Charles University in Prague
Faculty of Mathematics and Physics

DOCTORAL THESIS

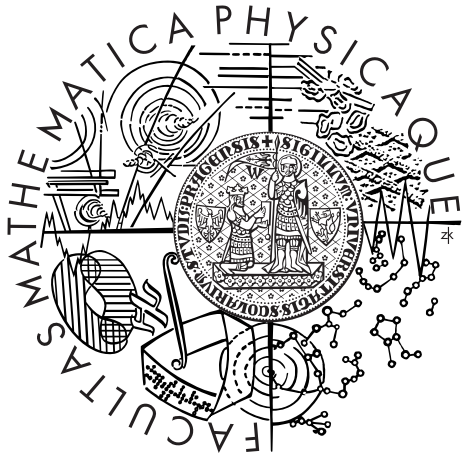

PETER RUBOVIČ

RECOMBINATION OF IONS IN PLASMA AT 50 – 300 K

Department of Surface and Plasma Science
Supervisor of the doctoral thesis: Prof. RNDr. Juraj Glosík, DrSc.
Study programme: Physics
Study branch: Physics of Plasmas and Ionized Media

« Only devil knows what is going on in the afterglow. »

— Manfred A. Biondi

ACKNOWLEDGMENTS

I would like to express my appreciation to everyone who helped to make this work possible, namely my colleagues Petr Dohnal, Michal Hejduk, Ábel Kálosi, Tomáš Kotrík, Pavol Jusko, Dmytro Mulin, Štěpán Roučka, and Illia Zymak. I want to thank Radek Plašil and especially prof. Juraj Glosík for their excellent supervision and guidance. My deepest thank goes to Petr Dohnal for his never ending enthusiasm, most of our results would not be obtained without him. I want also to thank prof. Rainer Johnsen for his cooperation with our group.

Ešte viac chcem ale poďakovať svojej rodine, všetkým priateľom a manželke Carmen za podporu počas celej doby môjho štúdia, a za to, že pri mne stáli vždy, keď som to najviac potreboval. Ďakujem.

DECLARATION

I declare that I carried out this doctoral thesis independently, and only with the cited sources, literature and other professional sources.

I understand that my work relates to the rights and obligations under the Act No. 121/2000 Coll., the Copyright Act, as amended, in particular the fact that the Charles University in Prague has the right to conclude a license agreement on the use of this work as a school work pursuant to Section 60 paragraph 1 of the Copyright Act.

Prague, June 2, 2014

Peter Rubovič

ABSTRAKT

Názov práce: Rekombinácia iónov v plazme pri $50 - 300\,\mathrm{K}$
Autor: Peter Rubovič
Vedúci doktorskej práce: Prof. RNDr. Juraj Glosík, DrSc.

Abstrakt: Hlavná časť tejto doktorskej práce spočíva v štúdiu rekombinácie atomárnych a molekulárnych iónov v nízkoteplotnom plazmatickom prostredí s dôrazom na efekt tretích telies. Boli použité metódy stacionárnej dohasínajúcej plazmy s cavity ring down spektrometrom a kryogénnej prúdiacej dohasínajúcej plazmy. Elektrónom asistovaná zrážkovo radiatívne rekombinácia iónov Ar^+ bola študovaná v teplotnom rozsahu $50 - 100\,\mathrm{K}$, héliom asistovaná zrážkovo radiatívna rekombinácia bola pozorovaná tiež. Ión H_3^+ a jeho izotopológ D_3^+ boli študované ako v prúdiacej dohasínajúcej plazme, tak aj spektroskopicky v stacionárnej dohasínajúcej plazme. Binárne rekombinačné koeficienty a ternárne rekombinačné koeficienty pre héliom asistovanú ternárnu rekombináciu boli určené v teplotnom rozsahu $50 - 250\,\mathrm{K}$. Tieto koeficienty boli stanované aj pre ortho- a para- konfigurácie spinu jadra iónu H_3^+ v teplotnom rosahu $80 - 200\,\mathrm{K}$.

Kľúčové slová: disociatívna rekombinácia, zrážkovo radiatívna rekombinácia, FALP, CRDS, H_3^+, D_3^+, Ar^+

ABSTRACT

TITLE: Recombination of Ions in Plasma at $50-300\,\mathrm{K}$
AUTHOR: Peter Rubovič
SUPERVISOR: Prof. RNDr. Juraj Glosík, DrSc.

ABSTRACT: Main part of this doctoral thesis lies in a study of recombination of atomic and molecular ions in low temperature plasmatic environment with emphasis on effect of third bodies. Stationary Afterglow equipped with Cavity Ring Down Spectrometer and Cryogenic Flowing Afterglow with Langmuir Probe II were used to obtain recombination rate coefficients. Electron assisted collisional radiative recombination of Ar^+ ion was studied in the temperature range of $50-100$ K and helium assisted collisional radiative recombination was observed too. Both H_3^+ and its isotopologue D_3^+ were studies in flowing afterglow and spectroscopically in stationary afterglow as well. Binary recombination rate coefficients and ternary recombination rate coefficients for helium assisted ternary recombination were determined in the temperature range of $50-250$ K. These coefficients were determined also for pure ortho- and para- nuclear spin configurations of H_3^+ in the temperature range of $80-200$ K.

KEYWORDS: dissociative recombination, collisional radiative recombination, H_3^+, D_3^+, Ar^+

CONTENTS

1 INTRODUCTION

This work summarizes four years of my doctoral studies under supervision of prof. Juraj Glosík in the Laboratory of Elementary Processes at Department of Surface and Plasma Science, Charles University in Prague. My study was entirely devoted to a process of recombination of ions with electron. It may sound as an easily understandable topic but reality is different. Complexity of this process remains challenging for physicisits, both theoretic and experimental, even at the beginning of 21^{st} century.

Even more challenging topic is H_3^+. This most simple triatomic molecular ion manages to puzzle physicists already for more than one hundred years! It is not without any reason that Bates et al. (1993) gave H_3^+ more than suitable nickname *"enigma"*. Over the time, there have been many discrepancies and contradictory studies. Some of them are resolved, some of them wait for their time to come.

Thus, one can only guess how unpredictable the conjuction of the aforementioned two topics - dissociative recombination of H_3^+ ions with electrons can be. Majority of this work is dedicated to its experimental study. Both stationary and flowing afterglow type experiments were used with emphasis on impact of third bodies, such as helium or electrons, on overall recombination process at temperatures down to 50 K.

This work is divided into 6 chapters according to the topics. Chapter 2 deals with theoretical description of recombinations of ions with electrons. Overview of experimental techniques used for recombination studies is also given. In Chapter 3 basic facts regarding H_3^+ ion are mentioned and review of its dissociative recombination measurements is included. Chapter 4 is devoted to the description of the experimental apparatuses used in this work and supplementary measurements of newly built Cryo-FALP II apparatus are shown. In Chapter 5 experimental results on recombination of Ar^+ ions, as well as of H_3^+ ions and its isotopologue D_3^+ are summarized.

1.1 GOALS OF THE THESIS

The focus of this work is concentrated on the topic of the recombination of ions with electrons in low temperature plasmatic environments with emphasis on the effect of third bodies on overall recombination.

The goals of the thesis can be summarized in the following points:

- Calibration of newly built Cryo-FALP II apparatus.
- Study of both electron assisted and helium assisted collisional radiative recombination of Ar^+ ions with electron in the temperature range of $50 - 100$ K.
- Study of binary and helium assisted ternary recombination of H_3^+ and D_3^+ ions in the temperature range of $50 - 250$ K.
- Recombination studies of specific nuclear spin state modifications of H_3^+ ion in the temperature range of $80 - 200$ K.
- Study of possible effect of H_2 as third body on H_3^+ recombination at 300 K.

2 RECOMBINATION OF IONS

Reaction of positive ion with electron is subject of study for more than one hundred years. If a singly ionized atomic ion is recombining, there are not many possibilities how to proceed. A free electron with a positive kinetic energy reacts with an ion whose energy can be removed, so it can enter a bound state. If there is no third body present, a photon radiation is one of the only possibilities for taking away excess energy. The process is called radiative recombination:

$$A^+ + e^- \xrightarrow{\alpha_{RR}} A + h\nu\,. \tag{1}$$

The other possibility is dielectronic recombination. It is worth remarking that both processes are quite inefficient and reaction rate coefficient for radiative recombination is $\alpha_{RR} < 10^{-10}\,cm^3s^{-1}$. When the third body is present in the aforementioned reaction, it can take away energy and thus make the reaction more efficient; the process is called *collisional-radiative recombination* (CRR) and it will be discussed thoroughly in section 2.3.

However, if a molecular ion is recombining instead of an atomic ion, the situation is different. A molecular ion has internal structure and thus it can transfer electron into a bound state while breaking one or even more chemical bonds. This process is called *dissociative recombination* (DR) because electron capture is stabilized by dissociation. The process is very efficient and its properties, as well as means of its experimental research, are to be discussed in the following sections 2.1 and 2.2.

2.1 DISSOCIATIVE RECOMBINATION

The first theoretical concept treating DR of molecular ions

$$AB^+ + e^- \xrightarrow{\alpha_{DR}} A + B \tag{2}$$

was given by Bates (1950). He suggested a two-step mechanism in which an unstable molecule is formed by capture of electron by molecular ion leading to formation of an unstable neutral molecule. It is followed by a rapid dissociation into neutral fragments. It is important to mention that incoming electron does not interact with molecular

nuclei but with the electron cloud, and the aforementioned fast dissociation prevents neutral molecule formed in the first step to autoionize. Rate coefficient of this process was estimated to be in the order of $\alpha_{DR} \sim 10^{-7}\,cm^3s^{-1}$. This mechanism of DR can be found in literature labelled as a *direct* one.

Another process was proposed in 1960's independently by Bardsley (Bardsley, 1968a; Bardsley, 1968b) and by Chen and Mittleman (Larsson and Orel, 2008). They proposed that kinetic energy of electron can be transformed by exciting a vibrational mode in the molecule while being captured into a Rydberg state. This step is followed by predissociation of the Rydberg state by an electronically doubly-excited, repulsive state. To distinguish this mechanism from that of Bates (1950) they labelled it as an *indirect* one.

Rydberg state is a state with a very high principal quantum number.

To illustrate the basic mechanisms of DR one need to hold all internuclear distances in a molecule constant except for the dissociation coordinate. A slice through the electron potential surfaces of the ion, Rydberg molecule, and dissociative states are displayed in Fig. 1.

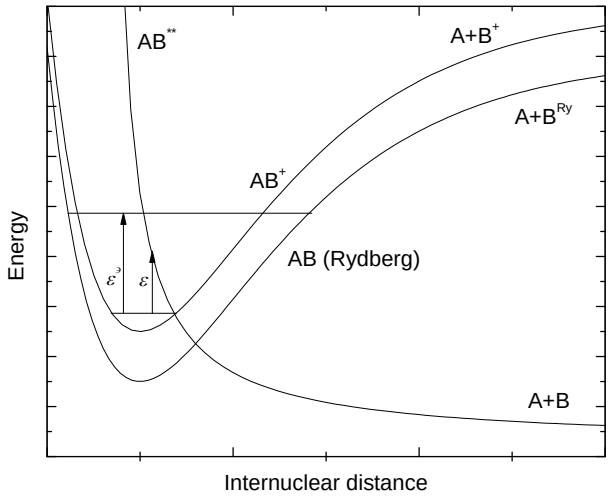

Figure 1: Schematics of both direct and indirect DR mechanisms. In direct mechanism, the molecular ion AB^+ in its ground vibrational states collides with an electron with kinetic energy ε and doubly excited neutral molecule AB^{**} is formed. Autoionization becomes prohibited due to rapid movement of atoms A and B and dissociation occurs on the potential curve. In indirect process, there is an intermediate step where a vibrationally excited Rydberg state if formed. Cross sections of DR depends on ε for direct mechanism and on ε' for indirect mechanism.

Complexity of DR lies in the fact that both direct and indirect mechanisms are paths to the same dissociation products and they can in-

terfere with each other. Thus every theoretical model dealing with DR must account for the interference and the results depend strongly on the details of molecular states.

2.2 EXPERIMENTAL TECHNIQUES

The experimental techniques used for DR investigation can be divided into two main categories: afterglow techniques and merged-beam techniques.

In afterglow techniques, reaction rate coefficients and products are derived from observed electron and ion densities, optical emissions, and neutral products during afterglow phase of plasma (Johnsen and Guberman, 2010). The analysis of an afterglow plasma can be complicated due to number of processes taking place, as it is common that not only one kind of DR process is happening. However, what one may see as complication, can be of interest for plasma physics in general.

On the other hand, merged-beam techniques and storage rings are free of these complications and they are closer to a theorists view of the problem. There is a single beam of a positive ion reacting with a beam of electrons at well defined mutual energy. It might sound as an ideal experiment for studying DR but as has been recently pointed out (Petrignani et al., 2011), the method has its own drawbacks.

2.2.1 *Afterglow Techniques*

Studies of ion chemistry are often carried out in so called swarm experiments. They are characterized by the presence of particles in ensembles, or swarms. These particles can be neutral molecules, atoms, ions or electrons. Most of swarm techniques are carried out in an afterglow plasma for several reasons. Firstly, it is a very accessible way to create low ionized environment with required atomic or molecular ions. Secondly, when using an active discharge, energetic, non-thermalized electrons are present but they are quickly thermalized (together with other particles in plasma) due to multiple collisions with buffer gas in the afterglow. Thus the afterglow is very well defined environment characterized by its temperature T and partial densities of reactants. An important feature of swarm experiments is that it is possible to measure only macroscopic values like temperature, rate coefficients of reactions, drift velocity etc. It is not possible to measure properties of individual particles (e. g. their actual energy); or properties of single

collisions (e. g. their cross sections which depend on the actual relative velocity of colliding particles).

Most of these techniques were developed in 1950's and 1960's and we will briefly discuss two of them which are relevant for this work. The first one is *Stationary Afterglow* (SA). This technique is based on measuring plasma properties during its decay. Stationary refers to a space configuration of the experiment. Discharge is repeatedly ignited in a gas mixture for a short period of time to form plasma dominated by ions which will be studied. Afterwards plasma decay is monitored, mainly by microwave diagnostic techniques often supplemented with a quadrupole mass spectrometer. A disadvantage of this method is that ion chemistry occurs also during active discharge where energy of electrons is not well defined and therefore the processes in plasma can be complicated. A good example of SA experiment is *Advanced Integrated Stationary Afterglow* (AISA) developed in our laboratory (Plašil et al., 2002), which can be seen in figure 2. SA equipped with *Cavity Ring Down Spectroscopy* (CRDS) will be described in Sec. 4.1 of this work.

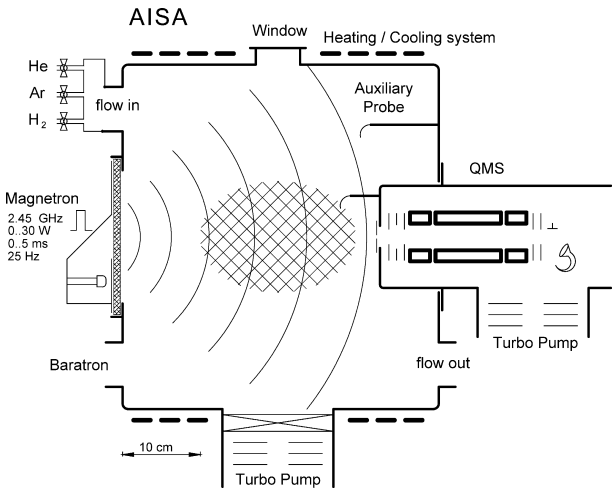

Figure 2: Overview of AISA apparatus (Plašil et al., 2002).

Main drawbacks of SA technique are improved in *Flowing Afterglow* (FA) experiments. In contrast to SA, a buffer gas introduced into a flow tube is flowing through an apparatus which is pumped usually by a large Roots pump. Velocity of flow v is used for conversion between the position on flow tube axis and time of plasma decay. Usually, helium or neon are used as a buffer gas. Plasma is formed by a discharge in the upper section of the flow tube. Downstream, where electrons are thermalized by collisions with buffer gas, reactant gases

are added. Space (and therefore time) separation of gas inlets is one of the main advantages of this technique – different regions dominated by different processes (removing metastables from buffer gas, ion formation, recombination dominated plasma, detection of ions or electrons) are separated and well defined. This method also offers great chemical variability.

There are many modifications of this technique and we will mention several of them. The original FA apparatus was developed by Fehsenfeld et al. (1966), see figure 3, and was equipped by a quadrupole mass spectrometer at the end of the flow tube. In 1970's, axially movable Langmuir probe was added to FA to monitore electron density in the flow tube (Mahdavi et al., 1971; Smith et al., 1975). This modification is commonly called *Flowing Afterglow with Langmuir Probe* (FALP). Another widely used modification of FA is *Selected Ion Flow Tube* (SIFT), where ions, produced in a separate ion source are then entering the flow tube, preselected by the quadrupole mass spectrometer (Adams and Smith, 1976). Rate coefficients of majority of ion molecule reactions studied up to now were measured by SIFT (Ikezoe et al., 1987). *Cryogenic Flowing Afterglow with Langmuir Probe II* (Cryo-FALP II), a modification of FALP with an ability to measure at stable temperature in the range $50 - 300$ K will be described in Sec. 4.2.

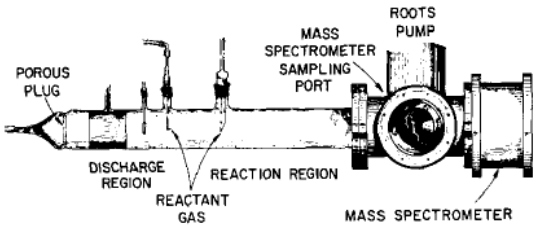

Figure 3: Drawing of the original FA apparatus (Fehsenfeld et al., 1966).

The methods for determining the recombination rate coefficient α are essentialy the same for both of the mentioned afterglow experiments. Under assumption that there is only one positive ion species present in plasma, which is quasineutral (the electron and number densities are equal $n_e = n_i$), the electron continuity equation is given as

$$\frac{\partial n_e(t, \vec{r})}{\partial t} = -\alpha n_e^2(t, \vec{r}) - D_a \nabla^2 n_e(t, \vec{r}), \tag{3}$$

where D_a is the ambipolar diffusion coefficient of the ion. If diffusion is slow enough the reciprocal electron number density can be written as

$$\frac{1}{n_e(t, \vec{r})} = \frac{1}{n_e(t = 0, \vec{r})} + \alpha t \tag{4}$$

and α can be obtained directly from the slope of the graph displaying time dependence of the measured reciprocal electron number density, so called "$1/n_e$" plot. However if diffusion losses are comparable to the recombination losses, one can fit the electron number density loss with the following equation:

$$\frac{dn_e(t)}{dt} = -\alpha n_e^2(t) - \frac{D_a n_e}{\Lambda^2}, \tag{5}$$

where Λ is the fundamental diffusion length of the plasma container, n_e is measured at the center of the container (in case of the flow tube its axis), and the position r is converted to time of plasma decay t. For a more sophisticated method of the aquired data analysis see Sec. 4.2.4 of this work.

2.2.2 *Merged Beam and Ion Storage Rings Experiments*

Altough the aforementioned techniques were not table top, they can be definitely called small scale experiment. However, this cannot be said of *Ion Storage Ring* (ISR) experiments which conquered the DR experiments in late 1980's and 1990's. Only the basic principles of this very complicated and complex technique will be given here. For more detailed review of these experiments please see Larsson and Orel (2008).

A single pass merged beam technique was developed in 1970's (Auerbach et al., 1977) and while it was an important step, it was superseded by the more powerful ISR technique. What is common for both of them is that electron-positive ion recombination takes place in two merged electron and ion beams of nearly the same velocity. In a single pass merged beam, the ion beam passes through the electron target beam only once and after analysis it is destroyed. However in ISR the ions circulate in the ring and pass through the interaction region multiple times. The advantage of ISR does not lay in higher efficiency of ion beam but in the solemn fact that the long storage time of ions in the ring results in deexcitation of all their excited states which radiate on the ion storage time scale.

It should be noted that the result from ISR studies is not a recombination rate coefficient for a single temperature T but set of ion-electron relative velocity dependent cross sections. Rate coefficients, as known

from afterglow experiments, can be inferred using Maxwellian velocity distribution.

2.3 COLLISIONAL-RADIATIVE RECOMBINATION

As was already indicated in the introduction of this chapter, ion-electron recombination, as essentialy two-body process, can be enhanced by involving the third body:

$$AB^+ + e^- + M \xrightarrow{K_{M\text{-}CRR}} A + B + M\,, \tag{6}$$

where M stands for the third body and $K_{M\text{-}CRR}$ is the ternary recombination rate coefficient of the process. *Collisional-radiative recombination*, as this process is often called (third body recombination can be found in literature too) can be divided into two essential categories depending on the nature of the third body. If M is neutral particle, the process is called *neutral-assisted collisional-radiative recombination* (N-CRR) and it will be discussed in section 2.3.1. If M is electron, the process is called *electron-assisted collisional-radiative recombination* (E-CRR) and it will be discussed in a separate section 2.3.2.

It has to be noted that effects of CRR can be usually negligible in afterglow experiments with the neutrals number densities $< 10^{17}\,\mathrm{cm}^{-3}$, temperatures $\sim 300\,\mathrm{K}$, and the electron number densities $< 10^{10}\,\mathrm{cm}^{-3}$. However, if one departs from these conditions by rising the neutral (electron) number densities or by lowering the temperature, the effects of the third bodies have to be taken into account, as they can substantially enlarge an impact of the recombination.

2.3.1 *Neutral-Assisted Collisional-Radiative Recombination*

In case of N-CRR, the excess energy originating from recombination is taken away by neutral particle. N-CRR can be described as

$$AB^+ + e^- + N \xrightarrow{\alpha_{N\text{-}CRR}} A + B + N\,, \tag{7}$$

where N stands for neutral particle and $\alpha_{N\text{-}CRR}$ is corresponding effective binary recombination rate coefficient of N-CRR. Corresponding ternary recombination rate coefficient $K_{N\text{-}CRR}$ can be obtained as

$$K_{N\text{-}CRR} = \frac{\alpha_{N\text{-}CRR}}{[N]}\,. \tag{8}$$

This process has been studied since early 1920's, starting with work of Thomson (1924). A successful diffusion model (Pitaevskii, 1962; Flan-

nery, 1991; Wojcik and Tachiya, 1999; Wojcik and Tachiya, 2000) treats the electron energy states as a continuum. Comparedg to experimental data, it gives a good estimation of the recombination rate coefficient. Flannery (1991) gives the following equation for the effective binary rate coefficient for atomic ions in their parent gas:

$$\alpha_{\text{N-CRR}} = 8\pi \frac{m_e}{M_{\text{atom}}} R_0 R_e^2 \sqrt{\frac{8 k_B T_e}{\pi m_e}} \sigma_{e,\text{atom}} \cdot [\text{N}] \,, \tag{9}$$

where m_e and m_{atom} are masses of electron and atoms respectively, R_0 is a trapping radius (in this theory electrons colliding with the atom inside the trapping radius recombine with unit probability and the probability outside of the radius is equal to zero), $R_e = e^2/4\pi\varepsilon_0 k_B T_e$, T_e is the electron temperature, and $\sigma_{e,\text{atom}}$ is an electron-atom momentum transfer cross section. Following assumption that $R_0 = R_e$ we get a $T^{-2.5}$ temperature dependence, which agrees also with that of Pitaevskii (1962) (for $R_0 = 2/3 R_e$) and Thomson (1924).

The model of Bates and Khare (1965) takes into account stepwise collisional deexcitation of Rydberg states of the ions and its values below 125 K are very similar to those of Pitaevskii (1962) and Flannery (1991). Due to more pronounced temperature dependence $\sim T^{-2.9}$ values at 300 K are two times lower.

The aforementioned theories treated system of atomic ion in its parent gas. Hence it is important to clarify the dependence of $\alpha_{\text{N-CRR}}$ on mass of neutral atom if it is different. The answer is still unclear, however Bates and Khare (1965) suggested that at low temperatures and neutral atom number densitied [N], $\alpha_{\text{N-CRR}}$ should be proportional to the reciprocal value of ion-atom reduced mass. Later calculations (Wojcik and Tachiya, 1999; Wojcik and Tachiya, 2000) only agreed with this.

Ternary effect for Ar^+ ions in helium buffer gas can be solved using (9) and (8), taking the momentum transfer cross section of electron-helium collisions $\sigma_{e,\text{He}} = 5.4 \times 10^{-16}\,\text{cm}^2$ (Crompton et al., 1967) as energy independent getting

$$K_{\text{He-CRR}} = 1.2 \times 10^{-27} \left(\frac{T_e}{300\,\text{K}} \right)^{-2.5} \text{cm}^6\text{s}^{-1} \,. \tag{10}$$

The experimental results obtained at temperatures above 300 K are in a good agreement with the theoretical calculations (Bates and Khare, 1965; Flannery, 1991) both in magnitude of the recombination rate coefficients and its temperature dependence. These experiments were conducted for atomic and also for molecular ions (He_2^+) (Berlande et

al., 1970; Deloche et al., 1976; Gousset et al., 1978; van Sonsbeek et al., 1992). Experimental data below 300 K are very rare. The experiment by Cao and Johnsen (1991) was performed in the temperature range of 80–150 K in a mixture of atmospheric ions (probably O_2^+, N_2^+ and NO^+) in helium buffer gas giving ternary recombination rate coefficients in agreement with theory and experiments at higher temperature.

One of the ions whose behaviour is not in agreement with the theory is the H_3^+ ion (together with its isotopologue D_3^+). Overview of the experimental data of H_3^+ DR together with their explanation will be given in sections 3.3 and 3.4. Data acquired during my doctoral work will be presented in section 5.2

2.3.2 *Electron-Assisted Collisional-Radiative Recombination*

When recombining by E-CRR, electron and positive ion form metastable complex colliding with another electron which carries away exceeding energy. Using Eq. (6), the process can be described by following chemical equation:

$$AB^+ + e^- + e^- \xrightarrow{\alpha_{\text{E-CRR}}} \text{neutral products} + e^- , \tag{11}$$

where $\alpha_{\text{E-CRR}}$ is the effective binary recombination rate coefficient of the E-CRR. In general, a single collision with another electron is insufficient and chain of several energy-reducing collisions is needed to prevent the autoionization of the neutral complex.

The E-CRR was described for the first time in the early 1960's and semi-classical theoreties of Bates et al. (1962), Mansbach and Keck (1969), and Stevefelt et al. (1975) followed very soon. These theories approach the E-CRR by solving the coupled equations of the three-body electron capture into the discrete Rydberg states, the ionization and the stepwise collisional and radiative reduction of the electron energy. Stevefelt et al. (1975) calculated the effective recombination rate coefficient and fitted it to a following equation:

$$\begin{aligned}\alpha_{\text{E-CRR}} = {} & 3.8 \times 10^{-9} T_e^{-4.5} n_e + 1.55 \times 10^{-10} T_e^{-0.63} \\ & + 6 \times 10^{-9} T_e^{-2.18} n_e^{0.37} \, \text{cm}^3 \text{s}^{-1} ,\end{aligned} \tag{12}$$

where n_e is the electron number density and T_e is the corresponding temperature. The first term of Eq. (12) describes purely collisional recombination, the second term treats contribution from purely radiative recombination, and the third term represents a correction for coupling of the previous two terms. Due to steep temperature dependence of

the collisional term ($\sim T^{-4.5}$), it becomes dominant at low temperatures and n_e typical for our experiments. Hence we can express the effective recombination rate coefficient of E-CRR as

$$\alpha_{\text{E-CRR}} = 3.8 \times 10^{-9} T_e^{-4.5} n_e \, \text{cm}^3 \text{s}^{-1} \, . \tag{13}$$

We can introduce the ternary recombination rate coefficient $K_{\text{E-CRR}}$ for low temperature environments:

$$K_{\text{E-CRR}} = \frac{\alpha_{\text{E-CRR}}}{n_e} = 3.8 \times 10^{-9} T_e^{-4.5} \, \text{cm}^6 \text{s}^{-1} \, . \tag{14}$$

The so-called Stevefelt formula (12) remains widely used, however, revised rates of electron capture into high Rydberg states and of the energy between the high Rydberg states and free electrons were published (Pohl et al., 2008). The new rates differ from the earlier ones, altough the recombination rate remains almost unchanged. Eq. (14) after Pohls revision would be

$$K_{\text{E-CRR}} = 2.77 \times 10^{-9} T_e^{-4.5} \, \text{cm}^6 \text{s}^{-1} \, . \tag{15}$$

However, we will use Stevefelts formula (14) throughout this work keeping in mind, that the actual data can differ from theory almost by one third.

Experimental studies of E-CRR were conducted mostly at electron temperatures above 300 K; see Mansbach and Keck (1969), Berlande et al. (1970), and Skrzypkowski et al. (2004), and references cited therein. E-CRR is also of interest for formation of antihydrogen (Killian et al., 1999; Pohl et al., 2008), and also for cold and ultra cold plasmas (Rennick et al., 2011). Experimental data for temperatures below 300 K are very scarce and all of them are from our laboratory (Kotrík et al., 2011a; Kotrík et al., 2011b; Dohnal et al., 2013). I participated on the latter two studies measured on Cryo-FALP II apparatus, which will be described in section 5.1. For the abovementioned articles see Article I and Article VI.

3

H_3^+ ION

H_3^+ ion was discovered in 1911 by J. J. Thomson using early mass spectrometry technique (Thomson, 1913). Containing only three protons and two electrons it is the simplest triatomic molecular ion and thus serving as "benchmark ion" for quantum mechanical calculations. However, as will be mentioned later, it does not mean that these calculations are always simple at the same time.

Process of H_3^+ formation

$$H_2^+ + H_2 \rightarrow H_3^+ + H + 1.7\,\text{eV} \tag{16}$$

was proposed by Hogness and Lunn (1925). As Oka (1983) pointed out, this reaction is not only exothermic but it has a large cross section without activation barrier too. The reaction rate coefficient was determined to be $k = 2 \times 10^{-9}\,\text{cm}^3\text{s}^{-1}$ at 300 K (Glosík, 1994). Martin et al. (1961) postulated the existence of H_3^+ in the *interstellar medium* (ISM). The importance of H_3^+ for the interstellar chemistry was recognized at the beginning of 1970's independently by Watson (1973) and by Herbst and Klemperer (1973). As H_2 has a low proton affinity of 4.5 eV and high cross-section of proton transfer to other atoms and molecules, H_3^+ serves as a universal proton donor and initiates a chain of ion-molecule reactions (McCall, 2006).

3.1 H_3^+ SPECTROSCOPY

H_3^+ ion has been widely studied in laboratory because it can be easily created in hydrogen discharge. However, it does lack both a stable electronic excited state needed for electronic spectrocopy, and a permanent dipole, this time needed for rotational spectroscopy, thus its spectroscopy is immensely difficult and only the infrared rotation-vibration spectrum is observable. A discovery of its spectrum took several years of work summed up in a pioneering article by Oka (1980) who observed the first 15 lines of the ν_2 fundamental band of H_3^+. Since then an enormous work was done in Oka's group and their results can be found in refs. Lindsay and McCall (2001) and McCall (2000).

The infrared transitions used to probe number densities of H_3^+ states in *Stationary Afterglow with Cavity Ring Down Spectroscopy* (SA-CRDS)

Table 1: Transitions monitored in the H_3^+ recombination studies. Details on spectroscopic notation can be found in Lindsay and McCall (2001). The energy levels are taken from Neale et al. (1996), the experimental line positions are from Ventrudo et al. (1994).

$\lambda\,(cm^{-1})$	SPECIES	$E_1\,(cm^{-1})$	$E_2\,(cm^{-1})$	TRANSITION
7234.957	$^oH_3^+$	315.349	7550.316	$3\nu_2^1(4,3) \leftarrow 0\nu_2^0(3,3)$
7237.285	$^pH_3^+$	64.1234	7301.4084	$3\nu_2^1(2,1) \leftarrow 0\nu_2^0(1,1)$
7241.245	$^oH_3^+$	86.9591	7328.2041	$3\nu_2^1(2,0) \leftarrow 0\nu_2^0(1,0)$

experiment are listed in Tab. 1. These transitions were used already in previous spectroscopic studies of H_3^+, see Ventrudo et al. (1994) and Mikosch et al. (2004). The lower energy levels of the transitions are displayed in Fig. 4.

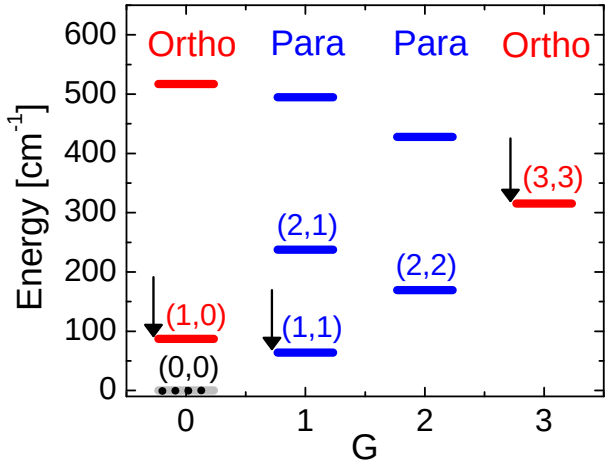

Figure 4: The lowest rotationaly energy levels (J, G) of the ground vibrational state of H_3^+. $(0,0)$ state is forbidden thus it is indicated by dashed line. Adapted from Hejduk et al. (2012).

3.2 H_3^+ IN INTERSTELLAR MEDIUM

H_3^+ was indentified in extraterrestrial enviroment in 1989 through emission spectroscopy of the Jovian atmosphere (Drossart et al., 1989), shortly followed by observations in atmosphere of Saturn (Trafton et al., 1993) and Uranus (Miller et al., 2000). The first identification of H_3^+ in the spectra of dense interstellar cloud came in 1996 (Geballe

and Oka, 1996) and in spectra towards diffuse interstellar cloud in 1998 (McCall et al., 1998).

The H_3^+ ion in molecular regions of ISM is formed in a two step process; H_2 molecule is ionized by cosmic rays with the rate coefficient ξ

$$H_2 \xrightarrow{\xi} H_2^+ + e^- , \tag{17}$$

followed by exothermic reaction (16). Destruction of H_3^+ in ISM is possible through ion-molecule reactions and through DR with electrons, which is determined by different conditions present in dense and diffuse interstellar cloud, respectively.

The fractional ionization in dense interstellar clouds is several orders of magnitude lower than in diffuse interstellar clouds. This is caused by a low abundance of free electrons, and by a low cosmic radiation flux causing radiation Herbst (2000). Thus the main H_3^+ destruction channel in dense interstellar clouds proton transfer to atoms and molecules like CO, N_2, and O.

On the other side, n_e in diffuse interstellar clouds, where the cosmic ray penetration is high, is more than four orders magnitude higher than in dense clouds Black (2000). As the reaction time of ion-molecule reactions scales down with the number density of reacting molecule, it becomes negligible at the number densities lower by several orders of magnitude. Hence the dominant loss channel becomes DR of H_3^+ with electrons.

As reaction (16) is much faster than reaction (17), ionization of H_2 by cosmic rays can be taken as a rate limiting step in formation of H_3^+ and it can be taken as a formation rate of H_3^+. Thus ξ can be calculated from the observed column densities of H_3^+ (Indriolo and McCall, 2012).

Another enigmatic face of H_3^+ is revealed here. Recent calculations of the H_3^+ nuclear spin excitation temperature T_{NS} from observations in diffuse sightlines show, that it is lower than the excitation temperature T_{01} of H_2, which can be taken as the kinetic temperature of the cloud (Indriolo and McCall, 2012; Crabtree et al., 2011) with $T_{01} \sim 70\,K$ and $T_{NS} \sim 30\,K$ implying enrichement in para-H_3^+ population. It was suggested that collisions between H_3^+ and H_2 can cause this nonthermal nuclear spin distribution of H_3^+ or that these collisions are infrequent or inefficient. However, recent study by Grussie et al. (2012) shows, that nuclear spin equilibrium of H_3^+ ions in collisions with H_2 is close to *thermal equilibrium* (TE). These observations demonstrate a strong need for accurate state selected studies of processes involving H_3^+, including its dissociative recombination.

3.3 DISSOCIATIVE RECOMBINATION OF H_3^+

The process of H_3^+ dissociative recombination with electrons has been studied continuously since the late 1940's. The long and often very interesting evolution of different experiments and theories accompanying this process is summarized in several reviews, notably in Mitchell (1990), Plašil et al. (2002), Florescu-Mitchell and Mitchell (2006), Larsson and Orel (2008), Johnsen and Guberman (2010), and Glosík et al. (2010). The list of experimental values, which is far from being complete, beginning with the study of Biondi and Brown (1949), is in Tab. 2.

The early H_3^+ recombination studies lacked the mass analysis and they were probably marked by nonnegligible presence of impurities. The observed fast recombination with rate coefficients in the order of $10^{-6}\,\mathrm{cm^3 s^{-1}}$ is partially caused by presence of H_5^+ ions and probably due to the aforementioned impurities. SA experimental method was significantly improved over the years and Leu et al. (1973), with the first mass spectrometer equipped afterglow experiment, obtained rate coefficient $\alpha = (2.3 \pm 0.3) \times 10^{-7}\,\mathrm{cm^3 s^{-1}}$ for H_3^+ in helium buffer gas. Similar results were obtained by Macdonald et al. (1984) in neon buffer gas.

However, Adams and Smith using FALP technique (Adams et al., 1984; Smith and Adams, 1984) obtained value lower by an order of magnitude $\alpha = 2 \times 10^{-8}\,\mathrm{cm^3 s^{-1}}$. Similar results were obtained in a MB experiment by Hus et al. (1988). Their "low" value was supported by calculations of Michels and Hobbs (1984). Amano in his two studies (Amano, 1988; Amano, 1990) used laser absorption spectroscopy and his results with $\alpha = (1.8 \pm 0.2) \times 10^{-7}\,\mathrm{cm^3 s^{-1}}$ supported "high" value. Fehér et al. (1994) tried to repeat Amano's spectroscopical experiment with addition of Langmuir probe but his results are unreliable due to the presence of various impurities.

The beginning of the 1990s saw an outbreak of ISR experiments, which supported the high value camp (Larsson et al., 1993; Sundström et al., 1994). So did the experiments of Johnsen and his coworkers (Gougousi et al., 1995). However, the low value camp was still supported by results of Smith and Španěl (Smith and Španěl, 1993a; Smith and Španěl, 1993b) and by Glosík using AISA experiment (Glosík et al., 2000). A whole series of experiments were done in Glosík's group in Prague. Their overview is given in the works by Korolov (2008) and Kotrík (2013). Here I will only mention the fact that a fast helium ternary recombination channel, which differs from that described by

Table 2: Overview of experimental values of H_3^+ recombination rate coefficient. Adapted from Plašil et al. (2002) and Dohnal (2013). Used acronyms are listed on p. 109.

SOURCE	$\alpha\,[10^{-7}\,cm^3s^{-1}]$	TECHNIQUE	COMMENT
Biondi and Brown (1949)	25	SA, μw	
Richardson and Holt (1951)	20; 60	SA, μw	pure H_2
Varnerin Jr. (1951)	3; 25	SA, μw	pure H_2
Persson and Brown (1955)	< 0.3	SA, μw	
Leu et al. (1973)	2.3	SA, μw	300 K
Peart and Dolder (1974)	2.5	IB	
Auerbach et al. (1977)	2.1	MB	
Mathur et al. (1978)	1.5	IT	
McGowan et al. (1979)	2.1	MB	
Adams et al. (1984)	< 0.2	FALP	
Macdonald et al. (1984)	1.5	SA	
Hus et al. (1988)	0.2	MB	
Adams and Smith (1989)	< 0.0001	FALP	estimate
Amano (1990)	1.8	SA, IR	273 K
Canosa et al. (1992)	1.5	FALP; QMS	
Smith and Španěl (1993a)	0.1	FALP	
Smith and Španěl (1993b)	0.2	FALP	
Fehér et al. (1994)	< 2	SA, IR	
Sundström et al. (1994)	1.15	ISR	Cryring
Gougousi et al. (1995)	$1.4 - 2$	FALP	
Laubé et al. (1998)	0.78	FALP, QMS	
Tanabe et al. (2000)	0.7	ISR	TARN II
Glosík et al. (2000)	< 0.13	AISA	low $[H_2]$
Jensen et al. (2001)	1	ISR	ASTRID
Glosík et al. (2003)	1.7	FALP	250 K
McCall et al. (2004)	0.68	ISR	Cryring
Macko et al. (2004)	1.6	SA-CRDS	330 K
Glosík et al. (2008)	0.75	FALP	260 K, comp.
Rubovič et al. (2013)	0.6	FALP	300 K, comp.

Bates and Khare (1965) (see also Sec. 2.3.1) was identified and theoretically explained (Glosík et al., 2009b).

Majority of the H_3^+ afterglow experimental values can be explained by the aforementioned ternary process (see Glosík et al. (2008)) which will be briefly described in a separate section 3.4. The only exception are values by Adams and Smith using FALP. Amano's experiment was the other exception for a long time but now it seems to be sufficiently explained by existence of H_2 ternary recombination channel. This recombination channel behaves differently than aforementioned He ternary channel and, of course, N-CRR as described in 2.3.1. This process will be discussed in Sec. 5.4 of this work.

Another surprise came when the value of pure binary recombination rate coefficient α_{bin}, which was obtained by extrapolating measured α_{eff} dependence on He number density to zero, gave values that are in agreement with the latest storage ring results (McCall et al., 2003; McCall et al., 2004; Kreckel et al., 2005) and even with theoretical calculations (Kokoouline and Greene, 2003; Kokoouline and Greene, 2005). Now, the generaly accepted value of thermal recombination rate coefficient at the temperature of 300 K is $\alpha = 7 \times 10^{-8}\,\mathrm{cm^3 s^{-1}}$ (Larsson and Orel, 2008).

Theory by Fonseca dos Santos et al. (2007) predicted that at temperatures below 300 K para-H_3^+ recombines faster than ortho-H_3^+. This prediction was partially confirmed in ISR experiments (Kreckel et al., 2005; Wolf et al., 2006; Kreckel et al., 2010). Tom et al. (2009) reported that para-H_3^+ recombines two times faster than ortho-H_3^+ at low collisional energies corresponding to 10 K. However, it was found that H_3^+ ions in the ISR experiments with low collisional energies had rotational temperature higher than 300 K (Kreckel et al., 2010; Petrignani et al., 2011; Kreckel et al., 2012).

Even greater difference in recombination rate coefficients was observed in SA-CRDS experiment at 77 K (Varju et al., 2011). Subsequently, a wide temperature range $77 - 200$ K was covered on that apparatus and the results are discussed in Sec. 5.3 of this work.

3.4 HELIUM ASSISTED TERNARY RECOMBINATION OF H_3^+

As mentioned in Sec. 2.3.1, helium assisted collisional radiative recombination of H_3^+ (and D_3^+) with electrons is an exception and it does not behave in accordance with standard theories (Bates and Khare, 1965; Flannery, 1991). The first studies of this process (Glosík et al., 2008; Glosík et al., 2009b; Glosík et al., 2009a; Glosík et al., 2010; Kotrík et

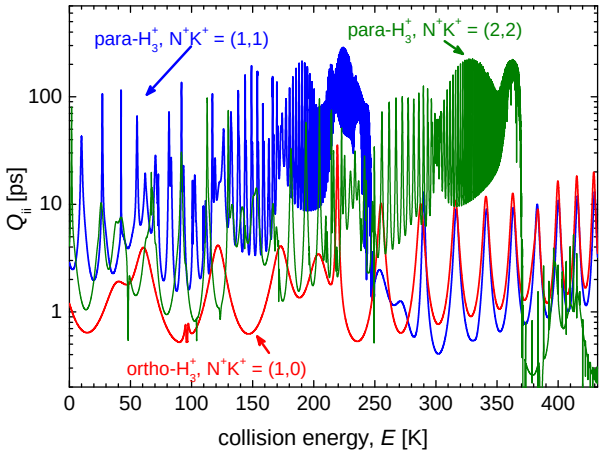

Figure 5: Diagonal elements of the calculated lifetime matrix **Q** of the three lowest rotational incident channels for the $e^- + H_3^+$ collisions. The lifetime of resonances is given by $Q_{ii}/4$. Adapted from Glosík et al. (2009b)

al., 2010) showed that the values of the ternary rate coefficient K_{He} exceeded the standard theoretical values by more than two orders of magnitude and morevover, they indicated nontrivial temperature dependence.

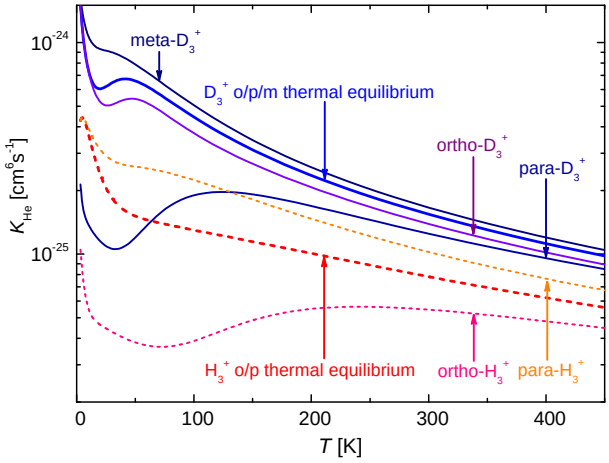

Figure 6: Theoretical ternary rate coefficient K_{He} of helium assisted collisional radiative recombination of H_3^+ and D_3^+ with electrons calculated for the ions in particular nuclear spin states and for the ions with internal state distribution according to thermal equilibrium. Adapted from Kotrík (2013).

This interesting process was moreless successfully described and calculated by C. H. Greene and V. Kokoouline (Glosík et al., 2009b)

as a multistep mechanism, where the electron collides with H_3^+ and a rotationally excited Rydberg state H_3^* with the lifetime $\sim 10^2$ ps is formed. Computed dependence of the lifetimes of the formed H_3^* on the incident electron energy is plotted in Fig. 5. Note that the diagonal element Q_{ii} of the calculated lifetime matrix $\mathbf{Q}$ is proportional to the H_3^* lifetime. If the number density of a neutral buffer gas, i. e. helium, is sufficient ($> 10^{17}\,\mathrm{cm}^{-3}$), the lifetime of H_3^* is long enough for a collision with neutral particle before autoionization of the H_3^*. It is supposed in Glosík et al. (2009b) that this collision changes the electronic angular momentum (l-changing collision) and prevents the autoionization.

Final ternary recombination rate coefficient is then calculated as

$$K_{He} = \alpha_* \cdot k^l \cdot \Delta t\,, \tag{18}$$

where α_* is the rate coefficient of H_3^* formation, Δt its lifetime, and k_l is the rate coefficient for the l-changing collision between He and H_3^*. Calculated ternary recombination coefficients are plotted in Fig. 6. A large difference between para- and ortho-H_3^+ ternary recombination below 300 K is predicted. This theory also treats D_3^+ ion.

3.5 D_3^+ ION

Importance of H_3^+ was discussed in the sections above. However, its deuterated isotopologues H_2D^+, HD_2^+, and D_3^+ are important as well. Beside from being a challenging task for theoretical physicists, deuteration of H_3^+ and formation of the aforementioned isotopologues enable us to characterize the enviroment where the deuteration takes place, including both interstellar plasma and enviroments, which are believed to be similar to that of pre-protostellar cores (Gay et al., 2011; Flower et al., 2004).

H_2D^+ and HD_2^+ unlike H_3^+ and D_3^+ have nonzero dipole moment, thus their detection should be less problematical than in the case of H_3^+ ion. H_2D^+ was observed in young stellar objects (Stark et al., 1999; Caselli et al., 2003), and in dense interstellar cloud (Cernicharo et al., 2007). HD_2^+ was detected shortly after that in dense interstellar medium of prestellar cores (Vastel et al., 2004; Parise et al., 2011). [1] These findings confirm the expectation that multiple deuterated ions play a key role the chemistry of the early universe (Gay et al., 2011). As a direct consequence, a higher D/H ratio is a result of gas phase

1 For molecules detected in space see The Cologne Database for Molecular Spectroscopy.

Table 3: Transitions monitored in the D_3^+ recombination studies. Details on spectroscopic notation can be found in Lindsay and McCall (2001). The energy levels are taken from Ramanlal and Tennyson (2004) and Tennyson (2012), the experimental line positions are from Dohnal et al. (2012a).

$\lambda\,(\mathrm{cm}^{-1})$	SPECIES	$E_1\,(\mathrm{cm}^{-1})$	$E_2\,(\mathrm{cm}^{-1})$	TRANSITION
5792.70	$^{m}D_3^+$	254.964	6047.645	$3\nu_2^1(3,2) \leftarrow 0\nu_2^0(4,2)$
5793.90	$^{o}D_3^+$	0	5793.917	$3\nu_2^1(1,0) \leftarrow 0\nu_2^0(0,0)$

models in ISM after inclusion of HD_2^+ and D_3^+ (Vastel et al., 2004). Unfortunately, D_3^+ has not been detected in space yet.

For spectroscopic study of D_3^+ recombination in SA-CRDS experiment we had to find transitions within the wavelength range of the used laser diode. The transitions listed in Tab. 3 were used to probe the decay of D_3^+ dominated plasma. The difference between the measured line positions and quantum mechanical calculations by Ramanlal and Tennyson (2004) and Tennyson (2012) was less than $0.02\,\mathrm{cm}^{-1}$, for additional details see Dohnal et al. (2012a).

For results of the D_3^+ recombination studies taken during my doctoral study refer to Sec. 5.2, where both binary and helium ternary channels are discussed. The studies were conducted in both SA-CRDS and Cryo-FALP II experiments.

4

EXPERIMENT

Two experimental apparatuses, SA-CRDS and Cryo-FALP II, were used during the course of my Ph.D. study. I describe their principles and configurations in the following sections. Subsidiary measurements, e. g. velocity calibration and O_2^+ recombination measurements used for calibration of Langmuir probe, both for Cryo-FALP II apparatus are included. Basic information about para enriched H_2 are mentioned too.

4.1 STATIONARY AFTERGLOW WITH CAVITY RING DOWN SPECTROSCOPY

Stationary afterglow technique, as described in section 2.2.1, has been used in Prague Laboratory of Elementary Processes in various configurations since late 1990s. A highly successful AISA apparatus was developed in order to study H_3^+ recombination at low pressures, for details see Plašil et al. (2002). CRDS was built in Prague in the early 2000s, first as an additional diagnostic method for AISA apparatus but later it was added to a small glass discharge tube, creating SA-CRDS apparatus. In this section the basics of absorption and cavity ring down spectroscopy will be given in sections 4.1.1 and 4.1.2, followed by description of SA-CRDS apparatus 4.1.3.

4.1.1 *Basics of Absorption Spectroscopy*

Intensity I of monochromatic light with frequency ν passing through a homogenous absorbing medium decreases according to Lambert-Beer law:

$$\frac{dI(x,\nu)}{dx} = -\alpha(\nu)I(x,\nu)\,, \tag{19}$$

where $\alpha(\nu)$ is the absorption coefficient related to the absorbing medium and x is the distance traveled by light in the medium. This equation has a simple solution

$$I(x,\nu) = I_0 e^{-\alpha(\nu)x}\,, \tag{20}$$

where I_0 is the initial light intensity.

We can characterize spectral line by its photo-absorption cross section $\sigma(\nu)$, which is defined through the absorption coefficient α and the number density of absorbing species N as

$$\alpha(\nu) = N(x)\sigma(\nu)\,. \tag{21}$$

A line-shape function $g(\nu)$ and an integral absorption coefficient (also known as spectral line intensity S) are introduced as

$$\sigma(\nu) = Sg(\nu)\,. \tag{22}$$

The line-shape function has to fullfill the following normalisation condition:

$$\int_0^\infty g(\nu)d\nu = 1\,. \tag{23}$$

Absorbance A is defined as

$$A = -\log\left(\frac{I}{I_0}\right)\,, \tag{24}$$

and we can rewrite this using Eq. (20) under assumption of homogenous medium:

$$A(\nu) = \alpha(\nu)L\,, \tag{25}$$

where L is the total distance traveled by light.

NUMBER DENSITY DETERMINATION

Population P of the energy level E_m in TE is given as

$$P(E_m) = \frac{g_m}{Q(T)}e^{-\frac{E_m}{k_B T}}\,, \tag{26}$$

where $Q(T)$ is a partition function and g_m is a degeneracy factor. We can calculate the value of the partition function at temperature T

$$Q(T) = \sum_m g_m e^{-\frac{E_m}{k_B T}} \tag{27}$$

from the following formula:

$$\log Q(T) = \sum_{i=0}^{n} a_i (\log T)^i\,, \tag{28}$$

where a_i are numerically calculated coefficients. It is important to keep in mind that at low temperatures only few energy levels are populated, so it is not needed to sum (27) over m running to infinity.

Table 4: Coefficients for the partition function expression (28) for H_3^+ (in TE), $^pH_3^+$, and $^oH_3^+$ taken from Hlavenka (2007).

	H_3^+ (in TE)	$^pH_3^+$	$^oH_3^+$
offset (cm^{-1})	0	64.123	86.9591
a_0	−35.2007	1.6702	0.5579
a_1	73.1854	−4.3613	2.8498
a_2	−68.1800	8.2473	−6.1672
a_3	37.2205	−7.6655	6.7433
a_4	−12.3723	3.6618	−3.9144
a_5	2.3413	−0.8479	1.1366
a_6	−0.1923	0.0764	−0.1275

The situation is similar also for Eq. (28) and it is sufficient to take finite series. Detailed information for rotational levels of H_3^+ can be found in Hlavenka (2007), Neale et al. (1996), and Tennyson (2011). The a_i parameters are listed in Tab. 4.

A detailed derivation of the formula for determining the number density can be found in Rothman et al. (1998) and Varju (2011). We will give only the final formulas for H_3^+ ions in rotational states J_n of the ground vibrational state. If the states are distributed in accordance with Maxwell-Boltzmann distribution, the integral absorption coefficient is calculated as

$$S = \frac{C g_n}{\nu_{nm}^2 Q(T)} e^{-\frac{E_m}{k_B T}} \left(1 - e^{-\frac{E_n - E_m}{k_B T}}\right) A_{nm} \,. \tag{29}$$

Variables and constants in this equation are listed in Tab. 5.

If the absorbance A is measured in the experiment, the number density N of the ions in the rotational state J_n at the centre of the Doppler broadened absorption line is

$$N = \frac{A\sqrt{2\pi}\sigma_D(T)}{S(T)L} \,, \tag{30}$$

where σ_D is the width of the spectral line, to be discussed below.

INTERNAL TEMPERATURES

In the previous paragraphs we considered temperature T as a temperature describing the system in TE. In reality, however, internal degrees

Table 5: Variables and constants in Eq. (29).

Symbol	Description	Units
S	integral absorption coefficient	cm
C	$1/8\pi c = 1.33 \times 10^{-12}$	$cm^{-1}s$
g_n	degeneracy factor for the upper level of the transition $g_n = (2S_n + 1) \times (2J_n + 1)$	
S_n	total nuclear spin of the upper level	
J_n	total angular momentum of the upper level	
E_m	energy of the lower state	J
E_n	energy of the upper state	J
A_{mn}	Einstein coefficient of the spontaneous emission	s^{-1}
ν_{mn}	transition frequency	cm^{-1}

of freedom are not necessarily thermalised. Therefore we have to distinguish specific temperatures, such as electronic T_e, vibrational T_{Vib}, or rotational T_{Rot} of the particles, particulary H_3^+ ions. Under TE, all of these temperatures are equal to the kinetic temperature T_{Kin}:

$$T = T_e = T_{Vib} = T_{Rot} = T_{Kin} = \dots \tag{31}$$

- **Kinetic Temperature**
  Kinetic temperature in absorption spectrocopy experiments is evaluated from Doppler broadening of a spectral line with central frequency ν_0. Its shape is given by a Gaussian function of the frequency ν:

$$g(\nu) = \frac{1}{\sqrt{2\pi}\sigma_D} e^{-\frac{(\nu-\nu_0)^2}{2\sigma_D^2}}, \tag{32}$$

  where $\nu_0 \equiv \nu_{mn}$ and

$$\sigma_D = \nu_0 \sqrt{\frac{k_B T_{Kin}}{Mc^2}}, \tag{33}$$

  where M is the particle mass. Please note, that commonly used *full width at half maximum* (FWHM) can be obtained by multiplying σ_D with factor $2\sqrt{2\log 2}$. The kinetic temperature T_{Kin} is then given by following expression:

$$T_{Kin} = \frac{\sigma_D^2 Mc^2}{\nu_0^2 k_B}. \tag{34}$$

Doppler broadening is not the only spectral line broadening type but it is the only relevant for this work. For H_3^+ ion in helium buffer gas with pressure 1000 Pa and at temperature of $T = 77\,K$, broadening of spectral line caused by Doppler effect is equal to 786 MHz while broadening due to collisions is only 36.1 MHz.

- **Nuclear Spin Temperature**
  At temperatures $\sim 80\,K$, only the two lowest rotational levels of H_3^+ ion are populated $(J, G) = (1, 1)$ and $(1, 0)$, so it is possible to introduce a nuclear spin temperature ($g_{o,p} = 2S + 1$):

$$\frac{^{o}f_3}{^{p}f_3} = \frac{g_o}{g_p} e^{-\frac{\Delta E}{k_B T_{NS}}} = 2e^{-\frac{32.9\,K}{T_{NS}}} \tag{35}$$

  and

$$T_{NS} = \frac{32.9}{\log(\frac{2\,^{p}f_3}{^{o}f_3})}\,. \tag{36}$$

  Of course, in TE $T = T_{NS}$. ln

- **Rotational Temperature**
  If Eq. (31) cannot be validated, T in Eq. (26) refers to rotational temperature T_{Rot}, which can be calculated from the ratio of populations of two rotational states J_m and $J_{m'}$:

$$\frac{P(E_m)}{P(E_{m'})} = \frac{g_m}{g_{m'}} e^{-\frac{E_m - E_{m'}}{k_B T_{Rot}}}\,. \tag{37}$$

  Vibrational temperature T_{Vib} can be introduced in a similar way. However, vibrational states are effectively thermalised by collisions with the buffer gas particles and with argon atoms, see detailed discussion in Article II.

4.1.2 *Cavity Ring Down Spectroscopy*

In this work, continuous wave modification of CRDS is used and a brief description of its principles will be given in this section. This spectroscopic technique was developed by Romanini et al. (1997). A laser light is coupled into an optical cavity with highly reflective mirrors (their reflectivity is $> 99.98\%$). They are periodically swept by piezo element until an optical resonator is formed (resonant cavity build-up) and the power of laser light in the cavity rises. Incoming laser beam is then interrupted by an acoustic-optic modulator after reaching a treshold intensity measured by PIN or avalanche photodiode behind one of

the mirrors. A basic scheme of the experimental setup can be seen in figure 7.

A laser light intensity I decreases with time t following the aforementioned interruption due to the losses at the mirrors and due to the absorption by the medium in the cavity, see Eq. (19):

$$I(t,\nu) = I_0 e^{-\frac{t}{\tau(\nu)}}. \tag{38}$$

Signal behaving in accordance with this equation is called a "ring-down signal". The characteristic time of the intensity decrease τ is a function of the light frequency and it is inversely proportional to the concentration of absorbing species in the medium:

$$\frac{1}{\tau(\nu)} = \frac{1}{\tau_0} + \frac{c}{d}A(\nu), \tag{39}$$

where d is a distance between the mirrors and A is the absorbance, see (25). τ_0 is the time constant of a light decay in the empty cavity, commonly called the baseline. Note, that it can be acquired almost "simultaneously" with $\tau(\nu)$ during one discharge-afterglow cycle. While $\tau(\nu)$ is acquired early after switching off the discharge, when the monitored ion density if sufficiently high, τ_0 is aquired at the end of the cycle, when there are almost no ions in the cavity. Frequency of ring-down events is $\sim 100\,\mathrm{Hz}$. Following (39) we can write

$$A(\nu) = \frac{d}{c}\left(\frac{1}{\tau(\nu)} - \frac{1}{\tau_0}\right). \tag{40}$$

4.1.3 *Stationary Afterglow with Cavity Ring Down Spectroscopy*

SA-CRDS is an implementation of CRDS technique to SA, see Fig. 8. The discharge tube is made of fused silica and distance between the mirrors is $\sim 75\,\mathrm{cm}$ and internal diameter $\sim 1.5\,\mathrm{cm}$. Its uniqueness lies in a synchronisation of the data aquisition system with a discharge switch. During the discharge-afterglow cycle repeating with period of several ms, the ring-down events are stochastic but after several hunderds of thousands cycles, the time evolution of the measured states is monitored with $\sim 20\,\mu\mathrm{s}$ resolution. Detailed description of the technique can be found in the following works: Varju (2011), Dohnal (2013), and Hejduk (2013).

As a light source, a fibre-coupled distributed feedback (DFB) laser diode is used. For studies with H_3^+ a laser with the central wavelength of 1381.55 nm was used. Its line-width is $< 2\,\mathrm{MHz}$ at 1 s time scale and

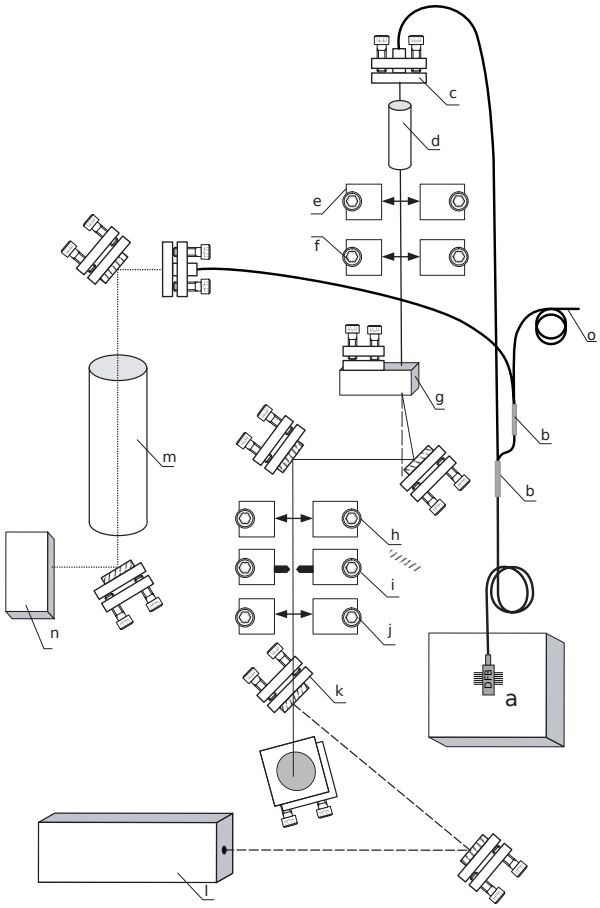

Figure 7: Top view of the placement of optical components. Adapted from Varju (2011). Optical fibre from the DFB laser (a) is connected to two 95:5 fibre beam splitters (b). The main fraction of the laser exits the fibre via the collimator (c). The optical isolator (d) follows. The beam shrinking telescope from lenses (e) and (f) focuses the beam on the active region of the acousto-optical modulator (g). The beam is focused on the pinhole (i) by the lens (h) and mode matched with lens (j). Laser light is guided into the optical resonator by mirror (k). The HeNe guiding laser (l) and Fabry-Perot resonator (m) are also placed on the same optical breadboard.

maximal output power is 20 mW. The laser beam undergoes carefuly set spatial filtering to form Gaussian profile matching to the optical resonator (Hejduk, 2013). Wavelength is monitored absolutely using wavemeter and relatively using a Fabry-Perot etalon. For an experimental setup scheme see Fig. 7.

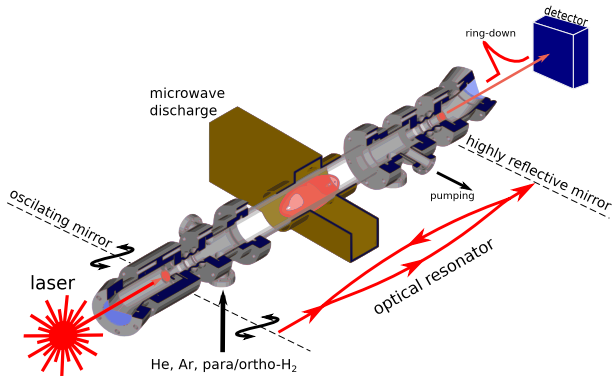

Figure 8: Scheme of SA-CRDS apparatus. The discharge in a gas mixture is ignited in the optical resonator consisting of two highly reflective mirrors. The oscillating mirror helps to establish the resonance, i. e. to inject the laser light into the cavity in random times. After the resonance is set and the resonator is filled with light, the laser light is switched off and the light travels several km in the cavity being gradually absorbed. Decrease of the optical signal escaping from the cavity, which is recorded by the detector is called ring-down. Higher concentration of monitored ions results in increased absorbance of the medium and shorter ring-down event. Adapted from Hejduk (2013).

A vacuum system used for SA-CRDS can be seen in Fig. 9. Its gas handling system is shared with Cryo-FALP II apparatus which will be described separately in section 4.2.3. He, Ar, and $^{n}H_2$ (or D_2) are sourced from it. Para enriched hydrogen $^{e}H_2$ is supplied directly from $^{e}H_2$ generator (see 4.3). Reasons for doing so are very simple. When passing through flow meter, para-to-ortho H_2 conversion can take place on its heated surface. We also do not want to store $^{e}H_2$ in a vessel kept at the room temperature. Hence the flow of $^{e}H_2$ is controlled by a temperature of the $^{e}H_2$ generator's cold head and calibrated by a pressure above turbomolecular pump TMU 261 seen in Fig. 9 measured by gauge P_f. Description of calibration procedure itself can be found in Hejduk (2013).

The discharge tube is cooled by liquid nitrogen (for the wall temperature of 77 K) or by its vapors. They are produced in a Dewar flask by heating liquid nitrogen with a resistant wire immersed in it. The

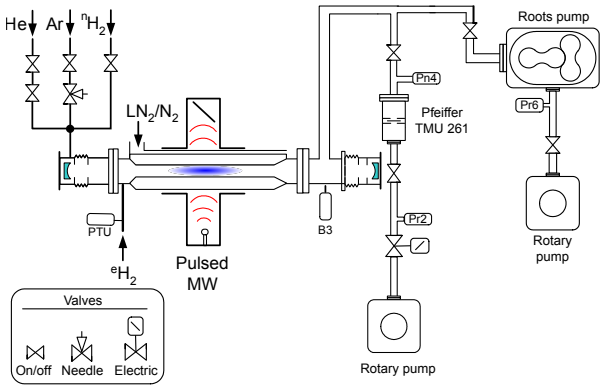

Figure 9: Vacuum system of SA-CRDS apparatus. Pr: Pirani gauge, B: capacitance gauge, Pn: full range gauge, PTU: piezoresistive strain gauge.

vapors are guided in an insulated metal tube into the space between a fused silica discharge tube and a microwave resonator afterwards.

For determining the recombination rate coefficient (2), we have to monitor the number density of the specific ion after the discharge is switched off. The number density of the ion in a specific state is calculated using Eq. (30) and the overall number density is calculated using Eq. (26). The advantage is that at low temperatures only several states are populated. If they are monitored, the sum of their number densitied forms the overall number density.

4.2 FLOWING AFTERGLOW WITH LANGMUIR PROBE

In this section, description of Cryo-FALP II apparatus will be given together with a necessary information on a diagnostic technique used and calibration measurements. FALP technique is used in our group for more than 30 years and there were several versions used in the last 15 years. These versions differed from the other ones used in the rest of the scientific community not only by the ability to measure at higher buffer gas pressures but also by the possibility to measure in a wide range of temperatures. Pinnacle of the efforts represents Cryo-FALP II apparatus, which can measure recombination at any temperature in the range of $50 - 300$ K.

4.2.1 *Langmuir Probe*

The Langmuir probe represents simple but very robust and reliable diagnostic method which is used for almost 100 years. Consisting of a small metallic electrode immersed in plasma, it was developed by Langmuir (1923), Mott-Smith and Langmuir (1926) and if several conditions are fulfilled, plasma parameters, such as the electron number density n_e, their temperature $T_e$and *electron energy distribution function* (EEDF) can be easily obtained from its current-voltage characteristic. These conditions are:

- The probe is not emitting.
- The electron and the ion currents are independent on each other.
- There are only singly charged particles present in plasma (ions and electrons) and their velocity distribution is maxwellian.
- The probe does not disturb plasma outside of a thin layer surrounding it.
- The mean free path of electron and ions is longer than the Debye shielding length.

There are several construction types of Langmuir probe but only a single cylindrical probe description will be given here, as it is the one used in Cryo-FALP II experiment. An example of a probe characteristic can be seen in Fig. 10.

A typical probe characteristic can be divided into several regions depending on a probe potential U:

1. $U = U_{fl}$
   If the probe is at the floating potential U_{fl}, the electron current on the probe is equal to the ion current, so the resulting current is equal to zero.
2. $U = U_p$
   Plasma potential U_p is defined as potential, where both ions and electrons are neither attracted nor repulsed by the probe. It is obtained as an inflection point of the probe characteristic (Smith et al., 1979).
3. $U < U_{fl}$
   If the probe potential is lower than the floating one, the region is called "saturated ion current", as majority of charged particles colliding with the probe surface are positive ions.

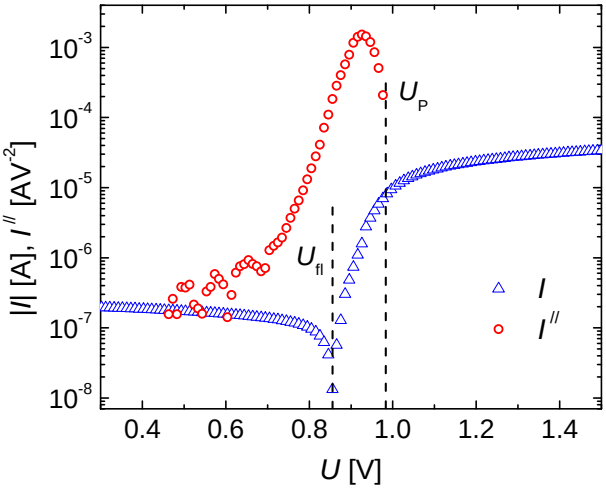

Figure 10: Absolute value of the current-voltage characteristic (open triangles) measured with Langmuir probe on Cryo-FALP II apparatus in Ar^+ dominated plasma at temperature of $T = 250\,K$ and He buffer gas pressure of 800 Pa. The second derivative of the probe characteristic is represented by open circles. Floating potential U_{fl} and plasma potential U_p are denoted by vertical dashed lines.

4. $U_{fl} \lesssim U \lesssim U_p$
   However, as the voltage increases, the electrons with higher energy can overcome the repulsive potential and they fall on the probe surface. Thus electron energy distribution can be obtained varying the probe potential in this region. Assuming maxwellian electron energy distribution, the electron current in this region can be expressed as (Pfau and Tichý, 2007)

$$i_- = -en_e A_{probe} \sqrt{\frac{k_B T_e}{2\pi m_e}} e^{-\frac{eU_S}{k_B T_e}} \tag{41}$$

   where A_{probe} is the probe surface and $U_S = U_p - U$. Hence the electron temperature T_e can be obtained from the following equation:

$$\ln i_- = \ln i_0 - \frac{eU_S}{k_B T_e}\,, \tag{42}$$

   where i_0 is constant independent on U_S. T_e can be obtained also from the second derivative of the electron current:

$$\ln \frac{d^2 i_-}{dU^2} = \ln C_T - \frac{eU_S}{k_B T_e}\,. \tag{43}$$

   Again, C_T is constant independent on U_S.

EEDF can be obtained from the second derivative of the electron current according to Druyvesteyn formula (Druyvesteyn, 1930):

$$f(eU_S) = \frac{2\sqrt{2m_e U_S}}{n_e e^3 A_{probe}} \cdot \frac{d^2 i_-}{dU^2}. \tag{44}$$

5. $U > U_p$
   This region is called "saturated electron current" region. As the name implies, the probe attracts electrons and repulses cations. The electron current collected by the single cylindrical probe is (Hutchinson, 2002)

$$i_- = \sqrt{\frac{2}{m_e}} \cdot \frac{A_{probe} e n_e}{\pi} \cdot \sqrt{eU_S + k_B T_e}. \tag{45}$$

   The electron number density can be obtained using the so-called "i-square method" (Mott-Smith and Langmuir, 1926) from the slope S of the i_-^2 dependence on U:

$$n_e = \sqrt{\frac{\pi^2 m_e}{2A_{probe}^2 e^3} S}. \tag{46}$$

4.2.2 *Cryogenic Flowing Afterglow with Langmuir Probe II*

As we have mentioned in the introductory part of this section, in Cryo-FALP II apparatus (for a schematic drawing see Fig. 11) the reaction section of the flow tube can be cooled down to 40 K and recombination processes can be studied down to 50 K. Effective binary recombination rate coefficients above $1 \times 10^{-8}\,cm^3 s^{-1}$ can be reliably measured. A very broad range of helium pressures and partial pressures of reactant gases can be covered which makes this apparatus an ideal instrument for measurements of rate coefficients of binary and ternary recombination processes. I will cover only basic facts in this work, as description of Cryo-FALP II can be found in the references Kotrík et al. (2011b) and Dohnal et al. (2013) and technical details can be found in Kotrík (2013) and Dohnal (2013).

The flow tube of Cryo-FALP II is divided into three sections, A, B, and C which differ by its wall temperature T_W. The internal diameter of the flow tube is ~ 5 cm, the length is ~ 80 cm. Helium buffer gas flows through the glass section (indicated as A in Fig. 11, kept at room temperature) where it is partially ionized in a microwave discharge (2.45 GHz, power of $10 - 30$ W). Downstream from the discharge Ar gas is added in order to remove helium metastable atoms

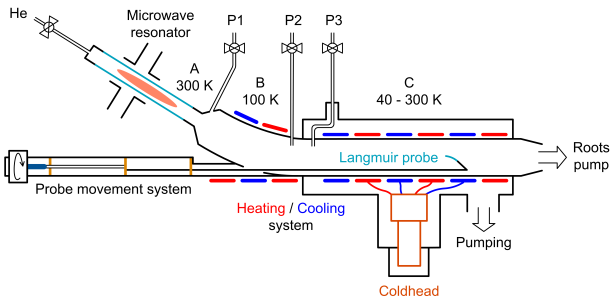

Figure 11: Scheme of Cryo-FALP II apparatus. Adapted from Kotrík (2013).

further downstream at the beginning of the stainless steel section B of the flow tube. This section is cooled to ~ 100 K by liquid nitrogen. It should be noted that in sections A and B with temperatures above 100 K the recombination is very slow and the plasma decay is caused mainly by ambipolar diffusion to the walls of the flow tube.

After precooling in section B the plasma enters stainless steel section C. This section is connected to the cold head (Sumitomo CH-110) by copper braids through a platform equipped with removable copper blocks and heating elements, so the cold head cooling power and the heath conductivity can be adjusted. Temperatures of the flow tube wall in the range of $40 - 300$ K can be achieved. To obtain good thermal insulation the whole section C and the cold head are placed in another vacuum chamber, see Sec. 4.2.3. Calculations showed that the buffer gas temperature T_{He} in section C is equal to the wall temperature T_W of the flow tube, and that the ion and electron temperatures (T_{ion} and T_e respectively) in the afterglow are equal to that of the buffer gas, i. e. $T_e = T_{ion} = T_{He} = T_W$. The temperature distribution along the flow tube and the resulting temperature of the He buffer gas was calculated by a computer model (see Kotrík et al., 2011b). The calculated relaxation time constant for the electron temperature is < 0.1 ms, i. e. electron temperature relaxes to the buffer gas temperature quickly after removal of the He metastables, see (Korolov et al., 2008; Glosík et al., 1999). We verified the electron thermalisation by analyzing characteristic times of ambipolar diffusion (see Sec. 5.1). These results support the assumption $T_W = T_e$. The ion thermalisation is many times faster (with time constant $< 0.1\,\mu$s) because the masses of ions are similar to those of the neutral atoms. This was also confirmed by spectroscopic measurements in H_3^+ and D_3^+ dominated plasma at otherwise very similar conditions (see Varju et al., 2011; Dohnal et al., 2012b; Dohnal et al., 2012a).

The recombination measurements are carried out in section C of the flow tube based on the electron density decays, which are determined by an axially movable Langmuir probe (length 7 mm, diameter 18 µm). To convert positions in the flow tube to afterglow time, the plasma velocity has to be known. We did plasma propagation velocity measurements summed up in Sec. 4.2.5.

The Langmuir probe characteristics are measured point by point on several possitions along the flow tube axis. The reliability of these measurements can be verified by measuring recombination rate coefficient of well-known recombination process, e. g. dissociative recombination of O_2^+ ions with electrons. For details see Sec. 4.2.6 of this work.

The temperature of the flow tube wall has to be monitored precisely. We use several silicone diode thermometers and common diodes attached at several positions along the flow tube, as well as on the platform and cold head itself. After building Cryo-FALP II apparatus we were trying several "*cooling regimes*", results of these measurements can be seen in Fig. 12. In the first, the B section of the flow tube was kept at room temperature instead of being kept at 100 K by *liquid nitrogen* (LN_2). After 4 hours of cooling temperature of section C was ~ 70 K. In the second regime, we cooled down section B and after the same time we approached the temperature of 68 K and afer 5 hours we got ~ 60 K. In the third case, we improved cooling using cryogenic grease Apiezon N which makes better thermal contact between the Cu braids and the platform and we saw very steep decrease of temperature resulting in ~ 50 K in 4 hours and ~ 40 K in almost 7 hours.

4.2.3 *Vacuum and Gas Handling System*

Vacuum and gas handling system of Cryo-FALP II apparatus will be briefly described in this section. The whole apparatus is based on *ultra high vacuum* (UHV) technology in order to keep level of impurities, such as H_2O, O_2, and N_2, as low as possible. These impurities react with ions in the afterglow forming fast recombining ions (see Eq. (48) and comments therein) which alter ionic composition of the afterglow.

Scheme of Cryo-FALP II vacuum and gas handling system is shown in Fig. 36. The system can be divided into three main parts: gas handling system, insulating vacuum chamber of the flow tube, and the flow tube itself.

The purpose of the gas handling system is to clean the gases before entering the flow tube and to mix the reactant gases. Helium (purity of

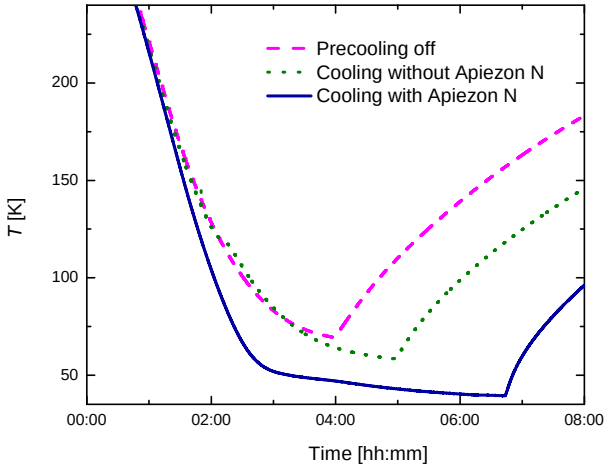

Figure 12: Measured temperature evolution of the section C of the flowtube at three regimes. In the first regime (dashed line), the B section of the flow tube was kept at room temperature instead of being kept at 100 K by LN_2. In the second regime (dotted line), section B was kept at 100 K. In the third regime (full line), we used Apiezon N cryogenic grease. Adapted from Rubovič et al. (2011).

5.7) is cleaned by passing two inline molecular sieve traps filled with zeolite, which are kept at LN_2 temperature. Before entering the flow tube, helium is passed through LN_2 cooled cryopump. Other gases (Ar, O_2, H_2, D_2) are purified only by passing cryopump cooled by LN_2 or by precooled ethanol (T ~ 170 K), depending on the boilng point of the gas. Ar gas is of 5.7 purity, H_2 and D_2 have declared purity of 5.0.

The flow of the gases is measured by mass flow meters (10000 sccm range for He, 10 sccm range for Ar) and flow of the reactant gases is regulated by mass flow controler with 10 sccm range. If desired reactant gas flow has to be even lower, it can be mixed with He in reservoirs, which can be seen in in Fig. 36. Reservoir system is equipped with a capacitance manometer with range $10^2 - 10^5$ Pa.

The gas handling system is routinely heated to ~ 340 K. Before every measurement a cleaning procedure lasting over 1 day takes place. Lines are heated, repeteadly filled with appropriate gas at pressure of several 10^5 Pa, and subsequently pumped. Molecular sieves are baked to ~ 390 K and repeteadly flushed with He. The background pressure after the cleaning procedure is in the order of ~ $9 \cdot 10^{-6}$ Pa. The resulting estimated level of impurities in the used gas mixture is of the order 10^{-2} ppm.

The purpose of the insulating vacuum chamber is, as was already mentioned in Sec. 4.2.2, to provide thermal insulation of the flow tube and cold head, i. e. to minimize the convection heat losses. The background pressure is usually $\sim 10^{-3}$ Pa.

The flow tube pressure is maintained by turbomolecular pump and ion sputter pump in between experiments, when it is heated to the temperature of 315 K. The background pressure is in the order of 10^{-6} Pa. During the experiment, buffer gas is pumped through the flow tube by a large Roots-type blower.

4.2.4 *Data Analysis*

As was already outlined in Sec. 2.2.1, data analysis in afterglow experiments is usually quite straightforward. However, few details have to be taken into account and they will be discussed in this section.

Electron number density n_e in Cryo-FALP II is evaluated using "i-square method", see Eq. (46) and corresponding comments in Sec. 4.2.1. Decay of n_e in quasineutral plasma dominated by singly charged ion A^+ is given by Eq. (3), which we modify a bit:

$$\frac{dn_e}{dt} = \frac{d[A^+]}{dt} = -\alpha_{eff} n_e [A^+] - k[A^+][B] - D_a \nabla [A^+] \,, \tag{47}$$

where α_{eff} stands for the effective (or apparent, overal) binary recombination rate coefficient and k is the rate coefficient of the ion-molecule reaction of A^+ with molecule B:

$$A^+ + B \xrightarrow{k} C^+ + D \,, \tag{48}$$

where C^+ is a fast recombining ion.

Using approximation of the fundamental diffusion mode (Chen, 1974) and aforementioned assumption (i. e. $n_e = A^+$), Eq. (47) can be written as

$$\frac{dn_e}{dt} = -\alpha_{eff} n_e^2 - k n_e [B] - \frac{D_a}{\Lambda^2} n_e \,, \tag{49}$$

where fundamental diffusion length Λ can be calculated as $\Lambda = r/J_0$, r being the flow tube radius and $J_0 = 2.405$ is the first root of Bessel function.

Time constant of the diffusion losses is taken as

$$\tau_D = \frac{\Lambda^2}{D_a} \tag{50}$$

and time constant of the losses due to ion-molecule reaction (48) is

$$\tau_R = \frac{1}{k[B]} \,. \tag{51}$$

The so called "*linear*" losses, which are proportional to n_e are then defined as

$$\frac{1}{\tau_L} = \frac{1}{\tau_D} + \frac{1}{\tau_R}\,. \tag{52}$$

Finally, we can rewrite Eq. (47) into a simpler form:

$$\frac{dn_e}{dt} = -\alpha_{eff} n_e^2 - \frac{1}{\tau_L} n_e\,. \tag{53}$$

The analytical solution of Eq. (53) has following form:

$$n_e(t) = \frac{n_0}{\alpha_{eff}\tau_L n_0 \cdot \left(e^{\frac{t-t_0}{\tau_L}} - 1\right) + e^{\frac{t-t_0}{\tau_L}}}\,, \tag{54}$$

where n_0 and t_0 represent initial conditions. Both coefficients α_{eff} and τ_L can be obtained directly by fitting the measured n_e to Eq. (54). Constants D_a for ambipolar diffusion are known for most of the cases and number density of B (i. e. impurities) can be estimated from τ_L. However, the dominant ion A^+ is usually formed from precursors and it does not have to be fully formed at the beginning of n_e measuring. To resolve this problem, an "*integral analysis*" was developed by O. Novotný (Korolov et al., 2008). Its core lies in the introduction of time dependent parameter ξ, which is defined as

$$\xi(t) = \frac{[A^+](t)}{n_e(t)}\,, \tag{55}$$

i. e. the fraction of A^+ number density to the overal ion number density. Using this parameter Eq. (53) can be rewritten as

$$\frac{dn_e}{dt} = -\alpha_{eff}\xi(t) n_e^2 - \frac{1}{\tau_L} n_e\,. \tag{56}$$

After integration we get

$$\ln\left[\frac{n_e(t_b)}{n_e(t_a)}\right] + \frac{t_b - t_a}{\tau_L} = -\alpha_{eff}\int_{t_a}^{t_b} \xi(t) n_e(t) dt\,, \tag{57}$$

where t_a and t_b are integration limits. After A^+ becomes dominant and $\xi = 1$, plot of Eq. (57) becomes linear with slope equal to $-\alpha_{eff}$. Time constant τ_L is taken as a parameter and it is calculated by minimizing χ^2 of the fit.

The derivation of Eq. (57) is valid under the assumption that α_{eff} does not depend on n_e. However when studying E-CRR, $\alpha_{eff}$is dependent on n_e, see Eq. (12). If no other recombination processes are present,

we can treat this case by modifying the procedure of (57) derivation. Firstly, we begin with Eq. (56):

$$\frac{dn_e}{dt} = -K_{E\text{-}CRR}\xi(t)n_e^3 - \frac{1}{\tau_L}n_e\,, \tag{58}$$

and after integrating we get the following expression:

$$\ln\left[\frac{n_e(t_b)}{n_e(t_a)}\right] + \frac{t_b - t_a}{\tau_L} = -K_{E\text{-}CRR}\int_{t_a}^{t_b}\xi(t)n_e^2(t)dt\,. \tag{59}$$

Derivation of $K_{E\text{-}CRR}$ and τ_L remains the same as for Eq. (57) and rate coefficient α_{eff}.

4.2.5 *Velocity Calibration*

As was already mentioned in Sec. 2.2.1, it is necessary to know the velocity of the plasma propagation v along the flow tube axis to convert distance z to time t. A simple *time of the propagation* method is used to obtain the velocity calibration. The discharge power is modulated periodically, so the electron number density n_e is modulated too. Time delay Δt of the n_e distortion is measured by Langmuir probe at different spatial positions and v can be obtained from the linear fit to the measured dependence of Δt on z, see Fig. 13, where several sets of plasma propagation velocity in He_2^+ dominated plasma are displayed. Note, that a change in these dependencies is caused by gradual cooling of plasma in the flow tube.

The results of the plasma velocity can be summarised as a function of semiempirical *similarity factor* (Kotrík, 2013) FT/p depending on the buffer gas flow rate F, its pressure p, and temperature T. This dependency is displayed in Fig. 14 for both He_2^+ and Ar^+ dominated plasma. As one would expect, it does not depend on the plasma composition.

A linear fit to the data in Fig. 14 (the dashed line) represents the calibrating curve used for the determination of the plasma velocity at given experimental conditions. This can be done using the following formula:

$$v = v_0 + S_v\left(\frac{F\cdot T}{p} - \frac{F_0\cdot T_0}{p_0}\right) \tag{60}$$

where v_0 represents velocity measured at F_0, T_0, and p_0, S_v denotes the slope of the calibrating curve. These values are: $v_0 = 8.451\,m\cdot s^{-1}$, $S_v = 3.047\,K^{-1}\cdot m^{-2}$, and $F_0\cdot T_0/p_0 = 2.483\,K\cdot m^3\cdot s^{-1}$.

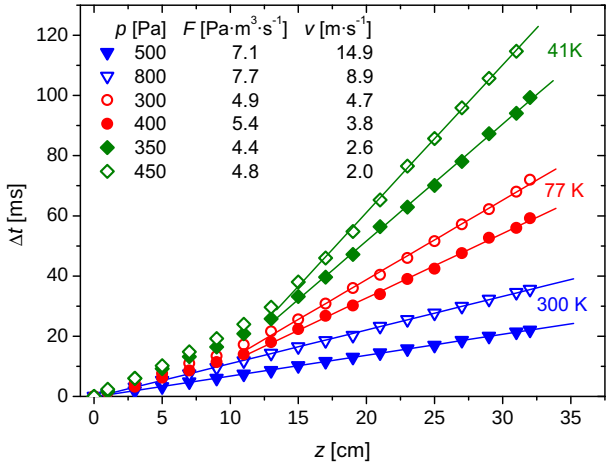

Figure 13: Plasma propagation velocity at the flow tube axis measurements in Cryo-FALP II. The discharge is modulated and the time delay Δt of n_e distortion is measured at the spatial position z. Data are obtained in He_2^+ dominated plasma, experimental conditions are listed in the figure. Adapted from Kotrík et al. (2011b).

4.2.6 *Recombination of O_2^+*

The Langmuir probe has to be calibrated due to several reasons. One of them is verifying the theoretical assumptions of the Langmuir probe theory 4.2.1. The other reason is to overcome the uncertainities in determination of Langmuir probe surface, i. e. its diameter and length needed for the electron number density measurements (46). The multiplication of n_e with eventual correction factor is equal to the multiplication of the measured recombination rate coefficient α. The key for determination of the correction factor C is to measure the recombination rate coefficient of a well known ion and in subsequent comparison with its generally accepted values. For this purpose, O_2^+ ion was used with the recombination rate temperature dependence (Španěl et al., 1993):

$$\alpha_{O_2^+} = 2.0 \times 10^{-7} (300\,\mathrm{K}/T)^{0.65}\,\mathrm{cm^3 s^{-1}}\,. \tag{61}$$

O_2^+ dominated plasma is formed in $He/Ar/O_2$ mixture involving the reactions listed in Tab. 6. A set of these reactions was used in the chemical kinetics model, which was computed before each measurement. The conditions have to be set to form O_2^+ dominated plasma. Number density of O_2 has to be high enough to assure fast O_2^+ formation but one has to avoid excessive O_4^+ formation at higher $[O_2]$. The flow and pressure of He buffer gas must be set correctly in order to

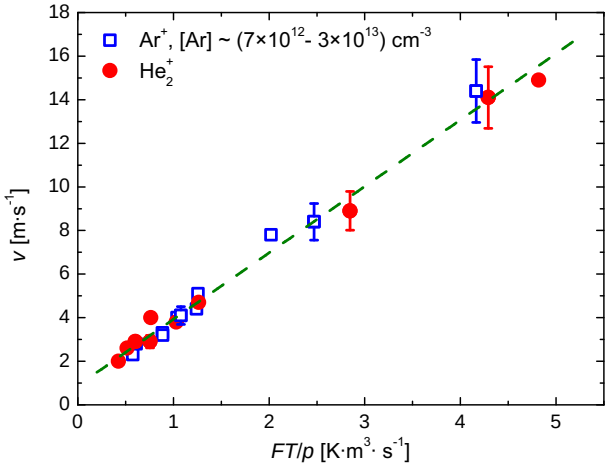

Figure 14: Velocity calibration curve of Cryo-FALP II apparatus. Velocity v dependence on *similarity parameter* representing experimental conditions is measured for plasma dominated by both He_2^+ and Ar^+(circles and squares, respectively). Fit to the data is represented by dashed line, which is used as the calibrating curve for determining the plasma velocity at given experimental conditions. Adapted from Kotrík et al. (2011b).

decrease losses caused by ambipolar diffusion. Example results of the model compared to the experimental data can be seen in Fig. 15

Helium buffer gas dependencies of the O_2^+ recombination rate coefficients for the temperatures of 155 K and 230 K are displayed in Fig. 16. The mean of the data shows that the agreement with values given by Španěl et al. (1993) is very good. Data were obtained at wide He buffer gas pressure range and no pressure dependence can be seen, nor any dependece on O_2^+ number density was seen, so we can assume that the recombination was not affected by O_4^+ recombination.

We measured at three different temperatures – 100 K, 155 K, and 230 K. The obtained results can be seen in Fig. 17 together with data obtained in other experiments (McLain et al., 2004; Alge et al., 1983; Walls and Dunn, 1974; Johnsen, 1987; Adams et al., 1984; Peverall et al., 2001; Španěl et al., 1993). The agreement with both afterglow and ISR experiments is obvious. Langmuir probe used in Cryo-FALP II experiment is the same one, as mentioned in Korolov (2008) and the aforementioned results indicate that the correction factor $C = 1.6$ (i. e. the probe itself) remains unchanged.

Table 6: List of the reactions which are included in the chemical kinetics model of O_2^+ dominated plasma in $He/Ar/O_2$ mixture. Characteristic times of the reactions are based on typical experimental conditions: $[He] = 5 \cdot 10^{17}\,cm^{-3}$, $[Ar] = 5 \cdot 10^{13}\,cm^{-3}$, $[O_2] = 5 \cdot 10^{13}\,cm^{-3}$, $[He^m] = 1 \cdot 10^{10}\,cm^{-3}$, $n_e = 10^9\,cm^{-3}$, $T = 230\,K$. When several loss processes are included for one species, the one with the smallest characteristic time is dominant. Adapted from Rubovič et al. (2012).

REACTION	α [$cm^{-3}s^{-1}$]; [$cm^{-6}s^{-1}$]	τ [ms]	SOURCE
$He^+ + He + He \rightarrow He_2^+ + He$	$1 \cdot 10^{-31}$	0.04	Ikezoe et al. (1987)
$He^+ + Ar \rightarrow Ar^+ + He$	$1 \cdot 10^{-13}$	200	Johnsen et al. (1973)
$He^m + Ar \rightarrow Ar^+ + He + e^-$	$7 \cdot 10^{-11}$	0.3	Glosík et al. (1999)
$He^m + He^m \rightarrow He_2^+ + e^-$	$5 \cdot 10^{-9}$	20	Urbain (1999)
$He^m + He^m \rightarrow He^+ + He + e^-$	$1.5 \cdot 10^{-9}$	67	Deloche et al. (1976)
$He_2^+ + Ar \rightarrow Ar^+ + 2He$	$2 \cdot 10^{-10}$	0.1	Ikezoe et al. (1987)
$He_2^+ + e^- \rightarrow 2He$	$< 3 \cdot 10^{-10}$	30	Deloche et al. (1976)
$Ar^+ + O_2 \rightarrow O_2^+ + Ar$	$4.5 \cdot 10^{-11} \cdot (300/T)^{0.67}$	0.4	Midey and Viggiano (1998)
$Ar^+ + e^- + He \rightarrow Ar + He$	$3 \cdot 10^{-26}$	67	Bates and Khare (1965)
$O_2^+ + e^- \rightarrow O + O$	$2.0 \cdot 10^{-7} \cdot (300/T)^{0.65}$	4.2	Španěl et al. (1993)
$O_2^+ + O_2 + He \rightarrow O_4^+ + He$	$8.9 \cdot 10^{-31} \cdot (300/T)^{2.74}$	22	Smirnov (1977) and Boehringer et al. (1983)
$O_2^+ + O_2 + O_2 \rightarrow O_4^+ + O_2$	$3.7 \cdot 10^{-30} \cdot (300/T)^3$	$47 \cdot 10^3$	Smirnov (1977)
$O_4^+ + e^- \rightarrow$ products	$2.3 \cdot 10^{-6}$	0.43	Kasner and Biondi (1968)

4.2.7 *Electron Temperature Verification*

Electron temperature T_e is one of the most important parameters affecting dissociative recombination. It is usually evaluated from the second derivative of the Langmuir probe current-voltage characteristics, see Sec. 4.2.1 and Eq. (43), but its determination at low temperatures is problematic.

However, a precise measurement of ambipolar diffusion losses in the late afterglow can serve as a "diffusion thermometer". In this case we used the data from our study of Ar^+ ion recombination at low temperatures, which can be found in Sec. 5.1. As we mentioned in Sec. 4.2.4, the measured time constant τ_L constists of two components; one representing ambipolar diffusion τ_D and the other representing losses due to ion-molecule reaction τ_R. The value of τ_D depends on temperature, helium buffer gas density, the characteristic diffusion length $\Lambda = R/2.405$ of the flow tube, and the zero-field re-

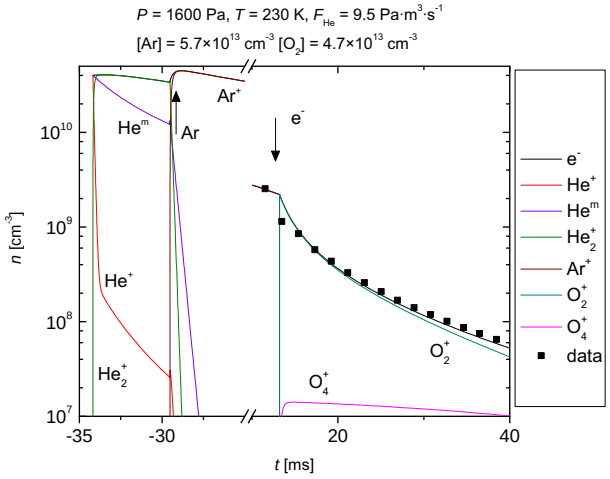

Figure 15: A comparison of the chemical kinetics model based on the reactions listed in Tab. 6 with measured data at displayed conditions. After the discharge ignition in helium gas, afterglow with He^+ and He_2^+ ions and He^m metastable atoms are created. After the addition of argon plasma is rapidly converged into the Ar^+ dominated plasma. Oxygen is added later and O_2^+ becomes the dominant ion. Adapted from Rubovič et al. (2012).

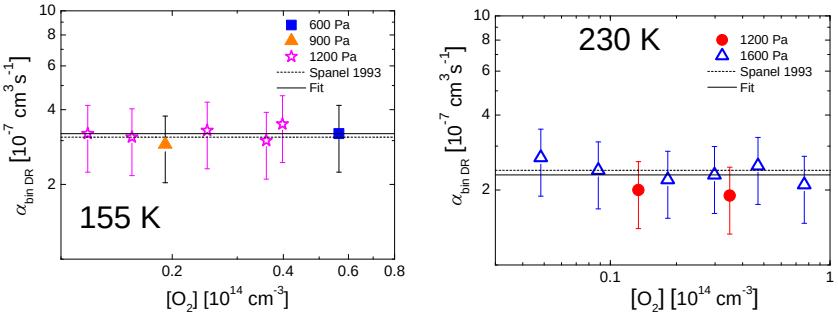

Figure 16: Measurements of the rate coefficients of dissociative recombination of O_2^+ with electrons at 155 K and 230 K at several pressures of He buffer gas and over 1 order of magnitude of $[O_2]$. There is a very good agreement between the mean of the data (continuous line) and the generally accepted value (Španěl et al., 1993). Adapted from Rubovič et al. (2012).

duced mobility K_0 of Ar^+ ions in He. Mason and McDaniel (1988) give the following formula for ambipolar diffusion characteristic time (as-

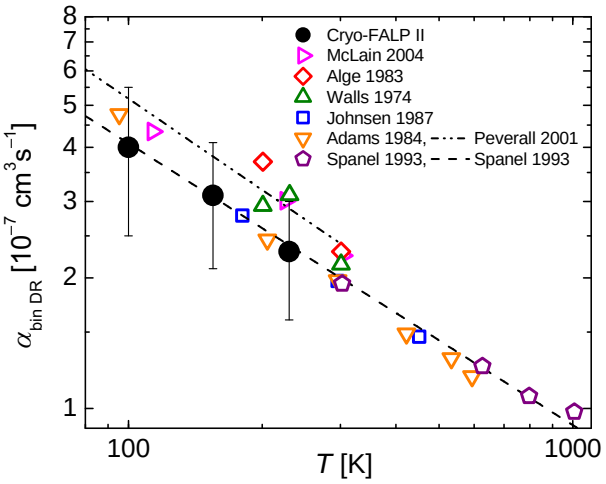

Figure 17: Temperature dependence of the measured recombination rate coefficient $\alpha_{bin\ DR}$ of the binary dissociative recombination of O_2^+ ions with electrons. The present Cryo-FALP II data (large circles) are compared to previous results (McLain et al., 2004; Alge et al., 1983; Walls and Dunn, 1974; Johnsen, 1987; Adams et al., 1984; Peverall et al., 2001; Španěl et al., 1993). Adapted from Dohnal et al. (2013).

suming that electrons, ions, and gas atoms have the same temperature $T_e = T_{ion} = T_{He} = T$):

$$\frac{1}{\tau_D} = 4.63 \times 10^{15} \frac{K_0(T)}{\Lambda^2} \frac{T}{[He]}\, s^{-1}\,. \tag{62}$$

Since the zero field reduced mobility of Ar^+ in He is nearly constant for temperatures below 300'K, a plot of $[He]/\tau_D$ versus T dependence should be almost linear, with small deviations if the dependence of K_0 on temperature is included, for details see (Kotrík et al., 2011a). Measured values of $[He]/\tau_D$ should be proportional to the temperature thus providing an independent measure of the otherwise difficult to determine electron temperature. Figure 18 shows the theoretical temperature dependence of $[He]/\tau_D$, where τ_D is calculated using zero-field reduced mobility K_0 (Viehland et al., 1991; Lindinger and Albritton, 1975; Johnsen and Biondi, 1979).

Even small changes in temperature imply rather large changes of $[He]/\tau_D$ and to illustrate this fact we included also values of $[He]/\tau_D$ calculated for the temperatures that are 10 K higher and lower in Fig. 18. As can be seen in Fig. 18, the "diffusion thermometer" becomes unreliable at temperatures below $\sim$ 70 K because the experimental values $[He]/\tau_L$ include a contribution $[He]/\tau_R$ caused by reactive losses in

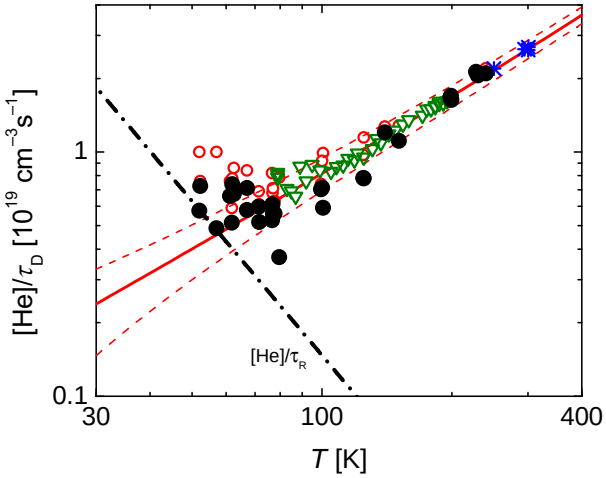

Figure 18: Temperature dependences of $[He]/\tau_D$ and $[He]/\tau_R$. Full line represents the theoretical temperature dependence of $[He]/\tau_D$. Dashed lines are calculated for 10 K higher or lower temperatures. The dash-dotted line labeled $[He]/\tau_R$ shows values corresponding to reactive losses due to Ar_2^+ formation. Data measured on previous FALP experiments (open triangles) are adapted from Kotrík et al., 2011a as well as data indicated by asterisk symbols measured at 250 and 300 K. Open circles indicate measured $[He]/\tau_L$ and closed circles indicate corresponding $[He]/\tau_D$ calculated for particular [He] and [Ar]. Adapted from Dohnal et al. (2013)

the late afterglow (see Eq. (52)). Thus we corrected the experimental values of $[He]/\tau_L$ (open circles) by subtracting an estimated reactive loss term $[He]/\tau_R$ in order to obtain the pure diffusion loss rate term $[He]/\tau_D$ (solid circles). The reactive loss term $[He]/\tau_R$ was ascribed to conversion of Ar^+ ions to fast recombining Ar_2^+ ions, using the experimental association ternary rate coefficient k_a of Bohme et al. (1969). For details of the actual analysis refer to Dohnal et al., 2013. This correction is included in Fig. 18 (dash-dotted line). Since the reactive losses increase rapidly at lower temperatures, while the diffusion losses become smaller, the accuracy of the "diffusion thermometer" becomes poor below 70 K and corrections for reactive losses do not improve it much. Nevertheless, this does not necessarily imply a difference between the flow tube wall temperature T_W, T_e and T_{ion} below 70 K as will be shown in Sec. 5.1. For comparison in Fig. 18 we also show data from the previous FALP and Cryo-FALP I experiments measured at 250 and 300 K (Kotrík et al., 2011a). In that case the whole flow tube was cooled by liquid nitrogen to the same temperature and there was no doubt about temperature equilibration.

4.3 PARA ENRICHED H_2 GENERATOR

Total fractions of para $^{p}H_2$ and ortho $^{n}H_2$ hydrogen states in hydrogen gas in TE ($^{n}H_2$) at 300 K are 1/4 for $^{p}H_2$ and 3/4 for $^{o}H_2$. These populations change only very slowly when the gas is cooled or heated. However, several mechanisms for realigning the proton spins exist (Hejduk, 2013). One of them is tu use a para-magnetic catalyst. If $^{n}H_2$ is brought into contact with such catalyst and cooled down to very low temperaturest, hydrogen gas in nearly complete $^{p}H_2$ population in the lowest rotational state ($v_0 = 0$, $J = 0$) can be prepared. Afterwards, without the presenceof the catalyst and subsequent heating of the gas, it maintains its "*low temperature composition of states*" for sufficiently long time to provide experiments with para-enriched hydrogen ($^{e}H_2$). Measured time constant for backward conversion to $^{n}H_2$ in a glass cavity kept at room temperature was 97 ± 4 hours.

Para enriched H_2 generator, inspired by Tam and Fajardo (1999), was built in our laboratory to work in conjuction with SA-CRDS experiment. For details, please, refer to the works of Varju (2011) and Hejduk (2013). In this device, Fe_2O_3 was used as a catalyst. A conversion chamber filled with the catalyst is cooled by a cold head. The actual fraction of $^{p}H_2$ measured by nuclear magnetic resonance is $[^{p}H_2]/[^{e}H_2] = (87 \pm 5)\,\%$. This is sufficient to form afterglow plasma with fraction of $^{p}H_3^+$ ($^{p}f_3$) higher than that in $^{n}H_2$, where $^{p}f_3 = 0.5$, see Fig. 19.

After the experiments on SA-CRDS, which are summarised in Dohnal et al. (2012b), the $HFeO_2$ catalyst was changed and heat activated in H_2 atmosphere. According to Zymak et al. (2013), who measured the reaction rate coefficient of $N^+ + H_2$ reaction, $^{p}f_3$ in the produced $^{e}H_2$ was $(99.5 \pm 0.5\%)$. This catalyst was used in the state selected H_3^+ studies using Cryo-FALP II, see Sec. 5.3.

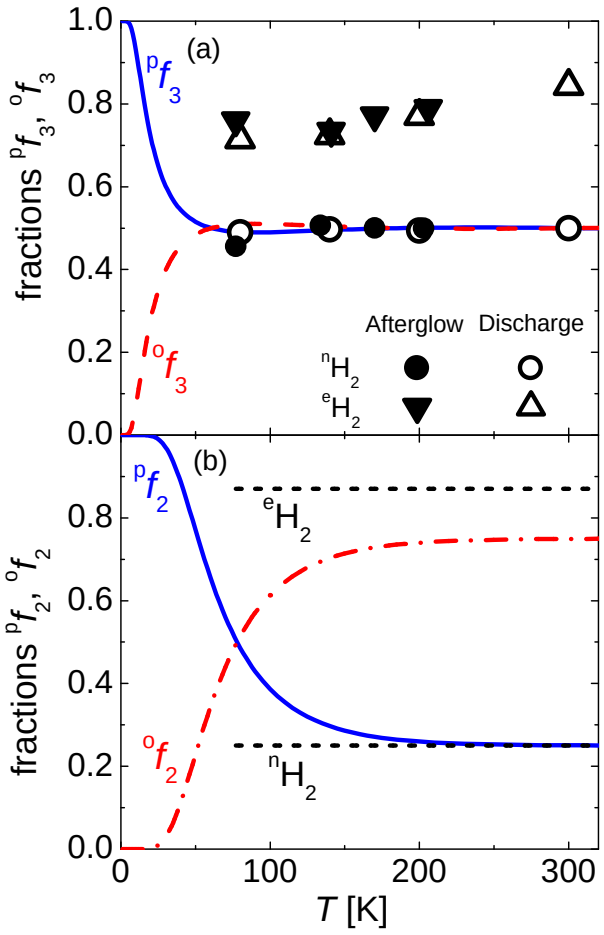

Figure 19: Panel (a): Calculated temperature variation of the fractions $^{p}f_3$ and $^{o}f_3$ in thermal equilibrium, compared to measured values of $^{p}f_3$ during the discharge phase (open triangles) and during the afterglow (closed circles and triangles) in experiments with either $^{n}H_2$ or $^{e}H_2$. Panel (b): Calculated thermal-equilibrium fractions $^{p}f_2$ and $^{o}f_2$. The dashed horizontal lines indicate the values of $^{p}f_2$ in experiments with either $^{n}H_2$ or $^{e}H_2$ (measured by NMR). Adapted from Dohnal et al. (2012b), see Article IV.

5 RESULTS

The following section will cover all the results of my doctoral study work. Their majority was already published and the publications are found in the attachment of this work.

5.1 Ar^+ RECOMBINATION

When measuring at room temperature, one does not have to take neutral assisted ternary recombination (N-CRR) nor electron assisted ternary recombination (E-CRR) into account due to their inverse and rather steep temperature dependence (see Sec. 2.3). Impact of those processes on the effective recombination rate coefficient of Ar^+ ions measured at conditions typical for most of the afterglow experiments is too small to be measured. However when reaching lower temperatures, they have to be considered.

After constructing the Cryo-FALP II apparatus, which can measure recombination rate coefficients at temperatures down to 50 K, we decided to study recombination of Ar^+ ion end effects of the aforementioned ternary recombination processes on its recombination. There were several reason for choosing this ion. Firstly, the processes leading to its formation in helium buffered afterglow plasma are well known. The second reason was that we could follow the study by Kotrík et al. (2011a) who studied E-CRR of Ar^+ ions at temperatures down to 77 K using Cryo-FALP I apparatus. And the last reason is that radiative recombination of $Ar^+$is negligible (see Eq. 1), so only the ternary processes exhibit.

5.1.1 *Ar^+ Formation in Plasma*

Discharge is ignited in the helium buffer gas flowing through a glass discharge tube of Cryo-FALP II apparatus, as displayed in Fig. 11. Argon reactant gas is added downstream via port P1 in order to form Ar^+ dominated plasma. This is achieved by Penning ionization of metastable helium atoms by Ar (reaction 6) and by reactions 5 and 7 in Tab. 7. Depending on the actual experimental conditions (temperature, buffer gas pressure, electron number density), N-CRR and/or

Table 7: List of the reactions taking place in a He/Ar plasma. Values of reaction rate coefficients are given for 80 K if the temperature dependence is known.

№	REACTION	α [$cm^{-3}s^{-1}$]; [$cm^{-6}s^{-1}$]	SOURCE
	He^+ dominated plasma formation		
1	$He^+ + He + He \rightarrow He_2^+ + He$	$1 \cdot 10^{-31}$	Ikezoe et al. (1987)
2	$He^m + He^m \rightarrow He_2^+ + e^-$	$5 \cdot 10^{-9}$	Urbain (1999)
3	$He^m + He^m \rightarrow He^+ + He + e^-$	$1.5 \cdot 10^{-9}$	Deloche et al. (1976)
4	$He_2^+ + e^- \rightarrow 2He$	$< 3 \cdot 10^{-10}$	Deloche et al. (1976)
	Ar^+ formation and destruction		
5	$He^+ + Ar \rightarrow Ar^+ + He$	$1 \cdot 10^{-13}$	Johnsen et al. (1973)
6	$He^m + Ar \rightarrow Ar^+ + He + e^-$	$7 \cdot 10^{-11}$	Yencha (1984)
7	$He_2^+ + Ar \rightarrow Ar^+ + 2He$	$2 \cdot 10^{-10}$	Ikezoe et al. (1987)
8	$Ar^+ + e^- + e^- \rightarrow Ar + e^-$	$1.1 \cdot 10^{-17}$	Stevefelt et al. (1975)
9	$Ar^+ + e^- + He \rightarrow Ar + He$	$2.7 \cdot 10^{-26}$	Bates and Khare (1965)
	Ar_n^+ formation and destruction		
10	$Ar^+ + Ar + He \rightarrow Ar_2^+ + He$	$1.3 \cdot 10^{-31}$	Smirnov (1977)
11	$Ar_2^+ + e^- \rightarrow 2Ar$	$8 \cdot 10^{-7}$	Okada and Sugawara (1993)
12	$Ar_2^+ + Ar + Ar \rightarrow Ar_3^+ + Ar$	$3.2 \cdot 10^{-30}$	Hiraoka and Mori (1989)
13	$Ar_2^+ + Ar + He \rightarrow Ar_3^+ + He$	$5.5 \cdot 10^{-31}$	Smirnov (1977)
14	$Ar_3^+ + e^- \rightarrow 3Ar$	$3.6 \cdot 10^{-6}$	estimate
15	$Ar_3^+ + Ar + He \rightarrow Ar_4^+ + He$	$5.5 \cdot 10^{-31}$	estimate
16	$Ar_4^+ + e^- \rightarrow 4Ar$	$3.6 \cdot 10^{-6}$	estimate

E-CRR process then takes place. It has to be noted, that at low temperatures the formation of fast recombining Ar_2^+ ions should be included in the data analysis (reactions nos. 10 and 12 in Tab. 7).

To set suitable experimental conditions, a chemical kinetics calculations using set of reactions listed in Tab. 7 was performed prior to the experiment (for additional details of the model see Korolov (2008) and Kotrík (2013)). To determine the influence of Ar_2^+ ions in the experiment we measured dependence of α_{eff} on Ar number density. Such dependencies measured at the temperature of 62 K are plotted in Fig. 20. As can be clearly seen, the measured α_{eff} is constant at $[Ar] < 10^{13}\,cm^{-3}$ and increases above this number density due to formation of Ar_2^+. Hence the typical [Ar] used in the study were $\sim 3 \times 10^{12}\,cm^{-3}$ which is sufficient to form Ar^+ dominated plasma prior entering cold section C of the flow tube (see Fig. 11). For additional comments about the nature of saturated values at $[Ar] > 10^{14}\,cm^{-3}$ please refer to Dohnal (2013).

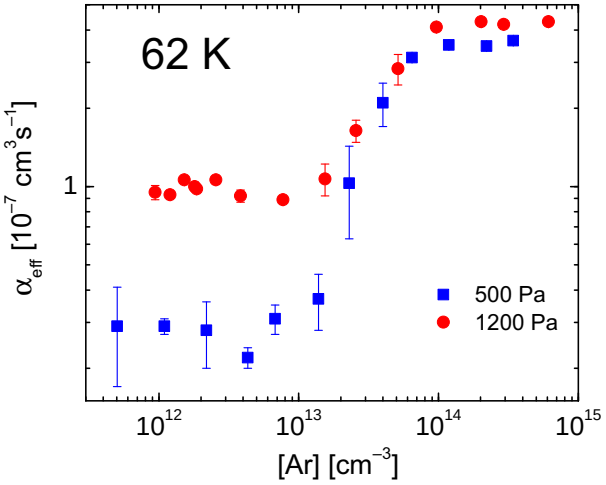

Figure 20: The dependence of measured effective binary recombination rate coefficient α_{eff} on Ar number density at 62 K and indicated pressures of He (full circles for the pressure of 1200 Pa and full squares for 500 Pa). Adapted from Dohnal et al. (2013).

5.1.2 *Data Analysis and Results*

We can write the following balance equation for Ar^+ dominated, quasineutral helium buffered afterglow plasma:

$$\frac{dn_e}{dt} = \frac{d[Ar^+]}{dt} = -K_{He\text{-}CRR}[He][Ar^+]n_e - K_{E\text{-}CRR}[Ar^+]n_e^2 - \frac{n_e}{\tau_L}, \quad (63)$$

where τ_L represent the linear losses as defined in Sec. 4.2.4. The effective recombination rate coefficient α_{eff} can be introduced as

$$\alpha_{eff} = K_{He\text{-}CRR}[He] + K_{E\text{-}CRR}n_e, \quad (64)$$

and Eq. (63) can be rewritten:

$$\frac{dn_e}{dt} = \frac{d[Ar^+]}{dt} = -\alpha_{eff}[Ar^+]n_e - \frac{n_e}{\tau_L}. \quad (65)$$

Linear addition of both N-CRR and E-CRR contributions in Eq. (64) might not be necessarily correct. According to Bates (1974), both processes can partly compete for the populations of the same energy levels. Hence Eq. (64) can be seen as a linear approximation valid if small fraction of the intermediate states is stabilized in collisions with neutrals or electrons.

In Fig. 21 the dependence of α_{eff} on He number density measured at indicated temperatures of 62, 72, and 100 K is shown. The initial

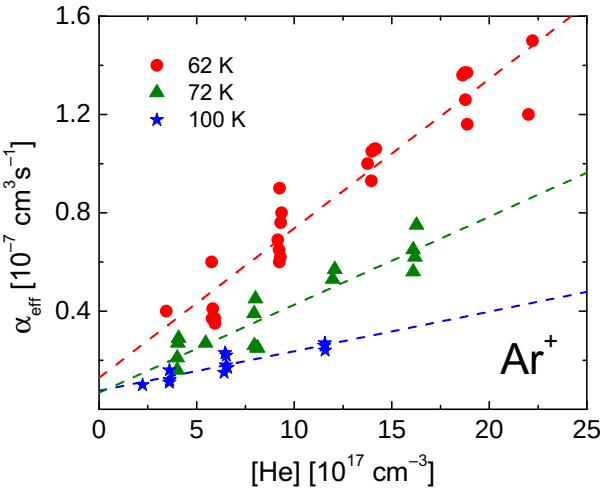

Figure 21: Measured dependence of the effective binary recombination rate coefficient $\alpha_{eff}(T, [He], n_e)$ of Ar^+ recombination with electrons on He number density at 62, 72, and 100 K. The lines represent the linear fits to the data.

n_e was in the range of $4 \times 10^{-8}\,cm^{-3} - 1.5 \times 10^{-9}\,cm^{-3}$. Linear dependence of α_{eff} on [He] is obvious and the ternary recombination rate coefficient $K_{He\text{-}CRR}$ can be obtained from the slope of such dependencies. Temperature dependence of $K_{He\text{-}CRR}$ is plotted in Fig. 22 together with data obtained by Berlande et al. (1970), Cao and Johnsen (1991), Deloche et al. (1976), and van Sonsbeek et al. (1992) and theoretical dependencies calculated according to Bates and Khare (1965) and Pitaevskii (1962).

Linear fits of α_{eff} vs. [He] plotted in Fig. 21 extrapolated to zero He number density give nonzero values caused by contribution of E-CRR. After dividing the extrapolated intercept by a mean electron number density in a specific measurement, we get a $K_{E\text{-}CRR}$ estimation displayed in Fig. 23. Although this method of obtaining $K_{E\text{-}CRR}$ can be seen as an approximation of the actual values, it agrees very well with the theoretical prediction of Stevefelt et al. (1975) and also with the previous results obtained in our group at higher $n_e \sim 3 \times 10^9\,cm^{-3}$ (Kotrík et al., 2011a; Kotrík et al., 2011b) where $K_{E\text{-}CRR}$ is obtained directly from the electron number density decays using Eq. (59). For more details see also Kotrík (2013).

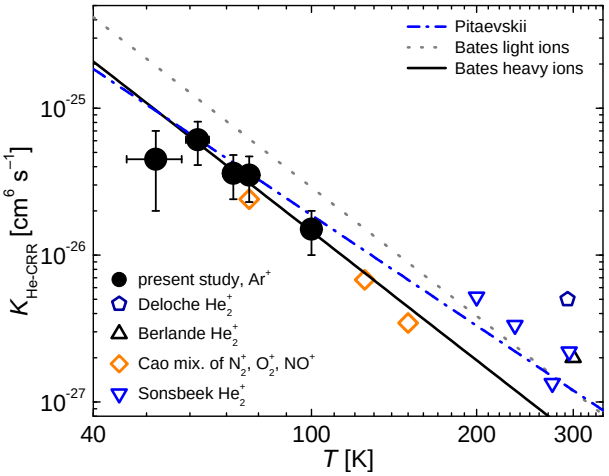

Figure 22: Temperature dependence of the measured ternary recombination rate coefficient $K_{He\text{-}CRR}$ of He assisted recombination of Ar^+ ions with electrons represented by full circles. Included are also data from previous experiments (Berlande et al., 1970; Cao and Johnsen, 1991; Deloche et al., 1976; van Sonsbeek et al., 1992). The dotted line follows calculation by Bates and Khare (1965), the solid line is scaled for this study using the dependence of the ternary recombination rate coefficient on reduced mass as suggested by Bates and Khare (1965). The dash-dotted line indicates theory of Pitaevskii (1962). Adapted from Dohnal et al. (2013).

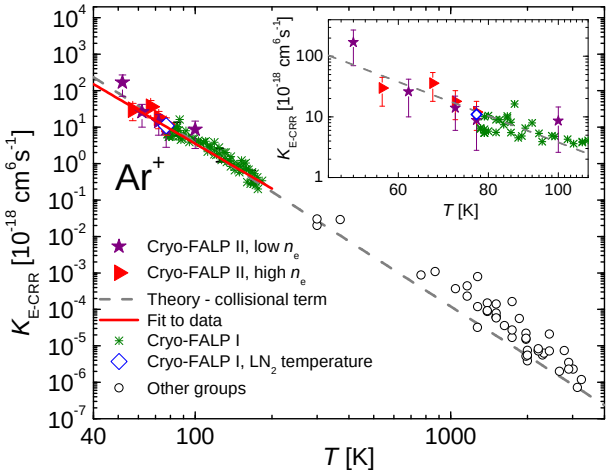

Figure 23: Temperature dependence of the measured ternary recombination rate coefficient $K_{E\text{-}CRR}$ of ternary electron assisted collisional radiative recombination of Ar^+ ion with electrons. The full stars represent data measured at lower n_e ($10^8 - 10^9$ cm^{-3}) using Cryo-FALP II apparatus (Dohnal et al., 2013). The full triangles denote values measured using the same apparatus at higher n_e (Kotrík et al., 2011b). Data depicted by open rhomboid are compiled from several measurements on Cryo-FALP I at 77 K. The crosses represent data measured on Cryo-FALP I at temperatures above 77 K (Kotrík et al., 2011a). The dashed line indicates $K_{E\text{-}CRR}$ calculated using collisional term of Stevefelt's formula (14). The full line is the fit to the Cryo-FALP I and Cryo-FALP II data. The open circles are values obtained by other groups (Mansbach and Keck, 1969; Berlande et al., 1970; Curry, 1970; Skrzypkowski et al., 2004). Adapted from Dohnal (2013).

5.2 H_3^+ AND D_3^+ RECOMBINATION

Dissociative recombination of H_3^+ has been studied in our laboratory since late 1990s and three types of experimental apparatuses were used. The first one was AISA experiment, modification of a clasic SA experiment, as described in Sec. 2.2.1, which used Langmuir probe and a mass spectrometer as a detection technique (Poterya et al., 2002; Plašil et al., 2002; Plašil, 2003). In order to determine internal state of the recombining H_3^+ ions, the Test Discharge Tube – Cavity Ring Down Spectroscopy (TDT-CRDS), today labelled as SA-CRDS, was built and a series of successful studies of both H_3^+ and D_3^+ recombination studies were performed using it (Macko et al., 2004; Varju et al., 2011; Dohnal et al., 2012b; Dohnal et al., 2012a). Several variants of FALP type experiments were used throughout the years, for details refer to Novotný (2006), Korolov (2008), and Kotrík (2013).

A nontrivial dependence of α_{eff} on H_2 number density was revealed in early studies of H_3^+ recombination which can be described by dividing into three regions characterized by its $[H_2]$:

- For $[H_2] < 10^{12}\,\text{cm}^{-3}$ α_{eff} lineary decreases with decreasing $[H_2]$ which explains the low value of α_{eff} given in Glosík et al. (2000). There are several explanations of this phenomenon. Johnsen (2011) suggests that H_3^+ is not the dominant ion and the presence of slowly recombining ArH^+ influences the measured recombination rate coefficient. However the mass spectra obtained during the actual experiment (Plašil et al., 2002) clearly exhibits that H_3^+ was dominant ion in AISA experiment. Another possibility is that at such low $[H_2]$ the number of collisions of H_3^+ ions with H_2 molecules is not sufficient to quench possible vibrational excitation of H_3^+ (Johnsen, 2005) or to maintain stable ortho- to para-H_3^+ ratio (Glosík et al., 2009b).

- For $10^{12}\,\text{cm}^{-3} < [H_2] < 10^{14}\,\text{cm}^{-3}$ the value of α_{eff} does not change with $[H_2]$, creating plateau. This region is called "saturated region" (Glosík et al., 2009b). Dependence of the α_{eff} value in this region on He buffer gas number density is caused by presence of ternary He assisted recombination channel.

- For $[H_2] > 10^{14}\,\text{cm}^{-3}$ α_{eff} increases due to formation of H_5^+ ions. However, this increase is seen also at conditions, where H_5^+ formation should be negligible, e. g. at the temperature of 300 K. The mechanism of this phenomenon assigned to H_2 assisted

ternary recombination of H_3^+, is not yet known. We will discuss this phenomenon in a separate section 5.4.

5.2.1 *H_3^+ and D_3^+ Formation in Plasma*

In Cryo-FALP II experiment, helium buffer gas is partially ionized in a microwave discharge in the upstream part of the flow tube; He^+, He_2^+, and He^m are created subsequently. Argon is added through port P1 (see Fig. 11 in Sec. 4.2.2) further downstream to form Ar^+ dominated plasma. Reaction nos. 1-9 listed in Tab. 7 are involved. Ar^+ dominated plasma is entering section B of the flow tube, which is cooled by LN_2. He buffer gas and subsequently Ar^+ ions are thermalized to the flow tube wall temperature T_W. Reactant gas, in this cas H_2 or D_2, is added through port P3, located in the beginning of cold head cooled section C of the flow tube. Ar^+ ions are converted to H_3^+ (or D_3^+) by a chain of ion-molecule reactions and after a short distance from the reactant entry port thermalized H_3^+ (D_3^+) dominated plasma is created. The reactions involved are listed in Tab. 8. When using SA-CRDS experiment, the discharge is ignited already in a $He/Ar/H_2(D_2)$ mixture.

5.2.2 *Data Analysis*

The effective recombination rate coefficient α_{eff} of H_3^+ dissociative recombination if measured in helium buffered afterglow experiment is dependent on temperature T, number density of both H_2 reactant gas and He buffer gas in the following way (Rubovič et al., 2013):

$$\begin{aligned}\frac{dn_e}{dt} = &-\alpha_{bin}[H_3^+]n_e - \alpha_5 R H_3^+ n_e - K_{He}[He][H_3^+]n_e \\ &- K_{E\text{-}CRR}[H_3^+]n_e^2 - \frac{n_e}{\tau_L},\end{aligned} \tag{66}$$

where α_{bin} is binary recombination rate coefficient of H_3^+ions, α_5 is recombination rate coefficient of H_5^+ ions, R is ratio of the H_5^+ number density to H_3^+ number density ($R = [H_5^+]/[H_3^+]$). Note, that $R \approx K_C[H_2]$ if R is constant in time; K_C is the equilibrium constant. K_{He} is the ternary recombination rate coefficient of He assisted ternary recombination, and $K_{E\text{-}CRR}$ is the ternary recombination rate coefficient of E-CRR. The effective recombination rate coefficient is introduced as

$$\alpha_{eff} = \alpha_{bin} + K_{E\text{-}CRR}n_e + K_{He\text{-}CRR}[He] + \alpha_5 K_C[H_2]\,. \tag{67}$$

To determine contributions of different processes in the measured α_{eff} as in Eq. (67), one has to separate them by measuring dependencies

Table 8: List of the reactions which are included in the chemical kinetics model of H_3^+ (D_3^+) dominated plasma in $He/Ar/H_2(D_3^+)$ mixture. The listed values are for the temperature of 300 K if available.

№	REACTION	α [$cm^{-3}s^{-1}$]; [$cm^{-6}s^{-1}$]	SOURCE
	H_3^+ formation and destruction		
1	$Ar^+ + H_2 \rightarrow ArH^+ + H$	$8 \cdot 10^{-10}$	Dotan and Lindinger (1982)
2	$Ar^+ + H_2 \rightarrow H_2^+ + Ar$	$1 \cdot 10^{-10}$	Dotan and Lindinger (1982)
3	$H_2^+ + Ar \rightarrow ArH^+ + H$	$2.3 \cdot 10^{-9}$	Glosík (1994)
4	$H_2^+ + H_2 \rightarrow H_3^+ + H$	$2.1 \cdot 10^{-9}$	Glosík (1994)
5	$ArH^+ + H_2 \rightarrow H_3^+ + Ar$	$1.5 \cdot 10^{-9}$	Villinger et al. (1982)
6	$H_3^+ + H_2 + He \rightarrow H_5^+ + He$	$< 10^{-29}$	Smirnov (1984)
7	$H_5^+ + He \rightarrow H_3^+ + H_2 + He$	$< \cdot 10^{-13}$	Glosík et al. (2003)
8	$H_3^+ + H_2 + H_2 \rightarrow H_5^+ + H_2$	$4.6 \cdot 10^{-30}$	Johnsen et al. (1976)
9	$H_3^+ + e^- \rightarrow$ products	$\sim 10^{-8} - 10^{-7}$	Rubovič et al. (2013)
10	$H_5^+ + e^- \rightarrow$ products	$2.5 \cdot 10^{-6}$	Glosík et al. (2003)
	D_3^+ formation and destruction		
11	$Ar^+ + D_2 \rightarrow ArD^+ + D$	$7.5 \cdot 10^{-10}$	Anicich (1993)
12	$Ar^+ + D_2 \rightarrow D_2^+ + Ar$	$7.5 \cdot 10^{-10}$	Anicich (1993)
13	$D_2^+ + Ar \rightarrow ArD^+ + D$	$1.5 \cdot 10^{-9}$	Clow and Futrell (1970)
14	$D_2^+ + D_2 \rightarrow D_3^+ + D$	$1.6 \cdot 10^{-9}$	Bowers et al. (1969)
15	$ArD^+ + D_2 \rightarrow D_3^+ + Ar$	$6 \cdot 10^{-10}$	Villinger et al. (1982)
16	$D_3^+ + D_2 + He \rightarrow D_5^+ + He$	$< 10^{-29}$	Novotný et al. (2006)
17	$D_5^+ + He \rightarrow D_3^+ + D_2 + He$	$< \cdot 10^{-13}$	Novotný et al. (2006)
18	$D_3^+ + D_2 + D_2 \rightarrow D_5^+ + D_2$	$6 \cdot 10^{-30}$	estimation
19	$D_3^+ + e^- \rightarrow$ products	$\sim 10^{-8} - 10^{-7}$	Rubovič et al. (2013)
20	$D_5^+ + e^- \rightarrow$ products	$3 \cdot 10^{-6}$	Novotný et al. (2006)

of α_{eff} on [He] and [H_2] at each temperature. α_{bin} is then equal to the limit of α_{eff} for the zero number densities of He and H_2. Dependency of α_{eff} on [H_2] can be seen in Fig. 24 for 90 K and 70 K. H_2 num-

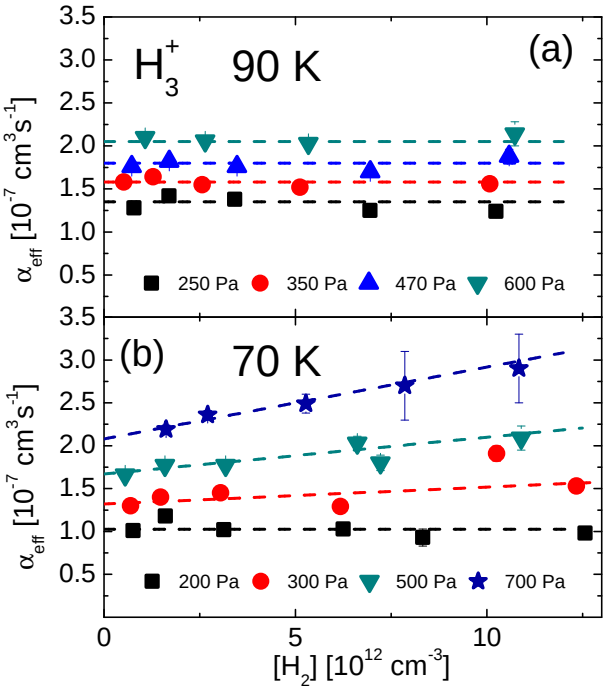

Figure 24: The measured dependencies of the effective recombination rate coefficient of the H_3^+ ions with electrons on H_2 number density as measured in Cryo-FALP II experiment at 90 K (**panel (a)**) and 70 K (**panel (b)**). The dashed lines represent linear fits to the data. Adapted from Rubovič et al. (2013).

ber densities has to be kept above $5 \times 10^{11}\,\mathrm{cm}^{-3}$ in order to form H_3^+ dominated plasma in adequate timeframe and also to maintain the constant ortho- to para-H_3^+ ratio. The dependencies of α_{eff} on He number density obtained in saturated region are plotted in Fig. 25.

Please note, that ternary recombination of H_3^+ assisted by H_2 is not taken in to the account in the actual data analysis and it does not affect obtained data. It will be discussed in Sec. 5.4 of this work.

5.2.3 *Experimental Results*

Experimental results were obtained in both SA-CRDS and Cryo-FALP II experiments. The infrared transitions used for probing the number densities of specific states for H_3^+ ion are listed in Tab. 1, lines monitored in studies using D_3^+ are listed in Tab. 3. H_3^+ ions with thermal

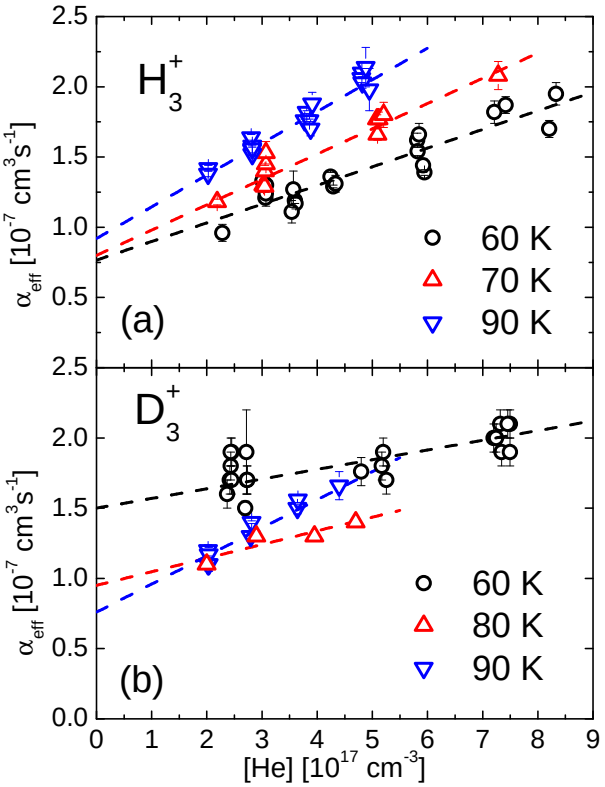

Figure 25: The dependence of the effective recombination rate coefficient measured in Cryo-FALP II experiment on He number density as measured for H_3^+ ion at 60, 70, and 90 K (**panel (a)**) and for D_3^+ ion at 60, 80, and 90 K (**panel (b)**). The dashed lines are linear fits to the data; the displayed errors are statistical errors. Adapted from Rubovič et al. (2013).

distribution of states were used in these measurements. For experiments with para enriched H_2 reactant gas, see Sec. 5.3.

In the previous FALP experiment, only the temperatures of 77 K and 300 K could be kept and intermediate temperatures were achieved during slow heating from the lowest temperature. The evaluation of data in these experiment is discussed in Glosík et al. (2009b). In contrast to them we could measure at any temperature in the range $50-300$ K using Cryo-FALP II apparatus which brought a possibility to obtain more precise results.

Ternary rate coefficient K_{He} was obtained from the dependence of α_{eff} on He number density, as plotted in Fig. 25, see Rubovič et al. (2013) and Johnsen et al. (2013). The results from this experiment, but also from Cryo-FALP and SA-CRDS are plotted in Fig. 26. Values of K_{He} for Ar^+ dominated plasma (see Sec. 5.1 and Dohnal et al. (2013))

and for a mixture of atmospheric ions (Cao and Johnsen, 1991) are plotted for comparison. The dashed line representing the scaled theory of Bates and Khare (1965) agrees with these values. However, values of K_{He} for H_3^+ ion at 250 K are greater by more than 2 orders of magnitude than those predicted by N-CRR theory (Bates and Khare, 1965). As the temperature decreases, measured K_{He} is, with maximum at ~ 200 K, closer to the theoretical prediction (Bates and Khare, 1965) and at 55 K agreement with the theory is achieved.

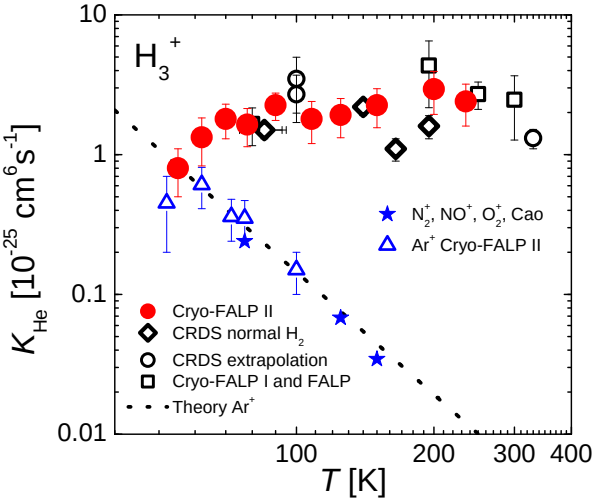

Figure 26: The temperature dependence of the ternary recombination rate coefficient K_{He} of H_3^+ ions using normal H_2 as obtained in Cryo-FALP II (full circles) (Johnsen et al., 2013), SA-CRDS (open rhomboids) (Varju et al., 2011; Dohnal et al., 2012b) and FALP experiments (open circles) (Glosík et al., 2009b). The open squares denote extrapolation of combined FALP and SA-CRDS data (see discussion in Glosík et al. (2009b)). The open triangles are values of $K_{He\text{-}CRR}$ obtained for Ar^+ ions in ambient helium gas (see Sec. 5.1). The full stars are values of Cao and Johnsen (1991) obtained in helium buffer gas with mixture of atmospheric ions. The dashed line is scaled theory of Bates and Khare (1965). Adapted from Johnsen et al. (2013).

In Fig. 27, values of K_{He} for D_3^+ ion measured in FALP, Cryo-FALP, Cryo-FALP II, and SA-CRDS experiments are plotted. Values for Ar^+ ion (Dohnal et al., 2013) and mixture of atmospheric ions (Cao and Johnsen, 1991) are included. The results are similar to those measured in H_3^+ dominated plasma, however, the value of K_{He} decreases faster at lower temperatures. It shows maximum at ~ 160 K and minimum at 70 K. K_{He} is similar as K_{He} for Ar^+ ions at lower temperatures. When scaling the theory of Bates and Khare (1965) by reciprocal reduced mass, value for atomic ions of mass 6 is higher by factor ~ 1.7 than for Ar^+ ions.

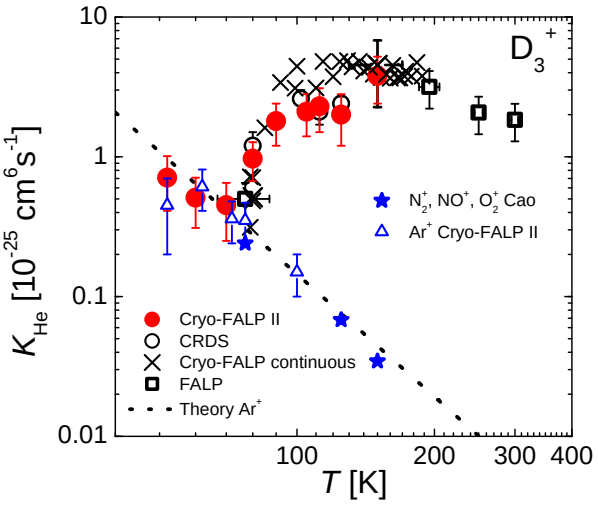

Figure 27: The temperature dependence of the ternary recombination rate coefficient K_{He} of D_3^+ ions. The full circles represent values obtained in Cryo-FALP II experiment (Johnsen et al., 2013), the open squares denote values measured in SA-CRDS experiment (Dohnal et al., 2012a), open circles are values measured in FALP and Cryo-FALP experiments (see discussion in Kotrík et al. (2010)). The crosses were obtained in Cryo-FALP experiment during warm up phase of the flow tube. The stars, triangles and the dashed line are the same as in Fig. 26. Adapted from Johnsen et al. (2013).

The evaluation of the binary recombination rate coefficient α_{bin} at temperatures below 70 K is complicated by the formation of fast recombining H_5^+ (D_5^+) ions. Thus special care has to be taken and dependencies of α_{eff} on H_2 (D_2) number density at each temperature and buffer gas pressure (i. e. He number density) has to be measured. Linear extrapolation of such dependence is made and from the dependence of the intercepts on He number density the actual values of α_{bin} and K_{He} are then taken. For more details see Rubovič et al. (2013).

Summarized values of α_{bin} for H_3^+ ion obtained in previous FALP experiments (represented by open circles), Cryo-FALP II (full circles), and SA-CRDS (full rhomboids) are shown in Fig. 28. The temperature dependence obtained in CRYRING ISR experiment is plotted by double dot-dashed line (McCall et al., 2004). Both dotted lines labelled as CRR_1 and CRR_2 reprepresent contribution of $\alpha_{E\text{-}CRR}$ calculated using Eq. (13) for the electron number densities of 1×10^9 cm^{-3} and 5×10^{10} cm^{-3}, former being adequate for Cryo-FALP II, the latter for SA-CRDS experiment. The dashed and the dot-dashed lines represent theoretical val-

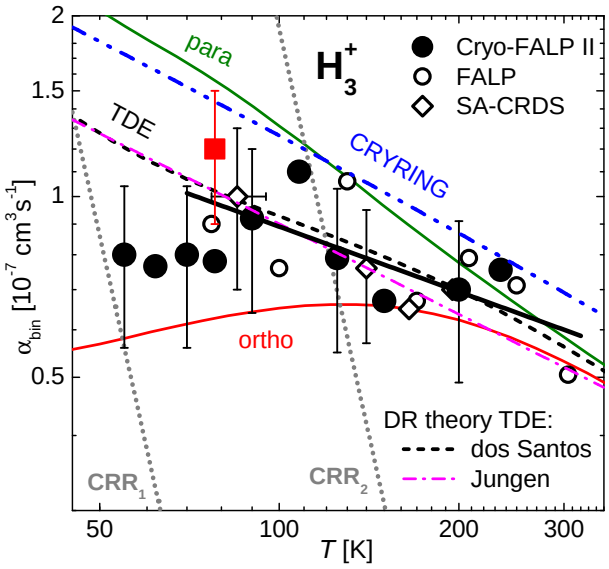

Figure 28: The temperature dependence of the binary recombination rate coefficient α_{bin} of H_3^+ ions. All displayed values were obtained in experiments with normal H_2 with the exception of full square at 80 K that was obtained in para enriched H_2. The full circles denote the values measured in Cryo-FALP II experiment (Rubovič et al., 2013). The values denoted by open circles were obtained in Cryo-FALP for the temperatures of 80 K, 100 K, and 300 K and in previous FALP experiments (see compilation in Glosík et al. (2009b)). The open rhomboids indicate values obtained in SA-CRDS experiment (Varju et al., 2011; Dohnal et al., 2012c; Dohnal et al., 2012b). The double dot-dashed line denotes values obtained in ISR experiment CRYRING (McCall et al., 2004). The dashed line and the dot-dashed line are theoretical calculations by Fonseca dos Santos et al. (2007) and Pratt and Jungen (2011), respectively. Dotted lines labeled CRR_1 and CRR_2 represent $\alpha_{E\text{-}CRR}$ relevant for the experimental conditions calculated using Eq. (13). The full line is the fit to the SA-CRDS, FALP, Cryo-FALP, and Cryo-FALP II data in the temperature range of $80 - 300$ K. Adapted from Rubovič et al. (2013).

ues of DR rate coefficient as calculated by Fonseca dos Santos et al. (2007) and Pratt and Jungen (2011), respectively.

The value of α_{bin} in Fig. 28 at 100 K denoted by open circle was obtained by fitting several experimental points from Cryo-FALP and SA-CRDS experiment, for details see Glosík et al. (2009b). The other datapoints were obtained from the α_{eff} pressure dependencies as displayed in Fig. 25.

The values of α_{bin} in the temperature range of $80 - 300$ K can be fitted as $\alpha_{bin} = (6.0 \pm 1.8) \times 10^{-8} (300/T)^{0.36 \pm 0.09}\,cm^3 s^{-1}$, which is

shown by full line in Fig. 28. As can be seen, this dependence agrees well with the theoretical predictions.

However, the values of α_{bin} begin to decrease and to deviate from the theoretical predictions below 100 K. Possible explanation of the deviation can be found in Rubovič et al. (2013). It might be caused by nonequilibrium population of ortho- and para-H_3^+ states as precursor gas to form H_3^+ dominated plasma in the experiment was hydrogen with populations of states according to TE at 300 K. Our results from experiment with para-enriched hydrogen (see Sec. 5.3) show that α_{bin} at 77 K is several times higher for para H_3^+ than for ortho-H_3^+. Distribution of H_3^+ states at 60 K according to TE is 1 : 1 for ortho-H_3^+ and para-H_3^+. If the ortho spin states were favoured at temperatures below 80 K, the resulting α_{bin} would be lower than with equilibrium popoulation of nuclear spin states. Unfortunately, we cannot distinguish specific nuclear spin states in Cryo-FALP II experiment and the working temperature of SA-CRDS experiment is limited by the temperature of LN_2.

The ratio of para-H_3^+ to ortho-H_3^+ at 80 K as measured in SA-CRDS is $(45 \pm 2)\%$. To observe the influence of various distributinos of H_3^+ nuclear spin states populations on α_{eff} in Cryo-FALP II experiment, we used para enriched H_2 as a precursor gas to form H_3^+ dominated plasma at otherwise identical experimental conditions as with normal H_2. It led to the increase of α_{bin} from $(0.8 \pm 0.3) \times 10^{-7}\,cm^3s^{-1}$ with normal H_2 to $(1.2 \pm 0.3) \times 10^{-7}\,cm^3s^{-1}$ with para enriched H_2 at 80 K. This value is represented as the full square in Fig. 28.

As the theory of E-CRR (see Sec. 2.3.2) is valid for atomic ions and our results for Ar^+ ions discussed in Sec. 5.1 show agreement with the theory of Stevefelt et al. (1975), value of $K_{E\text{-}CRR}$ for molecular H_3^+ ion is of particular interest. The values of α_{bin} obtained in both Cryo-FALP II and SA-CRDS are congruent within their errors. However, values from SA-CRDS experiment are systematically higher by $\sim$ 10% than those from Cryo-FALP II experiment. Contribution of E-CRR to measured α_{eff} in SA-CRDS experiment (for $n_e = 5 \times 10^{10}\,cm^{-3}$) should be, according to Eq. (13), $\alpha_{E\text{-}CRR} = 5 \times 10^{-7}\,cm^3s^{-1}$. This value is, surprisingly, higher, than overall recombination coefficient obtained in the experiments. This phenomenon is discussed widely in Dohnal et al. (2012b). There are two possible reasons. The first one is that the $K_{E\text{-}CRR}$ for H_3^+ ions is lower by the order of magnitude than predicted by Stevefelt et al. (1975). The other one is that the electron temperature T_e in the experiment was higher by $\sim$ 100 K than the buffer gas temperature T_G. However, our analysis of T_e for Ar^+ ions discussed in Sec.

4.2.7, as well as the agreement between theory and measured values of $K_{He\text{-}CRR}$ and $K_{E\text{-}CRR}$ for Ar^+ ions (see Sec. 5.1), suggests that both of the temperatures are equal.

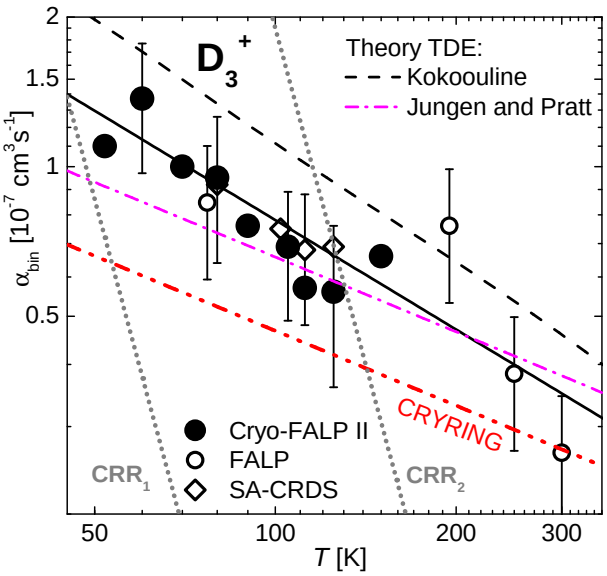

Figure 29: The temperature dependence of the binary recombination rate coefficient of D_3^+ ions measured in Cryo-FALP II (full circles) (Rubovič et al., 2013), SA-CRDS (open rhomboids) (Dohnal et al., 2012a), and FALP/Cryo-FALP experiments (open circles) (Kotrík et al., 2010). The values obtained in ISR experiment CRYRING is denoted by double dot-dashed line (Le Padellec et al., 1998) are plotted for comparison. The dashed line and the dot-dashed line represent the theoretical calculations by Kokoouline (Pagani et al., 2009) and by Pratt and Jungen (2011), respectively. The full straight line is the fit to the Cryo-FALP II, FALP, Cryo-FALP, and SA-CRDS data. Dotted lines labeled CRR_1 and CRR_2 represent $\alpha_{E\text{-}CRR}$ relevant for the experimental conditions calculated using Eq. (13). Adapted from Rubovič et al. (2013).

Values of α_{bin} for D_3^+ ion were obtained in a similar way as for H_3^+ ion in both Cryo-FALP II and SA-CRDS experiments. D_3^+ dominated plasma was created using D_2 reactant gas as a precursor and processes listed in the second part of Tab. 8 were involved. The temperature dependence of the binary recombination rate coefficient α_{bin} for D_3^+ ion as measured in older FALP experiments (open circles), Cryo-FALP II (full circles), and SA-CRDS (open rhomboids) is plotted in Fig. 29. Values obtained in CRYRING (Le Padellec et al., 1998) are represented by double dot-dashed line. Kokoouline's theoretical calculations (Pagani et al., 2009) is plotted by dashed line and the calculation by Pratt and Jungen (2011) is plotted by dot-dashed line. The full line is the

fit to the α_{bin} data giving the following dependence: $\alpha_{bin} = (3.5 \pm 1.1) \times 10^{-8}(300/T)^{0.73\pm0.09}\,cm^3s^{-1}$. Our results are in a good agreement with those obtained in CRYRING experiment, and they also agree well with the theoretical predicitons. The values measured in SA-CRDS experiment were measured at an order of magnitude higher n_e than values obtained in Cryo-FALP II experiment; both of them are identical within their experimental errors. It indicates a negligible contribution of E-CRR to the measured α_{eff}, as was the case for H_3^+ ion.

Predicted recombination rate coefficient for ortho, meta, and para nuclear spin states of D_3^+ are similar wihtin the studied temperature range (Pagani et al., 2009), hence the deviation from the theoretical dependence as seen for H_3^+ ion is not expected. For additional details see Rubovič et al. (2013).

5.3 STATE SELECTIVE H_3^+ RECOMBINATION

We mentioned in Sec. 3.3 already that the theory of Fonseca dos Santos et al. (2007) predicts a large difference between recombination of ortho- and para-H_3^+ nuclear spin state configurations at low temperatures, where para-H_3^+ should recombine faster.

In order to obtain the recombination rate coefficient for specific nuclear spin configuration of H_3^+ we used para enriched hydrogen reactant gas ($^eH_2$) produced by para enriched hydrogen generator (described in Sec. 4.3) in addition to normal hydrogen ($^nH_2$). The experiments with both reactant gases were conducted at otherwise similar experimental conditions in SA-CRDS experiment.

We can put a set of two linear equations based on the following idea together. If we measure the effective recombination rate coefficient α_{eff} for two different populations of ortho- and para-H_3^+, resulting α_{eff} will change in accordance with them:

$$^n\alpha_{eff} = {}^o\alpha_{eff} \cdot {}^{n,o}f_3 + {}^p\alpha_{eff} \cdot {}^{n,p}f_3\,, \tag{68}$$

$$^e\alpha_{eff} = {}^o\alpha_{eff} \cdot {}^{e,o}f_3 + {}^p\alpha_{eff} \cdot {}^{e,p}f_3\,, \tag{69}$$

where f_3 denotes fraction of H_3^+ ions in ortho (superscript "o") and para (superscript "p") spin state configuration for experiments with $^nH_2$ (superscript "n") and with $^eH_2$ (superscript "e"). The identity $^{n,o}f_3 + {}^{n,p}f_3 = {}^{e,o}f_3 + {}^{e,p}f_3 = 1$ is, of course, valid. The values of $^n\alpha_{eff}$ and $^e\alpha_{eff}$ obtained in SA-CRDS experiment at the temperature of (170 ± 10) K are plotted in panel (a) of Fig. 30. The values of both $^p\alpha_{eff}$ and $^o\alpha_{eff}$ inferred from $^n\alpha_{eff}$ and $^e\alpha_{eff}$ using Eqs. (68) and (69) are

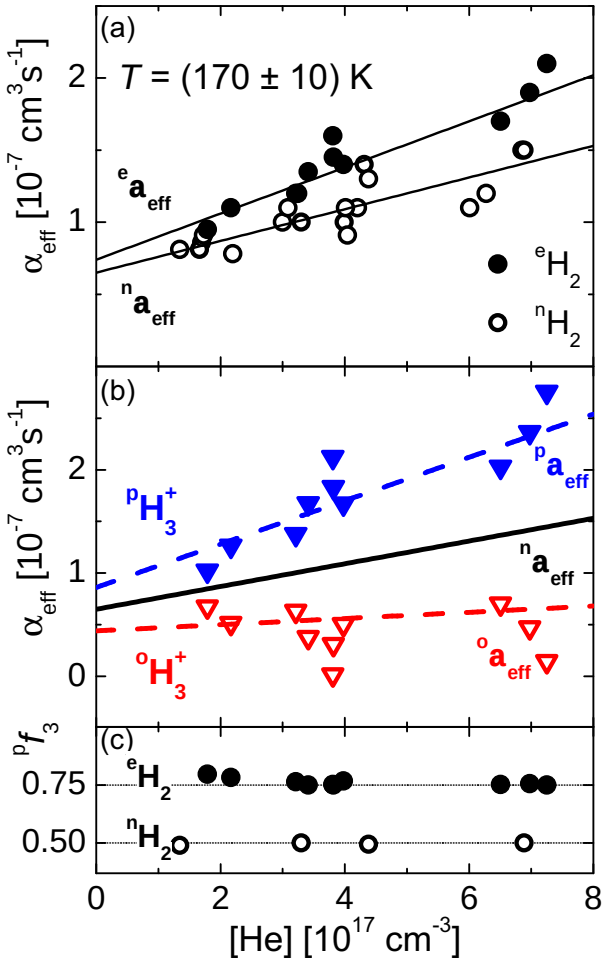

Figure 30: The dependence of measured effective recombination rate coefficients on helium number density at 170 K. **Panel (a):** The effective recombination rate coefficients measured using normal H_2 (open circles) and para enriched H_2 (full circles). The full lines are linear fits to the data. **Panel (b):** The values of $^{p}\alpha_{eff}$ and $^{o}\alpha_{eff}$ for pure para-H_3^+ and pure ortho-H_3^+ obtained from the values in panel (a) and panel (c). The dashed lines are linear fits to the data. The full line represents the linear fit to the values of $^{n}\alpha_{eff}$ displayed in panel (a). **Panel (c):** The fractions $^{n,p}f_3$ and $^{o,p}f_3$ of para-H_3^+ measured in the experiments with $^{n}H_2$ (open circles) and $^{e}H_2$ (full circles). Adapted from Dohnal et al. (2012b).

shown in panel (b); corresponding values of ${}^{n,p}f_3$ and ${}^{e,p}f_3$ are plotted in panel (c) of Fig. 30.

As was already mentioned in previous sections, α_{eff} is function of He number density and it applies also for ${}^{p}\alpha_{eff}$ and ${}^{o}\alpha_{eff}$:

$${}^{o}\alpha_{eff}(T,[He]) = {}^{o}\alpha_{bin}(T) + {}^{o}K_{He}(T)[He]\,, \tag{70}$$

$${}^{p}\alpha_{eff}(T,[He]) = {}^{p}\alpha_{bin}(T) + {}^{p}K_{He}(T)[He]\,, \tag{71}$$

with corresponding binary and helium assisted ternary recombination rate coefficients. They can be obtained from the linear fit to the ${}^{p}\alpha_{eff}$ and ${}^{e}\alpha_{eff}$ as shown by dashed lines in panel (b) of Fig. 30. Such dependencies were obtained also for temperatures of 80 K, 140 K, and 200 K using SA-CRDS and for 80 K also on Cryo-FALP II, see Glosík et al. (2014).

5.3.1 *Data Analysis*

Several assumptions have to be fulfilled in order to justify the evaluation of the acquired data:

- H_3^+ states are populated in accordance with TE in experiments with ${}^{n}H_2$.
- When using ${}^{e}H_2$, the states wihtin ortho and para manifold are populated according to TE even if the actual para to ortho ratio is nonthermal.
- Relative population of states remains stable during the afterglow.
- Plasma is thermalized, i. e. the kinetic and rotational temperature of H_3^+ ions (T_{Kin} and T_{Rot}), as well as the electons temperature T_e are equal to the buffer gas temperature T_G.
- H_3^+ is dominant ion in the afterglow.
- The shape of absorption lines is given by Doppler broadening.

The number density of the H_3^+ ion in specific rotational state can be calculated from measured absorption in SA-CRDS experiment, see description in Sec. 4.1.3. For evaluation of recombination rate coefficients, one needs to know the electron number density too. If H_3^+ is dominant ion in the afterglow, i. e. $n_e = [H_3^+]$, we can calculate α_{eff} from the decay of the overall number density of the ions. Under assumption of TE,

the overall number density of H_3^+ ion can be obtained from the absorption of single transition using Eqs. (29) and (30). So the number density of all para-H_3^+ states are determined from the measured population of para $(1,1)$ state and the number density of all ortho-H_3^+ states is computed from the population of ortho $(1,0)$ state. If ortho $(3,3)$ state is monitored, sum of both $(1,0)$ and $(3,3)$ states can be used.

The electron number density n_e was calculated as a sum of the overall ortho- and para-H_3^+ number densities measured at otherwise same experimental conditions. Such analysis was used in experiments with para enriched H_2. In the majority of experiments with normal H_2 the electron number density was determined from the population of ortho $(1,0)$ state. However, when the aforementioned analysis involving ortho $(1,0)$, ortho $(3,3)$, and para $(1,1)$ states was done, resulting α_{eff} was identical to the one determined from ortho $(1,0)$ state within its experimental error.

The measured time evolution of the number densities of ortho $(1,0)$, ortho $(3,3)$, and para $(1,1)$ H_3^+ states in early afterglow in experiment with para enriched H_2 is shown in panel (a) of Fig. 31. As can be seen in panel (c) of the figure, the relative populations of the states are constant during the decay and the ${}^{p}f_3$ fraction of all para-H_3^+ ions is constant too, see panel (c).

The relative populations of the measured ortho- and para-H_3^+ states measured during the discharge and in early afterglow using ${}^{n}H_2$ at the temperature range of $77-200$ K are shown in panel (a) of Fig. 32. The relative populations of the states were calculated by dividing measured absolute ion number densities in given state by the overall number density of H_3^+ ions under assumption of TE. They are in good agreement with calculated thermal populations of corresponding states (full lines in Fig. 32). The rotational temperature $T_{Rot\text{-}ortho}$ obtained from populations of both measured ortho H_3^+ states in the temperature range of $77-200$ K is plotted in panel (b) of Fig. 32. It was measured in the discharge and early afterglow periods in experiments with both ${}^{n}H_2$ and ${}^{e}H_2$. Kinetic temperature $T_{Kin}$was measured from Doppler broadening of the absorption lines, see Eq. (34). We also monitored temperature of the discharge tube wall tw using thermocouple and the obtained values were in the ± 10 K range when comparing to T_{Kin}.

As can be seen in Fig. 32, measured rotational temperature agree well with measured kinetic temperature of the ions even in experiment with para enriched H_2, where population of states is non-thermal, see Fig. 19. This finding indicate that assumption of the equilibrium

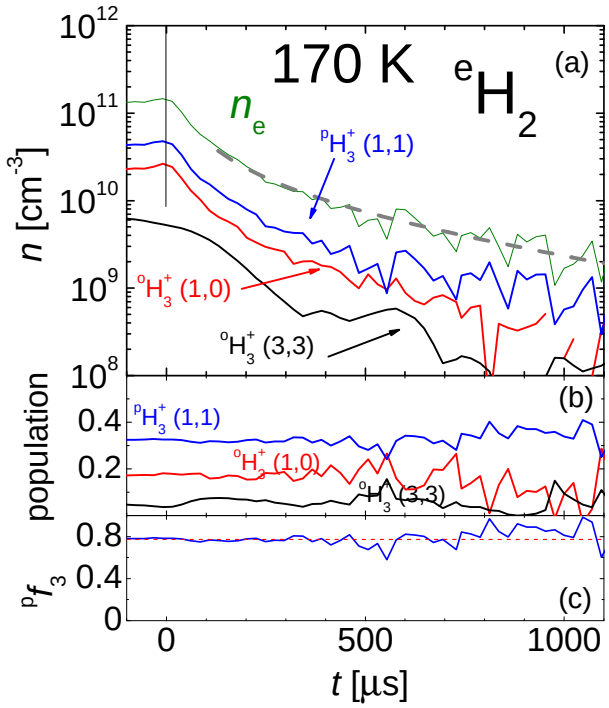

Figure 31: **Panel (a):** An example of decay curves of the H_3^+ ion number densities in para $(1,1)$, ortho $(1,0)$, and ortho $(3,3)$ state measured during the afterglow in He/Ar/H_2 gas mixture at 170 K, 1550 Pa of He, $H_2 = 1 \times 10^{14}\,\mathrm{cm}^{-3}$, and Ar $= 2 \times 10^{14}\,\mathrm{cm}^{-3}$. The vertical bar shows the end of the discharge period and the beginning of the afterglow. **Panel (b)**: The measured relative population of para $(1,1)$, ortho $(1,0)$, and ortho $(3,3)$ states of H_3^+. **Panel (c):** Measured fraction ${}^{p}f_3$ of para-H_3^+. Adapted from Dohnal et al. (2012b).

population within ortho H_3^+ manifold (and probably also within para H_3^+ manifold) is justified. For additional details on relaxation of H_3^+ dominated afterglow plasma see thorough discussion in Dohnal et al. (2012b).

5.3.2 *Results*

The binary recombination rate coefficients for pure ortho- and para-H_3^+measured in the temperature range of $80 - 200$ K are displayed in Fig. 33. A good agreement with the theory (Fonseca dos Santos et al., 2007) is obtained; difference between α_{bin} for ortho- and para-H_3^+ has its maximum at 80 K and the difference is diminishing with increasing temperature, exactly as predicted by the theory.

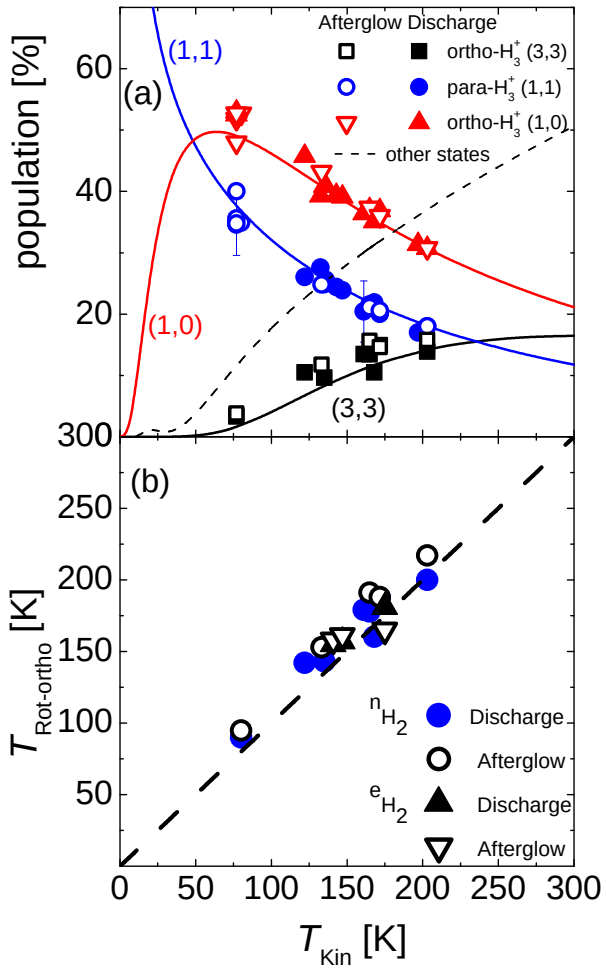

Figure 32: **Panel (a):** The dependence of measured relative population of H_3^+ ions in ortho $(1,0)$, ortho $(3,3)$, and para $(1,1)$ states on kinetic temperature in experiments with normal H_2. Closed symbols indicate data obtained at the end of the discharge period and open symbols during the afterglow, ~ 150 µs after switching off the discharge. The full lines indicate the calculated population of the displayed states in TE at temperatures given by T_{Kin}. The dashed line represents the sum of the other states populations. **Panel (b):** Measured rotational temperature of ortho manifold $T_{Rot\text{-}ortho}$ versus measured kinetic temperature T_{Kin}. Displayed data were obtained using both $^nH_2$ and $^eH_2$ gas precursors. The straight dashed line shows equality $T_{Rot\text{-}ortho} = T_{Kin}$. Adapted from Dohnal et al. (2012b).

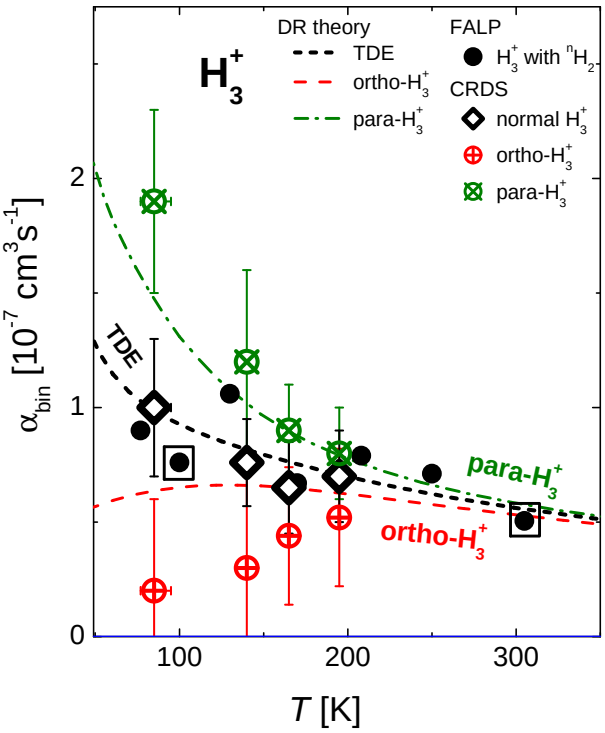

Figure 33: Temperature dependence of the binary recombination rate coefficient α_{eff} as obtained in SA-CRDS experiment (Varju et al., 2011; Dohnal et al., 2012b) for ortho-H_3^+, para-H_3^+ (crosses), and H_3^+ ions with population of states according to TE at given temperature (open rhomboids). The full circles denote values obtained in previous FALP experiments (Glosík et al., 2009b) and full circles in a square are extrapolations of values obtained Cryo-FALP and SA-CRDS. The full lines labeled as "ortho" and "para" are theoretical calculations for corresponding nuclear spin modifications of H_3^+ (Fonseca dos Santos et al., 2007). The dashed line is calculation by the same authors for H_3^+ ion with population of states according to TE. Adapted from Dohnal et al. (2012b).

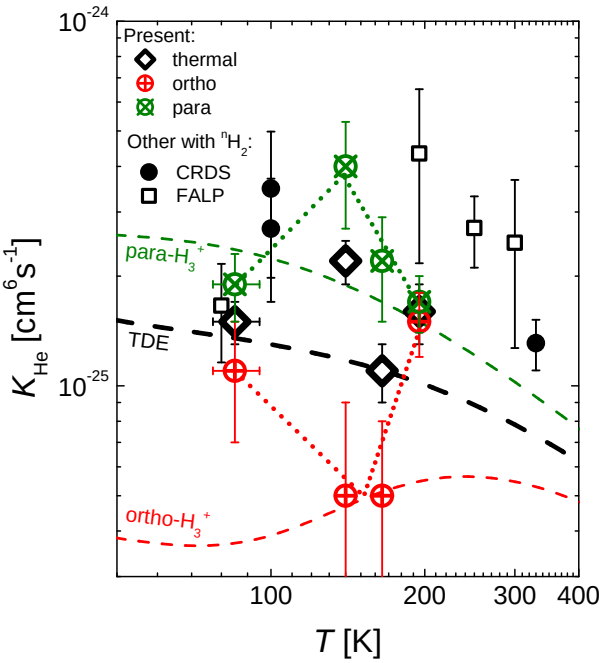

Figure 34: Temperature dependence of the ternary recombination rate coefficients K_{He} for ortho-H_3^+, para-H_3^+(crosses), and H_3^+ ions with population of states according to TE (open rhomboids) (Varju et al., 2011; Dohnal et al., 2012b). Values from previous FALP experiments (open squares) and values extrapolated from combination of Cryo-FALP and SA-CRDS data (full circles) are plotted for comparison. The dotted lines through "ortho" and "para" data are for eye guiding only. Dashed lines denote Kokoouline's theoretical caluclation (Glosík et al., 2009b). Adapted from Dohnal et al. (2012b).

The ternary recombination rate coefficients for pure ortho- and para-H_3^+ were calculated from the slopes of the effective recombination rate coefficients pressure dependences as plotted in Fig. 30. The results are shown in Fig. 34. The obtained ternary recombination rates are similar for both nuclear spin configurations at 80 K and 200 K but they differ at intermediate temperatures. Theoretical calculations of Kokoouline (Glosík et al., 2009b) are plotted by dashed line. Outline of the theory can be found also in Sec. 3.4 of this work. As can be seen in Fig. 34, we did not obtain agreement as in the case of the binary recombination coefficients.

5.4 H_2 ASSISTED TERNARY RECOMBINATION OF H_3^+

Most of the afterglow experiments measuring DR of H_3^+ ion was successfully explained by the existence of the helium ternary recombination channel discussed in Sec. 3.4. A study carried out by Amano (Amano, 1990) in pure H_2 gas at the pressure of ~ 100 Pa giving high value of $\alpha = 1.8 \times 10^{-7}\,\mathrm{cm^3 s^{-1}}$ at the temperature of 273 K has puzzled experimental physicists since its publishing. There was an attempt to repeat this experiment by Fehér et al. (1994) but it was marked by problems with impurities. The aforementioned facts make more than a sufficient motivation to perform a dedicated study at relatively high H_2 number densities using SA-CRDS experimental apparatus.

In order to avoid possible problems using high number densities of H_2, which can conflagrate in presence of oxygen, we decided to admix nitrogen gas at the entrance of the secondary pump, just behind the Roots pump (see Fig. 36). Subsequent modifications of the gas handling system allowed us to use the flow of H_2 reactant gas up to $0.17\,\mathrm{Pa\ m^3 s^{-1}}$ in order to measure dependence of α_{eff} over a wide range of $[H_2]$, as can be seen in Fig. 35.

As we mentioned in the introductory part of Sec. 5.2, dependence of the effective recombination coefficient α_{eff} for H_3^+ ions on H_2 number density can be divided into three different regions. At high $[H_2]$, α_{eff} increases due to formation of fast recombining H_5^+ ions. However, at the temperatures of 273 K and above, the observed increase of α_{eff} cannot be explained by formation of H_5^+, as it is not sufficiently fast at these temperatures. Full line in Fig. 35 shows the contribution of H_5^+ recombination if it is in thermodynamic equilibrium with H_3^+ ions,

which are created in ternary association reactions (see no. 8 in Tab. 8), computed as

$$\alpha_{H_5} = \alpha_5 K_C [H_2] , \tag{72}$$

where α_5 is the recombination rate coefficient of H_5^+, its value is taken as $\alpha_5 = 2 \times 10^{-6}\,cm^3 s^{-1}$ (Glosík et al., 2003; Macdonald et al., 1984) and K_C is the equilibrium constant taken as $K_C(300\,K) = 6.7 \times 10^{-19}\,cm^3$ (Hiraoka, 1987). Even smaller contribution, which is much more likely is represented by dot-dashed line denoted as M_{H_5} obtained from the chemical kinetics model indicates, that contribution due to H_5^+ recombination is negligible below $[H_2] = 2 \times 10^{16}\,cm^{-3}$ at 300 K.

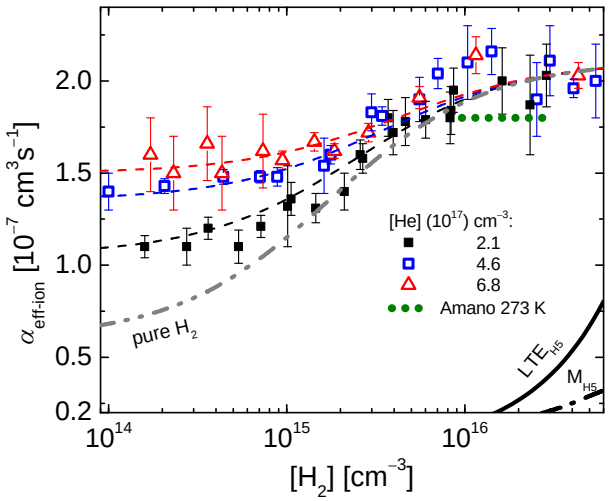

Figure 35: Experimental values of $\alpha_{eff\text{-}ion}$ for different $He/Ar/H_2$ mixtures. Dashed lines: Fits of Eq. (87) to the data. Double dot-dashed line: Three-body recombination in pure H_2. Solid line denoted (LTE_{H_5}): Approximate H_5^+ contribution taken as $\alpha_5 K_C [H_2]$. Dot-dashed line (M_{H_5}): H_5^+ contribution obtained from the kinetic model for $[He] = 2.1 \times 10^{17}\,cm^{-3}$. Dotted line: Data obtained by Amano (1990) in pure H_2 at 273 K.

To explain the obtained results we propose mechanism of H_3^+ recombination, explained in the following section.

5.4.1 *Recombination Mechanism*

The following loss processes of H_3^+ ion in the afterglow plasma are considered in the evaluation of the effective recombination rate coefficient of H_3^+:

1. The binary dissociative recombination with electrons:

$$H_3^+ + e^- \xrightarrow{\alpha_{bin}} \text{neutrals}\,. \tag{73}$$

2. The formation of the excited Rydberg state H_3^*:

$$H_3^+ + e^- \underset{\nu_a}{\overset{\alpha_F}{\longleftrightarrow}} H_3^* \underset{k_{SH_2}}{\overset{k_{SHe}}{\longrightarrow}} \text{neutrals}\,, \tag{74}$$

where α_F is rate coefficient of H_3^* formation, $\nu_a = 1/\tau_a$ is the autoionization rate (τ_a being the time constant of the autoionization), and k_{SH_2} and k_{SHe} are the rate coefficients for collisional stabilization of H_3^* with H_2 and He, respectively.

3. The formation of H_5^+ in ternary association reaction of H_3^+ with H_2 and He:

$$H_3^+ + H_2 + He \underset{k_{-3}}{\overset{k_3}{\longleftrightarrow}} H_5^+ + He\,, \tag{75}$$

followed by its recombination with electrons:

$$H_5^+ + e^- \xrightarrow{\alpha_5} \text{neutrals}\,, \tag{76}$$

where k_3 is the rate coefficient of the ternary association, k_{-3} is the rate coefficient of the backward reaction (collisional induced dissociation), α_5 is the recombination rate coefficient of H_5^+. We suppose that k_3 and k_{-3} coefficient are the same as corresponding coefficients for the association of H_3^+ with $2H_2$.

Hence we can write balance equations for H_3^+, H_3^*, and H_5^+:

$$\begin{aligned}\frac{d[H_3^+]}{dt} =& -\alpha_{bin}[H_3^+]n_e - \alpha_F[H_3^+]n_e + \frac{1}{\tau_a}[H_3^*] \\ & - k_3[H_3^+][H_2][He] + k_{-3}[H_5^+][He]\,,\end{aligned} \tag{77}$$

$$\frac{d[H_3^*]}{dt} = \alpha_F[H_3^+]n_e - \frac{1}{\tau_a}[H_3^*] - k_{SHe}[He][H_3^*] - k_{SH_2}[H_2][H_3^*]\,, \tag{78}$$

$$\frac{d[H_5^+]}{dt} = -\alpha_5[H_5^+]n_e + k_3[H_3^+][H_2][He] - k_{-3}[H_5^+][He]\,. \tag{79}$$

Under the assumption that both $[H_3^*]$ and $[H_5^+]$ remain constant in time (steady state approximation) and very small in comparison with the reactants number densities, we can write the corresponding number densities using Eqs. (78) and (79) as

$$[H_3^*] = \frac{\alpha_F n_e[H_3^+]}{\frac{1}{\tau_a} + k_{SHe}[He] + k_{SH_2}[H_2]} \tag{80}$$

and

$$[H_5^+] = \frac{k_3[H_2][He][H_3^+]}{k_{-3}[He] + \alpha_5 n_e} = K_C \frac{[H_2][H_3^+]}{1 + \frac{\alpha_5 n_e}{k_{-3}[He]}} = R[H_3^+], \tag{81}$$

where $K_C = k_3/k_{-3}$ is the equilibrium constant (Hiraoka, 1987) and $R = [H_5^+]/[H_3^+]$.

Assuming that only H_3^+ and H_5^+ ions are present in the afterglow plasma and $[H_3^+] + [H_5^+] = n_e$ we get

$$\frac{dn_e}{dt} = \alpha_{bin}[H_3^+]n_e - \alpha_F[H_3^+]n_e \frac{k_{SHe}[He] + k_{SH_2}[H_2]}{\frac{1}{\tau_a} + k_{SHe}[He] + k_{SH_2}[H_2]} - \alpha_5[H_5^+]n_e . \tag{82}$$

We can write the effective recombination rate coefficient as

$$\alpha_{eff} = \alpha_{bin} + \alpha_F \frac{k_{SHe}[He] + k_{SH_2}[H_2]}{\frac{1}{\tau_a} + k_{SHe}[He] + k_{SH_2}[H_2]} + \alpha_5 K_C[H_2] . \tag{83}$$

We define the ternary recombination rate coefficients for He and H_2 assisted recombination as

$$K_{He} = \alpha_F k_{SHe} \tau_a \tag{84}$$

and

$$K_{H_2} = \alpha_F k_{SH_2} \tau_a . \tag{85}$$

Balance equation for electrons can be rewritten:

$$\frac{dn_e}{dt} = -\left(\alpha_{bin} + \alpha_F \frac{K_{He}[He] + K_{H_2}[H_2]}{\alpha_F + K_{He}[He] + K_{H_2}[H_2]} + \alpha_5 K_C[H_2]\right) \cdot \cdot [H_3^+]n_e . \tag{86}$$

Because it is the number density of H_3^+ taht is being measured in the SA-CRDS xperiment we have to rewrite Eq. (86) using only $[H_3^+]$. Thus the effective recombination rate coefficient measured from the decay of the H_3^+ number density is expressed as

$$\alpha_{eff\text{-}ion} = \alpha_{bin} + \alpha_F \frac{K_{He}[He] + K_{H_2}[H_2]}{\alpha_F + K_{He}[He] + K_{H_2}[H_2]} + \alpha_5 K_C[H_2] . \tag{87}$$

It has to be noted, that in the limit of low He and H_2 number densities, where $\alpha_F \gg K_{He}[He] + K_{H_2}[H_2]$, we can make a "well known" linear approximation:

$$\alpha_{eff} = \alpha_{bin} + K_{He}[He] + K_{H_2}[H_2] + \alpha_5 K_C[H_2] . \tag{88}$$

5.4.2 *Discussion of the Results*

The value of the binary recombination coefficient $\alpha_{bin}(300\,K) = 6 \times 10^{-8}\,cm^3s^{-1}$ (Rubovič et al., 2013) was used in Eq. (87) when fitting the measured dependence of $\alpha_{eff\text{-}ion}$ on $[H_2]$. The inferred values of the other constants at the temperature of 300 K are the following: $K_{He} = (3.3 \pm 0.7) \times 10^{-25}\,cm^6s^{-1}$; $K_{H_2} = (8.7 \pm 1.5) \times 10^{-23}\,cm^6s^{-1}$; $\alpha_F = (1.5 \pm 0.1) \times 10^{-7}\,cm^3s^{-1}$. Note, that dependence of $\alpha_{eff\text{-}ion}$ on $[H_2]$ in pure hydrogen in figure 35 was obtained using these coefficients at zero He number density.

The significance of the coefficient α_F is well explained when measuring at high number densities of He and H_2. It can be clearly seen from Eq. (87) that the value of $\alpha_{eff\text{-}ion}$ then saturates on α_F. Our measurements proved this, as we have seen this for both cases within the experimental error. However, it is questionable if assumption of identical channel of H_3^* formation for both He and H_2 ternary recombination is correct and further experimental data are needed.

The obtained value of K_{He} agree well with our previous experimental results (Johnsen et al., 2013). On the other hand, the inferred value of K_{H_2}, which is in the order of $10^{-23}\,cm^6s^{-1}$ is surprisingly large. It is larger by two orders of magnitude than the corresponding value of K_{He} for H_3^+, not to mention the value of the ternary rate coefficient as predicted by Bates and Khare (1965), which is smaller by five orders of magnitude. In order to explain it, one has to take look at its definition in Eq. (85). The typical value of ion-molecule reaction rate coefficient is $10^{-9}\,cm^3s^{-1}$. When taking it as k_{SH_2}, one needs lifetime τ_a to be $\tau_a \sim 6 \times 10^{-7}$ s to obtain the observed K_{H_2}. The longest calculated lifetime is in the order of 10^{-10} s (Glosík et al., 2009b), however Mitchell (1990) observed lifetimes in the order of 10^{-7} s. The other possibility is to increase k_{SH_2}. It is known that l-mixing of the Rydberg electrons angular momentum by either plasma electrons (Gougousi et al., 1995) or neutral particles (Glosík et al., 2009b; Johnsen et al., 2013; Glosík et al., 2010) occurs and it can enhance H_3^* lifetime τ_a. Especially l-mixing of high Rydberg states with $n \gtrsim 40$ due to ambient plasma electrons is an exceedingly fast process. At electron number densitied $\sim 10^{11}\,cm^{-3}$ mixing would occur in a time of the order of 10^{-11} s to 10^{-10} s for $n = 40$ Rydberg atom (Dutta et al., 2001) and increases the lifetimes by a factor of $\sim n^2$. Yet a relevant theory is needed for sufficient explanation of this phenomenon.

As can be seen in Fig. 35, we came to the same results as Amano (Amano, 1990) successfully (even in pure H_2) and these can be ex-

plained by high H_2 number density used in his experiment. Our findings have, however, also other consequences. H_2 ternary assisted recombination channel may be present in Jovian-like planets with high H_2 number density and it should be definitely considered in numerical models of their ionospheres. Also a new question of the effective recombination rate coefficient saturation in afterglow experiments arises. One should be aware of this fact and careful measurements over a wide range of the reactants number densities are a must.

6 CONCLUSION

In this work we present studies of ion-electron recombination in the afterglow plasma at low temperatures. Both Cryo-FALP II and SA-CRDS apparatuses were properly described along with supplementary measurements proving their acclaimed advantages. Several new experimental results were obtained and they will be shortly summarized in this chapter.

CRYO-FALP II

Article I, *Article VI*

I took part in constructing Cryogenic Flowing Afterglow with Langmuir probe II apparatus which is described in Sec. 4.2 of this thesis. Several calibration measurements are mentioned, i. e. buffer gas velocity. The Langmuir probe was calibrated using well known temperature dependence of O_2^+ recombination. An analysis of ambipolar diffusion electron losses was used in order to verify thermalization of electrons. An excellent agreement with the wall temperature was obtained above the temperature of 70 K. However, we saw a deviation at lower temperatures ascribed to ion molecular reactions taking place in the late afterglow. However, we have an extremely reliable tool for measuring recombination rate coefficients in the temperature range of $50 - 300$ K in this apparatus what was unthinkable several years ago.

Ar^+ RECOMBINATION

Article I, *Article VI*

Recombination of Ar^+ ions with electron was studied using Cryo-FALP II apparatus in the temperature range of $50 - 100$ K following previous studies in our laboratory at higher temperature. Both helium and electron assisted collisional radiative recombination were studied and very good agreement with corresponding theories was achieved, see Figs. 22 and 23. These results represent the first experimental study of the aforementioned processes below 80 K.

H_3^+ AND D_3^+ RECOMBINATION

Article V, *Article VII*, *Article VIII*

Recombination of H_3^+ and its isotopologue D_3^+ with electrons was studied using both Cryo-FALP II and SA-CRDS experiments at temperatues of $50 - 250$ K. The measured temperature dependencies of corresponding binary recombination coefficients are plotted in Figs. 28 and 29. The ternary recombination rate coefficient for helium assisted H_3^+ and D_3^+ recombination are plotted in Figs. 26 and 27. Measurement of D_3^+ ion in SA-CRDS is the first one with spectroscopically resolved abundances of the recombining ions.

STATE SELECTED H_3^+ RECOMBINATION

Article II, *Article III*, *Article IV*

We were able to obtain hydrogen gas with nonthermal population of its states using para enriched hydrogen generator. By monitoring the lowest rotational states of H_3^+ ion on SA-CRDS apparatus we inferred temperature dependencies of the binary recombination rate coefficient (see Fig. 33) and of helium assisted ternary recombination rate coefficient (see Fig. 34) for pure para- and ortho-H_3^+. This is the first study of recombination of H_3^+ in specific states with *in situ* determination of rotational states population.

H_2 ASSISTED TERNARY RECOMBINATION OF H_3^+

Section 5.4

An extraordinaly large ternary rate coefficient of the process which would describe hydrogen assisted ternary recombination of H_3^+ ions was observed at the temperature of 300 K. We proposed a mechanism of this process but a solid theory is needed for its thorough explanation.

I dare to say that our understanding of ion-electron recombination due to contribution summarized in my doctoral thesis, is deeper than four years ago, when I started my doctoral study. Now, we know how third bodies affect recombination processes in afterglow plasmas and we have obtained very interesting results at temperatures below 80 K. However, there are still many open questions that we have answer before the topic of electron-ion recombination is fully understood. I hope that we managed to gather several pieces of the recombination mosaic and we will see a complete and fascinating result soon.

Part I

APPENDIX

A

DRAWINGS

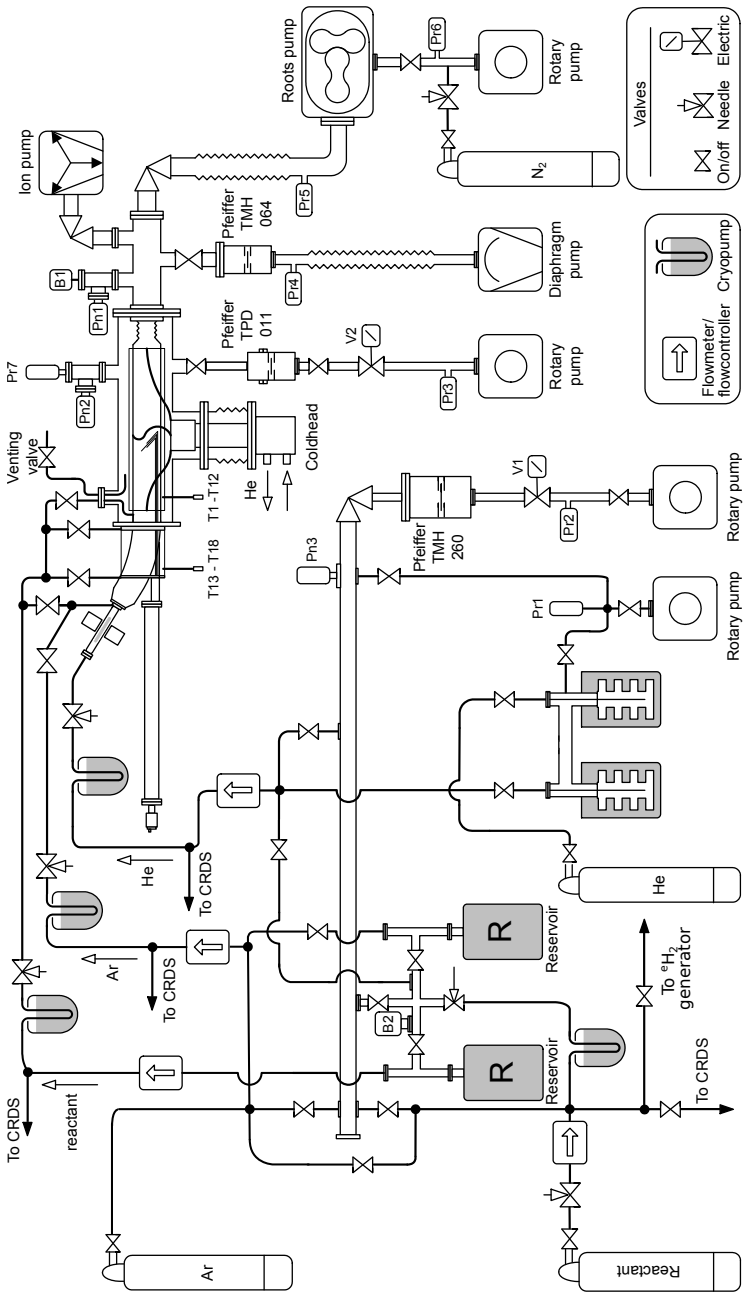

Figure 36: Vacuum and gas handling system of Cryo-FALP II apparatus. Adapted from Dohnal (2013) with subsequent modifications.

BIBLIOGRAPHY

Adams, N. G. and D. Smith (1976). "The selected ion flow tube (SIFT); A technique for studying ion-neutral reactions." In: *Int. J. Mass Spectrom.* 21, p. 349. DOI: 10.1016/0020-7381(76)80133-7 (cit. on p. 7).

Adams, N. G., D. Smith, and E. Alge (1984). "Measurements of dissociative recombination coefficients of H_3^+, HCO^+, N_2H^+, and CH_5^+ at 95 and 300 K using the FALP apparatus." In: *J. Chem. Phys.* 81, p. 1778. DOI: 10.1063/1.447849 (cit. on pp. 16, 17, 42, 45).

Adams, N. and D. Smith (1989). "FALP studies of positive ion/electron recombination coefficients." In: *Dissociative Recombination: Theory, Experiment and Applications*. Ed. by J. Mitchell and S. Guberman. World Scientific, Singapore, pp. 124–140 (cit. on p. 17).

Alge, E., N. G. Adams, and D. Smith (1983). "Measurements of the dissociative recombination coefficients of O_2^+, NO^+ and NH_4^+ in the temperature range 200-600K." In: *J. Phys. B: At. Mol. Phys* 16, p. 1433. DOI: 10.1088/0022-3700/16/8/017 (cit. on pp. 42, 45).

Amano, T. (1988). "Is the dissociative recombination of H_3^+ really slow? A new spectroscopic measurement of the rate constant." In: *Astrophys. J.* 329, pp. L121–L124. DOI: 10.1086/185190 (cit. on p. 16).

— (1990). "The dissociative recombination rate coefficients of H_3^+, HN_2^+, and HCO^+." In: *J. Chem. Phys.* 92, p. 6492. DOI: 10.1063/1.458594 (cit. on pp. 16, 17, 73, 74, 77).

Anicich, V. G. (1993). "Evaluated Bimolecular IonMolecule Gas Phase Kinetics of Positive Ions for Use in Modeling Planetary Atmospheres, Cometary Comae, and Interstellar Clouds." In: *J. Phys. Chem. Ref. Data* 22, p. 1469. DOI: 10.1063/1.555940 (cit. on p. 57).

Auerbach, D., R. Cacak, R. Caudano, T. D. Gaily, C. J. Keyser, J. W. McGowan, et al. (1977). "Merged electron-ion beam experiments. I. Method and measurements of (e-H_2^+) and (e-H_3^+) dissociative-recombination cross sections." In: *J. Phys. B: At. Mol. Phys* 10, p. 3797. DOI: 10.1088/0022-3700/10/18/033 (cit. on pp. 8, 17).

Bardsley, J. N. (1968a). "Configuration interaction in the continuum states of molecules." In: *J. Phys. B: At. Mol. Phys* 1, p. 349. DOI: 10.1088/0022-3700/1/3/303 (cit. on p. 4).

— (1968b). "The theory of dissociative recombination." In: *J. Phys. B: At. Mol. Phys* 1, p. 365. DOI: 10.1088/0022-3700/1/3/304 (cit. on p. 4).

Bates, D. R. (1950). "Dissociative Recombination." In: *Phys. Rev.* 78, pp. 492–493. DOI: 10.1103/PhysRev.78.492 (cit. on pp. 3, 4).

— (1974). "Recombination and Electrical Networks." In: *Proc. R. Soc. Lond. A* 337, pp. 15–20. DOI: 10.1098/rspa.1974.0036 (cit. on p. 51).

Bates, D. R., M. F. Guest, and R. A. Kendall (1993). "Enigma of H_3^+ dissociative recombination." In: *Planet, Space Sci.* Vol. 41, No. 1, pp. 9–15. DOI: 10.1016/0032-0633(93)90011-P (cit. on p. 1).

Bates, D. R. and S. P. Khare (1965). "Recombination of positive ions and electrons in a dense neutral gas." In: *Proc. Phys. Soc. Lond.* 85, p. 231. DOI: 10.1088/0370-1328/85/2/305 (cit. on pp. 10, 18, 43, 50, 52, 53, 60, 77).

Bates, D. R., A. E. Kingston, and W. P. McWhirter (1962). "Recombination Between Electrons and Atomic Ions. I. Optically Thin Plasmas." In: *Philos. T. Roy. Soc. A* 267, p. 297. DOI: 10.1098/rspa.1962.0101 (cit. on p. 11).

Berlande, J., M. Cheret, R. Deloche, A. Gonfalone, and C. Manus (1970). "Pressure and Electron Density Dependence of the Electron-Ion Recombination Coefficient in Helium." In: *Phys. Rev. A* 1, pp. 887–896. DOI: 10.1103/PhysRevA.1.887 (cit. on pp. 10, 12, 52–54).

Biondi, M. A. and S. C. Brown (1949). "Measurement of Electron-Ion Recombination." In: *Phys. Rev.* 76, p. 1697. DOI: 10.1103/PhysRev.76.1697 (cit. on pp. 16, 17).

Black, J. H. (2000). "The abundance and excitation of interstellar H_3^+." In: *Phil. Trans. R. Soc. Lond. A* 358, p. 2515. DOI: 10.1098/rsta.2000.0664 (cit. on p. 15).

Boehringer, H., F. Arnold, D. Smith, and N. G. Adams (1983). "A study of the temperature dependences of the $N_2^+ + N_2 \rightarrow N_4^+$ and $O_2^+ + O_2 \rightarrow O_4^+$ association reactions using the selected-ion flow-tube and drift-tube techniques." In: *Int. J. Mass Spectrom.* 52, p. 25. DOI: 10.1016/0020-7381(83)85089-X (cit. on p. 43).

Bohme, D. K., D. B. Dunkin, F. C. Fehsendeld, and E. E. Ferguson (1969). "Flowing Afterglow Studies of Ion-Molecule Association Reactions." In: *J. Chem. Phys.* 51, pp. 863–872. DOI: 10.1063/1.1672150 (cit. on p. 46).

Bowers, M. T., D. D. Elleman, and J. King Jr. (1969). "Analysis of the Ion–Molecule Reactions in Gaseous H_2, D_2, and HD by Ion Cyclotron Resonance Techniques." In: *J. Chem. Phys.* 50, p. 4787. DOI: 10.1063/1.1670971 (cit. on p. 57).

Canosa, A., J. C. Gomet, B. R. Rowe, J. B. A. Mitchell, and J. L. Queffelec (1992). "Further measurements of the $H_3^+(v = 0, 1, 2)$ dissocia-

tive recombination rate coefficient." In: *J. Chem. Phys.* 97, p. 1028. DOI: 10.1063/1.463282 (cit. on p. 17).

Cao, Y. S. and R. Johnsen (1991). "Neutralstabilized electron–ion recombination in ambient helium gas." In: *J. Chem. Phys.* 94, pp. 5443–5446. DOI: 10.1063/1.460505 (cit. on pp. 11, 52, 53, 60).

Caselli, P., F. F. S. van der Tak, C. Ceccarelli, and A. Bacmann (2003). "Abundant H_2D^+ in the pre-stellar core L1544." In: *Astron. Astrophys.* 403, p. L37. DOI: 10.1051/0004-6361:20030526 (cit. on p. 20).

Cernicharo, J., E. Polehampton, and J. R. Goicoechea (2007). "Far-Infrared Detection of H_2D^+ toward Sgr B2." In: *Astrophys. J.* 657, p. L21. DOI: 10.1086/512857 (cit. on p. 20).

Chen, F. F. (1974). *Introduction to plasma physics*. Plenum Press, New York (cit. on p. 38).

Clow, R. P. and J. H. Futrell (1970). "Ion-cyclotron resonance study of the kinetic energy dependence of ion–molecule reaction rates: I. Methane, hydrogen and rare gas–hydrogen systems." In: *Int. J. Mass Spectrom. Ion Proc.* 4, p. 165. DOI: 10.1016/0020-7381(70)85035-5 (cit. on p. 57).

Crabtree, K. N., N. Indriolo, H. Kreckel, B. A. Tom, and B. J. McCall (2011). "On the Ortho:Para Ratio of H_3^+ in Diffuse Molecular Clouds." In: *Astrophys. J.* 729, p. 15. DOI: 10.1088/0004-637X/729/1/15 (cit. on p. 15).

Crompton, R. W., M. T. Elford, and R. L. Jory (1967). "The Momentum Transfer Cross Section for Electrons in Helium." In: *Austr. J. Phys* 20, pp. 396–400. DOI: 10.1071/PH670369 (cit. on p. 10).

Curry, B. P. (1970). "Collisional Radiative Recombination in Hydrogen Plasmas and in Alkali Plasmas." In: *Phys. Rev. A* 1, p. 166. DOI: 10.1103/PhysRevA.1.166 (cit. on p. 54).

Deloche, R., P. Monchicourt, M. Cheret, and F. Lambert (1976). "High-pressure helium afterglow at room temperature." In: *Phys. Rev. A* 13, pp. 1140–1176. DOI: 10.1103/PhysRevA.13.1140 (cit. on pp. 11, 43, 50, 52, 53).

Dohnal, P. (2013). "Electron Ion Recombination in Low Temperature Plasma." PhD thesis. Charles University in Prague (cit. on pp. 17, 28, 34, 50, 54, 83).

Dohnal, P., M. Hejduk, P. Rubovič, J. Varju, Š. Roucka, R. Plašil, et al. (2012a). "Binary and ternary recombination of D_3^+ ions at 80–130 K: Application of laser absorption spectroscopy." In: *J. Chem. Phys.* 137, p. 194320. DOI: 10.1063/1.4767396 (cit. on pp. 21, 35, 55, 61, 64).

Dohnal, P., M. Hejduk, J. Varju, P. Rubovič, Š. Roučka, T. Kotrík, et al. (2012b). "Binary and ternary recombination of para-H_3^+ and ortho-H_3^+ with electrons: State selective study at 77-200 K." In: *J. Chem. Phys.* 136, p. 244304. DOI: doi:10.1063/1.4730162 (cit. on pp. 35, 47, 48, 55, 60, 62, 63, 66, 69–72).

Dohnal, P., M. Hejduk, J. Varju, P. Rubovič, Š. Roučka, T. Kotrík, et al. (2012c). "Binary recombination of para- and ortho-H_3^+ with electrons at low temperatures." In: *Phil. T. Roy. Soc. A* 370, pp. 5101–5108. DOI: 10.1098/rsta.2012.0097 (cit. on p. 62).

Dohnal, P., P. Rubovič, T. Kotrík, M. Hejduk, R. Plašil, R. Johnsen, et al. (2013). "Collisional-radiative recombination of Ar^+ ions with electrons in ambient helium at temperatures from 50 K to 100 K." In: *Phys. Rev. A* 87 (5), p. 052716. DOI: 10.1103/PhysRevA.87.052716 (cit. on pp. 12, 34, 45, 46, 51, 53, 54, 59, 60).

Dotan, I. and W. Lindinger (1982). "Energy dependencies of the reactions of Ar^+ with H_2, N_2, CO, O_2, CO_2, N_2O, and COS." In: *J. Chem. Phys.* 76, p. 4972. DOI: 10.1063/1.442843 (cit. on p. 57).

Drossart, P., J.-P. Maillard, J. Caldwell, S. J. Kim, J. K. G. Watson, W. A. Majewski, et al. (1989). "Detection of H_3^+ on Jupiter." In: *Nature* 340.6234, p. 539. DOI: 10.1038/340539a0 (cit. on p. 14).

Druyvesteyn, M. J. (1930). "Der Niedervoltbogen." In: *Zeitschrift für Physik* 64, p. 781. DOI: 10.1007/BF01773007 (cit. on p. 34).

Dutta, S. K., D. Feldbaum, A. Walz-Flannigan, J. R. Guest, and G. Raithel (2001). "High-Angular-Momentum States in Cold Rydberg Gases." In: *Phys. Rev. Lett.* 86 (18), pp. 3993–3996. DOI: 10.1103/PhysRevLett.86.3993 (cit. on p. 77).

Fehér, M., A. Rohrbacher, and J. P. Maier (1994). "Infrared laser kinetic spectroscopy of the H_3^+ ion." In: *Chem. Phys.* 185, pp. 357–364. DOI: 10.1016/0301-0104(94)00131-6 (cit. on pp. 16, 17, 73).

Fehsenfeld, F. C., E. E. Ferguson, and A. L. Schmeltekopf (1966). "ThermalEnergy Ion–Neutral Reaction Rates. III. The Measured Rate Constant for the Reaction $O^+(^4S)+CO_2(^1\Sigma) \rightarrow O_2 + (^2\Pi)+CO(^1\Sigma)$." In: *J. Chem. Phys.* 44, p. 3022. DOI: 10.1063/1.1727173 (cit. on p. 7).

Flannery, M. R. (1991). "Transportcollisional master equations for termolecular recombination as a function of gas density." In: *J. Chem. Phys.* 95(11), p. 8205. DOI: 10.1063/1.461300 (cit. on pp. 9, 10, 18).

Florescu-Mitchell, A. I. and J. B. A. Mitchell (2006). "Dissociative recombination." In: *Phys. Rep.* 430, pp. 277–374. DOI: 10.1016/j.physrep.2006.04.002 (cit. on p. 16).

Flower, D. R., G. Pineau des Forets, and C. M. Walmsley (2004). "Multiply-deuterated species in prestellar cores." In: *Astron. Astrophys.* 427, pp. 887–893. DOI: 10.1051/0004-6361:20041464 (cit. on p. 20).

Fonseca dos Santos, S., V. Kokoouline, and C. H. Greene (2007). "Dissociative recombination of H_3^+ in the ground and excited vibrational states." In: *J. Chem. Phys* 127, p. 124309. DOI: 10.1063/1.2784275 (cit. on pp. 18, 62, 65, 69, 71).

Gay, C. D., P. C. Stancil, S. Lepp, and A. Dalgarno (2011). "The Highly Deuterated Chemistry of the Early Universe." In: *Astrophys. J.* 737, p. 44. DOI: 10.1088/0004-637X/737/1/44 (cit. on p. 20).

Geballe, T. R. and T. Oka (1996). "Detection of H_3^+ in interstellar space." In: *Nature* 384, pp. 334–335. DOI: 10.1038/384334a0 (cit. on p. 14).

Glosík, J. (1994). "Measurement of the reaction rate coefficients of reactions of H_2^+ with Ne, Ar, Kr, Xe, H_2, D_2, N_2 and CH_4 at thermal energy." In: *Int. J. Mass Spectrom.* 1369, pp. 15–23. DOI: 10.1016/0168-1176(94)04069-9 (cit. on pp. 13, 57).

Glosík, J., G. Bánó, R. Plašil, A. Luca, and P. Zakouřil (1999). "Study of the electron ion recombination in high pressure flowing afterglow: recombination of $NH_{4\mathring{u}}^+(NH_3)_2$." In: *Int. J. Mass Spectrom.* 189, pp. 103–113. DOI: 10.1016/S1387-3806(99)00058-5 (cit. on pp. 35, 43).

Glosík, J., M. Hejduk, P. Dohnal, P. Rubovič, Á. Kálosi, and R. Plašil (2014). "State selective study of H_3^+ recombination in Cryo-FALP and SA-CRDS experiments at 77 K." In: *EPJ Web of Conf.* sent for publishing (cit. on p. 67).

Glosík, J., I. Korolov, R. Plašil, T. Kotrík, P. Dohnal, O. Novotný, et al. (2009a). "Binary and ternary recombination of D_3^+ ions with electrons in He-D_2 plasma." In: *Phys. Rev. A* 80, p. 042706. DOI: 10.1103/PhysRevA.80.042706 (cit. on p. 18).

Glosík, J., I. Korolov, R. Plašil, O. Novotný, T. Kotrík, P. Hlavenka, et al. (2008). "Recombination of H_3^+ ions in the afterglow of a He-Ar-H_2 plasma." In: *J. Phys. B-At. Mol. Opt.* 41, p. 191001. DOI: 10.1088/0953-4075/41/19/191001 (cit. on pp. 17, 18).

Glosík, J., O. Novotný, A. Pysanenko, P. Zakouřil, R. Plašil, P. Kudrna, et al. (2003). "The recombination of H_3^+ and H_5^+ ions with electrons in hydrogen plasma: dependence on temperature and on pressure of H_2." In: *Plasma Sci. Technol.* 12, S117–S122. DOI: 10.1088/0963-0252/12/4/027 (cit. on pp. 17, 57, 74).

Glosík, J., R. Plašil, I. Korolov, T. Kotrík, O. Novotný, P. Hlavenka, et al. (2009b). "Temperature dependence of binary and ternary recombination of H_3^+ ions with electrons." In: *Phys. Rev. A* 79, p. 052707.

DOI: 10.1103/PhysRevA.79.052707 (cit. on pp. 18–20, 55, 59, 60, 62, 71–73, 77).

Glosík, J., R. Plašil, T. Kotrík, P. Dohnal, J. Varju, M. Hejduk, et al. (2010). "Binary and ternary recombination of H_3^+ and D_3^+ ions with electrons in low temperature plasma." In: *Molec. Phys.* 108, p. 2253. DOI: 10.1080/00268976.2010.507555 (cit. on pp. 16, 18, 77).

Glosík, J., R. Plašil, V. Poterya, P. Kudrna, and M. Tichý (2000). "The recombination of H_3^+ ions with electrons: dependence on partial pressure of H_2." In: *Chem. Phys. Lett.* 331, p. 209. DOI: 10.1016/S0009-2614(00)01183-0 (cit. on pp. 16, 17, 55).

Gougousi, T., R. Johnsen, and M. F. Golde (1995). "Recombination of H_3^+ and D_3^+ ions in a flowing afterglow plasma." In: *Int. J. Mass Spectrom.* 149-150, pp. 131–151. DOI: 10.1016/0168-1176(95)04248-J (cit. on pp. 16, 17, 77).

Gousset, G., B. Sayer, M. Ferray, and J. Lonzigot (1978). "Role of atomic inelastic collisions in a Cs-He steady state discharge." In: *J. Quant. Spectrosc. Radiat. Transfer* 19, pp. 239–245. DOI: 10.1016/0022-4073(78)90059-6 (cit. on p. 11).

Grussie, F., M. H. Berg, K. N. Crabtree, S. Gärtner, B. J. McCall, S. Schlemmer, et al. (2012). "The Low-temperature Nuclear Spin Equilibrium of H_3^+ in Collisions with H_2." In: *Astrophys. J.* 759, p. 21. DOI: 10.1088/0004-637X/759/1/21 (cit. on p. 15).

Hejduk, M. (2013). "Reactions of Hydrogen Molecules with Ions and Recombination of H_3^+ Ions with Electrons at Cryogenic Temperatures." PhD thesis. Charles University in Prague (cit. on pp. 28, 30, 47).

Hejduk, M., P. Dohnal, J. Varju, P. Rubovič, T. Kotrík, R. Plašil, et al. (2012). "Nuclear spin state-resolved cavity ring-down spectroscopy diagnostics of a low-temperature H_3^+-dominated plasma." In: *Plasma Sources Sci. Technol.* 21, p. 024002. DOI: 10.1088/0963-0252/21/2/024002 (cit. on p. 14).

Herbst, E. (2000). "The astrochemistry of H_3^+." In: *Phil. Trans. R. Soc. Lond. A* 358, p. 2523. DOI: 10.1098/rsta.2000.0665 (cit. on p. 15).

Herbst, E. and W. Klemperer (1973). "The Formation and Depletion of Molecules in Dense Interstellar Clouds." In: *Astrophys. J.* 185, p. 505. DOI: 10.1086/152436 (cit. on p. 13).

Hiraoka, K. and T. Mori (1989). "Formation and stabilities of cluster ions Ar_n^+." In: *J. Chem. Phys.* 90, pp. 7143–7149. DOI: 10.1063/1.456245 (cit. on p. 50).

Hiraoka, K. (1987). "A determination of the stabilities of $H_3^+(H_2)_n$ with $n = 1$–9 from measurements of the gasphase ion equilibria $H_3^+(H_2)_{n-1} = H_3^+(H_2)_n$." In: *J. Chem. Phys* 87.7, pp. 4048–4055. DOI: 10.1063/1.452909 (cit. on pp. 74, 76).

Hlavenka, P. (2007). "The spectroscopic study of cold ions in plasma and ion trap." PhD thesis. Charles University in Prague (cit. on p. 25).

Hogness, T. R. and E. G. Lunn (1925). "The Ionization of Hydrogen by Electron Impact as Interpreted by Positive Ray Analysis." In: *Phys. Rev.* 26, p. 44. DOI: 10.1103/PhysRev.26.44 (cit. on p. 13).

Hus, H., F. Youssif, A. Sen, and J. B. A. Mitchell (1988). "Merged-beam studies of the dissociative recombination of H_3^+ ions with low internal energy." In: *Phys. Rev. A* 38, p. 658. DOI: 10.1103/PhysRevA.38.658 (cit. on pp. 16, 17).

Hutchinson, I. H. (2002). *Principles of Plasma Diagnostics*. Cambridge University Press, Cambridge (cit. on p. 34).

Ikezoe, Y., S. Matsuoka, M. Takebe, and A. Viggiano (1987). *Gas Phase Ion-Molecule Reaction Rate Constants*. The Mass Spectroscopy Society, Tokyo (cit. on pp. 7, 43, 50).

Indriolo, N. and B. J. McCall (2012). "Investigating the Cosmic-Ray Ionization Rate in the Galactic Diffuse Interstellar Medium through Observations of H_3^+." In: *Astrophys. J.* 745, p. 91. DOI: 10.1088/0004-637X/745/1/91 (cit. on p. 15).

Jensen, M. J., H. B. Pedersen, C. P. Safvan, K. Seiersen, X. Urbain, and L. H. Andersen (2001). "Dissociative recombination and excitation of H_3^+." In: *Phys. Rev. A* 63, p. 052701. DOI: 10.1103/PhysRevA.63.052701 (cit. on p. 17).

Johnsen, R. (1987). "Microwave afterglow measurements of the dissociative recombination of molecular ions with electrons." In: *Int. J. Mass Spectrom. Ion Processes* 81, p. 67. DOI: 10.1016/0168-1176(87)80006-X (cit. on pp. 42, 45).

— (2005). "A critical review of H_3^+ recombination studies." In: *J. Phys.: Conf. Ser.* 4, p. 83. DOI: 10.1088/1742-6596/4/1/011 (cit. on p. 55).

— (2011). "Discrepancies between H_3^+ recombination rate coefficients measured in ion storage rings, afterglows, and theory. Are they "real" or "pparent"?" In: *J. Phys.: Conf. Ser.* 300, p. 012024. DOI: 10.1088/1742-6596/300/1/012024 (cit. on p. 55).

Johnsen, R. and M. A. Biondi (1979). "Mobilities of singly and doubly charged rare-gas ions in helium and in neon." In: *Phys. Rev. A* 20, p. 221. DOI: 10.1103/PhysRevA.20.221 (cit. on p. 45).

Johnsen, R. and S. L. Guberman (2010). "Chapter 3 - Dissociative Recombination of H_3^+ Ions with Electrons: Theory and Experiment." In: *Advances in Atomic, Molecular, and Optical Physics*. Ed. by P. B. E. Arimondo and C. Lin. Vol. 59. Advances In Atomic, Molecular, and Optical Physics. Academic Press, pp. 75–128. DOI: http://dx.doi.org/10.1016/S1049-250X(10)59003-7 (cit. on pp. 5, 16).

Johnsen, R., C. Huang, and M. A. Biondi (1976). "Threebody association reactions of H^+ and H_3^+ ions in hydrogen from 135 to 300 K." In: *J. Chem. Phys.* 65, p. 1539. DOI: 10.1063/1.433209 (cit. on p. 57).

Johnsen, R., M. T. Leu, and M. A. Biondi (1973). "Studies of Nonresonant Charge Transfer between Atomic Ions and Atoms." In: *Phys. Rev. A* 8, pp. 1808–1813. DOI: 10.1103/PhysRevA.8.1808 (cit. on pp. 43, 50).

Johnsen, R., P. Rubovič, P. Dohnal, M. Hejduk, R. Plašil, and J. Glosík (2013). "Ternary Recombination of H_3^+ and D_3^+ with Electrons in He–H_2 (D_2) Plasmas at Temperatures from 50 to 300 K." In: *J. Phys. Chem. A* 117.39, pp. 9477–9485. DOI: 10.1021/jp311978n (cit. on pp. 59–61, 77).

Kasner, W. H. and M. A. Biondi (1968). "Temperature Dependence of the Electron–O_2^+-Ion Recombination Coefficient." In: *Phys. Rev.* 174, p. 139. DOI: 10.1103/PhysRev.174.139 (cit. on p. 43).

Killian, T. C., S. Kulin, S. D. Bergeson, L. A. Orozco, C. Orzel, and S. L. Rolston (1999). "Creation of an Ultracold Neutral Plasma." In: *Phys. Rev. Lett.* 83, pp. 4776–4779. DOI: 10.1103/PhysRevLett.83.4776 (cit. on p. 12).

Kokoouline, V. and C. H. Greene (2003). "Unified theoretical treatment of dissociative recombination of D_{3h} triatomic ions: Application to H_3^+ and D_3^+." In: *Phys. Rev. A* 68, p. 012703. DOI: 10.1103/PhysRevA.68.012703x (cit. on p. 18).

— (2005). "Theoretical study of dissociative recombination of C_{2v} triatomic ions: Application to H_2D^+ and D_2H^+." In: *Phys. Rev. A* 72, p. 022712. DOI: 10.1103/PhysRevA.72.022712 (cit. on p. 18).

Korolov, I. (2008). "Recombination and Reactions of Ions at Thermal Energies." PhD thesis. Charles University in Prague (cit. on pp. 16, 42, 50, 55).

Korolov, I., T. Kotrík, R. Plašil, J. Varju, M. Hejduk, and J. Glosík (2008). "Application of Langmuir Probe in Recombination Dominated Afterglow Plasma." In: *Contrib. Plasma Phys.* 48(5-7), p. 521. DOI: 10.1002/ctpp.200810084 (cit. on pp. 35, 39).

Kotrík, T. (2013). "Electron-Ion Recombination at Temperatures Below 300 K." PhD thesis. Charles University in Prague (cit. on pp. 16, 19, 34, 35, 40, 50, 52, 55).

Kotrík, T., P. Dohnal, I. Korolov, R. Plašil, Š. Roučka, J. Glosík, et al. (2010). "Temperature dependence of binary and ternary recombination of D_3^+ ions with electrons." In: *J. Chem. Phys.* 133, p. 034305. DOI: 10.1063/1.3457940 (cit. on pp. 18, 61, 64).

Kotrík, T., P. Dohnal, Š. Roučka, P. Jusko, R. Plašil, J. Glosík, et al. (2011a). "Collisional-radiative recombination Ar^+ + e + e: Experimental study at 77-180 K." In: *Phys. Rev. A* 83, p. 032720. DOI: 10.1103/PhysRevA.83.032720 (cit. on pp. 12, 45, 46, 49, 52, 54).

Kotrík, T., P. Dohnal, P. Rubovič, R. Plašil, Š. Roučka, S. Opanasiuk, et al. (2011b). "Cryo-FALP study of collisional-radiative recombination of Ar^+ ions at 40–200 K." In: *Eur. Phys. J. Appl. Phys.* 56, p. 24011. DOI: 10.1051/epjap/2011110158 (cit. on pp. 12, 34, 35, 41, 42, 52, 54).

Kreckel, H., M. Motsch, J. Mikosch, J. Glosík, R. Plašil, S. Altevogt, et al. (2005). "High-Resolution Dissociative Recombination of Cold H_3^+ and First Evidence for Nuclear Spin Effects." In: *Phys. Rev. Lett.* 95, p. 263201. DOI: 10.1103/PhysRevLett.95.263201 (cit. on p. 18).

Kreckel, H., O. Novotný, K. N. Crabtree, H. Buhr, A. Petrignani, B. A. Tom, et al. (2010). "High-resolution storage-ring measurements of the dissociative recombination of H_3^+ using a supersonic expansion ion source." In: *Phys. Rev. A* 82, p. 042715. DOI: 10.1103/PhysRevA.82.042715 (cit. on p. 18).

Kreckel, H., A. Petrignani, O. Novotný, K. Crabtree, H. Buhr, B. McCall, et al. (2012). "Review article: Storage ring measurements of the dissociative recombination of H_3^+." In: *Phil. Trans. R. Soc. A* 370, p. 1471. DOI: 10.1098/rsta.2012.0019 (cit. on p. 18).

Langmuir, I. (1923). "The pressure effect and other phenomena in gaseous discharges." In: *J. Franklin Inst.* 196, p. 751. DOI: 10.1016/S0016-0032(23)90859-8 (cit. on p. 32).

Larsson, M., H. Danared, J. R. Mowat, P. Sigray, G. Sundström, L. Broström, et al. (1993). "Direct high-energy neutral-channel dissociative recombination of cold H_3^+ in an ion storage ring." In: *Phys. Rev. Lett.* 70, p. 430. DOI: 10.1103/PhysRevLett.70.430 (cit. on p. 16).

Larsson, M. and A. Orel (2008). *Dissociative Recombination of Molecular Ions*. Cambridge University Press, Cambridge (cit. on pp. 4, 8, 16, 18).

Laubé, S., A. Le Padellec, O. Sidko, C. Rebrion-Rowe, J. B. A. Mitchell, and B. R. Rowe (1998). "New FALP-MS measurements of H_3^+, D_3^+ and HCO^+ dissociative recombination." In: *J. Phys. B-At. Mol. Opt.* 31, pp. 2111–2128. DOI: 10.1088/0953-4075/31/9/023 (cit. on p. 17).

Le Padellec, A., M. Larsson, H. Danared, A. Larson, J. R. Peterson, S. Rosén, et al. (1998). "A Storage Ring Study of Dissociative Excitation and Recombination of D_3^+." In: *Phys. Scr.* 57, p. 215. DOI: 10.1088/0031-8949/57/2/010 (cit. on p. 64).

Leu, M. T., M. A. Biondi, and R. Johnsen (1973). "Measurements of Recombination of Electrons with H_3^+ and H_5^+ Ions." In: *Phys. Rev. A* 8, pp. 413–419. DOI: 10.1103/PhysRevA.8.413 (cit. on pp. 16, 17).

Lindinger, W. and D. Albritton (1975). "Mobilities of various massidentified positive ions in helium and argon." In: *J. Chem. Phys.* 62, p. 3517. DOI: 10.1063/1.430988 (cit. on p. 45).

Lindsay, C. M. and B. J. McCall (2001). "Comprehensive Evaluation and Compilation of H_3^+ Spectroscopy." In: *J. Mol. Spectrosc.* 210, p. 60. DOI: 10.1006/jmsp.2001.8444 (cit. on pp. 13, 14, 21).

Macdonald, J. A., M. A. Biondi, and R. Johnsen (1984). "Recombination of electrons with H_3^+ and H_5^+ Ions." In: *Planet, Space Sci.* 32, pp. 651–654. DOI: 10.1016/0032-0633(84)90117-X (cit. on pp. 16, 17, 74).

Macko, P., G. Bánó, P. Hlavenka, R. Plašil, V. Poterya, A. Pysanenko, et al. (2004). "Afterglow studies of $H_3^+(v = 0)$ recombination using time resolved cw-diode laser cavity ring-down spectroscopy." In: *Int. J. Mass Spectrom.* 233, p. 299. DOI: 10.1016/j.ijms.2003.12.035 (cit. on pp. 17, 55).

Mahdavi, M. R., J. B. Hasted, and M. M. Nakshbandi (1971). "Electron-ion recombination measurements in the flowing afterglow." In: *J. Phys. B: Atom. Molec. Phys.* 4, p. 1726. DOI: 10.1088/0022-3700/4/12/020 (cit. on p. 7).

Mansbach, P. and J. Keck (1969). "Monte Carlo Trajectory Calculations of Atomic Excitation and Ionization by Thermal Electrons." In: *Phys. Rev.* 181, pp. 275–289. DOI: 10.1103/PhysRev.181.275 (cit. on pp. 11, 12, 54).

Martin, D. W., E. W. McDaniel, and M. L. Meeks (1961). "On the Possible Occurence of H_3^+ in Interstellar Space." In: *Astrophys. J.* 134, p. 1012. DOI: 10.1086/147232 (cit. on p. 13).

Mason, E. and E. McDaniel (1988). *Transport Properties of Ions in Gases*. Wiley, New York (cit. on p. 44).

Mathur, D., S. U. Khan, and J. B. Hasted (1978). "Dissociative recombination in low-energy e-H_2^+ and e-H_3^+ collisions." In: *J. Phys. B: At. Mol. Phys.* 11, p. 3615. DOI: 10.1088/0022-3700/11/20/021 (cit. on p. 17).

McCall, B. J. (2000). "Laboratory spectroscopy of H_3^+." In: *Phil. Trans. R. Soc. Lond. A* 358, p. 2385. DOI: 10.1098/rsta.2000.0655 (cit. on p. 13).

— (2006). "Dissociative recombination of cold H_3^+ and its interstellar implications." In: *Phil. Trans. R. Soc. A* 364, p. 2953. DOI: 10.1098/rsta.2006.1876 (cit. on p. 13).

McCall, B. J., T. R. Geballe, K. H. Hinkle, and T. Oka (1998). "Detection of H_3^+ in the Diffuse Interstellar Medium Toward Cygnus OB2 No. 12." In: *Science* 279, p. 1910. DOI: 10.1126/science.279.5358.1910 (cit. on p. 15).

McCall, B. J., A. J. Honeycutt, R. J. Saykally, N. Djuric, G. H. Dunn, J. Semaniak, et al. (2004). "Dissociative recombination of rotationally cold H_3^+." In: *Phys. Rev. A* 70, p. 052716. DOI: 10.1103/PhysRevA.70.052716 (cit. on pp. 17, 18, 61, 62).

McCall, B. J., A. J. Honeycutt, R. J. Saykally, T. R. Geballe, N. Djuric, G. H. Dunn, et al. (2003). "An enhanced cosmic-ray flux towards ζ Persei inferred from a laboratory study of the H_3^+–e^- recombination rate." In: *Nature* 422, p. 500. DOI: 10.1038/nature01498 (cit. on p. 18).

McGowan, J. W., P. M. Mul, V. S. D'Angelo, J. B. A. Mitchell, P. Defrance, and H. R. Froelich (1979). "Energy Dependence of Dissociative Recombination below 0.08 eV Measured with (Electron-Ion) Merged-Beam Technique." In: *Phys. Rev. Lett.* 42, p. 373. DOI: 10.1103/PhysRevLett.42.373 (cit. on p. 17).

McLain, J. L., V. Poterya, C. D. Molek, L. M. Babcock, and N. G. Adams (2004). "Flowing Afterglow Studies of the Temperature Dependencies for Dissociative Recombination of O_2^+, CH_5^+, $C_2H_5^+$, and $C_6H_7^+$ with Electrons." In: *J. Phys. Chem. A* 108, pp. 6704–6708. DOI: 10.1021/jp040215l (cit. on pp. 42, 45).

Michels, H. H. and R. H. Hobbs (1984). "Low-temperature dissociative recombination of e + H_3^+." In: *Astrophys. J.* 286, p. L27. DOI: 10.1086/184378 (cit. on p. 16).

Midey, A. J. and A. A. Viggiano (1998). "Rate constants for the reaction of Ar^+ with O_2 and CO as a function of temperature from 300 to 1400 K: Derivation of rotational and vibrational energy effects." In: *J. Chem. Phys.* 109, pp. 5257–5263. DOI: 10.1063/1.477142 (cit. on p. 43).

Mikosch, J., H. Kreckel, R. Wester, J. Glosík, R. Plašil, D. Gerlich, et al. (2004). "Action spectroscopy and temperature diagnostics of H_3^+ by chemical probing." In: *J. Chem. Phys.* 121(22), pp. 11030–11037. DOI: 10.1063/1.1810512 (cit. on p. 14).

Miller, S., N. Achilleos, G. . Ballester, T. R. Geballe, R. D. Joseph, R. Prangé, et al. (2000). "The role of H_3^+ in planetary atmospheres." In: *Phil. Trans. R. Soc. Lond. A* 358, p. 2485. DOI: 10.1098/rsta.2000.0662 (cit. on p. 14).

Mitchell, J. B. A. (1990). "The dissociative recombination of molecular ions." In: *Phys. Rep.* 186, p. 215. DOI: 10.1016/0370-1573(90)90159-Y (cit. on pp. 16, 77).

Mott-Smith, H. M. and I. Langmuir (1926). "The Theory of Collectors in Gaseous Discharges." In: *Phys. Rev.* 28, p. 727. DOI: 10.1103/PhysRev.28.727 (cit. on pp. 32, 34).

Neale, L., S. Miller, and J. Tennyson (1996). "Spectroscopic Properties of the H_3^+ Molecule: A New Calculated Line List." In: *Astrophys. J.* 464, p. 516. DOI: 10.1086/177341 (cit. on pp. 14, 25).

Novotný, O. (2006). "Experimental study of electron-ion recombination using Storage ring and Afterglow techniques." PhD thesis. Charles University in Prague (cit. on p. 55).

Novotný, O., R. Plašil, A. Pysanenko, I. Korolov, and J. Glosík (2006). "The recombination of D_3^+ and D_5^+ ions with electrons in deuterium containing plasma." In: *J. Phys. B-At. Mol. Opt.* 39, pp. 2561–2569. DOI: 10.1088/0953-4075/39/11/019 (cit. on p. 57).

Oka, T. (1983). "The H_3^+ Ion." In: *Molecular Ions: Spectroscopy, Structure, and Chemistry*. Ed. by T. Miller and V. Bondybey. North Holland, New York, p. 73 (cit. on p. 13).

Oka, T. (1980). "Observation of the Infrared Spectrum of H_3^+." In: *Phys. Rev. Lett.* 45 (7), pp. 531–534. DOI: 10.1103/PhysRevLett.45.531 (cit. on p. 13).

Okada, T. and M. Sugawara (1993). "Microwave determination of the coefficient of dissociative recombination of Ar_2^+ in Ar afterglow." In: *J. Phys. D: Appl. Phys.* 26, pp. 1680–1686. DOI: 10.1088/0022-3727/26/10/019 (cit. on p. 50).

Pagani, L., C. Vastel, E. Hugo, V. Kokoouline, C. H. Greene, A. Bacmann, et al. (2009). "Chemical modeling of L183 (L134N): an estimate of the ortho/para H_2 ratio." In: *Astron. Astrophys.* 494, p. 623. DOI: 10.1051/0004-6361:200810587 (cit. on pp. 64, 65).

Parise, B., A. Belloche, F. Du, R. Güsten, and K. Menten (2011). "Extended emission of D_2H^+ in a prestellar core." In: *Astron. Astrophys.* 526, A31. DOI: 10.1051/0004-6361/201015475 (cit. on p. 20).

Peart, B. and K. T. Dolder (1974). "Measurements of the dissociative recombination of H_3^+ ions." In: *J. Phys. B: At. Mol. Phys.* 7, p. 1948. DOI: 10.1088/0022-3700/7/14/018 (cit. on p. 17).

Persson, K.-B. and S. C. Brown (1955). "Electron Loss Process in the Hydrogen Afterglow." In: *Phys. Rev.* 100, p. 729. DOI: 10.1103/PhysRev.100.729 (cit. on p. 17).

Petrignani, A., S. Altevogt, M. H. Berg, D. Bing, M. Grieser, J. Hoffmann, et al. (2011). "Resonant structure of low-energy H_3^+ dissociative recombination." In: *Phys. Rev. A* 83, p. 032711. DOI: 10.1103/PhysRevA.83.032711 (cit. on pp. 5, 18).

Peverall, R., S. Rosén, J. R. Peterson, M. Larsson, A. Al-Khalili, L. Vikor, et al. (2001). "Dissociative recombination and excitation of O_2^+: Cross sections, product yields and implications for studies of ionospheric airglows." In: *J. Chem. Phys.* 114, p. 6679. DOI: 10.1063/1.1349079 (cit. on pp. 42, 45).

Pfau, S. and M. Tichý (2007). "Low Temperature Plasmas; Fundamentals, Technologies, and Techniques, Volume 1." In: ed. by R. Hippler, H. Kersten, M. Schmidt, and K. Schoenbach. WILEY-VCH Verlag, Berlin. Chap. Langmuir probe diagnostics of low-temperature plasmas, pp. 207–248 (cit. on p. 33).

Pitaevskii, L. P. (1962). "Electron Recombination in a Monatomic Gas." In: *Sov. Phys.-JETP* 1, p. 919 (cit. on pp. 9, 10, 52, 53).

Plašil, R. (2003). "Rekombinace molekulárních iontů v dohasínajícím plazmatu." PhD thesis. Charles University in Prague (cit. on p. 55).

Plašil, R., J. Glosík, V. Poterya, P. Kudrna, J. Rusz, M. Tichý, et al. (2002). "Advanced integrated stationary afterglow method for experimental study of recombination of processes of H_3^+ and D_3^+ ions with electrons." In: *Int. J. Mass Spectrom.* 218(2), pp. 105–130. DOI: 10.1016/S1387-3806(02)00714-5 (cit. on pp. 6, 16, 17, 23, 55).

Pohl, T., D. Vrinceanu, and H. R. Sadeghpour (2008). "Rydberg Atom Formation in Ultracold Plasmas: Small Energy Transfer with Large Consequences." In: *Phys. Rev. Lett.* 100, p. 223201. DOI: 10.1103/PhysRevLett.100.223201 (cit. on p. 12).

Poterya, V., J. Glosík, R. Plašil, M. Tichý, P. Kudrna, and A. Pysanenko (2002). "Recombination of D_3^+ Ions in the Afterglow of a He-Ar-D_2 Plasma." In: *Phys. Rev. Lett.* 88, p. 044802. DOI: 10.1103/PhysRevLett.88.044802 (cit. on p. 55).

Pratt, S. T. and C. Jungen (2011). "Dissociative Recombination of Small Polyatomic Molecules." In: *J. Phys.: Conf. Ser.* 300, p. 012019. DOI: doi:10.1088/1742-6596/300/1/012019 (cit. on pp. 62, 64).

Ramanlal, J. and J. Tennyson (2004). "Deuterated hydrogen chemistry: partition functions, equilibrium constants and transition intensities for the H_3^+ system." In: *Mon. Not. R. Astron. Soc.* 354, p. 161. DOI: 10.1111/j.1365-2966.2004.08178.x (cit. on p. 21).

Rennick, C. J., N. Saquet, J. P. Morrison, J. Ortega-Arroyo, P. Godin, L. Fu, et al. (2011). "Dissociative recombination and the decay of a molecular ultracold plasma." In: *J. Phys.: Conf. Ser.* 300, p. 012005. DOI: 10.1088/1742-6596/300/1/012005 (cit. on p. 12).

Richardson, J. M. and R. B. Holt (1951). "Decay of the Hydrogen Discharge." In: *Phys. Rev.* 81, p. 153. DOI: 10.1103/PhysRev.81.153.2 (cit. on p. 17).

Romanini, D., A. A. Kachanov, N. Sadeghi, and F. Stoeckel (1997). "CW cavity ring down spectroscopy." In: *Chem. Phys. Lett.* 264 (3-4), pp. 316–322. DOI: 10.1016/S0009-2614(96)01351-6 (cit. on p. 27).

Rothman, L. S., C. P. Rinsland, A. Goldman, S. T. Massie, D. P. Edwards, J.-M. Flaud, et al. (1998). "The HITRAN Molecular Spectroscopic Database and HAWKS (HITRAN Atomspheric Workstation): 1996 Edition." In: *J. Quant. Spectrosc. Radiat. Transfer* 60, p. 665. DOI: 10.1016/S0022-4073(98)00078-8 (cit. on p. 25).

Rubovič, P., P. Dohnal, T. Kotrík, R. Plašil, and J. Glosík (2012). "Dissociative Recombination of O_2^+ Ions with Electrons." In: *WDS'12 Proceedings of Contributed Papers: Part II–Physics of Plasmas and Ionized Media*. Ed. by J. Šafránková and J. Pavlů. Matfyzpress, Prague, pp. 7–11 (cit. on pp. 43, 44).

Rubovič, P., T. Kotrík, P. Dohnal, Š. Roučka, M. Hejduk, S. Opanasiuk, et al. (2011). "Swarm Experiments at 40–100 K, Cryo–FALP." In: *WDS'11 Proceedings of Contributed Papers: Part II–Physics of Plasmas and Ionized Media*. Ed. by J. Šafránková and J. Pavlů. Matfyzpress, Prague, pp. 146–151 (cit. on p. 37).

Rubovič, P., P. Dohnal, M. Hejduk, R. Plašil, and J. Glosík (2013). "Binary Recombination of H_3^+ and D_3^+ Ions with Electrons in Plasma at 50–230 K." In: *J. Phys. Chem. A* 117.39, pp. 9626–9632. DOI: 10.1021/jp3123192 (cit. on pp. 17, 56–59, 61–65, 77).

Skrzypkowski, M. P., R. Johnsen, R. E. Rosati, and M. F. Golde (2004). "Flowing-afterglow measurements of collisional radiative recombination of argon ions." In: *Chem. Phys.* 296, p. 23. DOI: 10.1016/j.chemphys.2003.09.032 (cit. on pp. 12, 54).

Smirnov, B. M. (1977). "Cluster ions in gases." In: *Sov. Phys. Usp.* 20, p. 119. DOI: 10.1070/PU1977v020n02ABEH005325 (cit. on pp. 43, 50).

— (1984). *Complex Ions*. Nauka, Moscow (cit. on p. 57).

Smith, D. and N. G. Adams (1984). "Dissociative recombination coefficients for H_3^+, HCO^+, N_2H^+, and CH_5^+ at low temperature - Interstellar implications." In: *Astrophys. J.* 284, p. L13. DOI: 10.1086/184342 (cit. on p. 16).

Smith, D., N. G. Adams, A. G. Dean, and M. J. Church (1975). "The application of Langmuir probes to the study of flowing afterglow plasmas." In: *J. Phys. D: Appl. Phys.* 8, p. 141. DOI: 10.1088/0022-3727/8/2/007 (cit. on p. 7).

Smith, D. and P. Španěl (1993a). "Dissociative recombination of H_3^+ and some other interstellar ions: a controversy resolved." In: *Int. J. Mass Spectrom.* 129, p. 163. DOI: 10.1016/0168-1176(93)87040-Y (cit. on pp. 16, 17).

— (1993b). "Dissociative recombination of H_3^+. Experiment and theory reconciled." In: *Chem. Phys. Lett.* 211, p. 454. DOI: 10.1016/0009-2614(93)87090-P (cit. on pp. 16, 17).

Smith, J. R., N. Hershkowitz, and P. Coakley (1979). "Inflectionpoint method of interpreting emissive probe characteristics." In: *Rev. Sci. Instrum.* 50, p. 210. DOI: 10.1063/1.1135789 (cit. on p. 32).

Španěl, P., L. Dittrichová, and D. Smith (1993). "FALP studies of the dissociative recombination coefficients for O_2^+ and NO^+ within the electron temperature range 300–2000 K." In: *Int. J. Mass Spectrom.* 129, pp. 183–191. DOI: 10.1016/0168-1176(93)87041-P (cit. on pp. 41–45).

Stark, R., F. F. S. van der Tak, and E. F. van Dishoeck (1999). "Detection of Interstellar H_2D^+ Emission." In: *Astrophys. J.* 521, p. L67. DOI: 10.1086/312182 (cit. on p. 20).

Stevefelt, J., J. Boulmer, and J. Delpech (1975). "Collisional-radiative recombination in cold plasmas." In: *Phys. Rev. A* 12, p. 1246. DOI: 10.1103/PhysRevA.12.1246 (cit. on pp. 11, 50, 52, 63).

Sundström, G., J. R. Mowat, H. Danared, S. Datz, L. Broström, A. Filevich, et al. (1994). "Destruction Rate of H_3^+ by Low-Energy Electrons Measured in a Storage-Ring Experiment." In: *Science* 263, p. 5148. DOI: 10.1126/science.263.5148.785 (cit. on pp. 16, 17).

Tam, S. and M. E. Fajardo (1999). "Ortho/para hydrogen converter for rapid deposition matrix isolation spectroscopy." In: *Rev. Sci. Instrum.* 70, p. 1926. DOI: 10.1063/1.1149734 (cit. on p. 47).

Tanabe, T., K. Chida, T. Watanabe, Y. Arakaki, H. Takagi, I. Katayama, et al. (2000). "Dissociative Recombination: Theory, Experiment and Applications IV." In: ed. by M. Larsson, J. Mitchell, and I. Schnei-

der. World Scientific, Singapore. Chap. Dissociative recombination at the TARN II storage ring, p. 170 (cit. on p. 17).

Tennyson, J. (2011). *Molecular Physics and Astrophysics Group Homepage*. URL: http://www.tampa.phys.ucl.ac.uk/ftp/astrodata/h3+/ (cit. on p. 25).

— (2012). In: *private communication* (cit. on p. 21).

Thomson, J. J. (1913). "Rays of Positive Electricity." In: *Proc. R. Soc. Lond. A* 89.607, pp. 1–20. DOI: 10.1098/rspa.1913.0057 (cit. on p. 13).

— (1924). "Recombination of gaseous ions, the chemical combination of gases, and monomolecular reactions." In: *Philos. Mag.* 47, p. 337. DOI: 10.1080/14786442408634372 (cit. on pp. 9, 10).

Tom, B. A., V. Zhaunerchyk, M. B. Wiczer, A. A. Mills, K. N. Crabtree, M. Kaminska, et al. (2009). "Dissociative recombination of highly enriched para-H_3^+." In: *J. Chem. Phys* 130, 031101, p. 031101. DOI: 10.1063/1.3065970 (cit. on p. 18).

Trafton, L., D. F. Lester, and K. L. Thompson (1993). "Detection of H_3^+ from Uranus." In: *Astrophys. J.* 405, p. 761. DOI: 10.1086/172404 (cit. on p. 14).

Urbain, X. (1999). "Dissociative recombination, Theory, Experiment and Applications IV." In: ed. by M. Larsson, J. B. A. Mitchell, and I. F. Schneider. World Scientific, Singapore, p. 131 (cit. on pp. 43, 50).

van Sonsbeek, R. J., R. Cooper, and R. N. Bhave (1992). "Pulse radiolysis studies of ion–electron recombination in helium. Pressure and temperature effects." In: *J. Chem. Phys.* 97, pp. 1800–1808. DOI: 10.1063/1.463167 (cit. on pp. 11, 52, 53).

Varju, J. (2011). "Study of H_3^+ Recombination in Selected Quantum States." PhD thesis. Charles University in Prague (cit. on pp. 25, 28, 29, 47).

Varju, J., M. Hejduk, P. Dohnal, M. Jílek, T. Kotrík, R. Plašil, et al. (2011). "Nuclear Spin Effect on Recombination of H_3^+ Ions with Electrons at 77 K." In: *Phys. Rev. Lett.* 106, p. 203201. DOI: 10.1103/PhysRevLett.106.203201 (cit. on pp. 18, 35, 55, 60, 62, 71, 72).

Varnerin Jr., L. J. (1951). "Electron Recombination and Collision Cross-Section Measurements in Hydrogen." In: *Phys. Rev.* 84, p. 563. DOI: 10.1103/PhysRev.84.563 (cit. on p. 17).

Vastel, C., T. G. Phillips, and H. Yoshida (2004). "Detection of D_2H^+ in the Dense Interstellar Medium." In: *Astrophys. J.* 606, p. L127. DOI: 10.1086/421265 (cit. on pp. 20, 21).

Ventrudo, B. F., D. T. Cassidy, Z. Y. Guo, S. Joo, S. S. Lee, and T. Oka (1994). "Near infrared $3\nu_2$ overtone band of H_3^+." In: *J. Chem. Phys.* 100, p. 6263. DOI: 10.1063/1.467088 (cit. on p. 14).

Viehland, L., A. Viggiano, and E. Mason (1991). "The Ar^+–He interaction potential and distribution function effects on swarm measurements of $Ar^+ + N_2$ reactionrate coefficients using helium buffer gas." In: *J. Chem. Phys.* 95, p. 7286. DOI: 10.1063/1.461406 (cit. on p. 45).

Villinger, H., J. H. Futrell, F. Howorka, N. Duric, and W. Lindinger (1982). "The proton transfer from ArH^+ to various neutrals." In: *J. Chem. Phys.* 76, p. 3529. DOI: 10.1063/1.443454 (cit. on p. 57).

Walls, F. L. and G. H. Dunn (1974). "Measurement of total cross sections for electron recombination with NO^+ and O_2^+ using ion storage techniques." In: *J. Geophys. Res.* 79, p. 1911. DOI: 10.1029/JA079i013p01911 (cit. on pp. 42, 45).

Watson, W. D. (1973). "The Rate of Formation of Interstellar Molecules by Ion-Molecule Reactions." In: *Astrophys. J.* 183.2, p. L17. DOI: 10.1086/181242 (cit. on p. 13).

Wojcik, M. and M. Tachiya (1999). "Electron-ion recombination rate constant in dense gaseous argon and krypton." In: *J. Chem. Phys.* 110, pp. 10016–10023. DOI: 10.1063/1.478875 (cit. on p. 10).

— (2000). "Electron-ion recombination in dense rare gases: Energy diffusion theory vs simulation." In: *J. Chem. Phys.* 112, pp. 3845–3850. DOI: 10.1063/1.480532 (cit. on p. 10).

Wolf, A., H. Kreckel, L. Lammich, D. Strasser, J. Mikosch, J. Glosík, et al. (2006). "Effects of molecular rotation in low-energy electron collisions of H_3^+." In: *Phil. T. Roy. Soc. A* 364.1848, pp. 2981–2997. DOI: 10.1098/rsta.2006.1881 (cit. on p. 18).

Yencha, A. J. (1984). "Penning Ionization and Related Processes." In: *Electron Spectroscopy: Theory, Techniques and Applications. Volume 5*. Ed. by C. R. Bundle and A. D. Baker. Academic Press, London (cit. on p. 50).

Zymak, I., M. Hejduk, D. Mulin, R. Plašil, J. Glosík, and D. Gerlich (2013). "Low-Temperature Ion Trap Studies of $N^+(^3P_{ja}) + H_2(j) \rightarrow NH^+ + H$." In: *Astrophys. J.* 768, p. 86. DOI: 10.1088/0004-637X/768/1/86 (cit. on p. 47).

LIST OF PUBLICATIONS

PUBLICATIONS IN IMPACTED JOURNALS

Dohnal, P., M. Hejduk, P. Rubovič, J. Varju, Š. Roučka, R. Plašil, et al. (2012a). "Binary and ternary recombination of D_3^+ ions at 80–130 K: Application of laser absorption spectroscopy." In: *J. Chem. Phys.* 137.19, p. 194320. DOI: 10.1063/1.4767396.

Dohnal, P., M. Hejduk, J. Varju, P. Rubovič, Š. Roučka, T. Kotrík, et al. (2012b). "Binary and ternary recombination of para-H_3^+ and ortho-H_3^+ with electrons: State selective study at 77–200 K." In: *J. Chem. Phys.* 136.24, p. 244304. DOI: 10.1063/1.4730162.

Dohnal, P., M. Hejduk, J. Varju, P. Rubovič, Š. Roučka, T. Kotrík, et al. (2012c). "Binary recombination of para- and ortho-H_3^+ with electrons at low temperatures." In: *Phil. Trans. R. Soc. A* 370.1978, pp. 5101–5108. DOI: 10.1098/rsta.2012.0097.

Dohnal, P., P. Rubovič, T. Kotrík, M. Hejduk, R. Plašil, R. Johnsen, et al. (2013). "Collisional-radiative recombination of Ar^+ ions with electrons in ambient helium at temperatures from 50 K to 100 K." In: *Phys. Rev. A* 87.5, p. 052716. DOI: 10.1103/PhysRevA.87.052716.

Hejduk, M., P. Dohnal, J. Varju, P. Rubovič, T. Kotrík, R. Plašil, et al. (2012c). "Nuclear spin state-resolved cavity ring-down spectroscopy diagnostics of a low-temperature H_3^+–dominated plasma." In: *Plasma Sources Sci. Technol.* 21.2, p. 024002. DOI: 10.1088/0963-0252/21/2/024002.

Johnsen, R., P. Rubovič, P. Dohnal, M. Hejduk, R. Plašil, and J. Glosík (2013). "Ternary Recombination of H_3^+ and D_3^+ with Electrons in He–H_2 (D_2) Plasmas at Temperatures from 50 to 300 K." In: *J. Phys. Chem. A* 117.39, pp. 9477–9485. DOI: 10.1021/jp311978n.

Kotrík, T., P. Dohnal, P. Rubovič, R. Plašil, Š. Roučka, S. Opanasiuk, et al. (2011b). "Cryo-FALP study of collisional-radiative recombination of Ar^+ ions at 40–200 K." In: *Eur. Phys. J.-Appl. Phys.* 56.2, p. 24011. DOI: 10.1051/epjap/2011110158.

Rubovič, P., P. Dohnal, M. Hejduk, R. Plašil, and J. Glosík (2013). "Binary Recombination of H_3^+ and D_3^+ Ions with Electrons in Plasma at 50–230 K." In: *J. Phys. Chem. A* 117.39, pp. 9626–9632. DOI: 10.1021/jp3123192.

Zymak, I., P. Jusko, Š. Roučka, R. Plašil, P. Rubovič, D. Gerlich, et al. (2011). "Ternary association of H^+ ion with H_2 at 11 K, experimental study." In: *Eur. Phys. J.-Appl. Phys.* 56.2, p. 24010. DOI: 10.1051/epjap/2011110172.

PUBLICATIONS IN OTHER PEER-REVIEWED JOURNALS

Hejduk, M., P. Dohnal, P. Rubovič, J. Varju, S. Opanasiuk, R. Plašil, et al. (2012b). "Equilibrium in Low Temperature H_3^+-dominated Plasma, Application of Cavity Ring-Down." In: *Acta Univ. Carolin. Math. Phys.* 53.1, pp. 51–59.

PUBLICATIONS IN CONFERENCE PROCEEDINGS

Dohnal, P., M. Hejduk, J. Varju, P. Rubovič, R. Plašil, and J. Glosík (2011). "Recombination of Para- and Ortho-H_3^+ with Electrons in Low Temperature Afterglow Plasma." In: *WDS'11 Proceedings of Contributed Papers: Part II–Physics of Plasmas and Ionized Media*. Ed. by J. Šafránková and J. Pavlů. Matfyzpress, Prague, pp. 169–174.

Dohnal, P., P. Rubovič, T. Kotrík, R. Plašil, and J. Glosík (2012d). "Recombination in He/Ar Afterglow Plasma at Low Temperatures." In: *WDS'12 Proceedings of Contributed Papers: Part II–Physics of Plasmas and Ionized Media*. Ed. by J. Šafránková and J. Pavlů. Matfyzpress, Prague, pp. 18–24.

Hejduk, M., P. Dohnal, P. Rubovič, S. Opanasiuk, R. Plašil, and J. Glosík (2012a). "Cavity ring-down spectroscopy of D_3^+-dominated low-temperature plasma." In: *39^{th} EPS Conference on Plasma Physics; 16^{th} International Congress on Plasma Physics*. Ed. by S. Ratynskaya, L. Blomberg, and A. Fasoli. Vol. 36F. Europhysics Conference Abstracts, P2.143.

Kotrík, T., P. Dohnal, S. Opanasiuk, P. Rubovič, Š. Roučka, R. Plašil, et al. (2011a). "New Cryo-FALP Experiment to Study Collisional Radiative Recombination of Ar^+ Ions at 40–200 K." In: *WDS'11 Proceedings of Contributed Papers: Part II–Physics of Plasmas and Ionized Media*. Ed. by J. Šafránková and J. Pavlů. Matfyzpress, Prague, pp. 136–140.

Kotrík, T., P. Dohnal, P. Rubovič, M. Hejduk, S. Opanasiuk, R. Plašil, et al. (2012). "Collisional radiative recombination of Ar^+ ions, experimental study at 40-300K." In: *J. Phys.: Conf. Ser.* 388, p. 062033. DOI: 10.1088/1742-6596/388/6/062033.

Opanasiuk, S., T. Kotrík, P. Dohnal, M. Hejduk, P. Rubovič, R. Plašil, et al. (2011). "Study of Collisional-radiative Recombination Using CRYO-FALP." In: *WDS'11 Proceedings of Contributed Papers: Part II–Physics of Plasmas and Ionized Media*. Ed. by J. Šafránková and J. Pavlů. Matfyzpress, Prague, pp. 141–145.

Rubovič, P., P. Dohnal, T. Kotrík, R. Plašil, and J. Glosík (2012a). "Dissociative Recombination of O_2^+ Ions with Electrons." In: *WDS'12 Proceedings of Contributed Papers: Part II–Physics of Plasmas and Ionized Media*. Ed. by J. Šafránková and J. Pavlů. Matfyzpress, Prague, pp. 7–11.

Rubovič, P., T. Kotrík, P. Dohnal, Š. Roučka, M. Hejduk, S. Opanasiuk, et al. (2011). "Swarm Experiments at 40–100 K, Cryo–FALP." In: *WDS'11 Proceedings of Contributed Papers: Part II–Physics of Plasmas and Ionized Media*. Ed. by J. Šafránková and J. Pavlů. Matfyzpress, Prague, pp. 146–151.

Rubovič, P., T. Kotrík, P. Dohnal, Š. Roučka, S. Opanasiuk, R. Plašil, et al. (2012b). "Recombination in low temperature Ar^+ dominated plasma." In: *39^{th} EPS Conference on Plasma Physics; 16^{th} International Congress on Plasma Physics*. Ed. by S. Ratynskaya, L. Blomberg, and A. Fasoli. Vol. 36F. Europhysics Conference Abstracts, P4.167.

LIST OF FIGURES

LIST OF TABLES

ACRONYMS

AISA *Advanced Integrated Stationary Afterglow*

CRDS *Cavity Ring Down Spectroscopy*

CRR *collisional-radiative recombination*

Cryo-FALP II *Cryogenic Flowing Afterglow with Langmuir Probe II*

DR *dissociative recombination*

E-CRR *electron-assisted collisional-radiative recombination*

EEDF *electron energy distribution function*

FA *Flowing Afterglow*

FALP *Flowing Afterglow with Langmuir Probe*

FWHM *full width at half maximum*

IB *Inclined Beam*

ISM *interstellar medium*

ISR *Ion Storage Ring*

IT *Ion Trap*

LN_2 *liquid nitrogen*

MB *Merged Beam*

N-CRR *neutral-assisted collisional-radiative recombination*

QMS *Quadrupole Mass Spectrometer*

SA *Stationary Afterglow*

SA-CRDS *Stationary Afterglow with Cavity Ring Down Spectroscopy*

SIFT *Selected Ion Flow Tube*

TE *thermal equilibrium*

UHV *ultra high vacuum*

Part II

ATTACHED ARTICLES

ARTICLE I

TITLE: Cryo-FALP study of collisional-radiative recombination of Ar^+ ions at 40–200 K

AUTHORS: Tomáš Kotrík, Petr Dohnal, Peter Rubovič, Radek Plašil, Štepán Roučka, Sergii Opanasiuk, and Juraj Glosík

JOURNAL: The European Physical Journal Applied Physics, 56:24011 (4 pp)

DATE: 28 October 2011

DOI: 10.1051/epjap/2011110158

Eur. Phys. J. Appl. Phys. **56**, 24011 (2011)
DOI: 10.1051/epjap/2011110158

THE EUROPEAN PHYSICAL JOURNAL
APPLIED PHYSICS

Regular Article

Cryo-FALP study of collisional-radiative recombination of Ar^+ ions at 40–200 K

T. Kotrík[a], P. Dohnal, P. Rubovič, R. Plašil, Š. Roučka, S. Opanasiuk, and J. Glosík

Department of Surface and Plasma Physics, Faculty of Mathematics and Physics, Charles University, V Holešovičkách 2, Praha 18000, Czech Republic

Received: 14 April 2011 / Received in final form: 26 July 2011 / Accepted: 25 August 2011
Published online: 28 October 2011 –

Abstract. New flowing afterglow apparatus, Cryo-FALP, was built to study ternary Collisional-Radiative Recombination (CRR) of Ar^+ ions with electrons in He/Ar afterglow plasma at temperatures 40–200 K. The obtained ternary recombination rate coefficient at 57 K is $K_{CRR} = (3\pm1)\times10^{-17}\,cm^6\,s^{-1}$. It is the first time that the K_{CRR} was measured below 77 K. The measured temperature dependence $K_{CRR} \sim T^{(-4.5\pm0.4)}$ is in a good agreement with theoretical prediction.

1 Introduction

A binary recombination of singly charged atomic cations with electrons is slow process comparing to a dissociative recombination (DR) of molecular ions (like O_2^+ or H_3^+, etc.). In low temperature plasma an overall recombination process can be enhanced by a ternary process where part of the recombination energy is transferred to a third particle (neutral or charged). When plasma electrons act as energy-removing third bodies, the process is referred to as collisional-radiative recombination, CRR. Schematically, the mechanism of collisional-radiative recombination can be described by the formula:

$$A^+ + e + e \xrightarrow{\alpha_{CRR}} A + e, \tag{1}$$

where A^+ denotes positive ion in general, e indicates electron and α_{CRR} corresponds to the effective binary recombination rate coefficient of CRR. The theory of CRR was originally developed by Bates et al. [1] and Mansbach and Keck [2]. The analytical formula derived by Stevefelt et al. [3] for the effective binary rate coefficient of CRR has the form:

$$\begin{aligned}\alpha_{CRR} &= 3.8\times10^{-9}T_e^{-4.5}n_e + 1.55\times10^{-10}T_e^{-0.63} \\ &\quad + 6\times10^{-9}T_e^{-2.18}n_e^{0.37}\,cm^3\,s^{-1},\end{aligned} \tag{2}$$

where T_e is the electron temperature given in K and n_e is the electron number density given in cm^{-3}. The first term belongs to the pure recombination through a collision with electron (note strong temperature dependence), the second term corresponds to the radiative recombination, where the exceeding energy is carried away by an emitted photon, and the third term accounts for the coupling between the collisional and radiative recombination. As only higher-order Rydberg states participate in the CRR process, formula (2) holds more or less for all atomic and to some extent also molecular ions (for details see Ref. [3] and references therein). This formula was confirmed also by the quantum mechanical calculations [4–6]. At our experimental conditions ($n_e \sim 10^9\,cm^{-3}, T_e < 200\,K$) the first term (pure recombination through collision with electron) is dominant and the other two terms can be neglected. Then the recombination process can be described by the simpler ternary recombination rate coefficient: $K_{CRR} = \alpha_{CRR}/n_e = 3.8\times10^{-9}T_e^{-4.5}\,cm^6\,s^{-1}$.

Previous experimental studies have been carried out mostly at higher electron temperatures (1000–4000 K, see compilation in [4]) and in only few cases also at 300 K [7–10]. It is not obvious that the Stevefelt formula holds also at low temperatures (below 300 K). Only very recently CRR was studied in our laboratory at temperatures below 200 K and K_{CRR} was obtained for temperatures from 77 up to 200 K [11]. Process of CRR has been studied also in ultracold plasmas in connection with the formation of neutral antihydrogen, where it is expected that at high positron number density the production of antihydrogen via recombination of positrons with antiprotons can be enhanced by CRR process. Nevertheless in these experiments CRR is influenced by the presence of strong magnetic field confining the plasma and neutralization process can have different character [12–14].

To study CRR in low temperature plasma we constructed a new flowing afterglow apparatus, Cryo-FALP, where afterglow plasma can be cooled down to 40 K. In this paper we present the first results of the study of recombination in plasma dominated by Ar^+ ions in the temperature range of 40–77 K. It is the first FALP apparatus ever built to operate at temperatures below the boiling point of liquid nitrogen.

[a] e-mail: kotrik.tomas@gmail.com

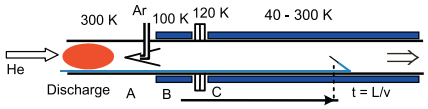

Fig. 1. (Color online) Scheme of the Cryo-FALP apparatus. The temperatures of sections A and B are fixed at 300 and 100–120 K respectively. The temperature of section C can be adjusted to a required value in the range of 40–300 K. The plasma decay time is given by the position in the flow tube. The axially movable Langmuir probe is used to monitor plasma decay along the flow tube, decay time $t = L/v_{\mathrm{PLASMA}}$.

2 Experiment

Modified version of the Flowing Afterglow with Langmuir Probe (FALP, for original design see Ref. [15]) apparatus – Cryo-FALP (for details on the previous versions of FALP apparatuses operating at higher pressure see Refs. [16–19]) was built and used to study CRR at temperatures down to 40 K. Scheme of the Cryo-FALP is shown in Figure 1. Helium buffer gas (300–800 Pa) is flowing through a glass discharge tube into a stainless steel flow tube. Plasma, consisting of helium ions (He^+, He_2^+), helium metastables (He^m) and electrons, is created in pure He by a microwave discharge (2.54 GHz, 10–20 W) ignited in a cavity attached to the glass discharge tube. Plasma is then driven along the flow tube by the flow of helium buffer gas. Downstream from the discharge region argon gas is added to the flow tube and Ar^+ dominated plasma is formed in the sequence of ion-molecule reactions:

$$\begin{aligned}
&\mathrm{He}^+ + 2\mathrm{He} \longrightarrow \mathrm{He}_2^+ + \mathrm{He},\\
&\mathrm{He}^m + \mathrm{He}^m \longrightarrow \mathrm{He}_2^+ + \mathrm{e},\\
&\mathrm{He}^+ + \mathrm{Ar} \longrightarrow \mathrm{Ar}^+ + \mathrm{He},\\
&\mathrm{He}^m + \mathrm{Ar} \longrightarrow \mathrm{Ar}^+ + \mathrm{He} + \mathrm{e},\\
&\mathrm{He}_2^+ + \mathrm{Ar} \longrightarrow \mathrm{Ar}^+ + 2\mathrm{He}. \qquad (3)
\end{aligned}$$

In order to set the optimal experimental conditions (He pressure and flow, Ar number density) at which Ar^+ ion is the dominant ion in afterglow plasma, a chemical kinetics model was developed and numerically solved (for details on reaction kinetics and the kinetics model see Refs. [16,17,20]).

The flow tube is divided into three sections with different temperature regime. The upstream section A of the flow tube, in which the microwave discharge is ignited, is kept at 300 K. The section further downstream, B, is cooled by liquid nitrogen to 100–120 K. The following section C is placed in a large insulating vacuum chamber and is connected via copper braids to a cold head of helium closed-cycle refrigerator (Sumitomo). The temperature of section C can be adjusted to a value between 40 and 300 K. Further details on the design and construction will be given in a separate publication.

Plasma, created in section A, undergoes many collisions with neutral particles. Through the collisions, after a short period of time outside of the discharge region (∼ms), electrons and ions thermalize to the temperature

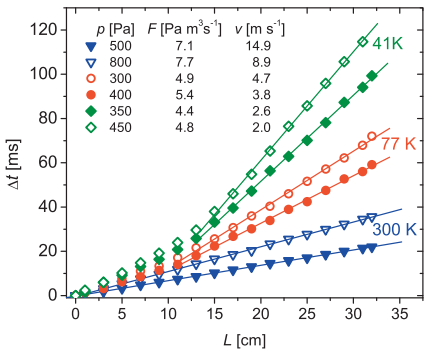

Fig. 2. (Color online) The measurements of plasma velocity. The microwave discharge is modulated and the dependence of the time delay (Δt) of the response is measured as a function of the probe position (L).

of the neutral species (i.e., temperature of the walls). The thermodynamic equilibrium is reached and instead of the temperature of electrons (T_e), ions (T_i) and neutrals (T_n) only one temperature can be used: $T = T_e = T_i = T_n$ (for details and discussion on plasma species thermalization in afterglow plasma see Refs. [11,21–23]). At the beginning of section B plasma is precooled via collisions with helium buffer gas to 100–120 K and in section C to the desired temperature adjusted in the range 40–300 K (see discussion later on). Temperature of the wall is monitored by sensors (silicon diodes, thermocouples type T) mounted along the wall of the flow tube.

Recombination rate coefficients are derived from the electron density decay monitored along section C by the axially movable cylindrical Langmuir probe [17,24]. While gas flow velocity (v) (i.e., plasma flow velocity) is known, spatial position (L) of the Langmuir probe along the flow tube can be transformed into the time (t) passed since the plasma creation by the relation $t = L/v$. The decay of the electron density due to CRR and diffusion in quasineutral plasma ($[Ar^+] = n_e$) is described by the balance equation:

$$\frac{\mathrm{d}n_e}{\mathrm{d}t} = -K_{\mathrm{CRR}}\,[\mathrm{Ar}^+]\,n_e^2 - \frac{n_e}{\tau_D} = -K_{\mathrm{CRR}}\,n_e^3 - \frac{n_e}{\tau_D}, \qquad (4)$$

where τ_D is characteristic diffusion time. K_{CRR} and τ_D can be obtained from the fit of the measured electron density decay under the assumption of K_{CRR} and τ_D being constant (for details on the data analysis see Ref. [11]).

Because of the temperature variation along sections B and C, gas density and flow velocity are changing along the flow tube. Plasma velocity v_{PLASMA} necessary for determination of the decay time is measured by the modulation of the discharge and by monitoring the time delay of the distortion along the flow tube (see Fig. 2). Plasma velocity depends on temperature (T), on gas flow (F) and on pressure (p). Because gas flow and pressure are constant along the flow tube, gas velocity is proportional to temperature (T). When the gas temperature relaxes to the wall temperature, velocity is constant (see linear fits in Fig. 2). In this region with constant temperature, from the decay of

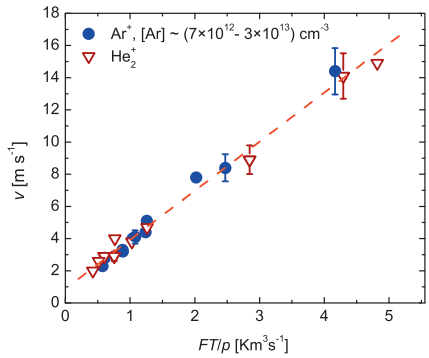

Fig. 3. (Color online) The measured dependence of plasma velocity on the "similarity parameter" $\phi = FT/p$, where F is the gas flow rate, T is the temperature and p is the pressure of the buffer gas. Indicated is dominant ion in the plasma.

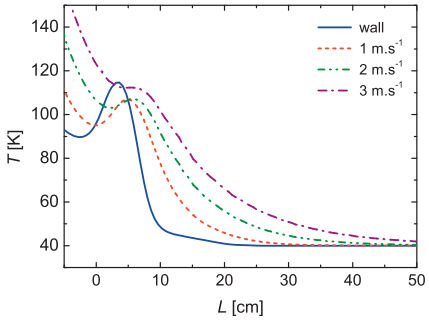

Fig. 4. (Color online) Evolution of buffer gas temperature in section C calculated for different flow velocities. Solid line denotes calculated temperature of the flow tube wall, the flow tube construction, materials and heat transfers are considered.

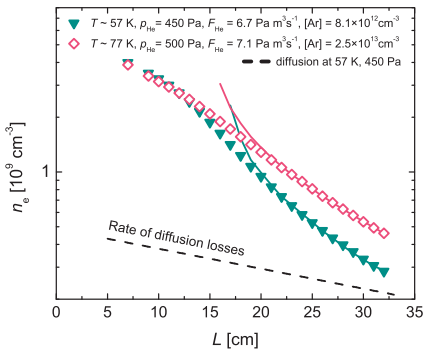

Fig. 5. (Color online) Examples of the electron decay curves measured at 57 and 77 K (temperature of section C). Experimental conditions are listed in the plot. From the fits of the plots in the region of constant plasma temperature (solid lines), the coefficients K_{CRR} are obtained. The dashed line indicates diffusion losses at 57 K, 450 Pa.

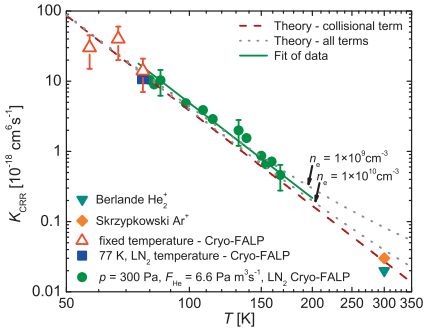

Fig. 6. (Color online) Measured K_{CRR} coefficient as a function of temperature. Dashed line corresponds to the theoretical value calculated from the collisional (first) term of equation (2). Dotted lines indicate the theoretical values of K_{CRR} for two electron densities calculated using all terms of relation (2). Closed square and triangle are data measured by Skrzypkowski et al. [8] and by Berlande et al. [10].

electron density, the effective recombination rate coefficient is obtained. Because of very strong temperature dependence of CRR, the measurements of the plasma velocity dependence on the flow parameters are very important in order to define conditions in which plasma is thermalized to the temperature of the flow tube wall. Measured dependence of the plasma velocity on "similarity parameter" $\phi = FT/p$ in Ar^+ and He_2^+ dominated plasma is plotted in Figure 3. To better understand the thermalization of buffer gas and plasma with the flow tube walls, a simple computer model of heat transport inside the flow tube was developed and numerically solved (the details on the computer model will be given in separate publication). The examples of gas temperature evolution calculated for different gas velocities at temperature of the flow tube ~40 K are plotted in Figure 4. The calculated buffer gas (and plasma) thermalization agrees well with the experimental insight gained from the plasma flow velocity measurements (linear fits in Fig. 2) and from the measurements of the diffusion losses (see Ref. [11]).

3 Results and conclusions

The examples of the measured electron density decay curves at particular experimental conditions are plotted in Figure 5. Measurements of the electron density decays were performed at various experimental conditions in order to control and verify the thermalization of plasma with the flow tube wall. At low temperatures and high enough argon number densities argon clusters Ar_2^+ with fast binary recombination rate coefficients ($\sim 10^{-6}\,cm^3\,s^{-1}$) can be created. As the present version of FALP apparatus is not equipped with a mass spectrometer, one needs to follow the optimal conditions suggested by the chemical kinetics model and/or examine the dependence of α_{eff} on [Ar] in order to exclude the formation of fast recombining Ar_2^+ ions. Such measurements were performed (the details on the results and discussion will be published in separate publication) and after careful examination of the results, the eventual electron assisted ternary recombination rate coefficient K_{CRR} of Ar^+ ion obtained at particular

temperature in the range 50–170 K is plotted in Figure 6. Open triangles denote experimental values obtained in the present version of FALP apparatus, full circles and squares correspond to values measured in the previous FALP experiment, where the flow tube was cooled by liquid nitrogen (for details see Ref. [11]). The theoretical dependence equation (2) is plotted by dashed line (collisional term only). Dotted lines denote theoretical K_{CRR} obtained from the formula $K_{\mathrm{CRR}} = \alpha_{\mathrm{eff}}/n_{\mathrm{e}}$ for two different electron number densities when all terms of equation (2) are involved in α_{eff} calculation. The results show an excellent agreement of the measured K_{CRR} with the theory down to 50 K. Further studies of CRR in Ar^+ dominated plasma are in progress.

This work is a part of the research plan MSM 0021620834 and Grant No. OC10046 financed by the Ministry of Education of the Czech Republic and was partly supported by GACR (202/07/0495, 202/08/H057, 205/09/1183, 202/09/0642), by GAUK 92410, GAUK 353811, GAUK 54010 and by COST Action CM0805 (The Chemical Cosmos).

References

1. D.R. Bates, A.E. Kingston, R.W.P. Mcwhirter, Proc. Roy. Soc. A **267**, 297 (1962)
2. P. Mansbach, J. Keck, Phys. Rev. **181**, 275 (1969)
3. J. Stevefelt, J. Boulmer, J.-F. Delpech, Phys. Rev. A **12**, 1246 (1975)
4. G.J. Pert, J. Phys. B: At. Mol. Opt. Phys. **23**, 619 (1990)
5. S.X. Hu, Phys. Rev. Lett. **98**, 133201-1 (2007)
6. T. Pohl, D. Vrinceanu, H.R. Sadeghpour, Phys. Rev. Lett. **100**, 223201 (2008)
7. M. Tsuji, T. Matsuzaki, T. Tsuji, Chem. Phys. **285**, 335 (2002)
8. M.P. Skrzypkowski, R. Johnsen, R.E. Rosati, M.F. Golde, Chem. Phys. **296**, 23 (2004)
9. G.E. Veatch, H.J. Oskam, Phys. Rev. A **1**, 1498 (1970)
10. J. Berlande, M. Cheret, R. Deloche, A. Gonfalone, C. Manus, Phys. Rev. A **1**, 887 (1970)
11. T. Kotrik, P. Dohnal, S. Roucka, P. Jusko, R. Plasil, J. Glosik, Phys. Rev. A **83**, 032720 (2011)
12. R.S. Fletcher, X.L. Zhang, S.L. Rolston, Phys. Rev. Lett. **99**, 145001-1 (2007)
13. S.X. Hu, D. Vrinceanu, S. Mazevet, L.A. Collins, Phys. Rev. Lett. **95**, 163402-1 (2005)
14. M. Amoretti et al., Phys. Lett. B **583**, 59 (2004)
15. D. Smith, N.G. Adams, A.G. Dean, M.J. Church, J. Phys. D **8**, 141 (1975)
16. J. Glosik, O. Novotny, A. Pysanenko, P. Zakouril, R. Plasil, P. Kudrna, V. Poterya, Plasma Sources Sci. Technol. **12**, 117 (2003)
17. I. Korolov, O. Novotný, J. Varju, T. Kotrík, R. Plašil, M. Hejduk, J. Glosík, Contrib. Plasma Phys. **48**, 521 (2008)
18. J. Glosík, R. Plašil, I. Korolov, T. Kotrík, O. Novotný, P. Hlavenka, P. Dohnal, J. Varju, V. Kokoouline, C.H. Greene, Phys. Rev. A **79**, 052707 (2009)
19. T. Kotrík, P. Dohnal, I. Korolov, R. Plašil, Š. Roučka, J. Glosík, C.H. Greene, V. Kokoouline, J. Chem. Phys. **133**, 034305 (2010)
20. R. Plasil, J. Glosik, V. Poterya, P. Kudrna, J. Rusz, M. Tichy, A. Pysanenko, Int. J. Mass Spectrom. **218**, 105 (2002)
21. H.J. Oskam, Philips Res. Rep. **13**, 335 (1958)
22. I. Korolov, T. Kotrik, P. Dohnal, O. Novotny, J. Glosik, Contrib. Plasma Phys. **48**, 461 (2008)
23. R. Plasil, I. Korolov, T. Kotrik, P. Dohnal, G. Bano, Z. Donko, J. Glosik, Eur. Phys. J. D **54**, 391 (2009)
24. J.D. Swift, M.J.R. Schwar, *Electrical Probes for Plasma Diagnostics* (Illiffe Books, London, 1970)

ARTICLE II

TITLE: Nuclear spin state-resolved cavity ring-down spectroscopy diagnostics of a low-temperature H_3^+–dominated plasma

AUTHORS: Michal Hejduk, Petr Dohnal, Jozef Varju, Peter Rubovič, Tomáš Kotrík, Radek Plašil, and Juraj Glosík

JOURNAL: Plasma Sources Science and Technology 21:024002 (9pp)

DATE: 4 April 2012

DOI: 10.1088/0963-0252/21/2/024002

IOP Publishing Plasma Sources Science and Technology

Plasma Sources Sci. Technol. **21** (2012) 024002 (9pp) doi:10.1088/0963-0252/21/2/024002

Nuclear spin state-resolved cavity ring-down spectroscopy diagnostics of a low-temperature H_3^+ -dominated plasma

Michal Hejduk, Petr Dohnal, Jozef Varju, Peter Rubovič, Radek Plašil and Juraj Glosík

Department of Surface and Plasma Physics, Faculty of Mathematics and Physics, Charles University, Prague, Czech Republic

E-mail: MichalLeeHejduk@matfyz.cz

Received 2 August 2011, in final form 31 October 2011
Published 4 April 2012
Online at stacks.iop.org/PSST/21/024002

Abstract

We have applied a continuous-wave near-infrared cavity ring-down spectroscopy method to study the parameters of a H_3^+-dominated plasma at temperatures in the range 77–200 K. We monitor populations of three rotational states of the ground vibrational state corresponding to para and ortho nuclear spin states in the discharge and the afterglow plasma in time and conclude that abundances of para and ortho states and rotational temperatures are well defined and stable. The non-trivial dependence of a relative population of para-H_3^+ on a relative population of para-H_2 in a source H_2 gas is described. The results described in this paper are valuable for studies of state-selective dissociative recombination of H_3^+ ions with electrons in the afterglow plasma and for the design of sources of H_3^+ ions in a specific nuclear spin state.

(Some figures may appear in colour only in the online journal)

1. Introduction

H_3^+ ions are one of the key components of interstellar space [1–3] and planetary atmospheres [4, 5]. For astrophysicists, it is crucial to understand how these ions are formed and destroyed [6, 7]. In the latter process, dissociative recombination (DR) of the H_3^+ ion with an electron plays one of the key roles.

Up to the end of the previous millennium, a number of mutually inconsistent experiments regarding DR were carried out [8–16] and no unifying theoretical explanation was available. This has changed recently when cross sections obtained at a storage ring [17–20] and theoretical values (calculated by going beyond the Born–Oppenheimer approximation and accounting for Jahn–Teller coupling [21–24]) started to converge. These experiments, however, succeeded in confirming different recombination cross sections for para and ortho nuclear spin states of the ion only qualitatively. The quantitative difference between the theory and the experiments was later explained to be caused by the fact that rotational temperatures were much higher [25] than those previously stated. Any further study about the recombination of H_3^+ would first have to show how well the internal temperature (population of internal states) is determined.

Our group has recently shown that, in addition to the two-body electron–ion recombination process, the ternary recombination process (He assisted, if helium buffer gas is used) plays a significant role in a laboratory afterglow plasma dominated by H_3^+ [26, 27]. Knowledge about both processes was exploited in our studies of the nuclear spin state-selective recombination of H_3^+ ions with electrons at a temperature of 77 K. Laser-aided continuous-wave cavity ring-down spectroscopy (cw-CRDS) was the chosen method. As a result of experiments with two different populations of para-nuclear spin states of H_3^+, we recently measured recombination rate coefficients for para and ortho H_3^+ ions [28], which are in quantitative accordance with the theoretical predictions [23].

In this paper, we describe our apparatus for the studies of the recombination and show how well the rotational and kinetic temperatures and population of the monitored states are determined. A description of the methods of precise determination of these parameters is useful not only for state-selective recombination studies but also for the investigation

of other nuclear spin state-selective processes involving H_3^+ ions in a low-temperature discharge plasma (nuclear spin conversion of H_3^+ ions in collision with H_2, for example, [29]). We also deal with the topic of production of an ensemble of H_3^+ ions with a specified population of para nuclear spin states, which may be interesting for the construction of para-H_3^+ ion sources.

In the following text, we use special notation for some terms. Para/ortho nuclear spin states of H_3^+, H_2 and H_2^+ are denoted by 'p'/'o' in the leading superscript position (like ${}^{p}H_3^+/{}^{o}H_3^+$). 'Normal' hydrogen gas (${}^{n}H_2$) is defined as H_2 gas with 25% of molecules in the para state and 75% in the ortho state. H_2 gas with any higher population of ${}^{p}H_2$ is called para-enriched and is marked ${}^{e}H_2$. We refer to a relative population of ${}^{p}H_3^+$ among H_3^+ ions as ${}^{p}f_3$, i.e. ${}^{p}f_3 = [{}^{p}H_3^+]/[H_3^+]$. The abundance of ${}^{p}H_2$ in H_2 gas is marked similarly: ${}^{p}f_2 = [{}^{p}H_2]/[H_2]$. Apart from ${}^{n}H_2$, we mainly use ${}^{e}H_2$ with ${}^{p}f_2 = 0.87$ in our experiments; this ${}^{e}H_2$ is marked ${}^{e}_{m}H_2$ (m indicates the maximum).

2. Experimental setup

Our experimental apparatus can be naturally divided into two subsystems: one is responsible for the production of cold H_3^+-dominated plasma and the other is a system of spectroscopic detection of specific rovibrational states of H_3^+ ions. A thorough description of the apparatus can be found in [30]. Here we provide only the most important details.

2.1. Production of H_3^+-dominated plasma with ions in specific states

H_3^+ ions are produced by a microwave discharge in a He–Ar–H_2 mixture with typical concentrations of 10^{17}, 10^{14} and 10^{14} cm^{-3}. The frequency of the microwaves is 2.5 GHz and input power is set in the range 4–12 W. The discharge is switched on for 2–2.5 ms and then switched off for around 4 ms to let the plasma decay. The discharge tube is made of silica glass and its inner diameter is 1.5 cm. The tube can be cooled down to 77 K by immersing it in liquid nitrogen and temperatures above 135 K are achieved by exposing it to cold nitrogen vapour. Helium ions and metastable atoms created during the microwave discharge are rapidly converted to H_3^+ by a sequence of ion–molecule reactions involving Ar^+ and ArH^+ as intermediate ions (for details on the kinetics of formation see [30–32]). The method of examination of the afterglow is actually semi-stationary, because the source gas mixture is always flowing through the discharge tube: each repetition of discharge on–off cycle is carried out in a completely renewed environment with almost all reaction products removed (see the discussion in section 3.1.4).

As briefly mentioned in section 1 and fully described in [28], at least two different measurements with two different relative populations of ${}^{p}H_3^+$ (${}^{p}f_3$) need to be carried out to study nuclear spin state-specific recombination. The value of ${}^{p}f_3$ is determined by H_2 and Ar densities, by the temperature and by nuclear spin selection rules of the reactions (see the discussions in [29, 33–37])

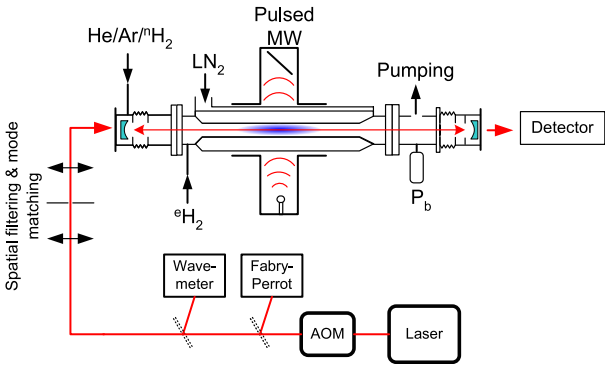

Figure 1. A scheme of the CRDS apparatus. The laser beam is directed into or out of the optical cavity by the acousto-optic modulator (AOM). The beam undergoes spatial filtering before it enters the optical cavity. The plasma is formed by the microwave discharge (MW) in the optical cavity. The pressure inside is measured by a baratron gauge (P_b). The discharge tube is cooled by liquid nitrogen (LN_2) or its vapour. The set wavelength is measured absolutely using a Michelson interferometer and relatively by a Fabry–Pérot interferometer. The inner diameter of the discharge tube is 15 mm.

$$ {}^{p,o}H_2^+ + {}^{p,o}H_2 \rightarrow {}^{p,o}H_3^+ + H, \quad (1) $$

$$ {}^{p,o}H_3^+ + {}^{p,o}H_2 \rightarrow {}^{p,o}H_3^+ + {}^{p,o}H_2, \quad (2) $$

and

$$ ArH^+ + {}^{p}H_2 \rightarrow {}^{p}H_3^+ + Ar \quad (3a) $$

$$ + {}^{o}H_2 \rightarrow {}^{p,o}H_3^+ + Ar, \quad (3b) $$

which allow the production of an ensemble of H_3^+ ions with higher or lower ${}^{p}f_3$ by raising or lowering the value of ${}^{p}f_2$. The maximal ${}^{p}f_2$ we are able to reach by conversion of ${}^{n}H_2$ in the presence of Fe_2O_3 catalyst at 10–18 K outside the discharge tube is 0.87 (value gained by nuclear magnetic resonance); we denote such a gas as ${}^{e}_{m}H_2$. The values of ${}^{p}f_3$ depend also on parameters other than ${}^{p}f_2$ as described in sections 3.1.4 and 3.1.5 of this paper.

2.2. Optical system—cavity ring-down spectroscopy

We have implemented cw-CRDS to track the population of specific rotational states of the ground vibrational state of H_3^+ ions in a discharge and an afterglow in time with high sensitivity and time resolution. Even though the concept of CRDS is widely known [38], its use in time spectroscopy is not common and requires a good synchronization of ring-down detection with other parts of the apparatus; for details about this topic, see [39].

A scheme of cw-CRDS, developed by Romanini *et al* [40], was employed in the construction of our spectrometer (see figure 1). A laser beam is coupled to an optical cavity whose highly reflective mirrors (reflectivity over 99.98%) are periodically swept until an optical resonator is formed. When the resonator is set up, the laser radiation power in the cavity

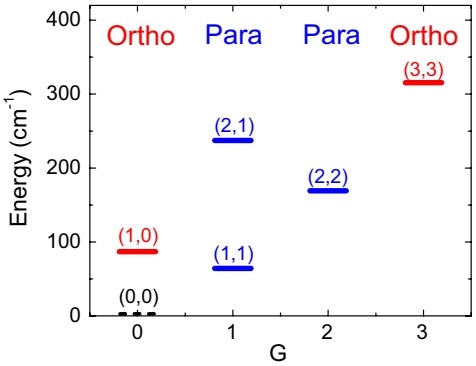

Figure 2. Lowest rotational levels (J, G) of the ground vibrational level of H_3^+. Populations of (1,1), (1,0) and (3,3) (corresponding to one para and two ortho states, respectively) are measured. For notation, see [41].

Table 1. Used transitions and their wavenumbers.

Transition	Wavenumber (cm^{-1})	Nuclear spin state
$3\nu_2^1(2,1) \leftarrow 0\nu_2^0(1,1)$	7237.285	Para
$3\nu_2^1(2,0) \leftarrow 0\nu_2^0(1,0)$	7241.245	Ortho
$3\nu_2^1(4,3) \leftarrow 0\nu_2^0(3,3)$	7234.957	Ortho

rises and the incoming laser beam is interrupted by an acousto-optic modulator as soon as the intensity measured by the PIN or avalanche diode behind one of the mirrors exceeds a threshold. After the laser beam is intercepted, the trapped light intensity decreases because of the losses at the mirrors and the absorption by the medium in the cavity. The characteristic time of the decrease in intensity is inversely proportional to the concentration of absorbing molecules in the medium. The frequency of ring-down events is ≈100 Hz.

As the light source, a fibre-coupled distributed feedback (DFB) laser diode was used. The central wavelength of the laser is 1381.55 nm. The line width of the laser is <2 MHz on 1 s timescales. The maximum output optical power is 20 mW. The beam from the laser undergoes spatial filtering to form Gaussian profile matching to the optical resonator. The set wavelength is measured absolutely using a Michelson interferometer and relatively by a Fabry–Pérot interferometer.

We were able to monitor three of the lowest rotational states of the ground vibrational state of H_3^+: $(J, G) = (1, 1)$, $(1, 0)$ and $(3, 3)$ corresponding to a para and two ortho states (respectively, see figure 2; for notation, see [41]). Specific transitions and their wavelengths are shown in table 1.

3. Experiment: examination of plasma parameters

As mentioned in section 1, our aim is to study the properties of the low-temperature discharge plasma in which we produce the ensemble of H_3^+ ions that is used to study the state-selective recombination of the eponymous ions. Apart from the discharge plasma, the early afterglow is also described in several places since the production processes can take place there as well. The CRDS method used in the presented experimental setup allows us to describe the plasma by kinetic and rotational temperatures of H_3^+ ions and by an abundance of these ions in para nuclear spin states ($^{\mathrm{p}}f_3$). We need to study the relationships between the aforementioned parameters and experimental conditions to be able to reproduce the results at any time.

In particular, the following questions need to be answered if we want to describe the studied plasma satisfactorily:

(Q-1) How does the kinetic temperature (T_{Kin}) of the ions evolve? What is its relation to the temperature of the discharge tube and the He buffer gas?
(Q-2) How does the population of rotational states of the ions change in time in the discharge and the early afterglow?
(Q-3) Does any subsystem of an ensemble of H_3^+ ions reach equilibrium in the discharge to be able to define a rotational temperature? How does the rotational temperature correspond to T_{Kin}?
(Q-4) How does the population of nuclear spin states develop in the discharge and in the early afterglow?
(Q-5) How can we produce the plasma with a specified value of $^{\mathrm{p}}f_3$ (specified para-to-ortho ratio)?
  (a) What is the relationship between $^{\mathrm{p}}f_2$ and $^{\mathrm{p}}f_3$?
  (b) What is the relationship between T_{Kin} and $^{\mathrm{p}}f_3$?

To answer these questions, it is preferable to clarify the processes taking place in the discharge plasma. A list of them is given in table 2. Here are some comments on the table.

1. *Ambipolar diffusion.* We know from recombination studies [28, 42] carried out in the experimental setup described in figure 1 (with [He] ≈ $10^{17}\,\mathrm{cm}^{-3}$ and temperature range 77–300 K) that the characteristic diffusion time in the afterglow (τ_{DAG}) is of the order of 1 ms. The characteristic diffusion time is evaluated from the ion number density decays measured in the afterglow together with the recombination rate coefficient—see equation (4) and figure 1 in [28]. Its value can also be calculated [43] from the mobility of the ion [44]. We assume that the electron temperature (T_{e}) in the discharge is of the order of $T_{\mathrm{e}} \approx 1\,\mathrm{eV}$ and that ions have kinetic temperature $T_{\mathrm{Kin}} \approx 0.01\,\mathrm{eV}$. Then the value of the characteristic time of the ambipolar diffusion in the discharge is

$$\tau_1 \sim 2 \times \tau_{\mathrm{DAG}} \frac{T_{\mathrm{Kin}}}{T_{\mathrm{e}}} \approx 2\,\mathrm{ms} \times \frac{0.01\,\mathrm{eV}}{1\,\mathrm{eV}} = 0.02\,\mathrm{ms}.$$

2. *Recombination of H_3^+ ions.* For electron temperature $T_{\mathrm{e}} \approx 1\,\mathrm{eV}$ and electron density [e] ≈ $10^{11}\,\mathrm{cm}^{-3}$ in the discharge, the recombination rate will be $\alpha \leqslant 10^{-8}\,\mathrm{cm}^3\,\mathrm{s}^{-1}$ [20]. Hence the characteristic time of recombination is

$$\tau_2 = 1/(\alpha[\mathrm{e}]) \approx 1/(10^{-8}\,\mathrm{cm}^3\,\mathrm{s}^{-1} \times 10^{11}\,\mathrm{cm}^{-3}) = 1\,\mathrm{ms}.$$

4, 6 and 7. Ions are supposed to get *cooled vibrationally* after several collisions with He atoms or H_2 molecules. The variables τ in the table are the time between two successive quenching collisions, and estimation of their values in the table is based on the collisional frequencies. We assume that the main process of *rotational cooling* is a quenching

Table 2. Processes in the discharge plasma in which H_3^+ ions are involved. Rotational quantum numbers $J' > J$, $G' > G$, vibrational quantum number $v' > v$ (symmetric or degenerate antisymmetric stretch). Prsmp. stands for the presumption. Rate coefficients k are approximate values applicable to the range of temperatures 77–300 K unless otherwise specified. If k is given, $\tau_n = 1/(k\,[\mathrm{X}])$ (where X is a reactant) and it is called the 'characteristic time' of the process. See the text for the definition of τ in the case of missing k.

n	Process type $H_3^+ + X$	[X] (cm^{-3})	k ($cm^3\ s^{-1}$)	τ_n (ms)	References, comments
1	Ambipolar diffusion of H_3^+	—	—	0.02	[28, 42]
2	$H_3^+ + e \rightarrow$ neutral products	10^{11}	10^{-8}	1	$T_e \approx 1$ eV, [20]
3	$H_3^+(J, G) + e \leftrightarrow H_3^+(J', G') + e$	10^{11}	10^{-7} [a]	0.1	$T_e \approx 1$ eV, [45]
4	$H_3^+(J', G') + He \rightarrow H_3^+(J, G) + He$	10^{17}	—	$<\tau_6$	prsmp., [46]
5	$H_3^+(v' \geqslant 2) + Ar \rightarrow ArH^+ + H_2$	10^{14}	10^{-9}	0.01	[47]
6	$H_3^+(v') + He \rightarrow H_3^+(v = 0) + He$	10^{17}	—	$<10^{-3}$	prsmp., [47, 48]
7	$H_3^+(v') + H_2 \rightarrow H_3^+(v = 0) + H_2$	10^{14}	—	10^{-3}	[49]
8, (2)	$^{p,o}H_3^+ + {}^{p,o}H_2 \rightarrow {}^{p,o}H_3^+ + {}^{p,o}H_2$	10^{14}	10^{-10}	0.01[b]	[36]

[a] Approximately same for both directions.

[b] Strongly dependent on the plasma temperature and initial nuclear spin states.

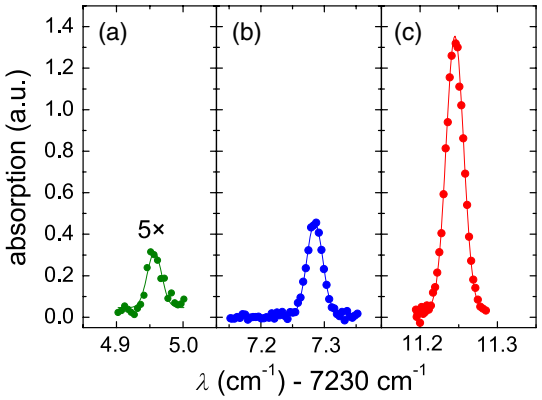

Figure 3. Doppler broadening of the monitored spectral lines in a $^nH_2$ discharge with the discharge tube immersed in LN_2. (*a*) transition $3\nu_2^1(4, 3) \leftarrow 0\nu_2^0(3, 3)$, (*b*) transition $3\nu_2^1(2, 1) \leftarrow 0\nu_2^0(1, 1)$, (*c*) transition $3\nu_2^1(2, 0) \leftarrow 0\nu_2^0(1, 0)$. The temperature evaluated from the broadening of the line corresponding to the (1,0) state is 80 ± 3 K. The mean values of temperature evaluated from all spectral lines are the same. The spectral line of the (3,3) state is multiplied by a factor of 5.

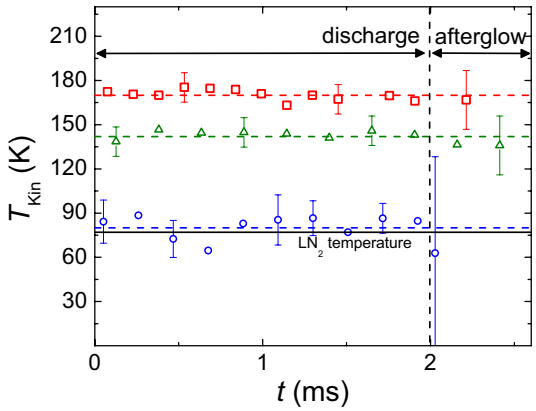

Figure 4. Evolution of kinetic temperatures for three different temperatures of the discharge tube (approximately 77, 140 and 170 K). Large errors in the early afterglow are caused by a fast decrease in the ion concentration due to the recombination with electrons. The mean values of the temperatures are shown as dashed lines. Note that data from a discharge tube cooled by LN_2 are close to the LN_2 temperature.

reaction of rotationally excited H_3^+ ions with He atoms and that this process has a higher rate than vibrational cooling. The CRDS method employed in our experimental setup should tell us whether H_3^+ ions are rotationally cooled down or not (see the discussion below).

From table 2 we can infer that mainly the ambipolar diffusion limits the lifetime of H_3^+ in the discharge. A significant fraction of H_3^+ ions have enough time to undergo rotational and vibrational cooling ($\tau_1 \approx \tau_5 > \tau_7 > \tau_6 > \tau_4$) and nuclear spin conversion (2): $\tau_8 \approx \tau_1$.

3.1. Answers to questions (Q-1)–(Q-5)

Measurements carried out to answer questions (Q-1)–(Q-5) and their results are discussed in this section.

3.1.1. (Q-1) Examination of kinetic temperature. The kinetic temperature of ions is evaluated from the Doppler broadening of the monitored transition lines given in table 1. An example of the broadening is shown in figure 3, which depicts the line profiles of all three used transitions in the $^nH_2$ discharge with the reaction area immersed in liquid nitrogen (LN_2). The value of the kinetic temperature (T_{Kin}) evaluated from the broadening of the line corresponding to the state (1,0) is 80 ± 3 K. The mean values of temperature corresponding to the other states are the same but the error is higher. In the graph, the (3,3) line is multiplied by a factor of 5 to be visible. The evaluated T_{Kin} agrees with the temperature of the discharge tube (77 K). Observations made in a $^c_mH_2$ discharge give similar results.

Figure 4 shows the evolution of T_{Kin} in the $^nH_2$ discharge and the early afterglow for three different temperatures of the tube (LN_2 temperature under standard conditions, 140 and 170 K). Data from the early afterglow are characterized by a large error because of a rapid decrease in the concentration due to the recombination. However, a significant change in T_{Kin} is not observed and the upper limit of the temperature given in the discharge seems to be preserved every time in the afterglow as well.

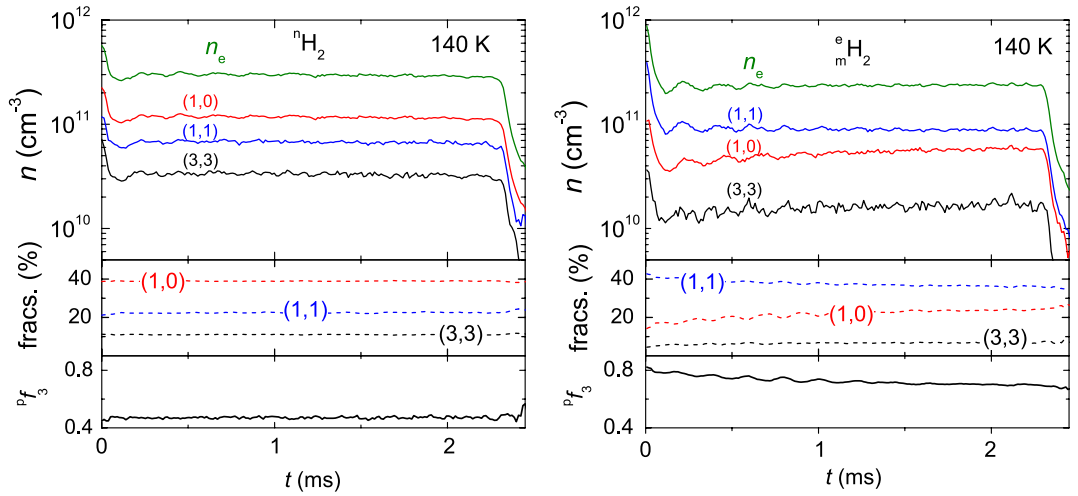

(a) discharge with $^nH_2$ (b) discharge with $^e_mH_2$

Figure 5. Evolution of the absolute and relative population of the states and the population of $^pH_3^+$ in the discharge and the early afterglow. Top panel: evolution of the concentrations of the ions in the indicated states and the corresponding electron density n_e. Middle panel: evolution of the fractions of the indicated states. Bottom panel: evolution of $^pf_3$.

Both figures 3 and 4 consist of data measured in the discharge with the microwave power in the range 4–8 W. During the discharge period, T_{Kin} maintains a more or less constant value, which means that collisional cooling of the translational degrees of freedom of the ions is very efficient. The agreement of T_{Kin} with the temperature of the discharge tube cooled by LN_2 allows us to take the measured T_{Kin} as a reference temperature for further experiments.

3.1.2. (Q-2) Evolution of populations of rotational states. Figure 5 shows the evolution of absolute and relative populations of the monitored states and an overall relative population $^pf_3$ of $^pH_3^+$ during the discharge and early afterglow for $^nH_2$ and $^e_mH_2$ discharges. These relative populations were computed by dividing the measured number density of the appropriate state by the number density of all H_3^+ ions. To calculate this overall number density, a Boltzmann distribution of rotational states was assumed. This assumption is justified later in the text (see section 3.1.3). The value of $^pf_3$ decreases slowly in the $^e_mH_2$ discharge, and in the $^nH_2$ discharge it is constant. Such a slow evolution of the value of $^pf_3$ towards a final constant (steady state) value observed in the $^e_mH_2$ discharge is common to all temperatures above 77 K, and it is discussed in section 3.1.4. In $^nH_2$ and $^e_mH_2$ discharges, the ratio of the fraction of the (1,0) state to the fraction of the (3,3) state is almost constant throughout the discharge period.

3.1.3. (Q-3) Definition of rotational temperature. In the previous section we concluded that relative populations of the rotational states within the ortho-nuclear spin manifold—states (1,0) and (3,3)—are constant (see figure 5). Most probably, this also holds for the para nuclear spin manifold. This allows us to define a rotational temperature $T_{Rot\text{-}ortho}$ based on the relative population of two ortho states. This rotational temperature is compared with T_{Kin} in figure 6. Data from measurements with $^e_mH_2$ and $^nH_2$ are scattered along the $T_{Rot\text{-}ortho} = T_{Kin}$ line.

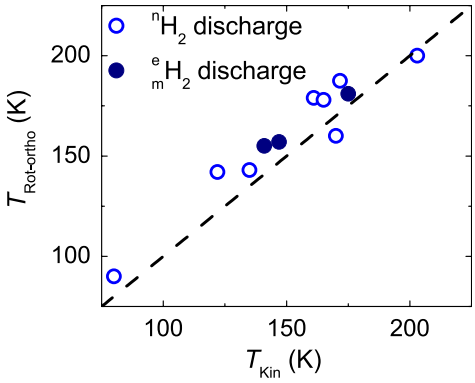

Figure 6. Comparison of the measured rotational $T_{Rot\text{-}ortho}$ and the kinetic T_{Kin} temperatures. Dashed line: $T_{Rot\text{-}ortho} = T_{Kin}$. The measurements were performed in discharges with $^nH_2$ and $^e_mH_2$.

To examine under which conditions we can define a rotational temperature of the H_3^+ ensemble (i.e. the ensemble of $^pH_3^+$ ions and $^oH_3^+$ ions mixed together), we plot the population of rotational states against T_{Kin} for the discharge with $^nH_2$ and $^e_mH_2$ in figure 7 (the plotted values were measured at the end of the discharge period, $t \doteq 2$ ms). The measured populations are supplemented by lines showing the populations in thermodynamic equilibrium (TDE). We can see that populations of all three monitored states agree with the TDE values in the case of the discharge with $^nH_2$ despite the fact that the value of $^pf_2$ does not correspond to TDE (note that $^pf_2$ is approximately 0.5 at 77 K in TDE, while $^pf_2$ of $^nH_2$ is 0.25). The effect is clear if we redraw the data from figure 7 to show the dependence of $^pf_3$ on T_{Kin}, as is shown in figure 8: the fractions $^pf_3$ for TDE are close to the values of $^pf_3$ measured in the $^nH_2$ discharge (approximately 0.5) in the whole temperature range 75–300 K.

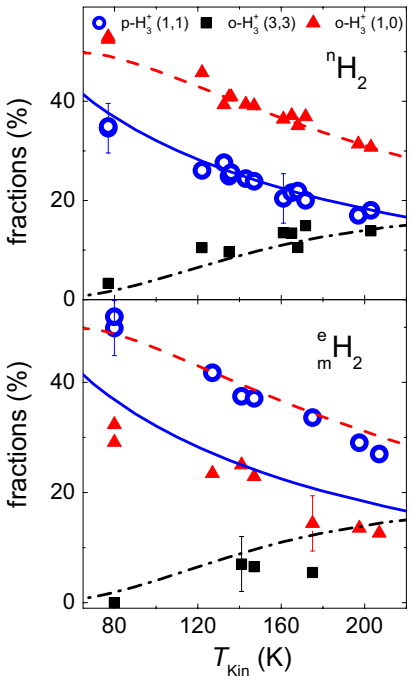

Figure 7. Dependence of the relative populations (fractions) of the monitored rotational states on T_{Kin} in the discharge with $^{\mathrm{n}}H_2$ (top panel) and with $^{\mathrm{e}}_{\mathrm{m}}H_2$ (bottom panel). Dashed lines, full lines, dashed-dotted lines: population of (1,0), (1,1) and (3,3) states corresponding to TDE, respectively. Note in the bottom panel that the measured values do not lie on the lines corresponding to TDE in the case of $^{\mathrm{e}}_{\mathrm{m}}H_2$ discharge; the fraction of $^{\mathrm{p}}H_3^+$ (1,1) (indicated by open circles) is substantially higher than the full line indicating the population at TDE.

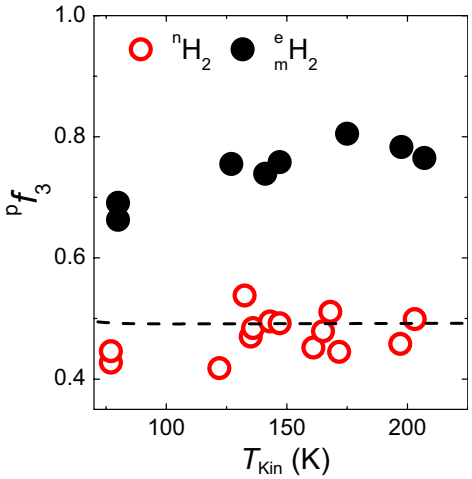

Figure 8. Measured dependence of $^{\mathrm{p}}f_3$ on T_{Kin} for the discharges with $^{\mathrm{n}}H_2$ and with $^{\mathrm{e}}_{\mathrm{m}}H_2$. Dashed line: $^{\mathrm{p}}f_3$ corresponding to TDE.

When using $^{\mathrm{e}}_{\mathrm{m}}H_2$ in the discharge, the population of the rotational states changes substantially against the values measured with $^{\mathrm{n}}H_2$ (see figure 7). The population of the states in the ortho sub-ensemble is thermalized, but the para-to-ortho ratio given by the value $^{\mathrm{p}}f_3$ is far from the TDE value (see figure 8).

Observations described in this section are useful for recombination studies. To compare the experimental recombination rate coefficients with theoretical values calculated for the distribution of the states in TDE for a temperature given in the range 77–300 K, we do not need to use $^{\mathrm{e}}H_2$ with $^{\mathrm{p}}f_2$ equal to the TDE value: the use of $^{\mathrm{n}}H_2$ is sufficient, because the resulting $^{\mathrm{p}}f_3 \approx 0.5$ is close to the value corresponding to TDE (see the dashed line in figure 8) and the rotational temperature is equilibrated with T_{Kin}.

Figures 6–8 show that it is possible to form plasmas with different values of $^{\mathrm{p}}f_3$ and with the rotational temperature defined well within each nuclear spin manifold by using H_2 with different values of $^{\mathrm{p}}f_2$ as a source gas. This is required in studies of the nuclear spin state-specific recombination of H_3^+ ions (see section 1, [28, 42])

3.1.4. (Q-4) Formation of the para–ortho steady state. The value of $^{\mathrm{p}}f_3$ in the discharge is determined by the nuclear spin selection rules of the processes (1), (2), (3*a*) and (3*b*). The evolution of $^{\mathrm{p}}f_3$ in time is given only by (2) if the value of $^{\mathrm{p}}f_2$ does not change in the discharge, i.e. if $^{\mathrm{e}}H_2$ does not convert to H_2 with a lower population of para states. This can happen because a certain amount of source $^{\mathrm{e}}H_2$ gas always stays in the discharge during the whole period, even though it is continuously supplied. In our experiments we could not observe the dependence of $^{\mathrm{p}}f_3$ on the length of the stay of the $^{\mathrm{e}}H_2$ gas in the discharge area. Moreover, data from experiments with density $[^{\mathrm{e}}_{\mathrm{m}}H_2]$ in the range from 5×10^{13} to 10^{15} cm^{-3} and with the temperature 130–210 K show that almost no dependence of $^{\mathrm{p}}f_3$ on $[^{\mathrm{e}}_{\mathrm{m}}H_2]$ exists—see figure 9. At each concentration, $^{\mathrm{p}}f_3$ from the beginning and from the end of the discharge period ('initial' and 'final value', respectively) is drawn (for an illustration of both terms, see the inset of the figure). The so-called 'nascent' fraction $^{\mathrm{p}}f_3$ originating from reaction (1) is also indicated (see also an extended discussion in [50]). The initial values are closer to the nascent values and change to the final value within the discharge period.

The slight slope of the lines fitted to data in the main frame of figure 9 seems to be an effect of temperature more than $[^{\mathrm{e}}_{\mathrm{m}}H_2]$ if we notice the error bar of $^{\mathrm{p}}f_3$ and where the mean values of data from each temperature range lie. The observation from this figure agrees with the trend of $^{\mathrm{e}}_{\mathrm{m}}H_2$ values in figure 8. Whether this effect is caused by the temperature dependence of the spin conversion reaction (2) is tested by measurements described in the next section.

3.1.5. (Q-5) Dependence of $^{\mathrm{p}}f_3$ on temperature. In the previous section we discussed figure 9 and introduced the idea that the slight slope of the line fitted to the experimental data can be caused by some temperature dependence, most probably by the temperature dependence of process (2). Such an effect can also be found in figure 8 (see the values for the discharge in $^{\mathrm{e}}_{\mathrm{m}}H_2$). To study this effect in detail we carried out measurements of the dependence of 'final' values of $^{\mathrm{p}}f_3$ on $^{\mathrm{p}}f_2$. Measurements were realized at temperatures of 77, 170 and 300 K. Data from 77 and 300 K are plotted in figure 10. The straight line marked 'nascent' shows the

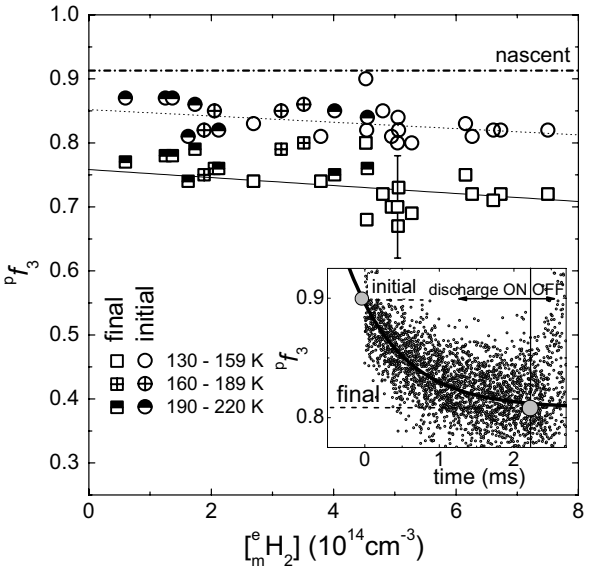

Figure 9. Dependence of the initial and final relative populations of $^{p}H_3^+$ on the concentration of $^{e}_{m}H_2$ in the discharge. The nascent value of $^{p}f_3$ originating from process (1) for $^{p}f_2 = 0.87$ (the value corresponding to $^{e}_{m}H_2$) is plotted by the dashed-dotted line. The inset serves as an illustration for the definition of the 'initial' and 'final' values.

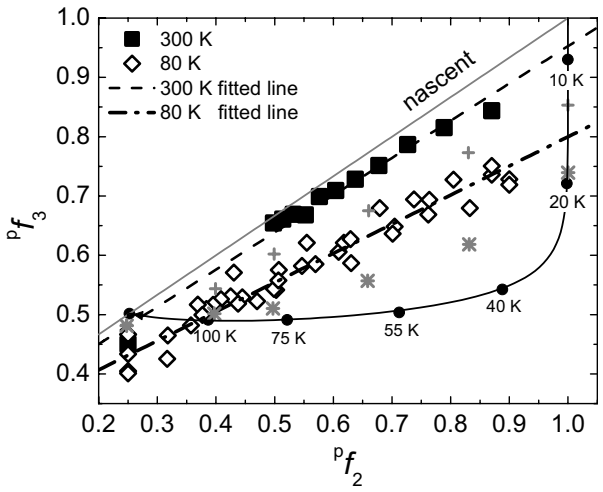

Figure 10. Dependence of the population of $^{p}H_3^+$ ($^{p}f_3$) on the para enrichment of $^{e}H_2$ ($^{p}f_2$) in experiments and TDE. Black dots: values corresponding to TDE at the indicated temperature (arrow shows the direction of rising temperature). The line marked as nascent is the population of $^{p}f_3$ and $^{p}f_2$ resulting from reaction (1) [50]. The experimental values come from measurements at 80 and 300 K. '+' and '∗' symbols: values measured in pure H_2 discharge [29] at pressures above 400 mTorr and temperatures 300 K and 77 K, respectively.

combination of $^{p}f_2$ and $^{p}f_3$ resulting from reaction (1) [50]. The experiment at 300 K was carried out at a discharge power of 12 W, $[H_2] \approx 10^{14}$ cm^{-3} and $[Ar] = 2 \times 10^{13}$ cm^{-3}. Data from 80 K were acquired at two different discharge powers (4 and 8 W) and three different concentrations of Ar (1×10^{14}, 3×10^{14} and 1×10^{15} cm^{-3}) and $[H_2] = 2.5 \times 10^{14}$ cm^{-3}. Significant influence of the discharge power and concentration of Ar was not observed.

The black dots in figure 10 show the values of $^{p}f_3$ and $^{p}f_2$ at TDE at the indicated temperature. Experimental values of $^{p}f_3$ for all temperatures at $^{p}f_2 = 0.25$ are close to the corresponding TDE values, as was discussed in section 3.1.3. We can see that the slices of the graph for $^{p}f_2 = 0.25$ and $^{p}f_2 = 0.87$ are in agreement with figures 8 and 9. Since it was shown by figure 9 that the influence of $[^{e}H_2]$ is weak and all data were measured at similar values of $[^{e}H_2]$, we can state that we do observe an influence of temperature dependence of reaction (2) on the final $^{p}f_3$ in the graph, i.e. $^{p}f_3 = {}^{p}f_3(^{p}f_2, T_{Kin})$.

The experimental data in figure 10 resemble those from a recently published paper of the McCall group on the nuclear spin selection rules of reaction (2) [29]. Their data are also plotted in the figure (+ and ∗ symbols). Unlike in the case of the McCall group data, the dependence of $^{p}f_3$ on $^{p}f_2$ measured by us is linear, not convex. This difference is probably due to the H_2 concentration: in our case, $[H_2]$ is 100 times lower [29] and almost no H_5^+ ions are formed [51]. Therefore, the nuclear spin conversion processes within the H_3^+ ensemble can be described much more simply in our experiment. However, further discussion about figure 10 with respect to the nuclear spin selection rules of process (2) is beyond the scope of this paper.

4. Conclusion

We tracked the population of three of the lowest rotational states of H_3^+ ions (corresponding to one para nuclear spin state and two ortho states) in a H_3^+-dominated microwave discharge plasma and the early afterglow plasma by cavity ring-down spectroscopy (CRDS). The relative population of $^{p}H_3^+$ ($^{p}f_3$) was varied by using $^{n}H_2$ or $^{e}H_2$. We characterized the properties of the ensemble of H_3^+ ions by the kinetic and rotational temperatures and the relative population of para nuclear spin states ($^{p}f_3$). The following conclusions were drawn for the considered experimental conditions:

- the ensemble of H_3^+ ions in the plasma has a stable kinetic temperature equalling the temperature of the discharge tube;
- the rotational temperature can be determined from the relative population of the two ortho states and it is equal to the kinetic temperature, i.e. $T_{Rot\text{-}ortho} = T_{Kin}$;
- the population of H_3^+ in the para states is given by the population of the para states of H_2 and the temperature of the system, i.e. $^{p}f_3$ is a function of $^{p}f_2$ and T_{Kin};
- a steady-state population of para-H_3^+ is reached in our discharge plasma.

These conclusions confirm our previous assumptions that our measurements of H_3^+ recombination rate coefficients performed with a He–Ar–$^{n}H_2$ afterglow plasma ([26–28, 42], i.e. under experimental conditions similar to those described in this paper) give values close to those in TDE.

Acknowledgments

This work is a part of the research plan MSM 0021620834 and grant OC10046 financed by the Ministry of Education of the Czech Republic and was partly supported by GACR (202/07/0495, 202/08/H057, 205/09/1183, 202/09/0642), by GAUK 92410, GAUK 353811, GAUK 54010 and by COST Action CM0805 (The Chemical Cosmos). The authors would like to thank Mgr. Mojmír Jílek for the design of the para-H_2 generator and RNDr. Jan Lang, PhD, for NMR experiments.

References

[1] Herbst E 2000 The astrochemistry of H_3^+ *Phil. Trans. R. Soc. Lond.* A **358** 2523–34
[2] Geballe T R and Oka T 1996 Detection of H_3^+ in interstellar space *Nature* **384** 334
[3] McCall B J, Geballe T R, Hinkle K H and Oka T 1998 Detection of H_3^+ in the diffuse interstellar medium toward Cygnus OB2 No. 12 *Science* **279** 1910–13
[4] Trafton L, Lester D F and Thompson K L 1989 Unidentified emission lines in Jupiter's northern and southern 2 micron aurorae *Astrophys. J.* **343** 73–6
[5] Miller S *et al* 2000 The role of H_3^+ in planetary atmospheres *Phil. Trans. R. Soc. Lond.* A **358** 2485–502
[6] des Forêts G P and Roueff E 2000 H_3^+ recombination and bistability in the interstellar medium *Phil. Trans. R. Soc. Lond.* A **358** 2549–59
[7] Le Petit F, Roueff E and Herbst E 2004 H_3^+ and other species in the diffuse cloud towards ζ Persei: a new detailed model *Astron. Astrophys.* **417** 993–1002
[8] Leu M T, Biondi M A and Johnsen R 1973 Measurements of recombination of electrons with H_3^+ and H_5^+ ions *Phys. Rev.* A **8** 413
[9] Adams N G, Smith D and Alge E 1984 Measurements of dissociative recombination coefficients of H_3^+, HCO^+, N_2H^+, and CH_5^+ at 95 and 300 K using the FALP apparatus *J. Chem. Phys.* **81** 1778
[10] Larsson M and Orel A 2008 *Dissociative Recombination of Molecular Ions* (Cambridge: Cambridge University Press)
[11] Oka T 2000 Introductory remarks *Phil. Trans. R. Soc. Lond.* A **358** 2363–9
[12] Johnsen R 2005 A critical review of H_3^+ recombination studies *J. Phys.: Conf. Ser.* **4** 83
[13] Smith D and Španěl P 1993 Dissociative recombination of H_3^+ and some other interstellar ions: a controversy resolved *Int. J. Mass Spectrom. Ion Processes* **129** 163–82
[14] Amano T 1990 The dissociative recombination rate coefficients of H_3^+, HN_2^+, and HCO^+ *J. Chem. Phys.* **92** 6492–501
[15] Plašil R *et al* 2002 Advanced integrated stationary afterglow method for experimental study of recombination of processes of H_3^+ and D_3^+ ions with electrons *Int. J. Mass Spectrom.* **218** 105–30
[16] Laubé S *et al* 1998 New FALP-MS measurements of H_3^+, D_3^+ and HCO^+ dissociative recombination *J. Phys. B: At. Mol. Opt. Phys.* **31** 2111
[17] Kreckel H *et al* 2005 High-resolution dissociative recombination of cold H_3^+ and first evidence for nuclear spin effects *Phys. Rev. Lett.* **95** 263201
[18] McCall B J *et al* 2003 An enhanced cosmic-ray flux towards zeta persei inferred from a laboratory study of the H_3^+-e^- recombination rate *Nature* **422** 500
[19] Petrignani A *et al* 2009 Spectroscopy and dissociative recombination of the lowest rotational states of H_3^+ *J. Phys.: Conf. Ser.* **192** 012022
[20] Tom B A *et al* 2009 Dissociative recombination of highly enriched para-H_3^+ *J. Chem. Phys.* **130** 031101
[21] Kokoouline V, Greene C H and Esry B D 2001 Mechanism for the destruction of H_3^+ ions by electron impact *Nature* **412** 891
[22] Kokoouline V and Greene C H 2003 Unified theoretical treatment of dissociative recombination of D_{3h} triatomic ions: application to H_3^+ and D_3^+ *Phys. Rev.* A **68** 012703
[23] dos Santos S F, Kokoouline V and Greene C H 2007 Dissociative recombination of H_3^+ in the ground and excited vibrational states *J. Chem. Phys.* **127** 124309
[24] Pagani L *et al* 2009 Chemical modeling of L183 (= L134N) : an estimate of the ortho/para H_2 ratio *Astron. Astrophys.* **494** 623
[25] Petrignani A *et al* 2011 Resonant structure of low-energy H_3^+ dissociative recombination *Phys. Rev.* A **83** 032711
[26] Glosík J *et al* 2008 Recombination of H_3^+ ions in the afterglow of a He/Ar/H_2 plasma *J. Phys. B: At. Mol. Opt. Phys.* **41** 191001
[27] Glosík J *et al* 2009 Temperature dependence of binary and ternary recombination of H_3^+ ions with electrons *Phys. Rev.* A **79** 052707
[28] Varju J, Hejduk M, Dohnal P, Jílek M, Kotrík T, Plašil R, Gerlich D and Glosík J 2011 Nuclear spin effect on recombination of H_3^+ ions with electrons at 77 K *Phys. Rev. Lett.* **106** 203201
[29] Crabtree K N, Kauffman C A, Tom B A, Becka E, McGuire B A and McCall B J 2011 Nuclear spin dependence of the reaction of H_3^+ with H_2: II. Experimental measurements *J. Chem. Phys.* **134** 194311
[30] Macko P *et al* 2004 Afterglow studies of $H_3^+(v = 0)$ recombination using time resolved cw-diode laser cavity ring-down spectroscopy *Int. J. Mass Spectrom* **233** 299–304
[31] Glosík J, Novotný O, Pysanenko A, Zakouril P, Plašil R, Kudrna P and Poterya V 2003 The recombination of H_3^+ and H_5^+ ions with electrons in hydrogen plasma: dependence on temperature and on pressure of H_2 *Plasma Sources Sci. Technol.* **12** S117–22
[32] Poterya V *et al* 2002 Recombination of D_3^+ ions in the afterglow of a He–Ar–D_2 plasma *Phys. Rev. Lett.* **88** 044802
[33] Quack M 1977 Detailed symmetry selection rules for reactive collisions *Mol. Phys.* **34** 477–504
[34] Cordonnier M *et al* 2000 Selection rules for nuclear spin modifications in ion–neutral reactions involving H_3^+ *J. Chem. Phys.* **113** 3181–93
[35] Oka T 2004 Nuclear spin selection rules in chemical reactions by angular momentum algebra *J. Mol. Spectrosc.* **228** 635–9
[36] Park K and Light J C 2007 Microcanonical statistical study of ortho–para conversion in the reaction $H_3^+ + H_2 \rightarrow (H_5^+)^* \rightarrow H_3^+ + H_2$ at very low energies *J. Chem. Phys.* **126** 044305
[37] Hugo E, Asvany O and Schlemmer S 2009 $H_3^+ + H_2$ isotopic system at low temperatures: microcanonical and experimental study *J. Chem. Phys.* **130** 164302
[38] O'Keefe A and Deacon D A G 1988 Cavity ring-down optical spectrometer for absorption measurements using pulsed laser sources *Rev. Sci. Instrum.* **59** 2544–51
[39] Hlavenka P *et al* 2006 Near infrared second overtone cw-cavity ringdown spectroscopy of D_2H^+ ions *Int. J. Mass Spectrom.* **255–256** 170–6
[40] Romanini D, Kachanov A A and Stoeckel F 1997 Diode laser cavity ring down spectroscopy *Chem. Phys. Lett.* **270** 538–45
[41] Lindsay C M and McCall B J 2001 Comprehensive evaluation and compilation of H_3^+ spectroscopy *J. Mol. Spectrosc.* **210** 60–83
[42] Varju J *et al* 2010 Application of NIR-CRDS for state selective study of recombination of para and ortho H_3^+ ions with

electrons in low temperature plasma *J. Phys.: Conf. Ser.* **227** 012026

[43] Kotrík T, Dohnal P, Roučka Š, Jusko P, Plašil R, Glosík J and Johnsen R 2011 Collisional-radiative recombination $Ar^+ + e + e$: experimental study at 77–180 K *Phys. Rev.* A **83** 032720

[44] Lindinger W and Albritton D L 1975 Mobilities of various mass-identified positive ions in helium and argon *J. Chem. Phys.* **62** 3517–22

[45] Kokoouline V, Faure A, Tennyson J and Greene C H 2010 Calculation of rate constants for vibrational and rotational excitation of the H_3^+ ion by electron impact *Mon. Not. R. Astron. Soc.* **405** 1195–1202

[46] McCall B J *et al* 2004 Dissociative recombination of rotationally cold H_3^+ *Phys. Rev.* A **70** 052716

[47] Mikosch J, Kreckel H, Wester R, Plašil R, Glosík J, Gerlich D, Schwalm D and Wolf A 2004 Action spectroscopy and temperature diagnostics of H_3^+ by chemical probing *J. Chem. Phys.* **121** 11030–7

[48] Ferguson E E 1986 Vibrational quenching of small molecular ions in neutral collisions *J. Phys. Chem.* **90** 731–8

[49] Yousif F B, Hinojosa G, de Urquijo J, Cisneros C and Alvarez I 1997 Generation of an H_3^+ ($v = 0$) beam and its diagnosis from the observation of its polar dissociation in collision with He *Int. J. Mass. Spectrom.* **171** 127–34

[50] Crabtree K N, Indriolo N, Kreckel H, Tom B A and McCall B J 2011 On the ortho:para ratio of H_3^+ in diffuse molecular clouds *Astrophys. J.* **729** 15

[51] Crabtree K N, Tom B A and McCall B J 2011 Nuclear spin dependence of the reaction of H_3^+ with H_2. I. Kinetics and modeling *J. Chem. Phys.* **134** 194310

ARTICLE III

TITLE: Binary recombination of para- and ortho-H_3^+ with electrons at low temperatures

AUTHORS: Petr Dohnal, Michal Hejduk, Jozef Varju, Peter Rubovič, Štěpán Roučka, Tomáš Kotrík, Radek Plašil, Rainer Johnsen, and Juraj Glosík

JOURNAL: Philosophical Transactions of The Royal Society A 370:5101-5108

DATE: 13 November 2012

DOI: 10.1098/rsta.2012.0097

PHILOSOPHICAL TRANSACTIONS OF THE ROYAL SOCIETY A

CrossMark click for updates

Phil. Trans. R. Soc. A (2012) **370**, 5101–5108
doi:10.1098/rsta.2012.0097

Binary recombination of para- and ortho-H_3^+ with electrons at low temperatures

By P. Dohnal[1], M. Hejduk[1], J. Varju[1], P. Rubovič[1,*], Š. Roučka[1], T. Kotrík[1], R. Plašil[1], R. Johnsen[2] and J. Glosík[1]

[1]*Faculty of Mathematics and Physics, Department of Surface and Plasma Science, Charles University, Prague, Czech Republic*
[2]*Department of Physics and Astronomy, University of Pittsburgh, Pittsburgh, PA 15260, USA*

Results of an experimental study of binary recombination of para- and ortho-H_3^+ ions with electrons are presented. Near-infrared cavity-ring-down absorption spectroscopy was used to probe the lowest rotational states of H_3^+ ions in the temperature range of 77–200 K in an H_3^+-dominated afterglow plasma. By changing the para/ortho abundance ratio, we were able to obtain the binary recombination rate coefficients for pure para-H_3^+ and ortho-H_3^+. The results are in good agreement with previous theoretical predictions.

Keywords: H_3^+; dissociative recombination; cavity ring down spectroscopy; afterglow plasma

1. Introduction

The fundamental characteristics of the H_3^+ dissociative recombination (DR) [1] have been the subject of much interest for both theoretical and experimental physicists [2]. The discrepancies between measurements of the binary dissociative reaction rate and the theoretical complexity of this seemingly simple reaction led to a great deal of fruitful research on this process. The history of H_3^+ recombination studies has been adequately covered in several review articles [3–9]. Recently, both theory and experiment have converged to a value for the rate of this particular reaction. The theoretical treatment took a crucial leap forward in the understanding of the DR process after including the Jahn–Teller mechanism as the critical step in the initial electron-capture step of the DR reaction [10]. This resulted in a convergence with experimental DR data reported from ion storage rings where experimentalists had realized the impact of rotational excitation of the H_3^+ ions on the DR reaction rate, especially with respect to the importance of the DR process in interstellar molecular clouds [11–13]. Final convergence between theory and the remaining important experimental techniques, stationary and flowing afterglow, was reached after recognizing that a

*Author for correspondence (peter.rubovic@gmail.com).

One contribution of 21 to a Theo Murphy Meeting Issue ‘Chemistry, astronomy and physics of H_3^+’.

fast third-body reaction, not previously considered, stabilizes the recombination process in such plasmas [4,14,15]. However, recently it has been shown [16,17] that the assumption of rotationally cold H_3^+ ions in storage rings was not entirely correct [17]. This is important if we realize that the quantum mechanical calculations [18] predict a large difference in the low-temperature recombination of ions in para-H_3^+ and ortho-H_3^+ states. This has been qualitatively confirmed in storage-ring experiments using hydrogen with an enriched para fraction [12,13,19]. However, as has just been stated, the actual rotational population of the recombining ions has not been proved experimentally. In the present experiments, the stationary afterglow (SA) technique with spectroscopic *in situ* determination of the abundances of the recombining ions was used. Near-infrared cavity-ring-down absorption spectroscopy (NIR-CRDS) enabled *in situ* determination of the spin states, together with the kinetic and the rotational temperatures of the recombining ions. A similar approach was used in our recent study of binary recombination of para-H_3^+ and ortho-H_3^+ ions at temperatures close to 77 K [20]. In the present studies, we have extended the range of temperatures up to 200 K. Our previous measurements in H_3^+- and D_3^+-dominated plasmas at conditions similar to those in the present experiment [4,14,15,21,22] have shown that the H_3^+ ions recombine by both a binary process with a rate coefficient α_{bin}, and a ternary helium-assisted recombination mechanism, with a rate coefficient K_{He}. The plasma decay can then be described by an overall effective recombination rate coefficient:

$$\alpha_{\mathrm{eff}} = \alpha_{\mathrm{bin}} + K_{\mathrm{He}}[\mathrm{He}]. \tag{1.1}$$

Both rate coefficients can be obtained by measuring the dependence of α_{eff} on the helium density [He]. The possible effects of another ternary process—collisional radiative recombination (CRR) [23,24]—are discussed in detail elsewhere [25].

In the following, we will use left indices p, o, n and e to denote 'para', 'ortho', 'normal' and 'para-enriched' hydrogen (i.e. ${}^{\mathrm{p}}H_2$, ${}^{\mathrm{o}}H_2$, ${}^{\mathrm{n}}H_2$ and ${}^{\mathrm{e}}H_2$) and ${}^{\mathrm{p}}f_2$ and ${}^{\mathrm{o}}f_2$ to denote para and ortho fractions. ${}^{\mathrm{p}}H_3^+$ and ${}^{\mathrm{o}}H_3^+$ stand for para-H_3^+ and ortho-H_3^+, while ${}^{\mathrm{p}}f_3$ and ${}^{\mathrm{o}}f_3$ denote their fractions (i.e. ${}^{\mathrm{p}}f_3 = [{}^{\mathrm{p}}H_3^+]/[H_3^+]$ and ${}^{\mathrm{o}}f_3 = [{}^{\mathrm{o}}H_3^+]/[H_3^+]$). If an index is missing, then the spin modification is not specified. Assuming that the plasma is quasi-neutral and that it contains no ions other than H_3^+ (i.e. $n_{\mathrm{e}} = [{}^{\mathrm{p}}H_3^+] + [{}^{\mathrm{o}}H_3^+]$), then following the derivation in the study of Varju *et al.* [20], we can write the continuity equation for the electron number density n_{e}:

$$\frac{\mathrm{d}n_{\mathrm{e}}}{\mathrm{d}t} = -({}^{\mathrm{p}}\alpha_{\mathrm{eff}}\,{}^{\mathrm{p}}f_3 + {}^{\mathrm{o}}\alpha_{\mathrm{eff}}\,{}^{\mathrm{o}}f_3)n_{\mathrm{e}}^2 - \frac{n_{\mathrm{e}}}{\tau_{\mathrm{D}}} = -\alpha_{\mathrm{eff}}\,n_{\mathrm{e}}^2 - \frac{n_{\mathrm{e}}}{\tau_{\mathrm{D}}}, \tag{1.2}$$

where ${}^{\mathrm{o}}\alpha_{\mathrm{eff}}$ and ${}^{\mathrm{p}}\alpha_{\mathrm{eff}}$ are the state-selected effective recombination rate coefficients for ${}^{\mathrm{o}}H_3^+$ and ${}^{\mathrm{p}}H_3^+$, respectively, $\alpha_{\mathrm{eff}} = {}^{\mathrm{p}}f_3\,{}^{\mathrm{p}}\alpha_{\mathrm{eff}} + {}^{\mathrm{o}}f_3\,{}^{\mathrm{o}}\alpha_{\mathrm{eff}}$ is the overall (apparent binary) recombination rate coefficient for a given mixture of ortho and para ions, and τ_{D} is the characteristic time constant of the ambipolar diffusion. A linear relation similar to equation (1.2) holds also for ${}^{\mathrm{p}}\alpha_{\mathrm{eff}}$ and ${}^{\mathrm{o}}\alpha_{\mathrm{eff}}$ [20].

The data (see §3) show that at the H_2 and He densities used in the experiment, the fractions ${}^{\mathrm{p}}f_3$ and ${}^{\mathrm{o}}f_3$ are nearly constant during the afterglow. A measurement of α_{eff} for two or more different values of ${}^{\mathrm{p}}f_3$, but under otherwise identical conditions (temperature, and density of He and H_2), then permits a determination

of the individual recombination rate coefficients ${}^{\mathrm{p}}\alpha_{\mathrm{eff}}$ and ${}^{\mathrm{o}}\alpha_{\mathrm{eff}}$. The fraction ${}^{\mathrm{p}}f_3$ can be enhanced from about 0.5 to 0.8 by using para-enriched hydrogen instead of normal hydrogen (for details, see [20,26]).

2. Experimental apparatus

The experimental apparatus is the same as that in our previous studies [20,26]. A pulsed microwave discharge generates a plasma in a tube (inner diameter of approx. 1.5 cm) cooled by liquid nitrogen. A mixture of He/Ar/H_2 with a typical composition $10^{17}/10^{14}/10^{14}\,\mathrm{cm}^{-3}$ flows continuously along the discharge tube. Details of the ion formation reactions are given elsewhere [4,5,27]. 'A para-hydrogen generator' prepares samples of para-enriched H_2 (${}^{\mathrm{e}}H_2$) [26]. The enrichment was measured by nuclear magnetic resonance spectroscopy (RNDr Jan Lang PhD 2010, personal communication). NIR-CRDS in the continuous wave modification (based on the configuration described by Romanini *et al.* [28]) was developed in our laboratory for time-resolved studies [26,29,30]. The light source is a fibre-coupled distributed feedback laser diode with a central wavelength of 1381.55 nm, line-width less than 2 MHz, and maximum output optical power of 20 mW. During the experiment, the time-dependent optical absorption signals from the discharge and the afterglow are recorded. The measured absorption is then converted to ion concentrations. The kinetic temperature of the H_3^+ ions and its evolution during the discharge and in the early afterglow were determined from the Doppler-broadened absorption line profiles by tuning the wavelength of the laser diode. All spectroscopic absorption measurements were performed on the second overtone transitions originating from the ground vibrational level of H_3^+. The lowest rotational levels (1,0) (ortho, transition $3v_2^1(2,0) \leftarrow 0v_2^0(1,0)$) and (1,1) (para, transition $3v_2^1(2,1) \leftarrow 0v_2^0(1,1)$) of the vibrational ground state were monitored routinely. In some experiments, we also probed the higher-lying level (3,3) (ortho, transition $3v_2^1(4,3) \leftarrow 0v_2^0(3,3)$). Here, and in the following discussion, the energy levels are labelled (J, G) by their quantum numbers J and G.

3. Experimental results: binary recombination of para-H_3^+ and ortho-H_3^+

The measured electron density decay curves were analysed to obtain α_{eff} for two particular values of ${}^{\mathrm{p}}f_3$ (further details can also be found in the study of Varju *et al.* [20]). We carried out a systematic set of measurements that differed only in the value of ${}^{\mathrm{p}}f_2$ (${}^{\mathrm{p}}f_2 = 0.25$ when using ${}^{\mathrm{n}}H_2$ and ${}^{\mathrm{p}}f_2 = 0.87$ using ${}^{\mathrm{e}}H_2$), but under otherwise very similar conditions. The densities of the para (1,1), ortho (1,0) and ortho (3,3) states of H_3^+ were monitored. Examples of data measured at 140 K with ${}^{\mathrm{n}}H_2$ and with ${}^{\mathrm{e}}H_2$ are plotted in figure 1*a*,*b*, respectively. The middle panels of figure 1*a*,*b* show a large difference in the measured populations of the particular rotational states of H_3^+ in both experiments. In this set of experiments, we obtained ${}^{\mathrm{p}}f_3 \sim 0.5$ for ${}^{\mathrm{n}}H_2$, and ${}^{\mathrm{p}}f_3 \sim 0.7$ for ${}^{\mathrm{e}}H_2$ (see the lower panels). Note that in both experiments, the values of ${}^{\mathrm{p}}f_3$ are nearly constant during the afterglow.

Assuming thermal equilibrium (TDE) within the para and ortho manifolds, we calculated from the densities of the ions in the (1,1) and (1,0) states the

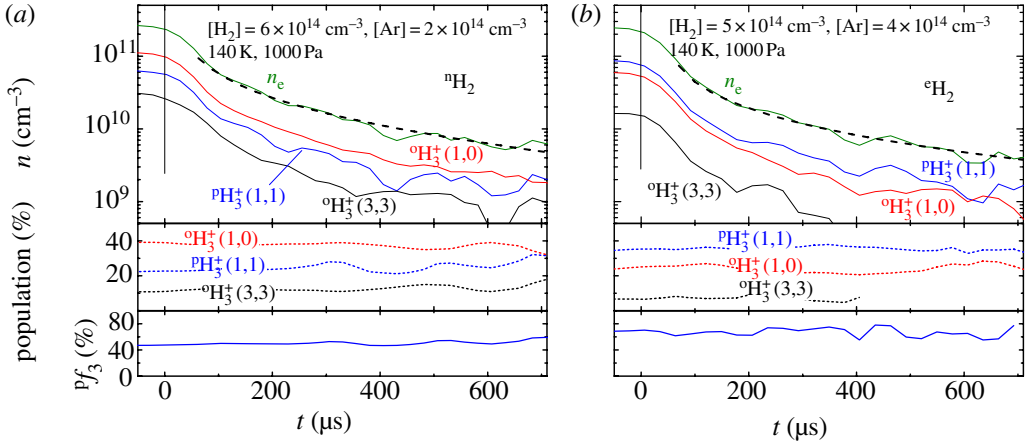

Figure 1. (*a*) Upper panel: a typical example of the ion and electron decay curves measured during the afterglow in a He/Ar/$^{n}H_2$ gas mixture. The time $t = 0$ is taken to be at the beginning of the afterglow when the discharge is switched off. The measurements were made at 140 K and 1000 Pa of He and at the indicated densities of H_2 and Ar. Middle panel: the measured relative populations of the para (1,1), ortho (1,0) and ortho (3,3) states of H_3^+. Lower panel: the measured fraction of $^{p}f_3$ of $^{p}H_3^+$. Note the constant value of $^{p}f_3$ during the afterglow. (*b*) Similar to (*a*), but for data measured in a He/Ar/$^{e}H_2$ gas mixture. (Online version in colour.)

total densities [$^{p}H_3^+$], [$^{o}H_3^+$] and n_e. We have proved experimentally [25,26] that the assumption of TDE under our experimental conditions is correct. To obtain α_{eff} from the measured electron density decay curves, we used direct fits to the data and, in addition, the more advanced 'integral analysis' technique [31]. We deliberately excluded the first 50–150 μs of the afterglow decay from the data analysis because some new ions were probably still being formed (for details see [4,20,26,31]). The observed dependences of $^{n}\alpha_{eff}$ and $^{e}\alpha_{eff}$ on [He] at 140 K are shown in figure 2*a*. The corresponding fractions $^{p}f_3$ are shown in figure 2*c*. Because $^{n}\alpha_{eff}$ and $^{e}\alpha_{eff}$ increase linearly with increasing [He], we can use equation (1.1) to obtain binary and ternary recombination rate coefficients for known para/ortho ratios. The values obtained with normal hydrogen ($^{p}f_3 = 0.5$) correspond to those expected under TDE. The present experiments with $^{n}H_2$ also confirmed that $^{p}f_3$ was 0.5 in our previous flowing afterglow with Langmuir probe (FALP) experiments [4,14,15,32]. Hence, the values of α_{bin} and K_{He} from these experiments correspond to TDE.

The dependences of $^{n}\alpha_{eff}$ and $^{e}\alpha_{eff}$ on [He] were measured for four temperatures in the 77–200 K range. From those dependences and from the corresponding $^{p}f_3$, we calculated the values of $^{p}\alpha_{eff}$ and $^{o}\alpha_{eff}$ for pure $^{p}H_3^+$ and for pure $^{o}H_3^+$, respectively. The binary recombination rate coefficients for pure $^{p}H_3^+$ and for pure $^{o}H_3^+$ were obtained by fitting the values of $^{p}\alpha_{eff}$ and $^{o}\alpha_{eff}$ (figure 2*b*) using equation (1.1). For further details on the data analysis, see Varju *et al.* [20]. The measured values of $^{p}\alpha_{bin}$, $^{o}\alpha_{bin}$, $^{n}\alpha_{bin}$ and values of $^{n}\alpha_{bin}$ from previous FALP experiments [4,14,15] are plotted in figure 3. The displayed errors of rate coefficients are 1σ errors, and systematic errors (mainly from determination of ion number densities) were estimated to be less than 10 per cent.

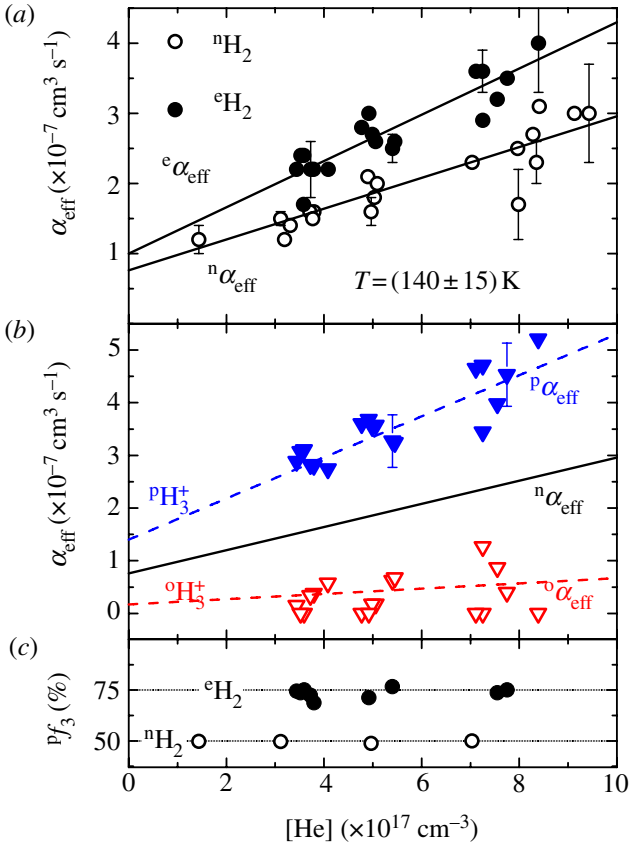

Figure 2. The measured dependences of the effective recombination rate coefficients on the He density at 140 K. (*a*) α_{eff} measured using $^{n}H_2$ (open circles) and α_{eff} measured using $^{e}H_2$ (filled circles). (*b*) The measured values $^{p}\alpha_{eff}$ and $^{o}\alpha_{eff}$ for pure $^{p}H_3^+$ (filled triangles) and pure $^{o}H_3^+$ (open triangles), respectively. (*c*) The fractions $^{p}f_3$ of $^{p}H_3^+$ measured in the experiments with $^{n}H_2$ and $^{e}H_2$. (Online version in colour.)

4. Discussion and conclusion

By using either normal or para-enriched hydrogen gas, we were able to form plasmas with different partial populations of $^{p}H_3^+$ (fractions, $^{p}f_3$) and $^{o}H_3^+$, and from the measured decay of the ion density, we evaluated the binary recombination rate coefficients for pure $^{p}H_3^+$ and $^{o}H_3^+$ ions. The temperature range covered in this study was 77–200 K. The results of this study show a strong dependence of the low-temperature binary recombination of H_3^+ ions on the nuclear spin states of the ions. The agreement between the experimental values ($^{n}\alpha_{bin}$, $^{p}\alpha_{bin}$ and $^{o}\alpha_{bin}$) and the theoretical values ($^{n}\alpha_{DR}$, $^{p}\alpha_{DR}$ and $^{o}\alpha_{DR}$) [18] is very good. Moreover, though the electron number density used in the present experiment was by an order of magnitude higher than in our previous FALP experiments using Langmuir probes [14], the agreement between the present $^{n}\alpha_{bin}$ values and those from the FALP experiments is very good over the whole temperature range. Because of this agreement at higher temperatures, where CRR is negligible, we conclude that the measured rate coefficients at 77 K do not depend on the electron density. From this, it follows that CRR has little to no effect on the plasma decay and that the obtained recombination rate coefficients

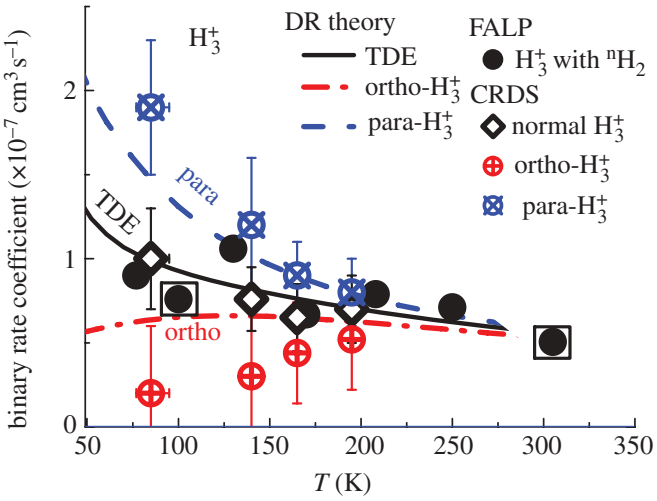

Figure 3. The measured temperature dependences of the binary recombination rate coefficients $^n\alpha_{bin}$, $^p\alpha_{bin}$ and $^o\alpha_{bin}$. 'Normal-H_3^+' refers to data measured in the present experiments with $^nH_2$. Previous FALP data [4,14,15] measured with $^nH_2$ are indicated by filled circles. Combined SA-CRDS/FALP data at 100 K and 305 K [4,14] are indicated by a filled circle in a square. The lines indicate the theoretical rate coefficients for $^pH_3^+$, $^oH_3^+$ and for H_3^+ ions in TDE [18]. (Online version in colour.)

$^p\alpha_{bin}$ and $^o\alpha_{bin}$ correspond to the binary DR (for details see discussion in the study of Dohnal *et al.* [25]). Further results concerning ternary recombination have been published elsewhere [25], together with a detailed discussion of the equilibrium conditions in the recombining afterglow plasma and with an estimation of the effect of the CRR process.

This work was partly financed by the research grant OC10046 from the Ministry of Education of the Czech Republic and was partly supported by GACR (205/09/1183, P209/12/0233), by SV 265 302, by GAUK 92410, GAUK 353811, GAUK 54010 and by COST Action CM0805 (The Chemical Cosmos).

References

1 Oka, T. 2006 Introductory remarks. *Phil. Trans. R. Soc. A* **364**, 2847–2853. (doi:10.1098/rsta.2006.1870)
2 Herbst, E. & Klemperer, W. 1973 The formation and depletion of molecules in dense interstellar clouds. *Astrophys. J.* **185**, 505–533. (doi:10.1086/152436)
3 Larsson, M. 2000 Experimental studies of the dissociative recombination of H_3^+. *Phil. Trans. R. Soc. Lond. A* **358**, 2433–2444. (doi:10.1098/rsta.2000.0658)
4 Glosík, J., Plašil, R., Kotrík, T., Dohnal, P., Varju, J., Hejduk, M., Korolov, I., Roučka, Š. & Kokoouline, V. 2010 Binary and ternary recombination of H_3^+ and D_3^+ ions with electrons in low temperature plasma. *Mol. Phys.* **108**, 2253–2264. (doi:10.1080/00268976.2010.507555)
5 Plašil, R., Glosík, J., Poterya, V., Kudrna, P., Rusz, J., Tichý, M. & Pysanenko, A. 2002 Advanced integrated stationary afterglow method for experimental study of recombination of processes of H_3^+ and D_3^+ ions with electrons. *Int. J. Mass Spectrom.* **218**, 105–130. (doi:10.1016/S1387-3806(02)00714-5)
6 Smith, D. & Španěl, P. 1993 Dissociative recombination of H_3^+ and some other interstellar ions: a controversy resolved. *Int. J. Mass Spectrom. Ion Process.* **129**, 163–182. (doi:10.1016/0168-1176(93)87040-Y)

7 Johnsen, R. 2005 A critical review of H_3^+ recombination studies. *J. Phys. Conf. Ser.* **4**, 83–91. (doi:10.1088/1742-6596/4/1/011)

8 Johnsen, R. & Guberman, S. L. 2010 Dissociative recombination of H_3^+ ions with electrons: theory and experiment. In *Advances in atomic, molecular, and optical physics*, vol. 59 (eds E. Arimondo, P. R. Berman & C. C. Lin), pp. 75–128. New York, NY: Academic Press.

9 Larsson, M. & Orel, A. E. 2008 *Dissociative recombination of molecular ions*. Cambridge, UK: Cambridge University Press.

10 Kokoouline, V. & Greene, C. H. 2003 Unified theoretical treatment of dissociative recombination of D_{3h} triatomic ions: application to H_3^+ and D_3^+. *Phys. Rev. A* **68**, 012703. (doi:10.1103/PhysRevA.68.012703)

11 McCall, B. J. *et al.* 2003 An enhanced cosmic-ray flux towards ζ Persei inferred from a laboratory study of the H_3^+–e^- recombination rate. *Nature* **422**, 500–502. (doi:10.1038/nature01498)

12 Kreckel, H. *et al.* 2005 High-resolution dissociative recombination of cold H_3^+ and first evidence for nuclear spin effects. *Phys. Rev. Lett.* **95**, 263201. (doi:10.1103/PhysRevLett.95.263201)

13 McCall, B. J. *et al.* 2004 Dissociative recombination of rotationally cold H_3^+. *Phys. Rev. A* **70**, 052716. (doi:10.1103/PhysRevA.70.052716)

14 Glosík, J. *et al.* 2009 Temperature dependence of binary and ternary recombination of H_3^+ ions with electrons. *Phys. Rev. A* **79**, 052707. (doi:10.1103/PhysRevA.79.052707)

15 Glosík, J. *et al.* 2008 Recombination of H_3^+ ions in the afterglow of a He–Ar–H_2 plasma. *J. Phys. B* **41**, 191001. (doi:10.1088/0953-4075/41/19/191001)

16 Kreckel, H. *et al.* 2010 High-resolution storage-ring measurements of the dissociative recombination of H_3^+ using a supersonic expansion ion source. *Phys. Rev. A* **82**, 042715. (doi:10.1103/PhysRevA.82.042715)

17 Petrignani, A. *et al.* 2011 Resonant structure of low-energy H_3^+ dissociative recombination. *Phys. Rev. A* **83**, 032711. (doi:10.1103/PhysRevA.83.032711)

18 dos Santos, S. F., Kokoouline, V. & Greene, C. H. 2007 Dissociative recombination of H_3^+ in the ground and excited vibrational states. *J. Chem. Phys.* **127**, 124309. (doi:10.1063/1.2784275)

19 Mikosch, J., Kreckel, H., Wester, R., Glosík, J., Plašil, R., Gerlich, D., Schwalm, D. & Wolf, A. 2004 Action spectroscopy and temperature diagnostics of H_3^+ by chemical probing. *J. Chem. Phys.* **121**, 11 030–11 037. (doi:10.1063/1.1810512)

20 Varju, J., Hejduk, M., Dohnal, P., Jílek, M., Kotrík, T., Plašil, R., Gerlich, D. & Glosík, J. 2011 Nuclear spin effect on recombination of H_3^+ ions with electrons at 77 K. *Phys. Rev. Lett.* **106**, 203201. (doi:10.1103/PhysRevLett.106.203201)

21 Glosík, J. *et al.* 2009 Binary and ternary recombination of D_3^+ ions with electrons in He–D_2 plasma. *Phys. Rev. A* **80**, 042706. (doi:10.1103/PhysRevA.80.042706)

22 Kotrík, T., Dohnal, P., Korolov, I., Plašil, R., Roučka, S., Glosík, J., Greene, C. H. & Kokoouline, V. 2010 Temperature dependence of binary and ternary recombination of D_3^+ ions with electrons. *J. Chem. Phys.* **133**, 034305. (doi:10.1063/1.3457940)

23 Bates, D. R., Kingston, A. E. & McWhirter, R. W. P. 1962 Recombination between electrons and atomic ions. I. Optically thin plasmas. *Proc. R. Soc. Lond. A* **267**, 297–312. (doi:10.1098/rspa.1962.0101)

24 Kotrík, T., Dohnal, P., Roučka, Š., Jusko, P., Plašil, R., Glosík, J. & Johnsen, R. 2011 Collisional-radiative recombination $Ar^+ + e + e$: experimental study at 77–180 K. *Phys. Rev. A* **83**, 032720. (doi:10.1103/PhysRevA.83.032720)

25 Dohnal, P., Hejduk, M., Varju, J., Rubovič, P., Roučka, Š., Kotrík, T., Plašil, R., Glosík, J. & Johnsen, R. 2012 Binary and ternary recombination of para- and ortho-H_3^+ with electrons: state selective study at 77–200 K. *J. Chem. Phys.* **136**, 244304. (doi:10.1063/1.4730162)

26 Hejduk, M., Dohnal, P., Varju, J., Rubovič, P., Kotrik, T., Plašil, R. & Glosík, J. 2012 Nuclear spin state-resolved cavity ring-down spectroscopy diagnostics of a low-temperature H_3^+-dominated plasma. *Plasma Sources Sci. Technol.* **21**, 024002. (doi:10.1088/0963-0252/21/2/024002)

27 Glosík, J., Plašil, R., Poterya, V., Kudrna, P., Tichý, M. & Pysanenko, A. 2001 Experimental study of recombination of H_3^+ ions with electrons relevant for interstellar and planetary plasmas. *J. Phys. B* **34**, L485–L494. (doi:10.1088/0953-4075/34/15/104)

28 Romanini, D., Kachanov, A. A., Sadeghi, N. & Stoeckel, F. 1997 CW cavity ring down spectroscopy. *Chem. Phys. Lett.* **264**, 316–322. (doi:10.1016/S0009-2614(96)01351-6)
29 Macko, P., Bano, G., Hlavenka, P., Plašil, R., Poterya, V., Pysanenko, A., Votava, O., Johnsen, R. & Glosík, J. 2004 Afterglow studies of H_3^+ ($\nu = 0$) recombination using time resolved cw-diode laser cavity ring-down spectroscopy. *Int. J. Mass Spectrom.* **233**, 299–304. (doi:10.1016/j.ijms.2003.12.035)
30 Hlavenka, P., Plašil, R., Bano, G., Korolov, I., Gerlich, D., Ramanlal, J., Tennyson, J. & Glosík, J. 2006 Near infrared second overtone cw-cavity ringdown spectroscopy of D_2H^+ ions. *Int. J. Mass Spectrom.* **255–256**, 170–176. (doi:10.1016/j.ijms.2006.02.002)
31 Plašil, R., Korolov, I., Kotrík, T. & Glosík, J. 2008 Recombination of KrD^+ and XeD^+ ions with electrons. *Int. J. Mass Spectrom.* **275**, 80–85. (doi:10.1016/j.ijms.2008.05.037)
32 Glosík, J., Plašil, R., Korolov, I., Novotný, O. & Kotrík, T. 2009 Multicollision character of recombination of H_3^+ ions in afterglow plasma. *J. Phys. Conf. Ser.* **192**, 012005. (doi:10.1088/1742-6596/192/1/012005)

ARTICLE IV

TITLE: Binary and ternary recombination of para-H_3^+ and ortho-H_3^+ with electrons: State selective study at 77–200 K

AUTHORS: Petr Dohnal, Michal Hejduk, Jozef Varju, Peter Rubovič, Štěpán Roučka, Tomáš Kotrík, Radek Plašil, Juraj Glosík, and Rainer Johnsen

JOURNAL: The Journal of Chemical Physics, 136:244304 (14pp)

DATE: 26 June 2012

DOI: 10.1063/1.4730162

Binary and ternary recombination of para-H_3^+ and ortho-H_3^+ with electrons: State selective study at 77–200 K

Petr Dohnal,[1] Michal Hejduk,[1] Jozef Varju,[1] Peter Rubovič,[1] Štěpán Roučka,[1] Tomáš Kotrík,[1] Radek Plašil,[1] Juraj Glosík,[1] and Rainer Johnsen[2]
[1]*Department of Surface and Plasma Science, Faculty of Mathematics and Physics, Charles University, Prague 18000, Czech Republic*
[2]*Department of Physics and Astronomy, University of Pittsburgh, Pittsburgh, Pennsylvania 15260, USA*

(Received 13 April 2012; accepted 1 June 2012; published online 26 June 2012)

Measurements in H_3^+ afterglow plasmas with spectroscopically determined relative abundances of H_3^+ ions in the para-nuclear and ortho-nuclear spin states provide clear evidence that at low temperatures (77–200 K) para-H_3^+ ions recombine significantly faster with electrons than ions in the ortho state, in agreement with a recent theoretical prediction. The cavity ring-down absorption spectroscopy used here provides an *in situ* determination of the para/ortho abundance ratio and yields additional information on the translational and rotational temperatures of the recombining ions. The results show that H_3^+ recombination with electrons occurs by both binary recombination and third-body (helium) assisted recombination, and that both the two-body and three-body rate coefficients depend on the nuclear spin states. Electron-stabilized (collisional-radiative) recombination appears to make only a small contribution. © *2012 American Institute of Physics*. [http://dx.doi.org/10.1063/1.4730162]

I. INTRODUCTION

The present experiments were motivated by the fundamental character of the recombination of H_3^+ ions,[1] its relevance to modeling of astrophysical diffuse clouds,[2] and electrical discharges in hydrogen. In cold diffuse clouds (temperatures from 50 to 100 K), H_3^+ ions are formed by cosmic-ray ionization of H_2, followed by the reaction $H_2^+ + H_2 \rightarrow H_3^+ + H$.[3] The H_3^+ ions subsequently either recombine by dissociative recombination (DR) with electrons or transfer protons to other atoms or molecules.[4] The recombination of H_3^+ ions competes with the rate of molecule formation in diffuse clouds and plays a pivotal role in the chemical evolution. Even though H_3^+ is the "simplest" triatomic ion, its recombination is a rather subtle process that has challenged theorists and experimentalists for many years. It has become clear in recent years that the ortho-modifications and para-modifications of H_3^+, distinguished by their nuclear spins and allowed rotational states, may recombine differently at low temperatures. The experiments described in this paper focus on this question. Unlike other previous experiments, they incorporate *in situ* spectroscopic identification of the recombining ion species in the recombining medium.

The spin dependence of H_3^+ recombination also plays a role in the interpretation of spectra observed in astrophysical clouds. For instance, a recent analysis by Crabtree *et al.*[5] of several diffuse molecular clouds suggests that the observed differences between the rotational excitation temperatures of H_2 and H_3^+ (denoted as $T_{(01)}(H_2)$ and $T(H_3^+)$) can be explained by a kinetic model that includes both reactive collisions of H_3^+ or para-H_3^+ with H_2 and recombination with electrons. The model makes specific allowance for the dependence of all relevant reaction rates on the ortho/para states of both H_2 and H_3^+. Surprisingly, reasonable agreement between observed and calculated excitation temperatures was found only when the DR rate coefficients of para-H_3^+ (nuclear spin $I = 1/2$) and H_3^+ (nuclear spin $I = 3/2$) were assumed to be nearly equal, which, however, is in conflict with the theoretical prediction[6] that the low-temperature DR rate coefficient of para-H_3^+ is considerably larger than that of H_3^+.

The history of H_3^+ recombination studies has been extensively covered in a number of reviews[7–12] and in the book by Larsson and Orel.[13] Many of the once puzzling disagreements among measured recombination coefficients have either been resolved or can be rationalized by invoking third-body stabilized recombination processes that occur in plasmas but not in beam-type experiments. Also, earlier serious discrepancies between experimental results and theory were largely resolved in 2001 when it was shown that the Jahn–Teller mechanism can account for the observed magnitude of dissociative recombination rates of H_3^+ ions.[14] Subsequent improvements of the theory[15] yielded a thermal rate coefficient of the dissociative recombination at 300 K of $\alpha_{DR} = 5.6 \times 10^{-8}$ cm^{3}s^{-1} which comes close to the magnitude of many experimental values. Theoretical predictions also agree quite well with the temperature dependence of the thermal rate coefficients inferred from ion-storage-rings (ISR) experiments. The more recent ISR studies employed ion sources specifically designed to produce rotationally cold ions ("cold ion sources")[16–18] and the results supported the theoretical thermal rate coefficients.[19] At that time it appeared that a satisfactory solution to the "H_3^+ enigma," the often-cited term coined by Bates *et al.* in 1993,[20] had been found. However, it proved difficult to verify experimentally that the H_3^+ ions circulating in the storage rings were truly rotationally cold

and this problem has not been entirely solved. It had been assumed that the "cold" rotational distributions inferred from spectroscopic observations in the ion source survived extraction into the storage ring and were not altered further in the ring, but recent experiments using high-resolution storage-rings indicate that these assumptions were not necessarily correct.[21,22] The problem awaits clarification by further experiments. Also, high-resolution storage rings data exhibit resonances at particular collision energies that have not been clearly assigned to specific recombination paths and are not predicted by theory.[22] Thus, a truly satisfactory convergence of theory and experiment has not been achieved. Petrignani *et al.*[22] summed up the current situation of storage-ring experiments: *"Presently no rate coefficient measurement with a confirmed temperature below 300 K exists."* Plasma afterglow measurements at reduced temperatures have been made, but those, as will be discussed later, have their own set of complications. Paraphrasing Bates *et al.*[20] and Larsson *et al.*,[19] we can sum up the state of the art today in the words: *"... the saga of the* H_3^+ *enigma continues...."*

Recent theoretical calculations[6] predict that the low-temperature DR rate coefficients for para-H_3^+ are larger than those for H_3^+ ions, by a factor of about ten at temperatures below 10 K. This prediction has been qualitatively confirmed at low electron-ion collision energies in storage-ring experiments using para-enriched H_3^+,[17,23] but, as has been mentioned before, the actual para/ortho abundance ratio of the recombining ions was not experimentally verified. This problem, of course, is closely linked to that of the rotational populations. Further progress will require direct *in situ* determination of the para/ortho ratio and rotational excitation of the stored H_3^+ ions. Experimental photodissociation measurements on H_3^+ ions in the ring may be one feasible approach (see discussion in Refs. 24 and 25).

The experiments described here make use of the plasma afterglow technique but add spectroscopic capabilities. Here, the ion densities are many orders of magnitude larger than those in storage rings which enables *in situ* spectroscopic absorption measurements of rotational populations of H_3^+ ions under recombination-controlled conditions. The feasibility of such experiments was demonstrated by us in a recent study in which we measured binary recombination rate coefficients for para-H_3^+ and ortho-H_3^+ ions ($^{p}\alpha_{bin}$ and $^{o}\alpha_{bin}$) at buffer gas temperature ~77 K.[26,27] The present study extends this work and provides recombination rate coefficients for pure para-H_3^+ and pure ortho-H_3^+ over a wider range of temperatures from 77 K to 200 K. As before, the experiments were carried out in a stationary afterglow (SA) in conjunction with a near-infrared cavity-ring-down absorption spectrometer (NIR–CRDS) for direct *in situ* determination of the kinetic temperature, the rotational temperature, and the spin states of the ions.

In a SA experiment[28] electrons and ions undergo multiple collisions with buffer gas atoms (here He and Ar) and reagent molecules (here H_2) prior to their recombination. The early phase of the afterglow is dominated by ion-formation and ion-conversion reactions, electron thermalization, and equilibration of internal degrees of freedom of the ions. Ideally, this early phase should be completed rapidly so that the only relevant processes during the recombination phase are binary electron-ion recombination and ambipolar diffusion of ions and electrons. However, the neutral constituents (He, H_2, and Ar in our case) and ambient electrons and ions can affect the overall recombination process as well as the para/ortho ratio and this requires careful consideration. There are two known ternary recombination processes that contribute to the plasma decay, ternary neutral-assisted recombination (largely due to the helium buffer),[29] and ternary electron-assisted collisional radiative recombination (CRR).[30–32] We have recently studied the ternary helium-assisted recombination of H_3^+ and D_3^+ ions with electrons at conditions similar to those of the present experiments[8,33–37] and found that H_3^+ ions recombine by both the binary process with rate coefficient α_{bin} and by ternary ("He-assisted") process with ternary rate coefficient K_{He}. The observed plasma decay yields an "effective" rate coefficient α_{eff} given by the sum $\alpha_{eff} = \alpha_{bin} + K_{He}[He]$ that can be decomposed into its parts by measuring the dependence of α_{eff} on helium density [He].

The role of electron-assisted CRR is less clear because experimental data and theoretical calculations exist only for atomic ions but not for molecular ions. For atomic ions the predicted very strong negative temperature dependence, $\alpha_{CRR} \sim n_e T^{-4.5}$, of the CRR rate coefficient, has been confirmed for temperatures above 300 K,[30,38,39] and recently also for Ar^+ ions at temperatures below 300 K.[32,40] In low-temperature plasmas most molecular ions are removed by fast dissociative recombination (see, e.g., book by Larsson and Orel[13]) and the contribution from collisional radiative recombination is usually negligible. However, at temperatures approaching 77 K the effective binary rate of CRR (Refs. 38 and 39) becomes comparable to typical DR rate coefficients for electron densities $>10^{10}$ cm^{-3}. Somewhat surprisingly, the H_3^+ afterglow studies of Amano[41,42] at gas temperatures near 77 K and electron densities $>10^{11}$ cm^{-3} seemed to indicate that CRR did not play a significant role. However, as Bates[20] pointed out, the occurrence of CRR is "inevitable," and to make matters worse, the observed plasma decay due to CRR can give the appearance of binary recombination since the energy released by CRR can lead to a time-dependent electron temperature. A quantitative re-analysis of Amano's experiments is beyond the scope of this paper. It is far from obvious that CRR made only a negligible contribution. It is also difficult to accept the author's conclusion that clustering of H_3^+ to form fast recombining H_5^+ ions was entirely absent.

In our flowing afterglow (FA, FALP (Ref. 34)) and stationary afterglow (SA (Refs. 26 and 43)) experiments we can measure at gas temperatures close to 77 K and cover a wide range of electron and ion densities, from 10^8 to 10^{11} cm^{-3}. This makes it possible to separate binary and helium-assisted ternary recombination of H_3^+ ions from CRR. We will conclude (see Appendix) that CRR may have a slight effect at the lowest temperature (77 K), but most likely it is completely negligible at higher temperatures.

II. EXPERIMENTAL METHODS

The basic methods of measuring recombination rates in afterglow plasmas are well known and will not be

discussed here in great detail. This section focuses on the interconversion processes between para-H_3^+ and ortho-H_3^+ ions, and their recombination. Technical details of the experiments will be presented in Sec. III.

A. Afterglow processes in para-H_3^+ and ortho-H_3^+ dominated plasma

In the following upper left indices p, o, n, and e denote "para," "ortho," "normal," and "para-enriched" hydrogen (e.g., ${}^{\mathrm{p}}H_2$, ${}^{\mathrm{o}}H_2$, ${}^{\mathrm{n}}H_2$, and ${}^{\mathrm{e}}H_2$) and ${}^{\mathrm{p}}f_2$ and ${}^{\mathrm{o}}f_2$ denote their fractions. Para-H_3^+ and ortho-H_3^+ ions denote ${}^{\mathrm{p}}H_3^+$ and ${}^{\mathrm{o}}H_3^+$, while ${}^{\mathrm{p}}f_3$ and ${}^{\mathrm{o}}f_3$ stand for their fractions (i.e., ${}^{\mathrm{p}}f_3 = [{}^{\mathrm{p}}H_3^+]/[H_3^+]$ and ${}^{\mathrm{o}}f_3 = [{}^{\mathrm{o}}H_3^+]/[H_3^+]$ with ${}^{\mathrm{p}}f_3 + {}^{\mathrm{o}}f_3 = 1$). Absence of an index implies that the spin modification is not specified.

In a low-temperature afterglow plasma in a gas mixture of helium (the "buffer gas") with small additions of argon and hydrogen the principal processes affecting the densities of ${}^{\mathrm{p}}H_3^+$ and ${}^{\mathrm{o}}H_3^+$ are recombination, ambipolar diffusion, para/ortho conversion in reactions with H_2, and formation of H_5^+ in ternary association, i.e.:

$$ {}^{\mathrm{p}}H_3^+ + e^- \xrightarrow{{}^{\mathrm{p}}\alpha_{\mathrm{eff}}} \text{neutral products}, \tag{1a} $$

$$ {}^{\mathrm{o}}H_3^+ + e^- \xrightarrow{{}^{\mathrm{o}}\alpha_{\mathrm{eff}}} \text{neutral products}, \tag{1b} $$

$$ {}^{\mathrm{p}}H_3^+ + H_2 \xrightarrow{\nu_{\mathrm{po}}} {}^{\mathrm{o}}H_3^+ + H_2, \tag{1c} $$

$$ {}^{\mathrm{o}}H_3^+ + H_2 \xrightarrow{\nu_{\mathrm{op}}} {}^{\mathrm{p}}H_3^+ + H_2, \tag{1d} $$

$$ {}^{\mathrm{p}}H_3^+ + H_2 + He \xrightarrow{{}^{\mathrm{p}}\tau_{\mathrm{R}}} H_5^+ + He, \tag{1e} $$

$$ {}^{\mathrm{o}}H_3^+ + H_2 + He \xrightarrow{{}^{\mathrm{o}}\tau_{\mathrm{R}}} H_5^+ + He, \tag{1f} $$

where ${}^{\mathrm{p}}\alpha_{\mathrm{eff}}$ and ${}^{\mathrm{o}}\alpha_{\mathrm{eff}}$ stand for effective (apparent binary) recombination rate coefficients of pure para-H_3^+ and pure ortho-H_3^+ ions, respectively. ν_{po} and ν_{op} are the frequencies of para-H_3^+/ortho-H_3^+ conversion due to reactions with H_2. The spin state of the neutral hydrogen molecule in reactions (1c) and (1d) will change also, but because the neutral hydrogen is far more abundant than the ions, the resulting change in ${}^{\mathrm{p}}f_2$ can be neglected. ${}^{\mathrm{p}}\tau_{\mathrm{R}}$ and ${}^{\mathrm{o}}\tau_{\mathrm{R}}$ are time constants for ternary association, later we will assume that ${}^{\mathrm{p}}\tau_{\mathrm{R}} = {}^{\mathrm{o}}\tau_{\mathrm{R}}$ for simplification. The continuity equations for the ion densities $[{}^{\mathrm{p}}H_3^+]$ and $[{}^{\mathrm{o}}H_3^+]$ during the afterglow are:

$$ \frac{\mathrm{d}[{}^{\mathrm{p}}H_3^+]}{\mathrm{d}t} = -{}^{\mathrm{p}}\alpha_{\mathrm{eff}}[{}^{\mathrm{p}}H_3^+]n_{\mathrm{e}} - \frac{[{}^{\mathrm{p}}H_3^+]}{\tau_{\mathrm{D}}} - \nu_{\mathrm{po}}[{}^{\mathrm{p}}H_3^+] + \nu_{\mathrm{op}}[{}^{\mathrm{o}}H_3^+] - \frac{[{}^{\mathrm{p}}H_3^+]}{{}^{\mathrm{p}}\tau_{\mathrm{R}}}, \tag{2} $$

$$ \frac{\mathrm{d}[{}^{\mathrm{o}}H_3^+]}{\mathrm{d}t} = -{}^{\mathrm{o}}\alpha_{\mathrm{eff}}[{}^{\mathrm{o}}H_3^+]n_{\mathrm{e}} - \frac{[{}^{\mathrm{o}}H_3^+]}{\tau_{\mathrm{D}}} + \nu_{\mathrm{po}}[{}^{\mathrm{p}}H_3^+] - \nu_{\mathrm{op}}[{}^{\mathrm{o}}H_3^+] - \frac{[{}^{\mathrm{o}}H_3^+]}{{}^{\mathrm{o}}\tau_{\mathrm{R}}}, \tag{3} $$

where n_{e} is electron density and τ_{D} is the time constant for ambipolar diffusion, assumed to be equal for both spin modification of H_3^+. Three-body association of H_3^+ with H_2 to form H_5^+ is at the hydrogen and helium densities used in the present experiments relatively slow in comparison with the rate of the recombination (for details see Refs. 9, 34, and 44) and we can conclude $[H_5^+] \ll [H_3^+]$. Assuming that the plasma is quasineutral and that it contains no ions other than H_3^+ (i.e., $n_{\mathrm{e}} = [{}^{\mathrm{p}}H_3^+] + [{}^{\mathrm{o}}H_3^+]$), the continuity equation for the electron density (obtained by summing Eqs. (2) and (3)) becomes

$$ \frac{\mathrm{d}n_{\mathrm{e}}}{\mathrm{d}t} = -({}^{\mathrm{p}}f_3\,{}^{\mathrm{p}}\alpha_{\mathrm{eff}} + {}^{\mathrm{o}}f_3\,{}^{\mathrm{o}}\alpha_{\mathrm{eff}})n_{\mathrm{e}}^2 - \frac{n_{\mathrm{e}}}{\tau_{\mathrm{D}}} - \frac{n_{\mathrm{e}}}{\tau_{\mathrm{R}}}. \tag{4a} $$

The experimental data (see Sec. V) show that the fractions ${}^{\mathrm{p}}f_3$ and ${}^{\mathrm{o}}f_3$ are nearly constant during the afterglow. This implies that the para/ortho ratio is maintained by reactions (1c) and (1d) on a time scale that is short compared to the recombination time scale. In that case, one can define an overall effective (apparent binary) recombination rate coefficient for a given mixture of ortho and para ions by $\alpha_{\mathrm{eff}} = {}^{\mathrm{p}}f_3\,{}^{\mathrm{p}}\alpha_{\mathrm{eff}} + {}^{\mathrm{o}}f_3\,{}^{\mathrm{o}}\alpha_{\mathrm{eff}}$. Equation (4a) then simplifies to

$$ \frac{\mathrm{d}n_{\mathrm{e}}}{\mathrm{d}t} = -\alpha_{\mathrm{eff}}n_{\mathrm{e}}^2 - \frac{n_{\mathrm{e}}}{\tau_{\mathrm{L}}}, \tag{4b} $$

where $1/\tau_{\mathrm{L}} = 1/\tau_{\mathrm{D}} + 1/\tau_{\mathrm{R}}$. The time constant τ_{L} characterizes losses due to diffusion and reactions (1e) and (1f).

A measurement of α_{eff} for two or more different values of ${}^{\mathrm{p}}f_3$, but under otherwise identical conditions (temperature and density of He and H_2), then permits a determination of the individual recombination rate coefficients ${}^{\mathrm{p}}\alpha_{\mathrm{eff}}$ and ${}^{\mathrm{o}}\alpha_{\mathrm{eff}}$. These rate coefficients still do not necessarily represent purely binary recombination. In earlier work we observed that H_3^+ recombination in low-temperature (<300 K) helium-buffered afterglows occurs not only by binary recombination but also by ternary helium-assisted recombination.[8,33,34,36] In those studies ${}^{\mathrm{n}}H_2$ was used as a precursor gas to form H_3^+. It was then found that the effective recombination coefficient α_{eff} varies linearly with helium density [He], i.e.,

$$ \alpha_{\mathrm{eff}}(T, [\mathrm{He}]) = \alpha_{\mathrm{bin}}(T) + K_{\mathrm{He}}[\mathrm{He}], \tag{5} $$

where α_{bin} and K_{He} are the binary and ternary recombination rate coefficients. Previous experiments at 77 K (Ref. 27) showed that the same linear relation holds for the state-selected effective recombination rate coefficients ${}^{\mathrm{p}}\alpha_{\mathrm{eff}}$ and ${}^{\mathrm{o}}\alpha_{\mathrm{eff}}$. Hence, least-square fits to data of α_{eff} as a function of the helium density for two different values of ${}^{\mathrm{p}}f_3$ can be analyzed to obtain α_{bin} and K_{He} for each of the two spin states of H_3^+.

In experiment, ${}^{\mathrm{p}}f_3$ can be enhanced from about 0.5 to 0.8 by substituting para-enriched hydrogen for normal hydrogen. This was tested by a preliminary set of experiments, to be discussed next. Technical details of the para H_2 generator and the optical absorption measurements will be presented in Sec. III.

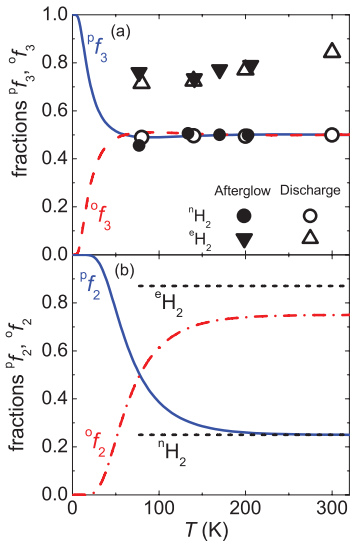

FIG. 1. Panel (a): Calculated temperature variation of the fractions $^{p}f_3$ and $^{o}f_3$ in thermal equilibrium, compared to measured values of $^{p}f_3$ during the discharge phase (open triangles) and during the afterglow (closed circles and triangles) in experiments with either $^{n}H_2$ or $^{e}H_2$. Panel (b): Calculated thermal-equilibrium fractions $^{p}f_2$ and $^{o}f_2$. The dashed horizontal lines indicate the values of $^{p}f_2$ in experiments with either $^{n}H_2$ or $^{e}H_2$ (measured by NMR).

B. Method of controlling the relative abundance of para-H_3^+ and ortho-H_3^+

In the experiment, normal $^{n}H_2$ is obtained by cooling normal hydrogen from 300 K to lower temperatures without ortho–para conversion, i.e., in a container without a catalyst. Hence, $^{n}H_2$ will have fraction $^{p}f_2 = 1/4$ and $^{o}f_2 = 3/4$. Para-enriched H_2 is produced by cooling normal hydrogen to cryogenic temperatures in the presence of a catalyst and then letting it warm up without the catalyst to the desired temperature. Our experiments confirmed earlier findings that an increase of $^{p}f_3$ in hydrogen discharges can be achieved by using $^{e}H_2$ instead of $^{n}H_2$ (see, e.g., Refs. 45 and 46), and that the increase of $^{p}f_3$ observed during the microwave discharge persists into afterglow phase.[26,27,43]

Figure 1 shows the equilibrium values $^{p}f_3$ and $^{o}f_3$ and $^{p}f_2$ and $^{o}f_2$ for temperatures from 0 to 300 K, calculated using published energy levels.[47,48] The same graph shows our experimental values of $^{p}f_3$ and $^{o}f_3$. In normal H_2 measured $^{p}f_3$ approach 0.5 at temperatures above ∼77 K, this is the value corresponding to thermal equilibrium at these temperatures. When para-enriched H_2 is used, measured $^{p}f_3$ becomes significantly larger (∼0.8).

III. EXPERIMENTAL APPARATUS

A. Stationary afterglow

The plasma is generated in a pulsed microwave discharge in a fused silica tube (inner diameter ∼ 1.5 cm) cooled by liquid nitrogen to nearly 77 K or by pre-cooled nitrogen gas for measurements in the range 80–220 K. The tube contains a mixture of He/Ar/H_2 with a typical composition

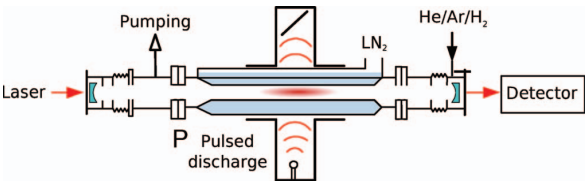

FIG. 2. Schematic diagram (not to scale) of the discharge tube and the optical resonator (cw–CRDS). The discharge tube at the center (containing a He/Ar/H_2 gas mixture) is immersed in liquid or pre-cooled gaseous nitrogen. The light signal exiting the optical cavity is measured by a photodetector (InGaAs avalanche photodiode).

$10^{17}/10^{14}/10^{14}$ cm^{-3} (details of the ion formation reactions are given in Refs. 8, 9, 34, 37, 44, and 49. The gas handling system includes a "para H_2 generator," used to prepare samples of para-enriched H_2, indicated here as $^{e}H_2$.[43] The microwave generator 2.45 GHz is equipped with an external fast high voltage switch to cut off the power to the magnetron within a fall time of < 30 μs. A fairly low microwave power in the range 5–15 W, with ∼50% duty cycle, was used to avoid excessive heating of the gas during the discharge.

B. CRDS spectroscopy

The principal diagnostic technique employs cavity ring down absorption spectroscopy in the continuous wave modification (cw-CRDS), based on the configuration described by Romanini *et al.*[50] The instrument used here was fabricated in our laboratory for spectroscopic time-resolved studies of elementary processes in plasmas, such as ion-electron recombination (see, e.g., Refs. 43 and 51–54). The light source is a fiber-coupled distributed feedback (DFB) laser diode with a central wavelength of 1381.55 nm, linewidth <2 MHz, and maximum output optical power of 20 mW. The wavelengths are measured by a wavemeter and a Fabry–Perot etalon. The ring-down signal exiting the optical cavity is detected by an InGaAs avalanche photodiode. A schematic picture of the apparatus is shown in Fig. 2.

The cw-CRDS instrument in conjunction with associated data processing electronics records the time-dependent optical absorption signals during the discharge and the afterglow. The observed absorption strengths are then converted to ion concentrations. By tuning the wavelength of the laser diode one can also determine the kinetic temperatures of the H_3^+ ions from the Doppler-broadened absorption line profiles, and their evolution during the discharge and in the early afterglow.

All spectroscopic absorption measurements were performed on the second overtone transitions originating from the ground vibrational level of H_3^+. The lowest rotational levels (1,0) (ortho) and (1,1) (para) of the vibrational ground state were monitored routinely, but the higher lying level (3,3) (ortho) was probed only occasionally. These first two transitions were chosen for routine scanning because they have closely spaced frequencies that can be covered by a single DFB laser. This made it possible to switch quickly from observing one to the other H_3^+ spin state. Figure 3 shows the relevant rotational levels and Table I lists the transitions. The

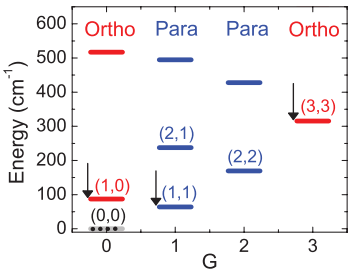

FIG. 3. Rotational energy levels of the ground vibrational state of H_3^+. The energy levels (J,G) are labeled by quantum numbers J and G.[55] The zero of the energy scale is taken at the forbidden (0,0) level, indicated by a dashed line. The rotational states, (1,0), (1,1), and (3,3) observed in the present study are indicated by arrows. Compiled from the data in Ref. 56.

energy levels are labeled (J,G) by their quantum numbers J and G.[55]

C. Para H_2 generator

Normal hydrogen gas at 300 K is a mixture of 1/4 para-hydrogen and 3/4 ortho-hydrogen (i.e., ${}^{\mathrm{p}}f_2 = 0.25$ and ${}^{\mathrm{o}}f_2 = 0.75$, see Fig. 1). It is well known that the composition changes extremely slowly when the hydrogen is cooled or heated, unless the gas is in contact with a suitable paramagnetic catalyst that facilitates re-alignment of the proton spins. By using a catalyst and cooling to low temperatures, nearly pure samples of para-hydrogen in the lowest rotational state ($J = 0$, $\nu = 0$) can be produced. When the catalyst is then removed and the gas is reheated, the hydrogen retains its low-temperature para/ortho composition for a sufficiently long time to carry out experiments with para-enriched hydrogen.

We produced para-enriched hydrogen in a closed-cycle helium cryostat that cools hydrogen in a conversion chamber[57] filled with the catalyst Fe_2O_3. Nuclear magnetic resonance (NMR) was used to check the actual para/ortho ratio in the enriched para-hydrogen ${}^{\mathrm{e}}H_2$. The experimental setup for measurement of para-hydrogen enrichment was similar to the one used in study by Tom.[58] The NMR measurements indicated (87 ± 5)% content of para-hydrogen, i.e., ${}^{\mathrm{p}}f_2 = 0.87$,[59] which is adequate for our experiments. In the following text we will use this value of ${}^{\mathrm{p}}f_2$ without explicitly mentioning its error. It suffices to enrich the hydrogen to a level where the fraction of para-H_3^+ significantly exceeds the value ${}^{\mathrm{p}}f_3 = 0.5$ in normal hydrogen. Figure 1 shows experimental data on the para-enrichment of H_3^+ measured in the discharge and in the afterglow for ${}^{\mathrm{e}}H_2$ and for ${}^{\mathrm{n}}H_2$.

IV. TEMPERATURES IN THE H_3^+ AFTERGLOW PLASMA

The different particles in a plasma afterglow and their internal degrees of freedom are not necessarily in complete thermal equilibrium with each other and with the walls of the plasma container. For instance, the electron temperature T_e can significantly exceed that of the ions T_{Kin} and gas atoms T_G because the energy transfer in electron collisions with heavy particles is inefficient. Also, the ion's rotational temperature T_{Rot} and vibrational temperature T_{Vib} do not have to be equal to the ion's translational temperature.

A. Ion and neutral gas kinetic temperatures

Since the exchange of translational energy between ions and neutral gas atoms is very efficient, the kinetic temperature of the H_3^+ ions during the afterglow should be nearly the same as the gas temperature, provided that the plasma is free of macroscopic electric fields that, in principle, can heat the ions. The ambipolar electric field is too weak to cause a significant heating. This expectation was confirmed by time-resolved scans of the Doppler-broadened absorption lines of H_3^+ ions over the experimental temperature range from 77 K to 220 K. The inferred temperatures of the H_3^+ ions during the discharge and the afterglow were equal to the wall temperature within ~10 K (see also Figs. 3 and 4 in Ref. 43). This also confirmed that the gas temperature in the discharge region approaches that of the walls. Previous afterglow studies in this lab performed under similar conditions,[60] but using absorption lines of H_2O rather than of H_3^+, led to the same conclusion.

B. Electron temperature T_e

The electron temperature T_e was not measured in these experiments. In previous FALP experiments[61–63] we used Langmuir probes to determine the electron energy distribution function in He and He/Ar buffered afterglow plasmas under conditions similar to those in the present study. It was found that the electrons gained a Maxwellian distribution with the gas temperature very quickly after the metastable helium atoms from the microwave discharge had been depleted by Penning ionization of argon atoms.[64] The electron cooling time constant at typical helium densities can also be estimated as the product of the electron-helium collision frequency (>1 GHz) and the mass ratio $2m_e/m_{He}$, which yields a cooling time of $\tau_\varepsilon < 10\ \mu$s.[65] We indirectly observed fast cooling of electrons by monitoring visible light emissions from the discharge and in the very early afterglow.[51] These estimates

TABLE I. Transitions monitored in the present study. For details on the spectroscopic notation see Ref. 55. Energy levels were taken from Ref. 56.

Wavenumber (cm^{-1})	Spin	Low. lvl. (cm^{-1})	Up. lvl. (cm^{-1})	Transition
7234.957	o	315.349	7550.316	$3\nu_2^1(4,3) \leftarrow 0\nu_2^0(3,3)$
7237.285	p	64.1234	7301.4084	$3\nu_2^1(2,1) \leftarrow 0\nu_2^0(1,1)$
7241.245	o	86.9591	7328.2041	$3\nu_2^1(2,0) \leftarrow 0\nu_2^0(1,0)$

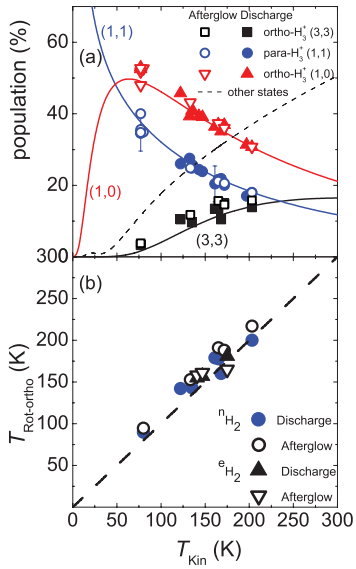

FIG. 4. Rotational temperatures of H_3^+ ions. Panel (a): Relative populations of H_3^+ ions in ortho (1,0) and (3,3) and para (1,1) states versus kinetic temperature of the ions measured in the experiments with normal H_2. The data obtained during the discharge (before switching it off) and during the afterglow (at ~ 150 μs) are indicated by the filled and the open symbols, respectively. The full lines indicate the calculated populations of the indicated states for ions in thermal equilibrium at temperatures equal to T_{Kin}. The dashed line indicates joint population of all other states. Panel (b): The measured rotational temperature of ortho manifold ($T_{Rot-ortho}$) versus measured kinetic temperature (T_{Kin}). The data were obtained in experiments with $^nH_2$ and with $^eH_2$. The dashed straight line indicates equality $T_{Rot-ortho} = T_{Kin}$.

need to be refined when the plasma contains energy sources that heat the electron gas, for instance, recombination of ions by collisional radiative recombination. It is shown in Appendix that this heating mechanism at used electron densities can elevate the electron temperature slightly in the early afterglow at gas temperatures near 77 K, but becomes unimportant at higher gas temperatures and lower electron densities.

C. Vibrational excitation of the H_3^+ ions

We expect that all excited vibrational states of H_3^+ are quenched in collisions with He, Ar, and H_2. The reaction $H_2^+ + H_2$ can produce H_3^+ ions with vibrational excitation up to $v = 5$ but the ions with internal energies above 0.57 eV are rapidly destroyed by proton transfer with Ar, leaving only ions in $v \leq 2$ (for details see Refs. 23 and 53). There is also a high probability that the vibrational excitation of H_3^+ will be quenched in collision with H_2. Kim *et al.*[66] obtained a rate coefficient 3×10^{-10} cm^{3}s^{-1} for vibrational relaxation of H_3^+ ions in H_2. At $[H_2] \sim 10^{14}$ cm^{-3} this leads to vibrational relaxation within 30 μs (see also discussion and references in Ref. 67). We conclude that at Ar and H_2 densities of the order of $\sim 10^{14}$ cm^{-3} vibrational excitation will be quenched within 30 μs after ion formation. Collisions with He atoms are more frequent by at least by three orders of magnitude, but vibrational quenching by helium can be very low, as it is, e.g., in collisions of He with vibrationally excited N_2^+ ions (see, e.g., Ref. 68). To estimate the rate of formation of H_3^+ ions (in reactions with H_2, Ar, and He) we studied the processes at very early afterglow at several He densities and at low H_2 and Ar densities ($[H_2]$, $[Ar] \sim 10^{12}$ cm^{-3}) in our previous study[69] and we found qualitative agreement with results obtained from kinetic model.

D. Rotational and nuclear spin states of the H_3^+ ions

The determination of the spin-dependent recombination rate coefficients of H_3^+ ions relies on accurate knowledge of the relative abundance of ions in the ortho-states and para-states and corresponding rotational states. In this experiment these quantities were measured by optical absorption, rather than by modeling the kinetic processes, but we will briefly describe the reactions of relevance.

The probability of changing the nuclear spin alignment by radiation is very low and likewise collisions with He or Ar atoms are inefficient in causing spin changes. The principal rotational equilibration and spin scrambling process is the proton-hopping or exchange reaction of H_3^+ with H_2 that proceeds via a short-lived $(H_5^+)^*$ reaction complex. The reaction has been studied in great detail.[5,27,70–75] It has been found that the ratio of $[^pH_3^+]/[^oH_3^+]$ in plasmas containing H_2 is constrained by nuclear spin selection rules and depends on the relative concentrations of $^pH_2$ and $^oH_2$ (Refs. 70–75) and on temperature. Rotational-state changes without changing the nuclear spin state, i.e., within the para or ortho manifold, are possible by radiation and in collisions with He or Ar. Electron collisions can change the rotational states within the para or the ortho manifold with rates approximately ten times faster than the rate of the dissociative recombination (for details see Ref. 76) which means than on average an H_3^+ ion has ten thermalizing collisions with electrons prior to its recombination at our conditions. For this reason, we expect that ions are rotationally thermalized within the para and ortho manifolds.

Rotational temperatures of the ions were inferred from measurements of absolute densities of ions in three rotational states. Panel (a) of Fig. 4 shows the populations of two ortho-states and one para-state, measured during the discharge and during the afterglow in experiments with normal H_2 at temperatures 77–200 K. The relative populations of the ortho- and para-states were computed by dividing the measured absolute ion densities in a given state by the density of all H_3^+ ions, assuming a thermal rotational state distribution. At temperatures where two H_3^+ absorption lines were observable, the rotational temperature $T_{Rot-ortho}$ within the ortho manifold was obtained also. The relation between the rotational temperature ($T_{Rot-ortho}$) and the kinetic temperature (T_{Kin}) of the ions is shown in panel (b) of Fig. 4. The data plotted in panel (b) were obtained in experiments with $^nH_2$ and with $^eH_2$. The agreement between $T_{Rot-ortho}$ and T_{Kin} is very good ($|T_{Rot-ortho} - T_{Kin}| < 15$ K). During the discharge, a slightly higher rotational temperature $T_{Rot-ortho}$ compared to the kinetic temperature T_{Kin} is expected since the ions are produced with higher rotational excitation and then relax by collisions to lower states. During the afterglow, the lifetime of the H_3^+ ions is longer (because ambipolar diffusion is slower) and

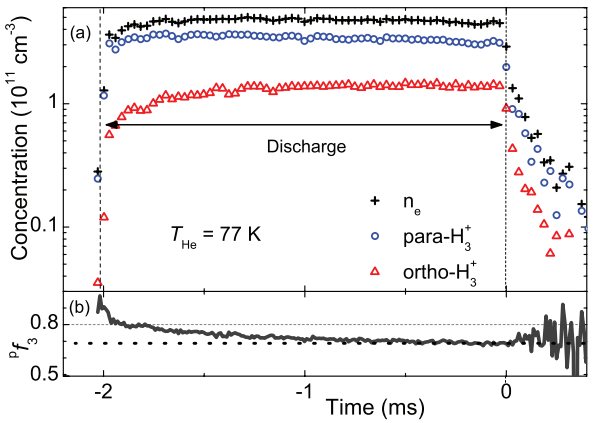

FIG. 5. Panel (a): Evolution of $[^pH_3^+]$, $[^oH_3^+]$, and n_e measured in experiments with enriched hydrogen, $^eH_2$, at $T_{He}\sim$ 77 K and [He] = 4 × 10^{17} cm^{-3}, $[^eH_2] = 3 \times 10^{14}$ cm^{-3}, [Ar] = 6 × 10^{13} cm^{-3}. The decay in the early afterglow is caused by recombination. Panel (b): Evolution of $^pf_3$. The final value of $^pf_3 \sim 0.7$ during the late discharge and in the early afterglow exceeds the equilibrium value of $^pf_3 \sim 0.5$ in normal hydrogen.

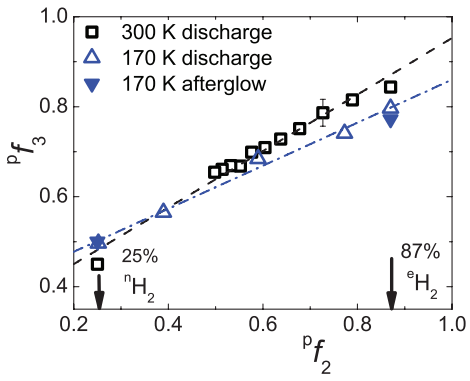

FIG. 6. Dependence of $^pf_3$ on $^pf_2$ measured in a He/Ar/H_2 mixture at 300 K (discharge) and 170 K (discharge and afterglow). Arrows point to the values of $^pf_2$ in $^nH_2$ and $^eH_2$ that were used in the recombination studies. Open symbols: Values in the discharge ($\tau_{Disch} \sim 2$ ms). Filled symbols: Values during the afterglow ($\tau_{Afterglow} \sim 150$ μs).

more time is available for rotational relaxation. Some production of rotationally excited H_3^+ ions may occur in very early afterglow. Therefore, in the determination of $T_{Rot-ortho}$ we excluded data obtained during the first $\sim$ 150 μs after switching off the discharge.

We concluded that the ions under study were kinetically and internally thermalized in plasmas containing $^nH_2$, within the experimental uncertainties of $T_{Rot-ortho}$, T_{Kin}, and $^pf_3$(see Figs. 1 and 4). In plasmas containing $^eH_2$, we also found that $T_{Rot-ortho} \sim T_{Kin} \sim T_{He}$ (see panel (b) of Fig. 4), but in this case the relative abundances of para-H_3^+ and ortho-H_3^+ ($^pf_3$ and $^of_3$) are not in thermal equilibrium (see panel (a) of Fig. 1). The enrichment of para-H_3^+ will be discussed next.

E. H_3^+ para to ortho ratio

We measured absolute densities $[^pH_3^+]$ and $[^oH_3^+]$ during the discharge and during the afterglow to determine the dependence of the para-H_3^+ and ortho-H_3^+ fractions on experimental conditions. The time resolution in our experiment suffices to record the temporal evolution during the discharge and during the early afterglow. Typical evolutions of $[^pH_3^+]$, $[^oH_3^+]$ and electron densities are plotted in panel (a) of Fig. 5 for the case where $^eH_2$ was the precursor gas. The electron density n_e is taken as the sum $[^pH_3^+] + [^oH_3^+]$. Panel (b) of Fig. 5 shows the measured fraction $^pf_3$ of $[^pH_3^+]$. After the rapid change in the early discharge the variation during the discharge becomes slow. The faster change of $^pf_3$ at the beginning reflects the transition from the nascent H_3^+, formed by proton transfer from ArH^+ or H_2^+ to H_2, to the steady state established in subsequent reactions with H_2. A thorough discussion of the reactions is contained in two recent papers by Crabtree *et al.*[45,46]). During the discharge, the para/ortho composition of H_2 ($^pf_2$) changes slowly as a consequence of H_2 dissociation and recombination and hence $^pf_3$ also changes during the discharge. When we refer to values (e.g., $T_{Rot-ortho}$, T_{Kin}) measured "during the discharge" we mean values measured shortly before switching off the discharge ($\tau_{Disch} \sim 2$ ms), unless stated otherwise (see also discussion in Ref. 43).

Our systematic measurements of the evolution of the para/ortho composition show that, under the conditions of this set of experiments, the fraction $^pf_3$ remains nearly constant during the afterglow, and that it can be varied by using normal or para enriched hydrogen. We also measured the dependence of $^pf_3$ on $^pf_2$ which was varied from $^pf_2$= 0.25 to ~0.87 by mixing $^nH_2$ with $^eH_2$, while keeping the overall hydrogen density ($[^nH_2] + [^eH_2]$) constant. The dependence of $^pf_3$ on $^pf_2$ measured at 300 K and at 170 K (see Fig. 6) is linear and the same was found to be true at other temperatures (for details see Ref. 43). The linearity is a consequence of the spin-scrambling reaction with hydrogen.[70–73] Crabtree *et al.*[45,46] have recently discussed in great detail the general dependence of $^pf_3$ on $^pf_2$ and other experimental conditions. For the present study of H_3^+ recombination a quantitative understanding of the reaction kinetics is not required; it is only important that $^pf_3$ is known and can be varied over a significant range.

V. EXPERIMENTAL RESULTS – STATE SELECTIVE RECOMBINATION

The measured electron-density decay curves were analyzed to obtain apparent binary recombination rate coefficients for two particular values of $^pf_3$(see Eqs. (2)—(4)). Further details can also be found in Ref. 27. We carried out a systematic set of measurements which differed only in the value of $^pf_2$, but employed otherwise very similar conditions. The densities of para (1,1), ortho (1,0), and ortho (3,3) states of H_3^+ were monitored. Examples of data measured at 170 K with $^nH_2$ and with $^eH_2$ are plotted in Figs. 7 and 8, respectively. Note the large difference in measured populations of particular rotational states of H_3^+ in both experiments (see panels (b) of both figuers). In this set of experiments we obtained $^pf_3 \sim 0.5$ for $^nH_2$ and $^pf_3 \sim 0.7$–0.8 for $^eH_2$ (see panels (c) of both figures). Note also that in both experiments the values of $^pf_3$ are nearly constant during the afterglow.

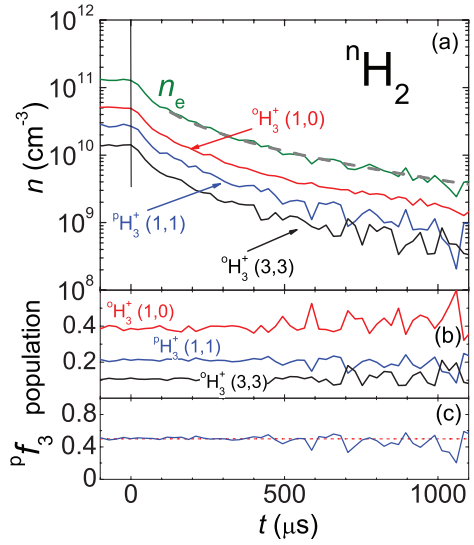

FIG. 7. Panel (a): Example of decay curves of densities of ions in para (1,1), ortho (1,0), and ortho (3,3) states of H_3^+, measured during the afterglow in a He/Ar/$^{n}H_2$ gas mixture at 170 K, 1440 Pa of He, $[H_2] = 1 \times 10^{14}$ cm^{-3}, and $[Ar] = 2 \times 10^{14}$ cm^{-3}. Time is set to zero at the beginning of the afterglow. The vertical bar shows the end of the discharge period and the beginning of the afterglow. Electron density is obtained as a sum of ion densities. Panel (b): The measured relative populations of para (1,1), ortho (1,0), and ortho (3,3) states of H_3^+, note the nearly constant values during whole afterglow. Panel (c): Measured fraction $^{p}f_3$ of para-H_3^+.

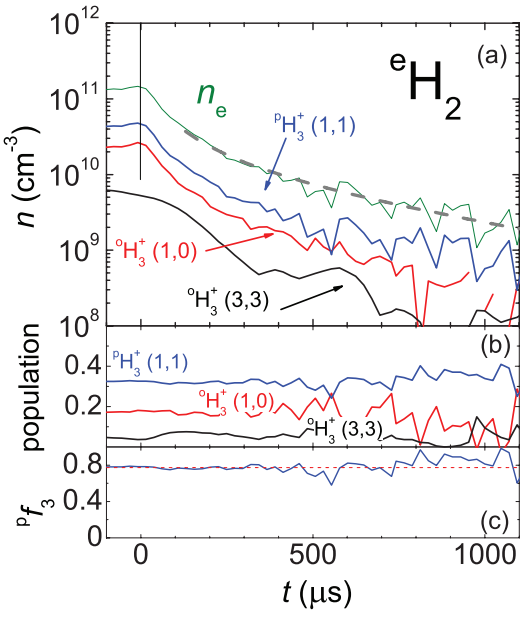

FIG. 8. Panel (a): Example of decay curves of densities of ions in para (1,1), ortho (1,0), and ortho (3,3) states of H_3^+, measured during the afterglow in a He/Ar/$^{e}H_2$ gas mixture at 170 K, 1550 Pa of He, $[H_2] = 1 \times 10^{14}$ cm^{-3}, and $[Ar] = 2 \times 10^{14}$ cm^{-3}. The vertical bar shows the end of the discharge period and the beginning of the afterglow. Panel (b): The measured relative populations of para (1,1), ortho (1,0), and ortho (3,3) states of H_3^+. Panel (c): Measured fraction $^{p}f_3$ of para-H_3^+.

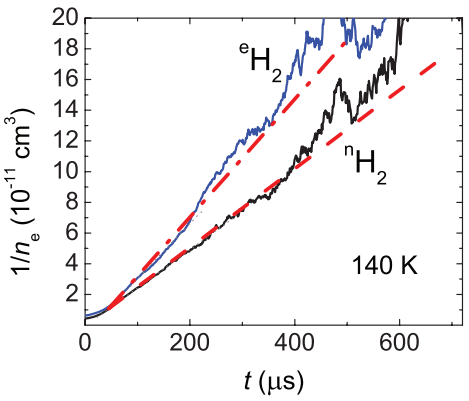

FIG. 9. Examples of the evolutions of the reciprocal number density $1/n_e$ during the afterglow when using normal $^{n}H_2$ or para-enriched $^{e}H_2$ at otherwise identical conditions. The effective (apparent) binary recombination rate coefficient is given by the slope of the linear part of the plot.

From the densities of the ions in (1,1) and (1,0) states we calculated, assuming thermal equilibrium (TDE) within the para-manifolds and ortho-manifolds, the total densities $[^{p}H_3^+]$ and $[^{o}H_3^+]$ and their sum, i.e., the electron density. The electron-density decay curves can be approximately analyzed by graphing $1/n_e$ versus decay time. The slope of the linear part of the plot yields the effective (apparent) binary recombination rate (for details see Ref. 61). Examples of such graphs of data obtained with $^{n}H_2$ and $^{e}H_2$ are shown in Fig. 9.

This simple form of analysis demonstrates that recombination in afterglows containing para-enriched hydrogen $^{e}H_2$, i.e., with higher relative population of para-H_3^+, is faster than when normal hydrogen is used. However, it neglects ambipolar diffusion and eventual reactive losses characterized in Eqs. (2) and (3). Hence, we used the more advanced "integral analysis" of the measured electron density decay curves (for details of "integral analysis" see Refs. 61 and 77). This analysis can separate α_{eff} from τ_L and minimize influence of ternary association (1e) and (1f) on determination of α_{eff}. The first 50–150 μs of the afterglow decay were excluded because probably new ions were still being formed (for details see Refs. 8, 27, 43, and 69. At 77 K special attention was paid to analysis of the decay curves because of a possible influence of the CRR process, which is discussed in Appendix.

The dependences of $^{n}\alpha_{eff}$ and $^{e}\alpha_{eff}$ on He density measured at 170 K are shown in panel (a) of Fig. 10. Panel (c) shows values of the corresponding fractions $^{p}f_3$. Note that the fractions $^{p}f_3$ are different in $^{n}H_2$ and in $^{e}H_2$, but are independent on helium density [He]. Both, $^{n}\alpha_{eff}$ and $^{e}\alpha_{eff}$ increase linearly with increasing [He]. Therefore (see Eq. (5)), we can obtain separate binary and ternary recombination rate coefficients for known para/ortho ratios. The values obtained with normal hydrogen refer to the thermal equilibrium H_3^+ with $^{p}f_3 \sim 0.5$. In our previous FALP experiments using $^{n}H_2$ we assumed but did not prove that $^{p}f_3 = 0.5$. The present experiments with $^{n}H_2$ confirmed that $^{p}f_3 = 0.5$ and $T_{Rot-ortho} = T_{Kin}$. In other words, the values of α_{bin} and K_{He} recombination rate coefficients obtained in our previous FALP experiments were the values appropriate for thermal equilibrium.[8,33–37]

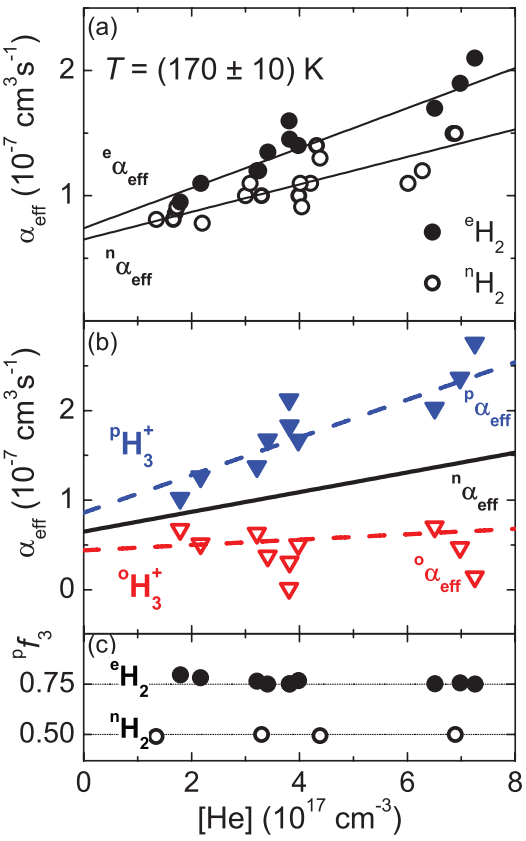

FIG. 10. Measured dependence of effective recombination rate coefficients α_{eff} on He density at 170 K. Panel (a): The values α_{eff} measured using $^nH_2$ as the precursor gas ($^n\alpha_{eff}$, open circles) and the values measured using $^eH_2$ ($^e\alpha_{eff}$, filled circles). Panel (b): The calculated values $^p\alpha_{eff}$ and $^o\alpha_{eff}$ for pure para-H_3^+ (filled triangles) and pure H_3^+ (open triangles), respectively. For comparison straight line obtained by fit of values $^n\alpha_{eff}$ in panel (a) is also plotted. Panel (c): The $^pf_3$ fractions of para-H_3^+ measured in the experiments with $^nH_2$ and $^eH_2$.

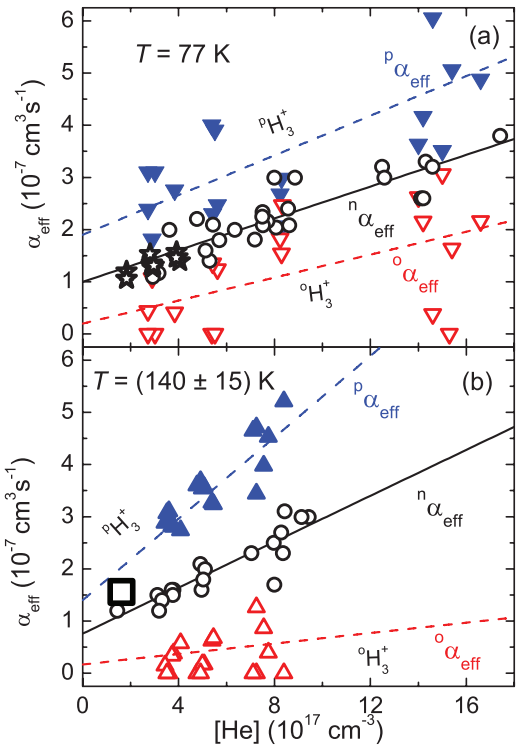

FIG. 11. Measured effective recombination rate coefficients $^p\alpha_{eff}$ and $^o\alpha_{eff}$ (closed and open triangles, respectively) as a function of He density at 77 K (panel (a), for details see also Ref. 27) and at 140 K (panel (b)). The full lines indicate $^n\alpha_{eff}$. The stars in panel (a) are data measured in previous FALP experiment at 77 K (Ref. 34) and the large square in panel (b) represents data measured in previous FALP and stationary afterglow experiments at 130 K.[34,79] The slopes of the straight-line fits yield the corresponding ternary recombination rate coefficients (K_{He}) while the intercept for [He] → 0 gives the corresponding α_{bin}.

We measured the dependences of $^n\alpha_{eff}$ and $^e\alpha_{eff}$ on [He] for temperatures in the range 77–200 K. From the dependences of $^n\alpha_{eff}$ and $^e\alpha_{eff}$ on [He] and the corresponding values of $^pf_3$ we calculated values $^p\alpha_{eff}$ and $^o\alpha_{eff}$ for pure para-H_3^+ and for pure ortho-H_3^+, respectively. In these calculations, linear fits to the data measured with $^nH_2$ were used as a reference (the full lines in panels (a) and (b) of the Fig. 10 indicated as $^n\alpha_{eff}$). The obtained negative values of $^o\alpha_{eff}$ were truncated to zero and the corresponding values of $^p\alpha_{eff}$ were corrected accordingly. By fitting the data $^p\alpha_{eff}$ and $^o\alpha_{eff}$ (panel (b) of Fig. 10) with a linear dependence (Eq. (5)) we obtained the corresponding binary ($^p\alpha_{bin}$ and $^o\alpha_{bin}$) and ternary ($^pK_{He}$ and $^oK_{He}$) recombination rate coefficients for pure para-H_3^+ and for pure ortho-H_3^+. This form of data analysis is also described in Ref. 27.

VI. RESULTS—TERNARY HE ASSISTED RECOMBINATION OF PARA-H_3^+ AND ORTHO-H_3^+

The present SA–CRDS experiments cover a range of pressures from 200 to 1600 Pa, corresponding to maximum He densities of 1.6×10^{18} cm^{-3} at 77 K and $\sim 6 \times 10^{17}$ cm^{-3} at 200 K. The ability to vary the He density over a large range of nearly a factor of 10 improves the accuracy of the inferred ternary rate coefficients. The dependences of α_{eff} on [He] were measured at four temperatures (77, 140, 170, and 200 K) using $^nH_2$ and $^eH_2$. The dependences of $^p\alpha_{eff}$ and $^o\alpha_{eff}$ on helium density obtained for 170 K are shown in panel (b) of Fig. 10 and dependences obtained for 77 K and for 140 K can be found in our previous papers[27,78] and are shown in Fig. 11 (the values of $^p\alpha_{eff}$ were omitted in Fig. 11 for better clarity). From the dependences of $^p\alpha_{eff}$ and $^o\alpha_{eff}$ on [He] we obtained (using Eq. (5)) the corresponding binary and ternary recombination rate coefficients α_{bin} and K_{He}. In spite of the fairly large scatter in the data it is clear that ternary recombination depends on the spin state of recombining ions (on $^pf_3$). This large scatter is mirrored in error bars of the values shown in Figs. 12 and 13. As can be seen from Fig. 11, zero values of extrapolated $^o\alpha_{bin}$ cannot be excluded at the lowest temperatures. For all three temperatures the ternary helium-assisted recombination of para-H_3^+ is faster than the recombination of H_3^+.

Figure 12 shows the ternary recombination rate coefficients $^pK_{He}$ and $^oK_{He}$ as a function of temperature, as

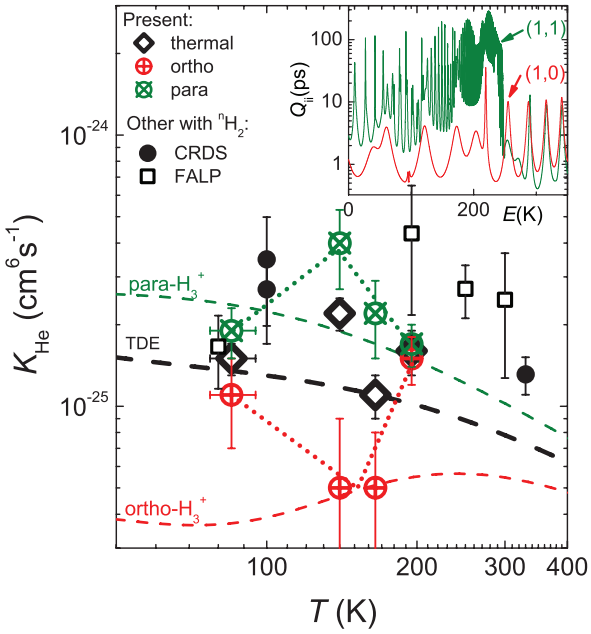

FIG. 12. Ternary recombination rate coefficients $^pK_{He}$, $^oK_{He}$, and $^nK_{He}$. The data obtained in previous CRDS (closed circles) and FALP/SA (open squares) experiments[33,34] are also shown. The dotted lines drawn through the para and ortho data are only meant to guide the eye. In the insert diagonal elements Q_{ii} of lifetime Matrix **Q** for the two lowest initial rotational states of H_3^+ are plotted. Each curve is labeled with the corresponding quantum numbers (J,G).[8,34]

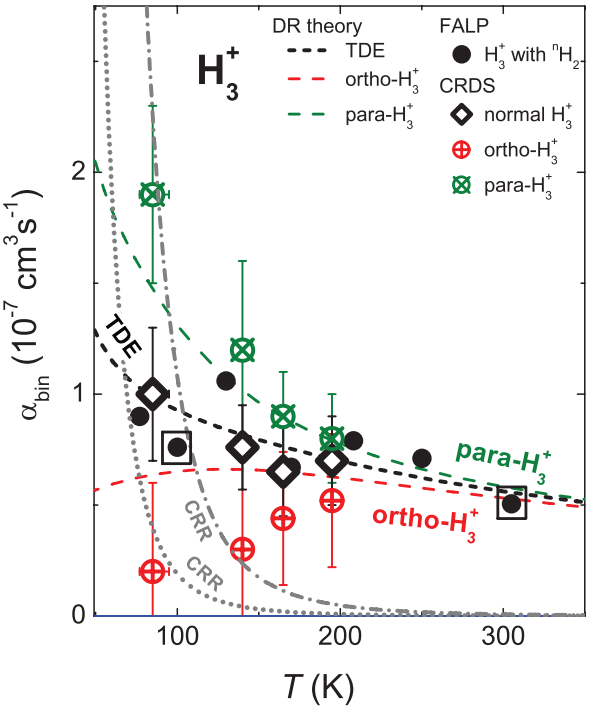

FIG. 13. Measured temperature dependences of the binary recombination rate coefficients $^n\alpha_{bin}$, $^p\alpha_{bin}$, and $^o\alpha_{bin}$ for normal-H_3^+ (measured in experiments with $^nH_2$), para-H_3^+, and ortho-H_3^+, respectively (see also Ref. 78). Previous FALP data[8,33,34] measured with $^nH_2$ are indicated by full circles. Combined SA–CRDS/FALP data at 100 K and 305 K (Refs. 8 and 34) are indicated by a full circle in a square. The temperature T in the SA–CRDS experiments is given by T_{Kin}, while in the FALP it is the temperature of the flow tube. That is why we use $T = 82$ K for data obtained in experiment made with discharge tube (SA–CRDS) immersed in liquid nitrogen, otherwise we indicate it as 77 K (e.g., in Fig. 5). Error bars (present CRDS data) represent statistical errors (see linear fits in Figs. 10 and 11). The dashed lines indicate the theoretical rate coefficients for para-H_3^+, ortho-H_3^+, and for H_3^+ ions in the thermal equilibrium (TDE).[6] The curves labeled CRR are the effective binary rate coefficients of collisional radiative recombination (CRR) calculated from the Stevefelt formula (see Refs. 31, 32, and 38) for electron densities $n_e = 5 \times 10^9$ cm^{-3} (dotted line) and $n_e = 3 \times 10^{10}$ cm^{-3} (dash-dotted line). For details see the Appendix.

obtained from the slopes of graphs of the kind shown in Figs. 10 and 11. The values $^nK_{He}$ corresponding to thermal equilibrium at 77, 140, 170, and 200 K (open rhomboids in Fig. 12) were obtained in the same way from $^n\alpha_{eff}$ (see Figs. 10 and 11). Particular attention was paid to experiments at 77 and 140 K (see Fig. 11) where we obtained high accuracy by measuring at larger helium density range (when comparing current CRDS data to FALP data, see Fig. 11). The CRDS data at 100 and 330 K (closed circles in Fig. 12) and FALP data at 200 K were measured in previous experiments and were obtained from the measured dependences of $^n\alpha_{eff}$ on hydrogen number density in the "saturated region." For details see Ref. 34. Values of K_{He} at 250 K and 300 K were obtained from the slopes of the linear dependence on helium number density from the data collection of SA and FALP data.[34] Because of the lower electron density in FALP experiment plasma decay is longer and formation of H_5^+ can influence the decay at higher helium densities. We have taken this effect into the account by enlarging error bars of the FALP data. Having in mind high He density and low temperature we used kinetic models to verify our assumptions on influence of H_5^+ formation on plasma decay and on determination of α_{eff}. Note that H_5^+ formed in association (1e) and (1f) is in used experimental conditions removed from plasma within $\sim 10\,\mu$s and the association is loss determining process. Possible error caused by H_5^+ formation is within statistical error of the data, as was confirmed by the chemical kinetics model. In Fig. 12 we did not include the data previously measured in "continuous regime" where FALP was first cooled to 77 K and after stopping cooling effective rate coefficients were measured at continuously increasing temperature (for details see Ref. 8). The accuracy of data obtained in "continuous regime" is lower when comparing with accuracy of present data obtained from dependences on helium density (Figs. 10 and 11).

In our previous studies[8,33,34] of recombination of H_3^+ with electrons we discussed the ternary recombination rate coefficient K_{He} in terms of the lifetimes of excited metastable Rydberg states H_3^* formed in collision of H_3^+ ion with electron.[8,33,34] At low collision energies the calculated values of the lifetimes depend on the spin state of the recombining ions and on collision energy. In the inset in Fig. 12 the calculated diagonal elements Q_{ii} of the lifetime Matrix **Q** for the two lowest initial rotational states of H_3^+ are plotted. The calculated lifetimes are long enough to enable l-changing collision of H_3^* molecule with helium buffer gas atom. The calculated ternary recombination rate coefficients[34] for para-H_3^+ and ortho-H_3^+, shown as dashed lines in Fig. 12,

are in qualitative agreement with measured values. ${}^{\mathrm{p}}K_{\mathrm{He}}$ is greater than ${}^{\mathrm{o}}K_{\mathrm{He}}$ due to the longer lifetimes of para-H_3^* Rydberg resonances. Although some rather rough assumptions were made in the theoretical calculations (mainly the independence of the rate coefficient of *l*-changing collision on temperature) the overall agreement with the measured data is quite good in comparison with older theories of ternary assisted recombination.[29,80] An alternative explanation of ternary recombination of H_3^+ has been suggested by Johnsen and Guberman.[12]

More accurate theory should address decrease of ternary rate coefficients at temperature decreasing towards 77 K and also observed small difference between ${}^{\mathrm{p}}K_{\mathrm{He}}$ and ${}^{\mathrm{o}}K_{\mathrm{He}}$ at 77 K (see also Ref. 27), which are in contradiction with calculated dependences.

VII. RESULTS—BINARY RECOMBINATION OF PARA-H_3^+ AND ORTHO-H_3^+

The values of ${}^{\mathrm{p}}\alpha_{\mathrm{bin}}$ and ${}^{\mathrm{o}}\alpha_{\mathrm{bin}}$ for pure para-H_3^+ and pure ortho-H_3^+ and values of ${}^{\mathrm{n}}\alpha_{\mathrm{bin}}$ measured in the present experiment are plotted versus temperature in Fig. 13. Plotted are also values ${}^{\mathrm{n}}\alpha_{\mathrm{bin}}$ for H_3^+ ions in thermal equilibrium obtained in our previous FALP experiments.[8,33,34] The theoretical rate coefficients for pure para-H_3^+, pure ortho-H_3^+, and for H_3^+ ions in thermal equilibrium[6] are also shown in Fig. 13. The agreement between experimental and theoretical binary recombination rate coefficients ${}^{\mathrm{n}}\alpha_{\mathrm{bin}}$, ${}^{\mathrm{p}}\alpha_{\mathrm{bin}}$, and ${}^{\mathrm{o}}\alpha_{\mathrm{bin}}$ is very good. Also, the agreement between the present ${}^{\mathrm{n}}\alpha_{\mathrm{bin}}$ values and those obtained in our earlier FALP experiments using Langmuir probes is very good over the whole temperature range, even though in the present experiments the electron densities in the early afterglow were higher by at least a factor of 20.[34] The agreement at higher temperatures (140, 170, and 200 K) indicates that the measured rate coefficients at 77 K do not depend on electron density (see overlap of FALP and CRDS data plotted in Fig. 11), which means that CRR has little effect on the binary recombination rate coefficients ${}^{\mathrm{p}}\alpha_{\mathrm{bin}}$ and ${}^{\mathrm{o}}\alpha_{\mathrm{bin}}$ (for details see discussion in the Appendix).

VIII. POSSIBLE CONTRIBUTION OF CRR

The afterglow experiments described here had to be performed at high ion and electron densities (approaching 10^{11} cm^{-3}) in order to obtain adequate optical absorption. Hence, we were concerned that electron-stabilized recombination (CRR) might contribute to the recombination loss, especially at the lowest gas temperature of 77 K. The dominant term in the "classical" treatment of CRR for atomic ions by Stevefelt *et al.*[30,38] yields a three-body CRR rate coefficient $K_{\mathrm{CRR}} = 3.8 \times 10^{-9}\, T_{\mathrm{e}}^{-4.5}$ cm^{6}s^{-1}. The formula (hereinafter referred to as the "Stevefelt formula") has been experimentally verified for recombination of atomic argon ions at temperatures down to 60 K (Refs. 32 and 40)). Its validity for molecular ions seems plausible but has not been tested.

An uncritical application of the commonly used "Stevefelt formula"[38] results in an effective binary CRR rate coefficient of 3×10^{-7} cm^{3}s^{-1} (at $T_{\mathrm{e}} = 77$ K and an electron density $n_{\mathrm{e}} = 3 \times 10^{10}$ cm^{-3}, see Fig. 13), larger than the binary H_3^+ recombination coefficient measured in normal H_2 at the same temperature. At later afterglow times, e.g., when the electron density has dropped below 5×10^9 cm^{-3}, the contribution of CRR becomes much smaller (see Fig. 13). However, the real situation is more complicated because the electrons that are captured by CRR transfer energy to other electrons, thereby raise the temperature of the electron gas, and reduce the rate of the strongly temperature-dependent CRR. The estimates of the electron heat balance described in the Appendix indicate that the electron temperature in the very early afterglow may be as high as 100 K, when the gas temperature is 77 K. This would reduce the contribution of CRR considerably but not make it entirely negligible. The model calculations described in the Appendix suggest that the effect of CRR is negligible, even at 77 K.

The fact that the present data for normal hydrogen are very close to those measured by us in flow tubes (FALP) at ten times smaller electron densities[34] supports our conclusion that CRR makes only a small contribution to recombination. While the exact contribution of CRR is difficult to determine, our main conclusion, namely that para-H_3^+ and ortho-H_3^+ recombine with different rates, remains unaffected since CRR should not distinguish between nuclear spin states, however this question is in need of further clarification. Under preparation is the SA–CRDS experiment where wall temperature will be below liquid nitrogen temperature, i.e., below 77 K.

IX. DISCUSSION AND CONCLUSION

Our investigations show that the low-temperature recombination of H_3^+ ions depends strongly on the nuclear spin states of the ions. CRDS proved eminently capable of quantifying the populations of para-H_3^+ and ortho-H_3^+ in the discharge and during the afterglow and to verify that the afterglow plasma was in thermal equilibrium with the He buffer gas. By adding normal and para enriched hydrogen to He buffer gas we were able to form plasmas with different partial populations of para-H_3^+ (fractions, ${}^{\mathrm{p}}f_3$) and ortho-H_3^+ (fractions, ${}^{\mathrm{o}}f_3$) and to deduce both binary and ternary (He-assisted) recombination rate coefficients for pure para-H_3^+ and ortho-H_3^+ ions. The rate coefficients were measured at temperatures from 77 to 200 K. As far as applications to astrophysical clouds are concerned, the binary rate coefficients are the most important. Applications to laboratory hydrogen plasmas will have to include the ternary coefficients as well. It is worth mentioning here that the recent observation of laser lines in hydrogen/rare gas discharge was explained by three-body recombination of H_3^+.[81]

This is the first time that binary and ternary recombination rate coefficients have been determined for H_3^+ ions with *in situ* measured abundances of the para and ortho nuclear spin state and actual kinetic and rotational temperature. The results support theoretical predictions and are compatible with the partial results obtained in storage-ring experiments.

ACKNOWLEDGMENTS

We would like to thank Mgr. Mojmir Jilek for the design of para-H_2 generator and RNDr. Jan Lang, Ph.D. for

TABLE II. Electron processes and corresponding characteristic times calculated for a plasma at $T_{He} = T_{Kin} = T_{Rot} = 77$ K, $T_e = 82$ K, $n_e = 5 \times 10^{10}$ cm^{-3}, and [He] $= 5 \times 10^{17}$ cm^{-3} (~500 Pa). Definition of symbols: v: electron velocity; $\sigma_{e/He}(v)$: tabulated cross section of electron-He elastic scattering; $\langle \ldots . \rangle$: average over relative velocity distribution; λ_D: Debye length; Λ: impact parameter for 90° coulombic scattering; m_{He}: mass of He atom; m_e: electron mass; λ: coulombic logarithm; $\Delta_{1,2}$: energy difference between rotational states (1,1) and (2,1); n_1, n_2: number density of H_3^+ ions in rotational states (1,1) and (2,1); α_{21}, α_{12}: rate coefficients for electron (de)excitation between the states 2 → 1 and vice versa; K_{He}: ternary rate coefficient of helium assisted dissociative recombination; α_{bin}: rate coefficient of binary dissociative recombination.

Reactants	Process	τ [μs]	Remark	Reference
e + He	Elastic scattering	0.0008	${}^{c}\tau_{e/He} = 1/[\mathrm{He}]\langle\sigma_{e/He} \cdot v\rangle$	85
e + e	Coulombic scattering	0.004	${}^{c}\tau_{e/e} = 1/n_e\langle v\pi\Lambda^2 \ln(\lambda_D/\Lambda)\rangle$	83,84
e + He	Elastic cooling	2.9	${}^{\varepsilon}\tau_{e/He} = {}^{c}\tau_{e/He}(m_{He}/2m_e)$	65
$e + H_3^+$	Coulombic cooling	3.4	${}^{\varepsilon}\tau_{e/i} = \frac{6\sqrt{2m_e}\varepsilon_0^2(\pi k_B T_e)^{3/2}}{n_e e^4 \lambda} \frac{m_i}{2m_e}$	86
$e + e + H_3^+$	CRR	43	$\tau_{CRR} = 1/n_e^2 K_{CRR}$	38
$e + H_3^+$	Rotational cooling	140	${}^{\varepsilon}\tau_{Rot} = \frac{3}{2}\frac{k_B(T_{Rot}-T_e)}{\Delta_{1,2}(n_2\alpha_{21}-n_1\alpha_{12})}$	76,87
$e + H_3^+ + He$	Ternary recombination	200	$\tau_{ternary} = 1/K_{He}[\mathrm{He}]n_e$	34
$e + H_3^+$	Binary recombination	250	$\tau_{bin} = 1/\alpha_{bin} n$	34

NMR measurements of para enrichment of ${}^{e}H_2$ gas. This work was partly financed by the research Grant No. OC10046 from the Ministry of Education of the Czech Republic and was partly supported by GACR (205/09/1183, P209/12/0233), SV 265 302, GAUK 92410, GAUK 353811, GAUK 54010, and COST Action CM0805 (The Chemical Cosmos).

APPENDIX A: ELECTRON HEATING AND EFFECT OF COLLISIONAL RADIATIVE RECOMBINATION

In this appendix we consider the heat balance for electrons in low temperature plasma. First we consider the heat balance between the heat released by CRR and heat transfer to ions and neutrals and the resulting increase of the electron temperature. In the second step we consider the effect of electron heating on the afterglow decay.

We denote characteristic times between electron collisions as ${}^{c}\tau$ (left superscript c) and characteristic times for equipartition of energy as ${}^{\varepsilon}\tau$ (left superscript ε). Right subscript will be used to denote collision partners. For example, the characteristic time for electron/He collisions is denoted as ${}^{c}\tau_{e/He}$ and the electron temperature relaxation time due to electron/He collisions is denoted as ${}^{\varepsilon}\tau_{e/He}$. Both quantities are related by the equation: ${}^{\varepsilon}\tau_{e/He} = {}^{c}\tau_{e/He}(m_{He}/2m_e)$.[65]

In these calculations we do not distinguish between the para and ortho nuclear spin states of H_3^+. In this approximation we treat the interactions as spin independent. The relevant collision processes are listed in Table II together with calculated characteristic times for conditions typical in our experiment: $T_{He} = T_{Kin} = T_{Rot} = 77$ K, $T_e = 82$ K, $n_e = 5 \times 10^{10}$ cm^{-3}, and [He] $= 5 \times 10^{17}$ cm^{-3} (~500 Pa). Collisional radiative recombination adds ΔE_{CRR} to the internal energy of the electron gas. We assume that this energy is of the order of $\Delta E_{CRR} = 0.13$ eV per recombined electron. This corresponds to the ionization potential of the lowest Rydberg state recombining predominantly by collisions rather than radiative transitions.[38,82] Varying the ΔE_{CRR} by a factor of 2 had no qualitative effect on the conclusions of our simulations. The CRR ternary rate coefficient is taken as $K_{CRR} = 3.8 \times 10^{-9} T_e^{-4.5}$ cm^{6}s^{-1}.[38] Heat transfer from the electron gas to neutrals (He) and ions occurs via electron/He collisions, electron-ion coulombic collisions, and by rotational excitation of H_3^+ between the rotational levels (1,1) and (2,1). We use recently calculated thermal rates (see Ref. 76) for rotational energy transfer. Electron-electron collisions establish and maintain a maxwellian energy distribution of the electron gas.

The maxwellization of the electron gas by electron-electron coulombic collisions[83,84] is much faster than the cooling processes under our conditions. Hence, we can define an electron temperature and write a simple equation for the internal energy of the electron gas U:

$$\frac{dU}{dt} = Q_{CRR} - Q_{elastic} - Q_{e/i} - Q_{Rot}, \tag{A1}$$

where the Q_{CRR}, $Q_{elastic}$, $Q_{e/i}$, and Q_{Rot} terms represent the heating by CRR, cooling by elastic collisions with neutrals, cooling by coulombic collisions with ions, and cooling by rotational excitation of ions, respectively. This equation can be rewritten in terms of relaxation times defined in Table II:

$$\frac{dT_e}{dt} = \frac{2\Delta E_{CRR}/3k_B}{\tau_{CRR}} - \frac{T_e - T_G}{{}^{\varepsilon}\tau_{e/He}} - \frac{T_e - T_{Kin}}{{}^{\varepsilon}\tau_{e/i}} - \frac{T_e - T_{Rot}}{{}^{\varepsilon}\tau_{Rot}}. \tag{A2}$$

In determining the electron temperature, the time derivative term can be neglected, because the relaxation processes are fast enough to maintain the equilibrium temperature at each time during the afterglow. The electron temperature is then obtained by numerically solving Eq. (A2) with zero time derivative.

For the beginning we use the theory of CRR of atomic ions[38] to estimate a rate of CRR of H_3^+ ions, then the effective binary rate of CRR should be comparable to the rate of effective binary recombination at 77 K and $n_e > 10^{10}$ cm^{-3} (see plots in Figs. 11 and 13). We deliberately chose conditions where a large influence of CRR can be expected. We then numerically model afterglow recombination in the presence of electron heating by CRR and compare the results to our experimental data. The evolution of electron density on axis of

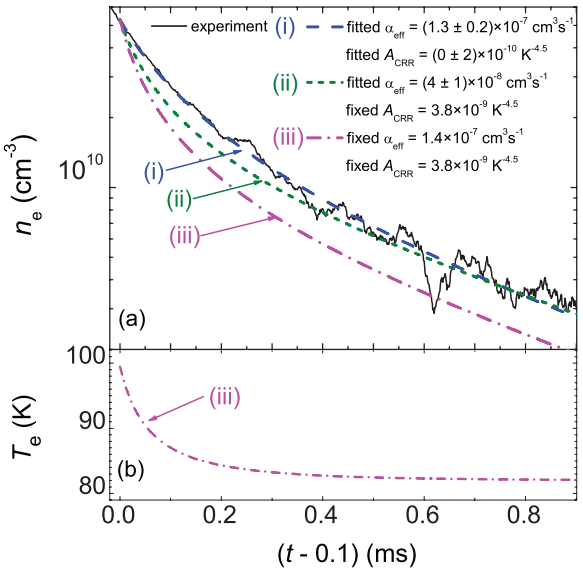

FIG. 14. Model fits of sample data measured in normal hydrogen at 77 K. Panel (a): The dashed line (i) shows the best fit to the data when α_{eff} and A_{CRR} are treated as free parameters. The short dashed line (ii) indicates the best fit when α_{eff} is treated as a free parameter, but A_{CRR} is taken as that given by the Stevefelt formula.[38] The dashed-dotted line (iii) shows model results assuming that both the Stevefelt value of A_{CRR} and the FALP values of α_{eff} (Ref. 34) are correct. Panel (b): The corresponding evolution of the electron temperature calculated for conditions corresponding to fit (iii).

the discharge tube is given by the differential equation (4b) augmented with the CRR term

$$\frac{dn_e}{dt} = -K_{CRR}(T_e)\, n_e^3 - \alpha_{eff} n_e^2 - \frac{n_e}{\tau_D}, \qquad (A3)$$

where T_e is given by Eq. (A2) and is dependent on n_e. In the numerical models, the value of K_{CRR} was taken as $K_{CRR} = A_{CRR} T_e^{-4.5}$ cm^{6}s^{-1} with either $A_{CRR} = 3.8 \times 10^{-9}$ K$^{4.5}$ or with A_{CRR} as a free fitting parameter.[38] The latter choice is permissible since no accurate measurement or theory of CRR for H_3^+ ions is available. Figure 14 compares numerical fits to sample data measured in normal hydrogen at 77 K. As before, the first 100 μs of the afterglow were excluded to eliminate possible effects of ion formation in the early afterglow.

It can be seen in Fig. 14 that the best fit to the data is obtained for a value of the CRR coefficient close to zero (line (i) in Fig. 14). The fit obtained under the constraint that K_{CRR} is given by the Stevefelt formula is noticeably worse, even when α_{eff} is reduced (line (ii)). An even worse agreement is obtained when α_{eff} is taken as the FALP value measured previously[34] (see panel (a) of Fig. 11) and the Stevefelt value is used for K_{CRR} (line (iii)). Since the previous FALP measurements were performed at lower electron densities, they should not be affected by CRR even if the Stevefelt value of K_{CRR} is appropriate for H_3^+.

The same fitting procedures were applied to several of our normal and enriched hydrogen datasets and led to the same conclusion that CRR has only a negligible effect. Hence, we did not correct the measured values of α_{eff} for CRR contributions. The apparent absence of CRR is surprising. It is known to occur for atomic ions and the high Rydberg states involved in CRR are essentially the same for molecular ions. On the other hand, it is also possible that the electron temperature in the experimental afterglow plasmas was somewhat higher than we estimate. This would greatly reduce the rate of CRR but make only a minor difference in the dissociative recombination coefficient of H_3^+.

[1] T. Oka, Philos. Trans. R. Soc. London, Ser. A **364**, 2847 (2006).
[2] E. Herbst and W. Klemperer, Astrophys. J. **185**, 505 (1973).
[3] N. Indriolo, G. A. Blake, M. Goto, T. Usuda, T. Oka, T. R. Geballe, B. D. Fields, and B. J. McCall, Astrophys. J. **724**, 1357 (2010).
[4] J. Glosik, Int. J. Mass Spectrom. **1369**, 15 (1994).
[5] K. N. Crabtree, N. Indriolo, H. Kreckel, B. A. Tom, and B. J. McCall, Astrophys. J. **729**, 15 (2011).
[6] S. F. dos Santos, V. Kokoouline, and C. H. Greene, J. Chem. Phys **127**, 124309 (2007).
[7] M. Larsson, Philos. Trans. R. Soc. London, Ser. A **358**, 2433 (2000).
[8] J. Glosik, R. Plasil, T. Kotrik, P. Dohnal, J. Varju, M. Hejduk, I. Korlov, S. Roucka, and V. Kokoouline, Mol. Phys. **108**, 2253 (2010).
[9] R. Plasil, J. Glosik, V. Poterya, P. Kudrna, J. Rusz, M. Tichy, and A. Pysanenko, Int. J. Mass Spectrom. **218**(2), 105 (2002).
[10] D. Smith and P. Spanel, Int. J. Mass Spectrom. **129**, 163 (1993).
[11] R. Johnsen, J. Phys.: Conf. Ser. **4**, 83 (2005).
[12] R. Johnsen and S. L. Guberman, Adv. At., Mol., Opt. Phys. **59**, 75 (2010).
[13] M. Larsson and A. Orel, *Dissociative Recombination of Molecular Ions* (Cambridge University Press, Cambridge, England, 2008).
[14] V. Kokoouline, C. H. Greene, and B. D. Esry, Nature (London) **412**, 891 (2001).
[15] V. Kokoouline and C. H. Greene, Phys. Rev. A **68**, 012703 (2003).
[16] B. J. McCall, A. J. Honeycutt, R. J. Saykally, T. R. Geballe, N. Djuric, G. H. Dunn, J. Semaniak, O. Novotny, A. Al-Khalili, A. Ehlerding, F. Hellberg, S. Kalhori, A. Neau, R. Thomas, F. Osterdahl, and M. Larsson, Nature (London) **422**, 500 (2003).
[17] H. Kreckel, M. Motsch, J. Mikosch, J. Glosik, R. Plasil, S. Altevogt, V. Andrianarijaona, H. Buhr, J. Hoffmann, L. Lammich, M. Lestinsky, I. Nevo, S. Novotny, D. A. Orlov, H. B. Pedersen, F. Sprenger, A. S. Terekhov, J. Toker, R. Wester, D. Gerlich, D. Schwalm, A. Wolf, and D. Zajfman, Phys. Rev. Lett. **95**, 263201 (2005).
[18] B. J. McCall, A. J. Huneycutt, R. J. Saykally, N. Djuric, G. H. Dunn, J. Semaniak, O. Novotny, A. Al-Khalili, A. Ehlerding, F. Hellberg, S. Kalhori, A. Neau, R. Thomas, A. Paal, F. Osterdahl, and M. Larsson, Phys. Rev. A **70**, 052716 (2004).
[19] M. Larsson, B. McCall, and A. Orel, Chem. Phys. Lett. **462**, 145 (2008).
[20] D. R. Bates, M. F. Guest, and R. A. Kendall, Planet. Space Sci. **41**(1), 9 (1993).
[21] H. Kreckel, O. Novotny, K. N. Crabtree, H. Buhr, A. Petrignani, B. A. Tom, R. D. Thomas, M. H. Berg, D. Bing, M. Grieser, C. Krantz, M. Lestinsky, M. B. Mendes, C. Nordhorn, R. Repnow, J. Stutzel, A. Wolf, and B. J. McCall, Phys. Rev. A **82**, 042715 (2010).
[22] A. Petrignani, S. Altevogt, M. H. Berg, D. Bing, M. Grieser, J. Hoffmann, B. Jordon-Thaden, C. Krantz, M. B. Mendes, O. Novotny, S. Novotny, D. A. Orlov, R. Repnow, T. Sorg, J. Stutzel, A. Wolf, H. Buhr, H. Kreckel, V. Kokoouline, and C. H. Greene, Phys. Rev. A **83**, 032711 (2011).
[23] J. Mikosch, H. Kreckel, R. Wester, J. Glosik, R. Plasil, D. Gerlich, D. Schwalm, and A. Wolf, J. Chem. Phys. **121**(22), 11030 (2004).
[24] A. Petrignani, D. Bing, O. Novotny, M. H. Berg, H. Buhr, M. Grieser, B. Jordon-Thaden, C. Krantz, M. B. Mendes, S. Menk, S. Novotny, A. D. A. Orlov, R. Repnow, J. Stutzel, X. Urbain, and A. Wolf, J. Phys. Chem. A **114**, 4864 (2010).
[25] U. Hechtfischer, Z. Amitay, P. Forck, M. Lange, J. Linkemann, M. Schmitt, U. Schramm, D. Schwalm, R. Wester, D. Zajfman, and A. Wolf, Phys. Rev. Lett. **80**, 2809 (1998).
[26] J. Varju, S. Roucka, T. Kotrik, R. Plasil, and J. Glosik, J. Phys.: Conf. Ser. **227**, 012026 (2010).
[27] J. Varju, M. Hejduk, P. Dohnal, M. Jilek, T. Kotrik, R. Plasil, D. Gerlich, and J. Glosik, Phys. Rev. Lett. **106**, 203201 (2011).
[28] D. Smith and P. Spanel, Methods Exp. Phys. **29**(A), 273 (1995).
[29] D. Bates and S. Khare, Proc. Phys. Soc. Lond. **85**, 231 (1965).
[30] D. R. Bates, A. E. Kingston, and W. P. McWhirter, Philos. Trans. R. Soc. London, Ser. A **267**, 297 (1962).

[31]E. W. McDaniel, J. B. A. Mitchell, and M. E. Rudd, *Atomic Collisions, Heavy Partricle Projectiles* (Wiley Interscience, New York, 1993).
[32]T. Kotrik, P. Dohnal, S. Roucka, P. Jusko, R. Plasil, J. Glosik, and R. Johnsen, Phys. Rev. A **83**, 032720 (2011).
[33]J. Glosik, I. Korolov, R. Plasil, O. Novotny, T. Kotrik, P. Hlavenka, J. Varju, I. A. Mikhailov, V. Kokoouline, and C. H. Greene, J. Phys. B **41**, 191001 (2008).
[34]J. Glosik, R. Plasil, I. Korolov, T. Kotrik, O. Novotny, P. Hlavenka, P. Dohnal, J. Varju, V. Kokoouline, and C. Greene, Phys. Rev. A **79**, 052707 (2009).
[35]J. Glosik, I. Korolov, R. Plasil, T. Kotrik, P. Dohnal, O. Novotny, J. Varju, S. Roucka, C. Greene, and V. Kokoouline, Phys. Rev. A **80**, 042706 (2009).
[36]J. Glosik, R. Plasil, I. Korolov, O. Novotny, and T. Kotrik, J. Phys.: Conf. Ser. **192**, 012005 (2009).
[37]T. Kotrik, P. Dohnal, I. Korolov, R. Plasil, S. Roucka, J. Glosik, C. Greene, and V. Kokoouline, J. Chem. Phys. **133**, 034305 (2010).
[38]J. Stevefelt, J. Boulmer, and J. Delpech, Phys. Rev. A **12**, 1246 (1975).
[39]T. Pohl, D. Vrinceanu, and H. R. Sadeghpour, Phys. Rev. Lett. **100**, 223201 (2008).
[40]T. Kotrik, P. Dohnal, P. Rubovic, R. Plasil, S. Roucka, S. Opanasiuk, and J. Glosik, Eur. Phys. J. Appl. Phys. **56**, 24011 (2011).
[41]T. Amano, J. Chem. Phys. **92**, 6492 (1990).
[42]T. Amano, Astrophys. J. **329**, L121 (1988).
[43]M. Hejduk, P. Dohnal, J. Varju, P. Rubovic, R. Plasil, and J. Glosik, Plasma Sources Sci. Technol. **21**, 024002 (2012).
[44]J. Glosik, O. Novotny, A. Pysanenko, P. Zakouril, R. Plasil, P. Kudrna, and V. Poterya, Plasma Sci. Technol. **12**, S117 (2003).
[45]K. N. Crabtree, B. A. Tom, and B. J. McCall, J. Chem. Phys. **134**, 194310 (2011).
[46]K. N. Crabtree, C. Kauffman, B. Tom, E. Beçka, B. McGuire, and B. J. McCall, J. Chem. Phys. **134**, 194311 (2011).
[47]J. Tennyson, see http://www.tampa.phys.ucl.ac.uk/ftp/astrodata/h3+/ for a list of H_3^+ transitions (2011).
[48]P. F. Goldsmith, T. Velusamy, D. Li, and W. D. Langer, Astrophys. J. **715**, 1370 (2010).
[49]J. Glosik, R. Plasil, V. Poterya, P. Kudrna, M. Tichy, and A. Pysanenko, J. Phys. B **34**(15), L485 (2001).
[50]D. Romanini, A. A. Kachanov, N. Sadeghi, and F. Stoeckel, Chem. Phys. Lett. **264**(3-4), 316 (1997).
[51]P. Macko, G. Bano, P. Hlavenka, R. Plasil, V. Poterya, A. Pysanenko, O. Votava, R. Johnsen, and J. Glosik, Int. J. Mass Spectrom. **233**, 299 (2004).
[52]P. Hlavenka, R. Plasil, G. Bano, I. Korolov, D. Gerlich, J. Ramanlal, J. Tennyson, and J. Glosik, Int. J. Mass Spectrom. **255-256**, 170 (2006).
[53]J. Glosik, P. Hlavenka, R. Plasil, F. Windisch, D. Gerlich, A. Wolf, and H. Kreckel, Philos. Trans. R. Soc. London, Ser. A **364**(1848), 2931 (2006).
[54]P. Hlavenka, I. Korolov, R. Plasil, J. Varju, T. Kotrik, and J. Glosik, Czech J. Phys. **56**, B749 (2006).
[55]C. M. Lindsay and B. J. McCall, J. Mol. Spectrosc. **210**, 60 (2001).
[56]L. Neale, S. Miller, and J. Tennyson, Astrophys. J. **464**, 516 (1996).
[57]S. Tam and M. Fajardo, Rev. Sci. Instrum. **70**, 1926 (1999).
[58]B. A. Tom, S. Bashler, Y. Miyamoto, T. Momose, and B. J. McCall, Rev. Sci. Instrum. **80**, 016108 (2009).
[59]J. Lang, private communication (2011).
[60]R. Plasil, P. Hlavenka, P. Macko, G. Bano, A. Pysanenko, and J. Glosik, J. Phys.: Conf. Ser. **4**, 118 (2005).
[61]I. Korolov, T. Kotrik, R. Plasil, J. Varju, M. Hejduk, and J. Glosik, Contrib. Plasma Phys. **48**(5–7), 521 (2008).
[62]R. Plasil, I. Korolov, T. Kotrik, J. Varju, P. Dohnal, Z. Donko, G. Bano, and J. Glosik, J. Phys.: Conf. Ser. **192**, 012023 (2009).
[63]R. Plasil, I. Korolov, T. Kotrik, P. Dohnal, G. Bano, Z. Donko, and J. Glosik, Eur. Phys. J. D **54**, 391 (2009).
[64]J. Glosik, G. Bano, R. Plasil, A. Luca, and P. Zakouril, Int. J. Mass Spectrom. **189**, 103 (1999).
[65]Y. P. Raizer, *Gas Discharge Physics* (Springer–Verlag, Berlin, 1991) p. 14.
[66]J. Kim, L. Theard, and W. Huntres, Int. J. Mass Spectrom. **15**, 223 (1974).
[67]F. B. Yousif, G. Hinojosa, J. de Urquijo, C. Cisneros, and I. Alvarez, Int. J. Mass Spectrom. **171**(1–3), 127 (1997).
[68]E. Ferguson, J. Phys. Chem. **90**, 731 (1986).
[69]R. Plasil, J. Varju, M. Hejduk, P. Dohnal, T. Kotrik, and J. Glosik, J. Phys.: Conf. Ser. **300**(1), 012023 (2011).
[70]M. Quack, Mol. Phys. **34**, 477 (1977).
[71]M. Cordonnier, D. Uy, R. M. Dickson, K. E. Kerr, Y. Zhang, and T. Oka, J. Chem. Phys. **113**, 3181 (2000).
[72]T. Oka and E. Epp, Astrophys. J. **613**, 349 (2004).
[73]D. Gerlich, F. Windisch, P. Hlavenka, R. Plasil, and J. Glosik, Philos. Trans. R. Soc. London, Ser. A **364**, 3007 (2006).
[74]K. Park and J. C. Light, J. Chem. Phys. **126**, 044305 (2007).
[75]E. Hugo, O. Asvany, and S. Schlemmer, J. Chem. Phys. **130**, 164302 (2009).
[76]V. Kokoouline, A. Faure, J. Tennyson, and C. Greene, Mon. Not. R. Astron. Soc. **405**, 1195 (2010).
[77]R. Plasil, I. Korolov, T. Kotrik, and J. Glosik, Int. J. Mass Spectrom. **275**, 80 (2008).
[78]P. Dohnal, M. Hejduk, J. Varju, P. Rubovic, S. Roucka, T. Kotrik, R. Plasil, R. Johnsen, and J. Glosik, "Binary recombination of para and ortho-H_3^+ with electrons at low temperatures," Philos. Trans. R. Soc. London, Ser. A (in press) (Conference Proceeding 2012).
[79]J. Glosik, R. Plasil, A. Pysanenko, O. Novotny, P. Hlavenka, P. Macko, and G. Bano, J. Phys.: Conf. Ser. **4**, 104 (2005).
[80]M. R. Flannery, J. Chem. Phys. **95**(11), 8205 (1991).
[81]R. J. Saykally, E. A. Michael, J. Wang, and C. H. Greene, J. Chem. Phys. **133**, 234302 (2010).
[82]S. Byron, R. C. Stabler, and P. I. Bortz, Phys. Rev. Lett. **8**, 376 (1962).
[83]F. F. Chen, *Introduction to Plasma Physics* (Plenum, New York, 1974).
[84]D. Trunec, P. Spanel, and D. Smith, Chem. Phys. Lett. **372**, 728 (2003).
[85]A. V. Phelps, see http://jila.colorado.edu/~avp/collision_data/ for compilation of electron cross sections (2011)
[86]A. A. Dougal and L. Goldstein, Phys. Rev. **109**, 615 (1958).
[87]J. Ramanlal and J. Tennyson, Mon. Not. R. Astron. Soc. **354**, 161 (2004).

ARTICLE V

TITLE: Binary and ternary recombination of D_3^+ ions at 80–130 K: Application of laser absorption spectroscopy

AUTHORS: Petr Dohnal, Michal Hejduk, Peter Rubovič, Jozef Varju, Štěpán Roučka, Radek Plašil, and Juraj Glosík

JOURNAL: The Journal of Chemical Physics 137:194320 (8pp)

DATE: 20 November 2012

DOI: 10.1063/1.4767396

Binary and ternary recombination of D_3^+ ions at 80–130 K: Application of laser absorption spectroscopy

Petr Dohnal, Michal Hejduk, Peter Rubovič, Jozef Varju, Štěpán Roučka, Radek Plašil, and Juraj Glosík
Department of Surface and Plasma Science, Faculty of Mathematics and Physics, Charles University, Prague, Czech Republic

(Received 14 August 2012; accepted 24 October 2012; published online 20 November 2012)

Recombination of D_3^+ ions with electrons at low temperatures (80–130 K) was studied using spectroscopic determination of D_3^+ ions density in afterglow plasmas. The use of cavity ring-down absorption spectroscopy enabled an *in situ* determination of the abundances of the ions in plasma and the translational and the rotational temperatures of the recombining ions. Two near infrared transitions at $(5792.70 \pm 0.01)\,\mathrm{cm}^{-1}$ and at $(5793.90 \pm 0.01)\,\mathrm{cm}^{-1}$ were used to probe the number densities of the lowest ortho state and of one higher lying rotational state of the vibrational ground state of D_3^+ ion. The results show that D_3^+ recombination with electrons consists of the binary and the third-body (helium) assisted process. The obtained binary recombination rate coefficients are in agreement with a recent theoretical prediction for electron-ion plasma in thermodynamic equilibrium with $\alpha_{\mathrm{bin}}(80\,\mathrm{K}) = (9.2 \pm 2.0) \times 10^{-8}\,\mathrm{cm}^3\,\mathrm{s}^{-1}$. The measured helium assisted ternary rate coefficients K_{He} are in agreement with our previously measured flowing afterglow data giving a value of $K_{\mathrm{He}}(80\,\mathrm{K}) = (1.2 \pm 0.3) \times 10^{-25}\,\mathrm{cm}^6\,\mathrm{s}^{-1}$. © *2012 American Institute of Physics*. [http://dx.doi.org/10.1063/1.4767396]

I. INTRODUCTION

The astronomical importance of trihydrogen cation H_3^+ has been driving research in many areas of both physics and chemistry[1] for a long time. This simplest of all polyatomic ions and its isotopologues are also very important for theory, because their properties including interactions with electrons, can be calculated. Processes leading to formation and destruction of H_3^+ ions and similar processes in which deuterated isotopologues are formed or destroyed are important for astronomy and fundamental physics. Deuteration of H_3^+ and formation of H_2D^+, HD_2^+, and D_3^+ are important processes that enable us to characterize the environment in which the deuteration takes place.[2] This also includes interstellar plasma and plasmas under physical conditions believed to be appropriate for pre-protostellar cores.[2,3] The particular importance of H_3^+, but also of H_2D^+ and HD_2^+, was recognized and they were detected in interstellar plasma.[4–7] These detections confirm expectations that multiple deuterated ions play a key role in the chemistry of the early universe.[2] The inclusion of HD_2^+ and D_3^+ in the models leads to predictions of higher values of the D/H ratio in the gas phase.[4] Unfortunately, D_3^+ has not been directly observed in the interstellar medium or in other astronomical object up to now.

Because of its fundamental character, the recombination of H_3^+ and D_3^+ ions with electrons has been studied for over 60 years with emphasis on H_3^+ (see, e.g., the book by Larsson and Orel[8]). For details on recombination studies of the D_3^+ ion, see Refs. 9–19. For both H_3^+ and D_3^+ significant differences between recombination rate coefficients were obtained in different types of experiments[10,12–15,19,20] over many years and the differences between the experimental values and the theoretical ones were very large.[21] Moreover, recombination studies of H_2D^+ and HD_2^+ ions are very rare.[22–25]

Only in the early 2000s the modern theory of binary dissociative recombination (DR) of these ions was formulated.[24–28] Agreement between this theory and experiments achieved in the late 1990s and in the years 2000–2003 was only partial. The remaining discrepancies were assumed to be in internal excitation of recombining ions, which can play a role at low collision energies. Because of this assumption ion storage rings were equipped with "cold ion sources" and better agreement was obtained for H_3^+ recombination.[29–31] In these experiments, it had been assumed that the "cold" rotational distributions measured in the ion source, survived the injection and storage in the ring. Recent high-resolution storage ring experiments indicate that these assumptions were not necessarily correct.[32,33] At this moment, there are no reliable storage ring data for H_3^+ recombination below 300 K (see discussion in Refs. 32 and 33). We assume that the situation with D_3^+ is similar to H_3^+ (i.e., no reliable data from storage ring experiments exist for low temperature recombination of the D_3^+ ion).

In our laboratory, we have studied D_3^+ recombination using stationary afterglow (AISA experiment[14,34]) and also flowing afterglow (FALP).[15] In our recent studies, we discovered a fast ternary neutral assisted recombination of H_3^+ and D_3^+ ions in plasma.[16–18,35–37] At temperatures between 77 and 300 K in helium buffer gas, the losses due to this ternary process are comparable with the losses due to binary dissociative recombination already at a buffer gas pressure of few hundred Pa. When this process is accounted for, then the rate coefficient of binary process can be obtained from afterglow experiments. In H_3^+ experiments, we obtained very good agreement

of the measured binary recombination rate coefficients with the ones theoretically predicted for thermodynamic equilibrium (TDE) and for pure para- and pure ortho-H_3^+.[38–41]

Among the H_3^+ studies only few were made using spectroscopic identification of the recombining ions (e.g., Refs. 42–46). The study by Amano done in pure hydrogen[42,43] is well known. Nevertheless, his value of the recombination rate coefficient is up to three times larger than other measured values.[30,37,41] We can speculate that in his experiments the H_3^+ recombination was enhanced by the ternary H_2 assisted process.

The situation with D_3^+ is different. To our knowledge, there was no spectroscopic study of D_3^+ recombination up to now. Only few studies were made using afterglow experiments[9,10,12,14,15] and storage ring experiments.[13,19] There are few storage ring experiments[22] and no afterglow experiments with H_2D^+ and HD_2^+. Usable, near infrared (NIR) absorption frequencies are known[47,48] and we have made spectroscopic investigation of plasma containing a mixture of these ions.[47] Recombination study of these ions using cavity ring down spectroscopy (CRDS) in the afterglow experiment is possible, but it would be very complicated. As was already mentioned, there are no recent storage ring studies of these ions and none at all with "cold ion source". The recent theory predicts the rate coefficients for DR of these ions to be smaller than the one of H_3^+ at temperatures ~300 K.[27,49,50]

In the present study, we formed D_3^+ dominated plasma in local thermodynamic equilibrium and we measured the binary recombination rate coefficient α_{bin} and the helium assisted ternary recombination rate coefficient K_{He} of D_3^+ recombination with electrons. To our knowledge, this is the first spectroscopic study concerning recombination of D_3^+ ions with electrons.

II. EXPERIMENTAL METHODS

The method of measuring the recombination rate coefficients in stationary afterglow plasma is well known, so only a very short description will be given here (see, e.g., Refs. 14 and 34). In pulsed discharge, quasi-neutral D_3^+ dominated plasma is formed and when the discharge is switched off a decrease of the ion number density is monitored during the afterglow. At these conditions the decay of the afterglow plasma is governed by ambipolar diffusion to the walls and by electron-ion recombination. Here, in addition to the mentioned processes, we also consider the conversion of D_3^+ ions to D_5^+ in ternary helium assisted association reaction.[15] The main processes are

$$D_3^+ + e^- \xrightarrow{\alpha_{bin}} \text{neutral products}, \quad (1)$$

$$D_3^+ + e^- + He \xrightarrow{K_{He}} \text{neutral products}, \quad (2)$$

$$D_3^+ + D_2 + He \xrightarrow{k_5} D_5^+ + He, \quad (3)$$

$$D_5^+ + e^- \xrightarrow{\alpha_5} \text{neutral products}, \quad (4)$$

where α_{bin} is the binary recombination rate coefficient of D_3^+ ions, K_{He} is the ternary recombination rate coefficient of He assisted recombination, k_5 is the ternary rate coefficient of He assisted association, and α_5 is the binary recombination rate coefficient of D_5^+ ions with electrons.[15,51] If the recombination of D_5^+ is fast and the ternary association (3) is the rate determining reaction in the sequence of processes (3) and (4), then the balance equation can be written in the form

$$\frac{d[D_3^+]}{dt} = -\alpha_{bin}[D_3^+]n_e - K_{He}[He][D_3^+]n_e - \frac{n_e}{\tau_D} - \frac{n_e}{\tau_R}, \quad (5)$$

where τ_D is the characteristic diffusion time, τ_R the time constant characterizing losses due to ternary association followed by a rapid recombination of D_5^+. If we assume quasineutrality and if we introduce the time constant τ_L for "linear losses" by equation $1/\tau_L = 1/\tau_D + 1/\tau_R$, then the balance equation can be rewritten as

$$\frac{dn_e}{dt} = -\alpha_{eff} n_e^2 - \frac{n_e}{\tau_L}, \quad (6)$$

where we introduced the effective binary recombination rate coefficient α_{eff} which can be written in the form

$$\alpha_{eff}(T, [He]) = \alpha_{bin}(T) + K_{He}(T)[He]. \quad (7)$$

We have demonstrated in our previous studies[16–18] and here we will demonstrate again, that the overall recombination of D_3^+ in afterglow plasma can be described in this way. To obtain α_{bin} and K_{He} one has to measure the dependence of α_{eff} on [He] at fixed temperature T.

III. EXPERIMENT

The plasma is generated in a pulsed microwave discharge in a fused silica tube (inner diameter ~1.5 cm). The tube is cooled to 80 K by liquid nitrogen or by pre-cooled nitrogen vapors for measurements in the temperature range of 80–220 K. To form a D_3^+ dominated plasma a mixture of He/Ar/D_2 with a typical composition $10^{17}/10^{14}/10^{14}$ cm^{-3} is flowing through the discharge tube. The D_3^+ ions are formed in a sequence of ion molecule reactions. The details of the kinetics of the ion formation are well known (see Refs. 14, 15, 18, 34, and 52). The microwave generator ($f = 2.45$ GHz) is equipped with an external fast high-voltage switch to cut off the HV power to the magnetron. The switch off transient time is less than 30 μs. This was indirectly confirmed by monitoring the spontaneous emission of the plasma.[45] A fairly low microwave power in the range 5–15 W, with ~50% duty cycle, was used to avoid excessive heating of the gas during the discharge. A NIR-CRDS was used as the main diagnostic tool, the principal layout is shown in Figure 1. The discharge tube, equipped with an optical resonator (not in scale), forms the main part of the continuous wave modification of CRDS. Because the apparatus was described elsewhere (see Refs. 38–41, 45, and 46) only a short description will be given here.

A distributed feedback laser diode covering the spectral range of 5788–5798 cm^{-1} was used in the present study. During the measurement the laser current was kept constant and wavelength change was done by means of computer controlled temperature change. An interference signal from the Fabry-Perot etalon was used to linearize the wavenumber

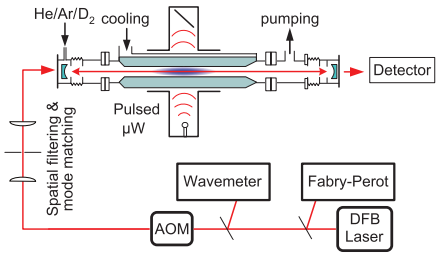

FIG. 1. Stationary afterglow with the CRDS absorption spectrometer. A discharge is periodically ignited in the microwave resonator (μW) in the middle part of the discharge tube. A He/Ar/D_2 gas mixture is used to form a D_3^+ dominated afterglow plasma. The laser light modulated by the acousto-optic modulator (AOM) is injected through the mirror on one side and photons exiting the cavity through the mirror on the other side are detected by an InGaAs avalanche photodiode. The absolute wavelength is measured using a Michelson wavemeter and relatively by a Fabry-Perot etalon.

scale. Two H_2O lines at 5789.65 cm^{-1} and 5793.03 cm^{-1} (line positions taken from HITRAN database[53]) were used to transform the relative value given by Fabry-Perot etalon to absolute wavelength. The resulting precision of wavelength determination is better than 0.01 cm^{-1}. At conditions used in the present experiment, where D_3^+ was the dominant ion, only two absorption lines $(5792.70 \pm 0.01)\,cm^{-1}$ and $(5793.90 \pm 0.01)\,cm^{-1}$ were visible during the discharge and early afterglow. The difference between the measured line positions and those predicted by quantum mechanical calculations is less than $0.02\,cm^{-1}$.[54] Given this fact and that those two absorption lines were only in plasma with D_2 present, we concluded that they belong to D_3^+ ion. The conclusion was also supported by measuring the temperature dependence of the intensities of both lines. The examples of measured profiles of absorption lines are shown in Figure 2. In this study we used the transitions, which we assigned (after discussion with Tennyson[54]) as $3\nu_2^1(1,0) \leftarrow 0\nu_2^0(0,0)$ and $3\nu_2^1(3,2) \leftarrow 0\nu_2^0(4,2)$ for ortho-D_3^+ (0,0) and meta-D_3^+ (4,2), respectively. The rotational levels are labeled by corresponding quantum numbers (J,G), for details on notation and calculations of transitions frequencies see Ref. 55.

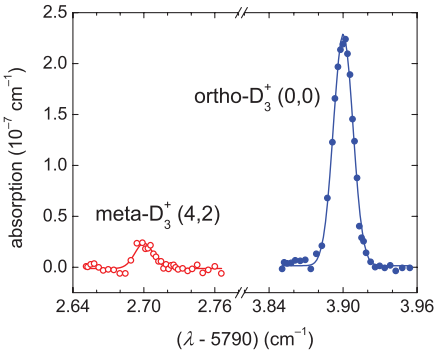

FIG. 2. Example of absorption line profiles of D_3^+ ions measured at the wall temperature of $T_{Wall} = 112$ K and $P = 560$ Pa of He. The kinetic temperature $T_{Kin} = (112 \pm 10)$ K was obtained from the Doppler broadening of the absorption lines. The line center positions are: $(5793.90 \pm 0.01)\,cm^{-1}$ and $(5792.70 \pm 0.01)\,cm^{-1}$ for ortho-D_3^+ (0,0) and meta-D_3^+ (4,2), respectively. The calculated values are 5793.92 cm^{-1} for $3\nu_2^1(1,0) \leftarrow 0\nu_2^0(0,0)$ and 5792.68 cm^{-1} for $3\nu_2^1(3,2) \leftarrow 0\nu_2^0(4,2)$ for ortho-D_3^+ (0,0) and meta-D_3^+ (4,2), respectively.[54,55]

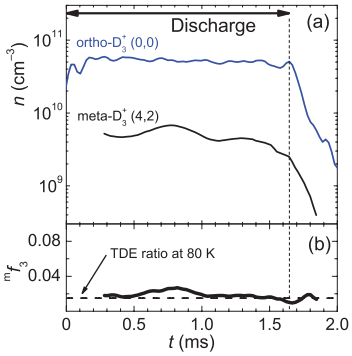

FIG. 3. Panel (a) Measured number densities of the ions in ortho (0,0) and meta (4,2) states of D_3^+ during the discharge and early afterglow. Panel (b) Measured fraction $^m f_3$ of meta-D_3^+ (4,2), $^m f_3 = [\text{meta-}D_3^+\ (4,2)]/[D_3^+]$. The value of the ratio corresponding to the TDE at 80 K is indicated by the dashed horizontal line. Used conditions are $T_{He} = 80$ K, $P = 400$ Pa of He, $[D_2] = 4 \times 10^{14}$ cm^{-3} and $[Ar] = 2 \times 10^{14}$ cm^{-3}.

An example of measured ion number density evolutions in discharge and early afterglow is shown in panel (a) of Figure 3. The dashed vertical line indicates the end of the discharge and the beginning of the afterglow. The measured evolution of the fraction $^m f_3$ of the number density of the meta-D_3^+ (4,2) to the number density of D_3^+ is shown in the lower panel of Figure 3. The horizontal dashed line indicates the calculated ratio corresponding to the TDE at 80 K.

IV. TEMPERATURE IN THE D_3^+ DOMINATED AFTERGLOW PLASMA

In general, in an afterglow plasma the different particles and their internal degrees of freedom are not necessarily in complete thermal equilibrium with each other and with the walls of the plasma container. For instance, the electron temperature T_e can significantly exceed the kinetic temperature of the ions T_{Kin} and the buffer gas atoms temperature T_{He} because the transfer of kinetic energy in electron collisions with heavy particles is less efficient than the kinetic energy transfer in collisions of ions and gas atoms. Also, the ions' rotational temperature T_{Rot} and vibrational temperature T_{Vib} do not have to be equal to the ions' translational temperature if the corresponding relaxation times are long in comparison with the characteristic time of the ion density decay. We have discussed this problem for H_3^+ dominated plasma in Refs. 40, 41, and 56. In the present studies, we determine kinetic temperature (T_{Kin}) of ions from the Doppler broadening of measured absorption lines. In Figure 4 an example of the evolution of T_{Kin} measured at a wall temperature of $T_{Wall} = (112 \pm 1)$ K is plotted. The obtained equality $T_{Wall} = T_{Kin}$ means also $T_{Wall} = T_{He}$. We have made such measurements for the whole range of pressures and temperatures used in the present study with the same conclusion.

The electron temperature T_e in the afterglow was not measured in these experiments. The time constant for

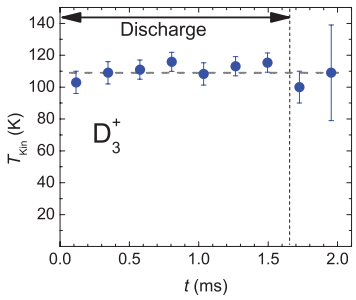

FIG. 4. The measured evolution of the kinetic temperature of the ions (T_{Kin}) during the discharge and during the early afterglow, while a wall temperature was $T_{Wall} = (112 \pm 1)$ K and rotational temperature was $T_{Rot} = (112 \pm 3)$ K. Used helium buffer gas concentration was [He] $= 3.6 \times 10^{17}$ cm^{-3}. The mean value of the measured T_{Kin} is indicated by a horizontal dashed line.

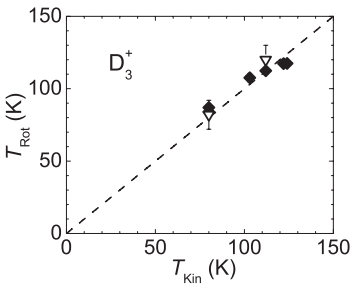

FIG. 5. The measured rotational temperature T_{Rot} of the D_3^+ ions versus the measured kinetic temperature T_{Kin}. The dashed straight line indicates the equality $T_{Rot} = T_{Kin}$. The open triangles and filled rhomboids indicate data measured during the early afterglow and during the discharge, respectively.

electron cooling at a typical helium density used in the experiment can be estimated from the electron-helium collision frequency (>1 GHz) and the mass ratio $2m_e/m_{He}$. The calculated time constant for electron cooling is $\tau_\varepsilon < 10\,\mu$s. In previous FALP experiments, we measured the electron energy distribution function (EEDF) in He and He/Ar buffered afterglow plasmas under conditions similar to those in the present study.[57–59] It was found that EEDF is close to a Maxwellian distribution with a temperature close to the buffer gas temperature.[60] In stationary afterglow with CRDS, we indirectly observed fast cooling of electrons after switching off the discharge by monitoring visible light emissions from the discharge and very early afterglow. Using analogy with H_3^+, we also expect that all excited vibrational states of D_3^+ are quenched in multiple collisions with He, Ar, and D_2 (see discussion for H_3^+ in Ref. 41).

Using FALP, we also studied the collisional radiative recombination (CRR) in an Ar^+ dominated plasma in a He/Ar gas mixture and we measured the corresponding ternary recombination rate coefficient K_{CRR} which has a very pronounced temperature dependence, $K_{CRR} \sim T_e^{-9/2}$.[61–63] In this study, we also measured the temperature dependence of ambipolar diffusion. In both cases, we obtained very good agreement with theory for temperatures of 77–300 K.[62,63] This is an excellent confirmation that at the given experimental conditions $T_e = T_{He} = T_{Wall}$. These estimates need to be refined when the plasma contains energy sources that can lead to heating of the electron gas. One such source can be He metastables.[59,60] In the present experiments, metastables are destroyed in reaction with Ar (by Penning ionization[58,60]). At low temperatures and high electron densities the electron heating can be caused by CRR; we will discuss this possibility later. In our previous studies of H_3^+ recombination,[41] we showed that at the used electron densities, the CRR can elevate the electron temperature only slightly in the early afterglow at gas temperatures near 77 K, but becomes unimportant at higher gas temperatures and lower electron densities.

From the measured relative population of the ions in the two monitored states we determined the rotational temperature T_{Rot}. The rotational temperature T_{Rot} was measured not only during the discharge but also during the early afterglow when the signal from meta-D_3^+ (J,G) = (4,2) was still sufficient. The measured dependence of T_{Rot} on T_{Kin} is shown in Figure 5.

Recently, we studied relaxation processes and equilibrium in H_3^+ dominated plasma using very similar experimental conditions, the only difference being that now we use D_2 instead of H_2.[38–41,56] In H_3^+ studies, we monitored the population of two ortho states and one para state and the used transitions were more suitable for measurements of rotational temperatures at He buffer gas temperatures in the range of 80–200 K. We were also able to monitor the para to ortho ratio, [para-H_3^+]/[ortho-H_3^+]. In addition, in the H_3^+ experiments we used normal and para enriched hydrogen to manipulate the fraction of para-H_3^+ in the plasma. From the obtained results we also concluded that $T_{Rot} = T_{Kin} = T_{He} = T_{Wall}$ for H_3^+. Later on, for present experiments we will use temperature measured from the Doppler broadening of the absorption lines (mean value from several measurements at the same wall temperature). For previous FALP data, we will use the measured temperature of the flow tube. On the basis of the present experiments and using comparison and analogy with the results obtained in H_3^+ experiments, we concluded that the plasma in the afterglow is in the thermodynamic equilibrium at a temperature given by the wall of the discharge tube.

V. RESULTS AND DISCUSSION

We measured the variation of light absorption in afterglow plasma using CRDS. Under the assumption that the plasma is in thermal equilibrium and D_3^+ is the dominant ion we calculated the electron density decay. Examples of data measured at 112 K are plotted in Figure 6. The measured number densities of the ions in ortho (0,0) and meta (4,2) states of D_3^+, the calculated electron density and the partial density of ions in (4,2) state (fraction $^m f_3$ of meta-D_3^+ (4,2), $^m f_3$ = [meta-D_3^+ (4,2)]/[D_3^+]) are plotted.

We studied plasma decay at temperatures of 80–130 K over a wide range of He pressures. The decay curves were analyzed using "integral analysis" (for details see Refs. 57 and 64). This analysis can separate α_{eff} from τ_L (see Eqs. (5) and (6)) and minimize the influence of D_5^+ formation followed by a rapid recombination on the determination of α_{eff}. The first 50–150 μs of the afterglow decay were not taken into

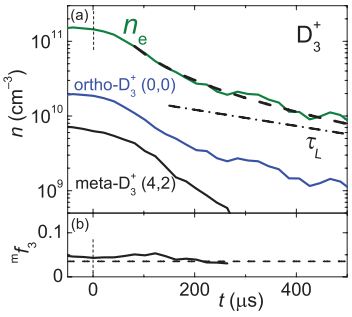

FIG. 6. Panel (a) Example of the decay of densities of ions in ortho (0,0) and meta (4,2) states of D_3^+, measured during the afterglow in a He/Ar/D_2 gas mixture at 112 K, 550 Pa of He, $[D_2] = 1.7 \times 10^{14}$ cm^{-3} and $[Ar] = 8.4 \times 10^{13}$ cm^{-3}. Time is set to zero at the beginning of the afterglow (indicated by vertical dashed line). The electron density (n_e) is obtained from the partial density of ions in the (0,0) state under assumption of TDE. The dashed-dotted line indicates losses due to diffusion and reactions with the time constant τ_L, the dashed line indicates the fit of the electron number density decay, see Eqs. (5) and (6). Panel (b) Measured fraction $^mf_3$ of meta-D_3^+ (4,2), $^mf_3$ = [meta-D_3^+ (4,2)]/[D_3^+].

account from the analysis to exclude eventual formation of D_3^+ in very early afterglow (for details see Refs. 18, 39, and 65). Dependencies of the effective recombination rate coefficient α_{eff} on [He], measured at 80 and 100 K are shown in panels (a) and (b) of Figure 7, respectively. Linear dependence of α_{eff} on [He] is obvious. Similar dependencies were measured also at 112 and 125 K. The data from previous FALP experiment are plotted in Figure 7 as open squares.[17] In addition, we performed series of experiments using new Cryo-FALP II apparatus (for details on experimental setup see Ref. 63) at

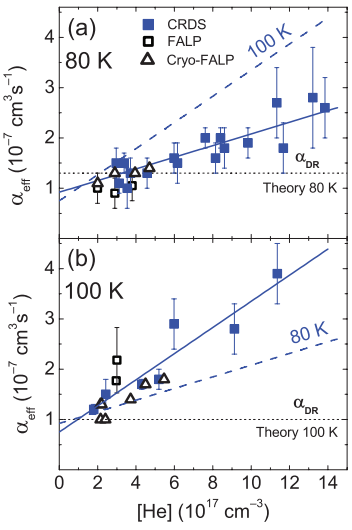

FIG. 7. Measured dependence of the effective recombination rate coefficients on [He] at 80 K - panel (a) and 100 K - panel (b). The data indicated by filled squares were measured in present experiments using CRDS and the data indicated by open squares were measured using a Langmuir probe in previous FALP experiment (see compilation in Ref. 17). The data indicated by open triangles were measured in this study using a new Cryo-FALP II apparatus. For comparison straight lines obtained by a fit of CRDS data at indicated temperatures are plotted in both panels. The horizontal dotted lines indicate theoretical values of α_{DR} at corresponding temperatures.[27,50]

the same conditions (temperature, number density of Ar and D_2) as in the already mentioned FALP experiment but in a broader pressure range and with better temperature control. These data are plotted in Figure 7 as open triangles.

Special attention was paid to the analysis of the decay curves measured at 80 and 100 K because of a possible influence of CRR process described by Bates.[66,67] To demonstrate and evaluate the effect of CRR we used the fact that the overall binary rate coefficient α_{CRR} of the ternary CRR process is dependent on the electron density, $\alpha_{CRR} = K_{CRR} \cdot n_e$, where K_{CRR} is the ternary rate coefficient, only dependent on the temperature. We measured α_{eff} in two types of experiments, in FALP with a typical initial electron density of $n_{e_0} = 2 \times 10^9$ cm^{-3} and in SA-CRDS with a typical initial electron density $n_{e_0} = 3 \times 10^{10}$ cm^{-3}. The measured α_{eff} are plotted in Figure 7. Within experimental accuracy, the data measured at the same temperature but with very different electron densities give the same value of α_{eff}. From this we concluded that CRR contribution, which should be dependent on n_{e_0} is small in comparison with the contribution from processes with their rate coefficients independent of electron density. This conclusion can be surprising, but it agrees with conclusions from more detailed studies of this phenomenon made for recombination of H_3^+ ions, for details see Ref. 41. For comparison if one uses the classical Stevefelt formula for calculation of α_{CRR} at $T = 77$ K and $n_e = 3 \times 10^{10}$ cm^{-3} then the value of $\alpha_{CRR} \sim 3 \times 10^{-7}$ cm^3 s^{-1} is obtained (for details see Refs. 41 and 61). From the data plotted in Figure 7 it is clear that Stevefelt's calculated value of α_{CRR}[61] is three times higher than the measured overall recombination rate coefficient α_{eff} at low [He]. We experimentally verified the validity of Stevefelt formula for atomic ions by measuring α_{CRR} in Ar^+ dominated plasma at temperature range of 60–300 K and we obtained a good agreement.[62,63] Up to now we do not have an explanation for not observing CRR for H_3^+ nor D_3^+ molecular ions while we can observe it for atomic Ar^+(bearing in mind the differences between both the experiments).

We calculated binary and ternary recombination rate coefficients α_{bin} and K_{He} from the measured dependencies of α_{eff} on [He] (see Eq. (7)). Present measurements are made over a broad range of [He], so the accuracy of obtained α_{bin} and K_{He} is higher in comparison with previous FALP and AISA studies.[17] The obtained values of α_{bin} and K_{He} are plotted in Figures 8 and 9 as a function of the temperature and summarized in Table I. The thermal rate coefficients α_{DR} calculated for binary dissociative recombination[27,28,50] are also plotted in Figure 8 (recombination rate coefficient plotted in Figure 8 as theory of Pratt and Jungen was calculated from the dependence of the recombination rate on energy published in Ref. 28). We also included several values of rate coefficients measured in previous afterglow experiments at 300 K.[10–12] These rate coefficients were corrected by taking the He density into account in particular experiments and the actual values of ternary rate coefficients as measured in the FALP experiment.[17] We also plotted the rate coefficients calculated from the corresponding cross section measured in storage ring experiment CRYRING.[13,19] For comparison of the measured α_{bin} with α_{CRR}, we also plotted expected

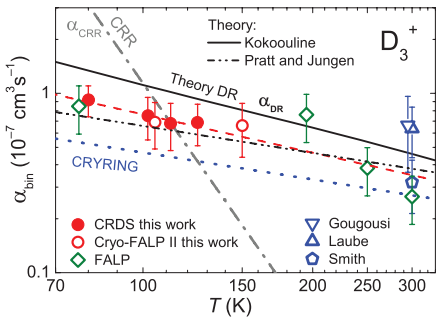

FIG. 8. D_3^+ binary recombination rate coefficients. The solid line and the dashed double dotted line indicate the values for the binary dissociative recombination (α_{DR}) at a thermal population of the para-/ortho-/meta-states of D_3^+ calculated by Kokoouline[27,50] and by Pratt and Jungen,[28] respectively. The values α_{bin} indicated by filled circles were obtained in present study from the dependencies of α_{eff} on [He] at particular T. The open circles denote the data obtained in this study using Cryo-FALP II apparatus. The values indicated by open diamonds were obtained in previous FALP experiments from dependencies of α_{eff} on [He] at fixed T.[16–18] The dotted line indicates the rate coefficients measured in storage ring experiment CRYRING.[13,19] Previous FALP data obtained in other laboratories are indicated as Gougousi,[11] Laube,[10] and Smith;[12] these data were corrected (see text). The steep dashed-dotted line labeled CRR is the effective binary rate coefficient α_{CRR} of CRR calculated using Stevefelt formula (see Refs. 41 and 61) for electron density $n_e = 3 \times 10^{10}$ cm^{-3}). The dashed line is a fit to FALP, Cryo-FALP II, and CRDS data.

α_{CRR} in Figure 8 calculated for $n_e = 3 \times 10^{10}$ cm^{-3} using the Stevefelt formula.[41,61]

The measured ternary recombination rate coefficients K_{He} are in good agreement with previous data measured in FALP experiments. In our previous studies, we discussed the ternary helium assisted recombination in terms of the life-times of excited Rydberg states D_3^* formed in the collision of D_3^+ ions with electrons.[16–18] Because of long life-time of D_3^* (up to several hundreds of picoseconds) the process can be, depending on the temperature, hundred times more effective

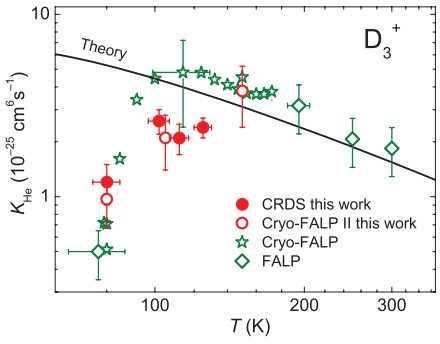

FIG. 9. The ternary recombination rate coefficient, $K_{He}(T)$, for He assisted ternary recombination of D_3^+ ions. The filled circles indicate the present values obtained from the measured linear dependencies of α_{eff} on [He] at fixed T, see full lines in Figure 7. The open circles were obtained in present study with Cryo-FALP II apparatus from the dependence of α_{eff} on [He]. The open diamonds indicate data obtained from dependence of α_{eff} on [He] measured in FALP experiment (for more details see Refs. 16–18). The data measured using Cryo-FALP with the continuously increasing temperature are labeled by stars.[17,18] The full line indicates theoretical ternary rate coefficients calculated for D_3^+ ions in thermal equilibrium.[16–18]

TABLE I. Measured binary α_{bin} and ternary K_{He} recombination rate coefficients of D_3^+. The displayed temperature T is the temperature obtained from Doppler broadening of absorption lines in the present study and temperature of the metal wall of the flow tube in FALP experiments.[17]

T[K]	α_{bin} (10^{-8} cm^3 s^{-1})	K_{He} (10^{-25} cm^6 s^{-1})	Reference
77	8.5 ± 2.5	0.5 ± 0.2	FALP[17]
80	9.2 ± 2.0	1.2 ± 0.3	This study
100	7.5 ± 2.0	2.6 ± 0.4	This study
112	6.5 ± 2.0	2.1 ± 0.4	This study
125	6.9 ± 1.8	2.4 ± 0.3	This study
300	2.7 ± 0.8	1.8 ± 0.6	FALP[17]

than classical neutral assisted ternary recombination predicted by Thomson[68] and by Bates and Khare.[69] The process is essentially different from the process considered by Thomson. The present studies confirmed the previously measured strong increase of K_{He} with temperatures starting from 80 K.

VI. CONCLUDING REMARKS

We studied electron-ion recombination in D_3^+ dominated afterglow plasma in He/Ar/D_2 gas mixture using CRDS for measuring ion density decays during the afterglow and for characterizing kinetic and rotational temperature of ions. From this measurements and using similarity with H_3^+ dominated afterglow plasma[39,41,56] we concluded that at used conditions D_3^+ dominated afterglow plasma is in thermal equilibrium with He buffer gas. The study confirmed that the decay of D_3^+ dominated afterglow plasma is controlled by the binary recombination and in parallel by the three body helium assisted recombination process. The magnitude and temperature dependence of rate coefficients of these processes as measured with CRDS are in agreement with our previous flowing afterglow studies using Langmuir probe.[16–18] The binary and the ternary recombination rate coefficients were obtained in the temperature range of 80–130 K yielding $\alpha_{bin}(80\,K) = (9.2 \pm 2.0) \times 10^{-8}$ cm^3 s^{-1}, $\alpha_{bin}(125\,K) = (6.9 \pm 1.8) \times 10^{-8}$ cm^3 s^{-1}, $K_{He}(80\,K) = (1.2 \pm 0.3) \times 10^{-26}$ cm^6 s^{-1} and $K_{He}(125\,K) = (2.4 \pm 0.3) \times 10^{-26}$ cm^6 s^{-1}.

As in our previous recombination study of H_3^+ dominated plasma, neither for recombination of D_3^+ ions we have seen any substantial dependence of recombination rate coefficient on electron number density as predicted by theory of collisional radiative recombination.[61] This rather surprising result is supported by comparison of effective recombination rate coefficients obtained at the temperature of 80 K in this study and in previous flowing afterglow measurement[17] (see Figure 7 for details) at electron number densities different by an order of magnitude.

This is the first study on the recombination of D_3^+ ions with electrons with spectroscopically resolved abundances of the recombining ions. The results support theoretical predictions and are in agreement with previous flowing afterglow measurements[16–18] and with storage ring data.[13,19]

ACKNOWLEDGMENTS

This work was partly financed by the research grant OC10046 from the Ministry of Education of the Czech Republic and was partly supported by GACR (205/09/1183, P209/12/0233), by SV 265 302, by GAUK 92410, GAUK 353811, GAUK 54010, and by COST Action CM0805 (The Chemical Cosmos).

[1] T. R. Geballe and T. Oka, Science **312**, 1610 (2006).
[2] C. D. Gay, P. C. Stancil, S. Lepp, and A. Dalgarno, Astrophys. J. **737**, 44 (2011).
[3] D. R. Flower, G. P. des Forets, and C. M. Walmsley, Astron. Astrophys. **427**, 887 (2004).
[4] C. Vastel, T. G. Phillips, and H. Yoshida, Astrophys. J. **606**, L127 (2004).
[5] R. Stark, F. F. S. van der Tak, and E. F. van Dishoeck, Astrophys. J. **521**, L67 (1999).
[6] R. Stark, G. Sandell, S. C. Beck, M. R. Hogerheijde, E. F. van Dishoeck, P. van der Wal, F. F. S. van der Tak, F. Schafer, G. J. Melnick, M. L. N. Ashby, and G. de Lange, Astrophys. J. **608**, 341 (2004).
[7] E. Roueff, J. Phys.: Conf. Ser. **4**, 1 (2005).
[8] M. Larsson and A. Orel, *Dissociative Recombination of Molecular Ions* (Cambridge University Press, Cambridge, 2008).
[9] P. van der Donk, F. B. Yousif, and J. B. A. Mitchell, Phys. Rev. A **43**, 5971 (1991).
[10] S. Laube, A. L. Padellec, O. Sidko, C. Rebrion-Rowe, J. B. A. Mitchell, and B. R. Rowe, J. Phys. B **31**, 2111 (1998).
[11] T. Gougousi, R. Johnsen, and M. F. Golde, Int. J. Mass Spectrom. **149-150**, 131 (1995).
[12] D. Smith and P. Spanel, Int. J. Mass Spectrom. **129**, 163 (1993).
[13] M. Larsson, H. Danared, A. Larson, A. L. Padellec, J. R. Peterson, S. Rosen, J. Semaniak, and C. Stromholm, Phys. Rev. Lett. **79**, 395 (1997).
[14] V. Poterya, J. Glosik, R. Plasil, M. Tichy, P. Kudrna, and A. Pysanenko, Phys. Rev. Lett. **88**, 044802 (2002).
[15] O. Novotny, R. Plasil, A. Pysanenko, I. Korolov, and J. Glosik, J. Phys. B **39**, 2561 (2006).
[16] J. Glosik, I. Korolov, R. Plasil, T. Kotrik, P. Dohnal, O. Novotny, J. Varju, S. Roucka, C. Greene, and V. Kokoouline, Phys. Rev. A **80**, 042706 (2009).
[17] T. Kotrik, P. Dohnal, I. Korolov, R. Plasil, S. Roucka, J. Glosik, C. Greene, and V. Kokoouline, J. Chem. Phys. **133**, 034305 (2010).
[18] J. Glosik, R. Plasil, T. Kotrik, P. Dohnal, J. Varju, M. Hejduk, I. Korlov, S. Roucka, and V. Kokoouline, Mol. Phys. **108**, 2253 (2010).
[19] A. L. Padellec, M. Larsson, H. Danared, A. Larson, J. R. Peterson, S. Rosen, J. Semaniak, and C. Stromholm, Phys. Scr. **57**, 215 (1998).
[20] T. Tanabe, I. Katayama, and H. Kamegaya, *Dissociative Recombination: Theory, Experiments and Applications III* (World Scientific, Singapore, 1996), pp. 84–93.
[21] A. E. Orel, I. F. Schneider, and A. Suzor-Weiner, Philos. Trans. R. Soc. London, Ser. A **358**, 1445 (2000).
[22] J. B. A. Mitchell, C. T. Ng, L. Forand, R. Janseen, and J. W. McGowan, J. Phys. B **17**, L909 (1984).
[23] V. Zhaunerchyk, R. D. Thomas, W. D. Geppert, M. Hamberg, M. Kaminska, E. Vigren, and M. Larsson, Phys. Rev. A **77**, 034701 (2008).
[24] V. Kokoouline and C. H. Greene, Phys. Rev. A **72**, 022712 (2005).
[25] C. Jungen and S. T. Pratt, Phys. Rev. Lett **1021**, 023201 (2009).
[26] V. Kokoouline, C. H. Greene, and B. D. Esry, Nature (London) **412**, 891 (2001).
[27] V. Kokoouline and C. H. Greene, Phys. Rev. A **68**, 012703 (2003).
[28] S. T. Pratt and C. Jungen, J. Phys.: Conf. Ser. **300**, 012019 (2011).
[29] B. J. McCall, A. J. Honeycutt, R. J. Saykally, T. R. Geballe, N. Djuric, G. H. Dunn, J. Semaniak, O. Novotny, A. Al-Khalili, A. Ehlerding, F. Hellberg, S. Kalhori, A. Neau, R. Thomas, F. Osterdahl, and M. Larsson, Nature (London) **422**, 500 (2003).
[30] H. Kreckel, M. Motsch, J. Mikosch, J. Glosik, R. Plasil, S. Altevogt, V. Andrianarijaona, H. Buhr, J. Hoffmann, L. Lammich, M. Lestinsky, I. Nevo, S. Novotny, D. A. Orlov, H. B. Pedersen, F. Sprenger, A. S. Terekhov, J. Toker, R. Wester, D. Gerlich, D. Schwalm, A. Wolf, and D. Zajfman, Phys. Rev. Lett. **95**, 263201 (2005).
[31] B. J. McCall, A. J. Huneycutt, R. J. Saykally, N. Djuric, G. H. Dunn, J. Semaniak, O. Novotny, A. Al-Khalili, A. Ehlerding, F. Hellberg, S. Kalhori, A. Neau, R. Thomas, A. Paal, F. Osterdahl, and M. Larsson, Phys. Rev. A **70**, 052716 (2004).
[32] H. Kreckel, O. Novotny, K. N. Crabtree, H. Buhr, A. Petrignani, B. A. Tom, R. D. Thomas, M. H. Berg, D. Bing, M. Grieser, C. Krantz, M. Lestinsky, M. B. Mendes, C. Nordhorn, R. Repnow, J. Stutzel, A. Wolf, and B. J. McCall, Phys. Rev. A **82**, 042715 (2010).
[33] A. Petrignani, S. Altevogt, M. H. Berg, D. Bing, M. Grieser, J. Hoffmann, B. Jordon-Thaden, C. Krantz, M. B. Mendes, O. Novotny, S. Novotny, D. A. Orlov, R. Repnow, T. Sorg, J. Stutzel, A. Wolf, H. Buhr, H. Kreckel, V. Kokoouline, and C. H. Greene, Phys. Rev. A **83**, 032711 (2011).
[34] R. Plasil, J. Glosik, V. Poterya, P. Kudrna, J. Rusz, M. Tichy, and A. Pysanenko, Int. J. Mass Spectrom. **218**(2), 105 (2002).
[35] J. Glosik, R. Plasil, I. Korolov, O. Novotny, and T. Kotrik, J. Phys.: Conf. Ser. **192**, 012005 (2009).
[36] J. Glosik, I. Korolov, R. Plasil, O. Novotny, T. Kotrik, P. Hlavenka, J. Varju, I. A. Mikhailov, V. Kokoouline, and C. H. Greene, J. Phys. B **41**, 191001 (2008).
[37] J. Glosik, R. Plasil, I. Korolov, T. Kotrik, O. Novotny, P. Hlavenka, P. Dohnal, J. Varju, V. Kokoouline, and C. Greene, Phys. Rev. A **79**, 052707 (2009).
[38] J. Varju, S. Roucka, T. Kotrik, R. Plasil, and J. Glosik, J. Phys.: Conf. Ser. **227**, 012026 (2010).
[39] J. Varju, M. Hejduk, P. Dohnal, M. Jilek, T. Kotrik, R. Plasil, D. Gerlich, and J. Glosik, Phys. Rev. Lett. **106**, 203201 (2011).
[40] M. Hejduk, P. Dohnal, J. Varju, P. Rubovic, T. Kotrik, R. Plasil, and J. Glosik, Plasma Sources Sci. Technol. **21**, 024002 (2012).
[41] P. Dohnal, M. Hejduk, J. Varju, P. Rubovic, S. Roucka, T. Kotrik, R. Plasil, J. Glosik, and R. Johnsen, J. Chem. Phys. **136**, 244304 (2012).
[42] T. Amano, J. Chem. Phys. **92**, 6492 (1990).
[43] T. Amano, Astrophys. J. **329**, L121 (1988).
[44] M. Feher, A. Rohrbacher, and J. P. Maier, Chem. Phys. **185**, 357 (1994).
[45] P. Macko, G. Bano, P. Hlavenka, R. Plasil, V. Poterya, A. Pysanenko, O. Votava, R. Johnsen, and J. Glosik, Int. J. Mass Spectrom. **233**, 299 (2004).
[46] P. Macko, R. Plasil, P. Kudrna, P. Hlavenka, V. Poterya, A. Pysanenko, G. Bano, and J. Glosik, Czech. J. Phys. **52**, 695 (2002).
[47] P. Hlavenka, R. Plasil, G. Bano, I. Korolov, D. Gerlich, J. Ramanlal, J. Tennyson, and J. Glosik, Int. J. Mass Spectrom. **255**, 170 (2006).
[48] J. Glosik, P. Hlavenka, R. Plasil, F. Windisch, D. Gerlich, A. Wolf, and H. Kreckel, Philos. Trans. R. Soc. London, Ser. A **364**(1848), 2931 (2006).
[49] S. F. dos Santos, V. Kokoouline, and C. H. Greene, J. Chem. Phys. **127**, 124309 (2007).
[50] L. Pagani, C. Vastel, E. Hugo, V. Kokoouline, C. H. Greene, A. Bacmann, E. Bayet, C. Ceccarelli, R. Peng, and S. Schlemmer, Astron. Astrophys. **494**, 623 (2009).
[51] M. T. Leu, M. A. Biondi, and R. Johnsen, Phys. Rev. A **8**, 413 (1973).
[52] J. Glosik, R. Plasil, V. Poterya, P. Kudrna, M. Tichy, and A. Pysanenko, J. Phys. B **34**(15), L485 (2001).
[53] L. S. Rothman, I. E. Gordon, A. Barbe, D. C. Benner, P. F. Bernath, M. Borik, V. Boudon, L. R. Brown, A. Campargue, J.-P. Champion, K. Chance, L. H. Coudert, V. Dana, V. M. Devi, S. Fally, J.-M. Flaud, R. R. Gamache, A. Goldman, D. Jacquemart, I. Kleiner, N. Lacome, W. J. Lafferty, J.-Y. Mandin, S. T. Massie, S. N. Mikhailenko, C. E. Miller, N. Moazzen-Ahmadi, O. V. Naumenko, A. V. Nikitin, J. Orphai, V. I. Perevalov, A. Perrin, A. Predoi-Cross, C. P. Rinsland, M. Rotger, M. Simeckova, M. A. H. Smith, K. Sung, S. A. Tashkun, J. Tennyson, R. A. Toth, A. C. Vandaele, and J. V. Auwera, J. Quant. Spectrosc. Radiat. Transf. **110**, 533 (2009).
[54] J. Tennyson, private communication (2012).
[55] J. Ramanlal and J. Tennyson, Mon. Not. R. Astron. Soc. **354**, 161 (2004).
[56] P. Dohnal, M. Hejduk, J. Varju, P. Rubovic, S. Roucka, T. Kotrik, R. Plasil, R. Johnsen, and J. Glosik, Philos. Trans. R. Soc. London, Ser. A **370**, 5101 (2012).
[57] I. Korolov, T. Kotrik, R. Plasil, J. Varju, M. Hejduk, and J. Glosik, Contrib. Plasma Phys. **48**(5−7), 521 (2008).
[58] R. Plasil, I. Korolov, T. Kotrik, J. Varju, P. Dohnal, Z. Donko, G. Bano, and J. Glosik, J. Phys.: Conf. Ser. **192**, 012023 (2009).
[59] R. Plasil, I. Korolov, T. Kotrik, P. Dohnal, G. Bano, Z. Donko, and J. Glosik, Eur. Phys. J. D **54**, 391 (2009).
[60] J. Glosik, G. Bano, R. Plasil, A. Luca, and P. Zakouril, Int. J. Mass Spectrom. **189**, 103 (1999).
[61] J. Stevefelt, J. Boulmer, and J. Delpech, Phys. Rev. A **12**, 1246 (1975).
[62] T. Kotrik, P. Dohnal, S. Roucka, P. Jusko, R. Plasil, J. Glosik, and R. Johnsen, Phys. Rev. A **83**, 032720 (2011).
[63] T. Kotrik, P. Dohnal, P. Rubovic, R. Plasil, S. Roucka, S. Opanasiuk, and J. Glosik, Eur. Phys. J.: Appl. Phys. **56**, 24011 (2011).
[64] R. Plasil, I. Korolov, T. Kotrik, and J. Glosik, Int. J. Mass Spectrom. **275**, 80 (2008).

[65]R. Plasil, J. Varju, M. Hejduk, P. Dohnal, T. Kotrik, and J. Glosik, J. Phys.: Conf. Ser. **300**(1), 012023 (2011).
[66]D. R. Bates, A. E. Kingston, and W. P. McWhirter, Philos. Trans. R. Soc. London, Ser. A **267**, 297 (1962).
[67]E. W. McDaniel, J. B. A. Mitchell, and M. E. Rudd, *Atomic Collisions, Heavy Partricle Projectiles* (Wiley Interscience, New York, 1993).
[68]J. J. Thomson, Philos. Mag. **47**, 337 (1924).
[69]D. Bates and S. Khare, Proc. Phys. Soc. London **85**, 231 (1965).

ARTICLE VI

TITLE: Collisional-radiative recombination of Ar^+ ions with electrons in ambient helium at temperatures from 50 K to 100 K

AUTHORS: Petr Dohnal, Peter Rubovič, Tomáš Kotrík, Michal Hejduk, Radek Plašil, Rainer Johnsen, and Juraj Glosík

JOURNAL: Physical Review A

DATE: 29 May 2013

DOI: 10.1103/PhysRevA.87.052716

Collisional-radiative recombination of Ar^+ ions with electrons in ambient helium at temperatures from 50 K to 100 K

Petr Dohnal,[1] Peter Rubovič,[1] Tomáš Kotrík,[1] Michal Hejduk,[1] Radek Plašil,[1] Rainer Johnsen,[2] and Juraj Glosík[1]
[1]*Department of Surface and Plasma Science, Faculty of Mathematics and Physics, Charles University in Prague, Czech Republic*
[2]*Department of Physics and Astronomy, University of Pittsburgh, Pittsburgh, Pennsylvania 15260, USA*
(Received 26 April 2013; published 29 May 2013)

Ternary electron-assisted collisional radiative recombination (E-CRR) and neutral-assisted radiative recombination (N-CRR) have very strong negative temperature dependencies and hence dominate electron recombination in some plasmas at very low temperatures. However, there are only few data for molecular ions and almost none for atomic ions at temperatures much below 300 K. In this experimental study we used a cryogenic afterglow plasma experiment (Cryo-FALP II) at temperatures from 50 K to 100 K to measure ternary recombination rate coefficients for Ar^+ ions in ambient helium gas. The measured magnitudes and the temperature dependencies of the ternary recombination rate coefficients for electron-assisted and neutral-assisted collisional radiative recombination agree well with theoretical predictions ($K_{\text{E-CRR}} \sim T^{-4.5}$ and $K_{\text{He-CRR}} \sim T^{-2.5}$ to $T^{-2.9}$) over a broad range of electron and He densities.

DOI: 10.1103/PhysRevA.87.052716 PACS number(s): 34.80.Lx, 52.27.Aj, 52.20.−j

I. INTRODUCTION

Electron-ion recombination in cold plasmas can occur by several mechanisms. When the ions in the plasma are molecular, dissociative recombination (DR) [1] is almost always much faster than third-body-assisted recombination, unless the densities of third particles (electrons, ions, and neutrals) are very high or the temperature is very low. Hence, in many afterglow determinations of DR rate coefficients of molecular ions at temperatures near 300 K, neutral densities below 1×10^{17} cm^{-3}, and electron densities $< 1 \times 10^{10}$ cm^{-3}, third-body-assisted recombination can usually be neglected. Experimental methods have now been developed that are capable of measuring DR rate coefficients at the very low temperatures (near 50 K) that exist in cold interstellar clouds. At those temperatures, third-body-assisted recombination becomes competitive with DR and must be clearly separated from binary DR. The studies described here test existing theories of ternary recombination at very low temperatures in helium-buffered plasmas containing predominantly atomic argon ions, thus largely eliminating DR. The remaining recombination processes consist of ternary recombination in which electrons and helium atoms act as third bodies and a slow conversion of atomic argon ions to molecular Ar_2^+ ions that recombine by DR. As will be shown, the relative contributions of the three mechanisms can be separated and the results confirm theoretical calculations.

In the following we will refer to ternary electron-assisted collisional radiative recombination (see, e.g., [2]) as E-CRR and to the ternary neutral-assisted recombination process (see, e.g., [3]) as N-CRR, where N denotes the neutral atom (e.g., He). The overall reaction equations for atomic argon ions in the presence of electrons and helium atoms can be written as

$$Ar^+ + e^- + e^- \xrightarrow{K_{\text{E-CRR}}} Ar + e^- \tag{1}$$

and

$$Ar^+ + e^- + He \xrightarrow{K_{\text{He-CRR}}} Ar + He, \tag{2}$$

where $K_{\text{E-CRR}}$ and $K_{\text{He-CRR}}$ are ternary recombination rate coefficients (in units of cm^6 s^{-1}). Writing the reactions in this form is not meant to imply that a single three-particle collision completes the recombination. In general, several energy-reducing collisions are required to render the product atom stable against reionization. Both E-CRR and N-CRR have been extensively treated by semiclassical theories (see, e.g., [2,4]) that solve the coupled equations for three-body electron capture into discrete Rydberg states, ionization, and stepwise collisional and radiative reduction of the electron energy. Results of numerical calculations of E-CRR by Stevefelt *et al.* [2] can be expressed by the following formula for the effective binary rate coefficient:

$$\alpha_{\text{E-CRR}} = 3.8 \times 10^{-9} T_e^{-4.5} n_e + 1.55 \times 10^{-10} T_e^{-0.63} + 6 \times 10^{-9} T_e^{-2.18} n_e^{0.37} \text{ cm}^3 \text{ s}^{-1}, \tag{3}$$

where T_e is the electron temperature in K and n_e is the electron number density in cm^{-3}. At low temperatures the second and third terms on the right-hand side tend to be small in comparison with the first term and one can define a three-body rate coefficient $K_{\text{E-CRR}}$ by dividing E-CRR by the electron density:

$$K_{\text{E-CRR}} = \alpha_{\text{E-CRR}}/n_e \cong 3.8 \times 10^{-9} T_e^{-4.5} \text{ cm}^6 \text{ s}^{-1}. \tag{4}$$

Recently, Pohl *et al.* [5] have revised the rates of electron capture into high Rydberg states and of the energy exchange between high Rydberg states and free electrons. In the limit of small energy transfer the revised rates differ drastically from the earlier rates, however, the steady-state recombination rate is only weakly affected. The numerical coefficient in Eq. (4) is reduced to 2.77×10^{-9}. The only experimental data on E-CRR for temperatures below 300 K are those of our Cryo-FALP I studies of Ar^+ ions [6] at 77–180 K, and our recent study at temperatures 57–200 K [7]. Those agreed well with theory. However, our studies of the recombination of H_3^+ and D_3^+ ions with electrons gave no indication of E-CRR, a rather puzzling result since E-CRR should have been faster than binary dissociative recombination at very low temperatures [8–10]. Those observations motivated us

to conduct the present studies of E-CRR in a range of temperatures that is largely unexplored. Ternary recombination in cold and ultracold plasmas is also of interest in the formation of antihydrogen [5,11].

As a consequence of the small electron-to-neutral mass ratio, transfer of electronic energy to heavy particles is slow and N-CRR is less efficient than E-CRR by many orders of magnitude. A good estimate of the recombination rate coefficient can be derived from the energy-diffusion model [3,12–14] that treats the electron energy states as a continuum, as discussed in great detail by Flannery [3]. Flannery derived the following rate coefficient for the case of atomic ions in their parent gas:

$$\alpha_{\text{N-CRR}} = 8\pi \frac{m_e}{M_{\text{atom}}} R_0 R_e^2 \left(\frac{8k_B T_e}{\pi m_e}\right)^{1/2} \sigma_{e,\text{atom}} n_{\text{atom}}. \quad (5)$$

Here, k_B is the Boltzmann constant, m_e and M_{atom} denote the masses of the electron and gas atoms (e.g., helium), $\sigma_{e,\text{atom}}$ is the electron-atom momentum transfer cross section, and $R_e = e^2/k_B T_e (=5.6 \times 10^{-6}$ cm at 300 K). R_0 is a "trapping radius," the assumption being made that electrons that collide with an atom inside this radius recombines with unit probability, while those colliding outside that radius will escape recombination. If R_0 is taken as $2R_e/3$, the recombination coefficient decreases with temperature as $T_e^{-2.5}$ and agrees with the energy-diffusion model of Pitaevskii [12].

The more elaborate theory of Bates and Khare [4], in which recombination proceeds by stepwise collisional deexcitation of excited Rydberg states of the ion, yields nearly identical recombination coefficients (for He^+ in He) at temperatures below 125 K, but lower values (by approximately a factor of 2) at 300 K. Much larger values ($\sim 10^{26}$ cm^6 s^{-1} at 300 K) have been calculated by Whitten *et al.* [15], but, as has been pointed out by Wojcik and Tachiya [13,14], the results of Whitten *et al.* depend sensitively on several assumptions, for instance, that the Rydberg populations of states with binding energies less than $4k_B T$ are in thermal equilibrium.

It is not quite clear how the theoretical results should be modified when the ions and neutrals have different masses, the case of interest in our experiments. Bates and Khare [4] suggest that the recombination rate at low temperatures and densities is approximately proportional to the reciprocal of the ion-atom reduced mass, i.e., that the mass M_{atom} in Eq. (5) should be replaced by $2M_{\text{red}}$, where M_{red} is the reduced mass of the ion and gas atoms. If one adopts that rule, the recombination of Ar^+ ions in helium should be slower by a factor of 0.54 than that for He^+ in helium. This scaling agrees with the conclusion of Wojcik and Tachiya [13,14] that the energy-diffusion model for heavy ions yields smaller rates by a factor of 2 than for ions of the same mass as the gas atoms.

In the case of recombination of atomic argon ions in ambient helium of density [He] Eq. (5) reduces to

$$\alpha_{\text{He-CRR}}(T_e) = 1.2 \times 10^{-27} (T_e/300)^{-2.5} [\text{He}]\ \text{cm}^3\ \text{s}^{-1}. \quad (6)$$

The momentum transfer cross section for electron-helium collisions was taken as 5.4×10^{-16} cm^2 [16], independent of energy.

The ternary rate coefficient $K_{\text{He-CRR}}$ is obtained by dividing $\alpha_{\text{He-CRR}}$ by the helium number density:

$$K_{\text{He-CRR}} = \alpha_{\text{He-CRR}}/[\text{He}]\ \text{cm}^6\ \text{s}^{-1}. \quad (7)$$

Experimental data on ternary neutral-assisted recombination N-CRR at temperatures $\geqslant$300 K have mostly confirmed theoretical predictions [3,4], including the expected $T^{-2.5}$ temperature dependence. Deloche *et al.* [17] found similar coefficients for both atomic and molecular ions. The only experimental measurements at low temperatures (77–150 K) by Cao and Johnsen [18] yielded rate coefficients close to those expected for atomic ions, even though the ions were most likely simple diatomic ions (N_2^+,O_2^+,NO^+). On the other hand, our recent low-temperature studies of recombination of H_3^+ and D_3^+ ions, summarized in [9,10,19–23], gave much faster ternary He-assisted recombination with rate coefficients $K_{\text{He-CRR}}(300\ \text{K}) > 10^{-25}$ cm^6 s^{-1}, indicating that ternary recombination of H_3^+ and D_3^+ ions can also proceed by dissociation of long-lived intermediate rotationally excited H_3^* and D_3^* Rydberg molecules.

In this paper, after describing the Cryo-FALP II apparatus, methods of data analysis, and test measurements on O_2^+ ions, we will discuss the determination of the electron temperature in the afterglow plasma by monitoring the decay of the electron density due to ambipolar diffusion. Finally we will present new data on ternary electron- and helium-assisted recombination of Ar^+ at temperatures down to 50 K.

II. EXPERIMENTS

A. Experimental apparatus

The recombination measurements described here were carried out in a decaying fast-flowing plasma, created by passing helium gas through a continuous microwave discharge and converting the primary active particles (mainly helium metastables) to argon ions by adding argon through a gas inlet downstream from the discharge. When the decay of the electron density is monitored by a Langmuir probe, a thin tungsten wire, the technique is referred to as the flowing afterglow Langmuir probe (FALP) method. Afterglow optical emissions from the decaying plasma, for instance, argon emission lines resulting from recombination, are present but were not analyzed in these experiments. While the FALP method has been used extensively to study recombination in decaying plasmas, the extension to very low temperatures required construction of the Cryo-FALP II apparatus to be described below. Also, additional efforts are needed to characterize the thermal properties of the plasma.

We note in passing that it might have been simpler to construct a cryogenic pulsed "stationary afterglow." However, the FALP arrangement offers better control of plasma parameters and avoids exposing all reagent gases directly to an intense discharge, which can lead to undesired excitation of atomic or molecular species.

In the Cryo-FALP II apparatus (see Fig. 1) the reaction section of the flow tube can be cooled down to 40 K and recombination processes can be studied down to 50 K. Effective binary recombination rate coefficients above 1×10^{-8} cm^3 s^{-1} can be reliably measured. A very broad range of helium pressures and partial pressures of reactant gases

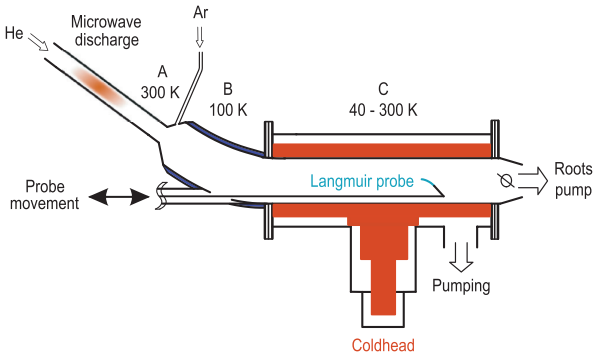

FIG. 1. (Color online) Simplified diagram of the Cryo-FALP II apparatus (not to scale). The three sections A, B, and C have temperatures of 300, 100, and 40–300 K, respectively. The axially movable Langmuir probe measures the decaying electron density along the section C of the flow tube.

can be covered which enables accurate measurements of rate coefficients of binary and ternary recombination processes. Using Cryo-FALP II we recently studied E-CRR of Ar^+ at temperatures 57–200 K and at electron number densities $n_e \sim 10^9 - 10^{10}$ cm^{-3} [6,7] and we found good agreement with theoretical predictions (see, e.g., [2]). At those electron densities E-CRR of Ar^+ was the dominant loss process during the afterglow. The present work focuses mainly on He-assisted ternary recombination (He-CRR) of Ar^+ ions at very low temperatures and lower electron densities. However, the relative contributions of E-CRR and He-CRR are often of similar magnitude and the data analysis (see Sec. II B) necessarily involves both processes.

A detailed description of the FALP technique can be found in the papers by Mahdavi [24] and by Smith [25] and in the book by Larsson and Orel [1]. The high-pressure version of the FALP and Langmuir probe technique is described in [26]. A short description of Cryo-FALP II is also given in Refs. [7,22,23].

The flow tube of Cryo-FALP II has three sections A, B, and C with different temperatures. The internal diameter of the flow tube is ∼5 cm and the length is ∼80 cm. Helium buffer gas flows through the glass section (A, 300 K) where it is partially ionized in a microwave discharge (2.45 GHz, power of 10–30 W). Downstream from the discharge the plasma contains mainly helium metastables (He^m), He^+ ions, and electrons. At high helium densities ([He] $\sim (1-25) \times 10^{17}$ cm^{-3}) most He^+ ions are converted by ternary association to He_2^+. The addition of Ar gas ([Ar] $\sim (0.01-10) \times 10^{14}$ cm^{-3}) further downstream from the discharge region at the beginning of the stainless steel section B of the flow tube converts the He_2^+ ions by charge transfer reaction to Ar^+ ions. The metastables He^m are converted to Ar^+ ions by Penning ionization [27,28]. The Ar^+-dominated plasma is carried along the section B of the flow tube that is cooled to ∼100 K by liquid nitrogen. In sections A and B at temperatures above 100 K the recombination of He_2^+ and Ar^+ ions is very slow and the plasma decay is caused mainly by ambipolar diffusion to the walls of the flow tube.

After precooling in section B the plasma enters section C, made from stainless steel. This section is connected to the cold head (Sumitomo CH-110) by copper braids, and temperatures of the flow tube wall in the range of 40–300 K can be achieved. To obtain good thermal insulation the whole section C and the cold head are placed in another vacuum chamber. Calculations showed that the buffer gas temperature T_{He} in section C is equal to the wall temperature T_W of the flow tube, and that the ion and electron temperatures (T_{ion} and T_e, respectively) in the afterglow are equal to that of the buffer gas, i.e., $T_{ion} = T_e = T_{He} = T_W$. The temperature distribution along the flow tube and the resulting temperature of the He buffer gas was calculated by a computer model (see [7]). The calculated relaxation time constant for the electron temperature is <0.1 ms, i.e., electron temperature relaxes to the buffer gas temperature immediately after removal of the He metastables (see [26,29]). We verified the electron thermalization by analyzing characteristic times of ambipolar diffusion (see Sec. II D). The results supported the assumption $T_W = T_e$. The ion thermalization is many times faster (with time constant < 0.1 μs) because the masses of ions are similar to those of the neutral atoms. This was also confirmed by spectroscopic measurements in H_3^+- and D_3^+-dominated plasma at otherwise very similar conditions (see [8–10]). In the following we will refer to the kinetic temperatures simply as T without subscripts.

The gas handling system and the flow tube itself employ UHV technology and high-purity He and Ar are used. Helium is further purified by passing it through two in-line liquid-nitrogen-cooled molecular sieve traps, resulting in an estimated level of impurities of the order of 10^{-2} ppm. A throttle valve at the downstream end of the flow tube (prior to the Roots pump) adjusts the working pressure and the flow velocity of the buffer gas to the desired values.

The recombination measurements, carried out in section C of the flow tube, rely on the electron density decays as determined by an axially movable Langmuir probe (length 7 mm, diameter 18 μm). To convert positions in the flow tube to afterglow time, the plasma velocity is needed. It is measured by modulating the discharge and observing the time of the Langmuir probe response at certain positions on the flow tube axis. The plasma velocities range from 1 to 20 m s^{-1}, depending on pressure, helium flow rate, and on the flow tube temperature (see Fig. 2 in [7]). The plasma velocity is not constant along the whole flow tube because the wall temperature is different in different sections.

The Langmuir probe characteristics are measured point by point along the flow tube, and the actual values of the electron densities are obtained from the saturated electron current to the probe at positive probe potential [30,31]. The reliability of Langmuir probes used in this mode has been established many times, e.g., by comparing recombination rate coefficients obtained with laser absorption spectroscopy (CRDS technique [32]) to those obtained with Langmuir probes [8–10] or by measuring recombination rate coefficients of well-known recombination processes, e.g., dissociative recombination of O_2^+ ions with electrons (see Sec. II C).

To establish optimal conditions for the measurements of the ternary rate coefficients we developed a kinetic model which includes all significant processes taking place during the

afterglow [33,34]. The temperature evolution along the flow tube was explicitly taken into the account. The calculations show that Ar^+ is the dominant ion at the beginning of the section C, and that the plasma is completely thermalized at that position.

B. Data analysis and conditions of measurement

In a quasineutral afterglow plasma, dominated by a single ion species A^+ in ambient helium gas, the loss rate of electrons and ions is given by

$$\frac{dn_e}{dt} = \frac{d[A^+]}{dt} = -\alpha_{\text{bin}}[A^+]n_e - K_{\text{He-CRR}}[\text{He}][A^+]n_e - K_{\text{E-CRR}}[A^+]n_e^2 - \frac{n_e}{\tau_{\text{D}}} - \frac{n_e}{\tau_{\text{R}}}, \quad (8)$$

where α_{bin} is the rate coefficient of binary recombination (e.g., DR) and τ_{D} is the time constant of ambipolar diffusion. The additional term containing time constant τ_{R} accounts for a loss due to possible reactions (for details see Sec. II D). By combining the recombination terms into an effective binary rate coefficient α_{eff} and combining the diffusion and reaction loss terms into a linear loss term characterized by a time constant τ_{L} one obtains

$$\frac{dn_e}{dt} = \frac{d[A^+]}{dt} = -\alpha_{\text{eff}}n_e^2 - \frac{n_e}{\tau_{\text{L}}}, \quad (9)$$

where

$$\alpha_{\text{eff}}(T,[\text{He}],n_e) = \alpha_{\text{bin}} + K_{\text{He-CRR}}[\text{He}] + K_{\text{E-CRR}}n_e \quad (10)$$

and

$$\frac{1}{\tau_{\text{L}}} = \frac{1}{\tau_{\text{D}}} + \frac{1}{\tau_{\text{R}}}. \quad (11)$$

We note that a linear addition of the contributions of He-CRR and E-CRR in Eq. (8) is not necessarily correct, as Bates pointed out [35], since both processes can partly compete for the populations of the same energy levels. Hence, we regard Eq. (10) as a first (linear) approximation that is valid only in the limit when a small fraction of the intermediate levels is stabilized by collision with electrons or neutrals. We will discuss this again in Sec. IV.

The effective binary recombination rate coefficients for ternary processes depend on electron and neutral density. For atomic Ar^+ ions purely binary recombination can be neglected so that the overall effective (measured) binary rate coefficient can be taken as $\alpha_{\text{eff}} = \alpha_{\text{E-CRR}} + \alpha_{\text{He-CRR}} = K_{\text{E-CRR}}n_e + K_{\text{He-CRR}}[\text{He}]$. Different experimental conditions must be chosen to separate the two contributions: To determine $K_{\text{E-CRR}}$, n_e should be large but [He] should be small. On the other hand, to determine $K_{\text{He-CRR}}$, [He] should be as high as possible, while n_e should be small. Figure 2 shows decay curves measured at a temperature of 60 K for two different sets of parameters. For the decay curve (i) [He] was minimized and n_e maximized, so that E-CRR dominates. For the decay curve (ii) [He] was maximized and n_e minimized, so that He-CRR dominates. The temperature distribution model showed that for both data sets in Fig. 2 the temperature in the recombining plasma is relaxed to 60 ± 2 K. This was confirmed by measuring the plasma velocity along the flow tube [7].

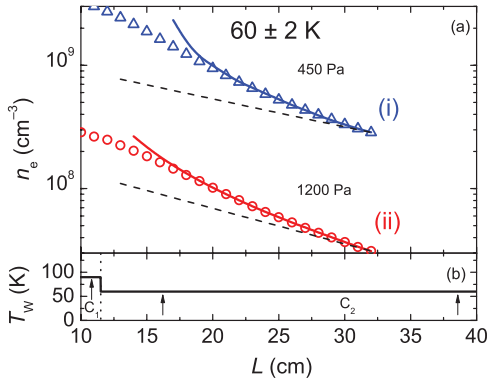

FIG. 2. (Color online) (a) Measured electron density decay in an Ar^+-dominated afterglow plasma for two helium pressures, 450 (open triangles) and 1200 Pa (open circles). Symbols show measured data, full lines represent fits of these data, and dashed lines indicate diffusion losses. The effective recombination rate coefficients at 1200 and 450 Pa are 1.0×10^{-7} and 3.3×10^{-8} cm^3 s^{-1}, respectively. (b) Measured temperatures of the flow tube wall (T_W) at the positions of the temperature sensors (indicated by arrows). Section C is divided into two subsections C_1 and C_2 in the figure indicating different measured temperature.

In a low-temperature Ar^+-dominated plasma in He buffer gas with a small admixture of Ar gas the reactive loss term in Eq. (8) accounts for the relatively slow ternary association of Ar^+ with atomic argon, i.e., the reaction $Ar^+ + Ar + He \longrightarrow Ar_2^+ + He$ [36,37]. Since the Ar_2^+ product ions recombine rapidly with electrons [1,38], the rate determining step at low argon concentrations is ternary association. The association reaction essentially constitutes an additional electron loss process that can be represented by a time constant τ_{R} as written in Eq. (8). In this particular case, τ_{R} depends on the ternary association rate coefficient k_{a} and on Ar and He densities, $\tau_{\text{R}} = 1/(k_{\text{a}}[\text{Ar}][\text{He}])$. The temperature dependence of τ_{R} is given by the temperature dependence of k_{a} (details will be discussed below). At higher Ar and He densities and lower temperatures the formation of Ar_2^+ is faster and the recombination of Ar_2^+ is the rate determining process. The effect of Ar_2^+ ions on observed effective binary recombination (on α_{eff}) was determined by measuring the effective binary recombination rate coefficient as a function of argon density. Examples of such dependencies are plotted in Fig. 3 for 62 K and He pressure 500 and 1200 Pa. The measured effective binary recombination rate coefficients are constant below $[\text{Ar}] = 1 \times 10^{13}$ cm^{-3} but increase above this value, in accordance with our kinetics model that includes the formation of Ar_2^+. To minimize the influence of Ar_2^+ formation on the measured α_{eff} the typical number density of Ar used in the present experiment was limited to $[\text{Ar}] \sim 3 \times 10^{12}$ cm^{-3}, which is still sufficient to form an Ar^+-dominated plasma before entering zone C of the flow tube. The final data were taken under conditions where the effect of Ar_2^+ on measured α_{eff} was negligible.

Figure 4 shows data for α_{eff} as a function of helium density [He] for three different temperatures. The slopes of the linear dependencies yield $K_{\text{He-CRR}}(T)$ [see Eq. (10)], and the

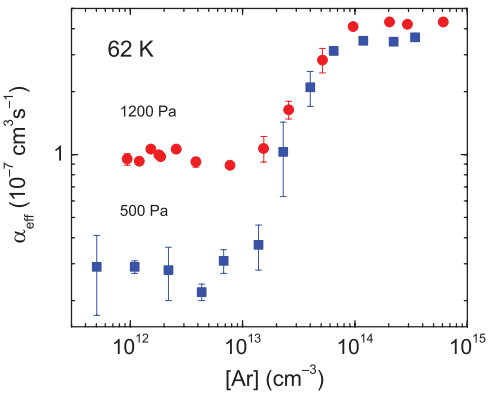

FIG. 3. (Color online) The dependence of measured effective binary recombination rate coefficient $\alpha_{\rm eff}$ on Ar number density at 62 K and indicated pressures of He (full circles for the pressure of 1200 Pa and full squares for 500 Pa). Displayed errors are statistical.

intercept at [He] = 0 gives the sum $\alpha_{\rm bin} + K_{\rm E\text{-}CRR} n_e$. Since previous work [6] has shown that $\alpha_{\rm bin} = 0$ (see Fig. 4 and discussion in [6]), we can write $\alpha_{\rm eff} = K_{\rm E\text{-}CRR} n_e$ at [He] = 0. This is in agreement with the expectation of slow radiative recombination of atomic Ar^+.

C. Test measurements on recombination of O_2^+ ions

Some of the present studies were conducted under conditions (helium densities, temperatures, flow velocities, etc.) that have not been used much in earlier work. Also, the data analysis relies on modeling of the temperature distribution and flow velocities. As a precaution, we performed a series of test measurements of the well-known binary recombination rate coefficient of dissociative recombination $\alpha_{\rm bin\ DR}$ of O_2^+ ions, which is much simpler to measure than ternary recombination. Our test results (see Fig. 5) agreed very well with previous data [39–45]. The rate coefficients were measured for three temperatures and over a broad range of He pressures and O_2 number densities. The results of these tests clearly confirm the validity of the methods used in present experiments.

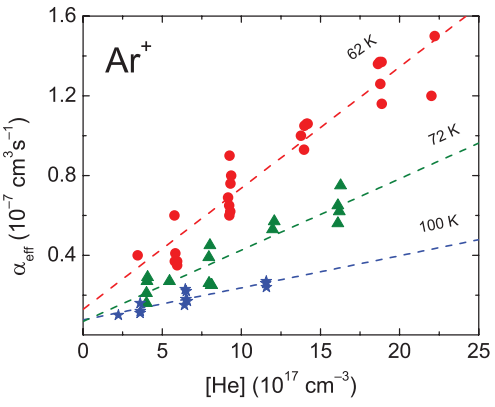

FIG. 4. (Color online) Measured dependence of the effective binary recombination rate coefficient $\alpha_{\rm eff}(T,[{\rm He}],n_e)$ of recombination of Ar^+ ions with electrons on He number density at 62 (full circles), 72 (full triangles), and 100 K (full stars). The lines represent the linear fits of the data.

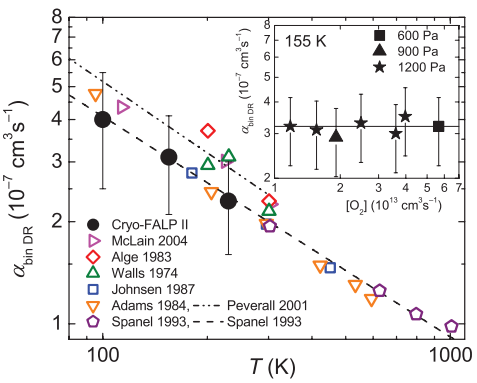

FIG. 5. (Color online) Temperature dependence of the measured recombination rate coefficient $\alpha_{\rm bin\ DR}$ of the binary dissociative recombination of O_2^+ ions with electrons. The present Cryo-FALP II data (large circles) are compared to previous results [39–45]. The dashed line represents a fit given by [43,45]. Inset: Data obtained at different O_2 number densities, measured at 155 K and at several helium pressures. The full line is the mean of the measured values.

D. Verification of the electron temperature by measuring ambipolar diffusion losses

The strong temperature dependencies of $K_{\rm E\text{-}CRR}$ and $K_{\rm He\text{-}CRR}$ make the electron temperature a crucial parameter that is not directly measured, but within some limitations a precise measurement of ambipolar diffusion losses in the late afterglow can serve as a "diffusion thermometer." Ambipolar diffusion losses also enter directly [see Eq. (8)] in the determinations of $\alpha_{\rm eff}$ and $\tau_{\rm L}$. The measured time constant $\tau_{\rm L}$ has two components: one representing ambipolar diffusion ($\tau_{\rm D}$) and the second representing reactive losses ($\tau_{\rm R}$) (see Sec. II B). The value of $\tau_{\rm D}$ depends on temperature, helium density, the characteristic diffusion length Λ of the flow tube, and the zero-field reduced mobility K_0 of Ar^+ ions in He (for details see [6]). For a long flow tube of radius R the characteristic diffusion length is $\Lambda = R/2.405$. Using the relations given by Mason and McDaniel [46] one can show that if electrons, ions, and gas atoms have the same temperature $T_e = T_{\rm ion} = T_{\rm He} = T$ then

$$\frac{1}{\tau_{\rm D}} = 4.63 \times 10^{15} \frac{K_0(T)}{\Lambda^2} \frac{T}{[{\rm He}]}\ {\rm s}^{-1}. \qquad (12)$$

The units are [He] in cm^{-3}, T in K, Λ in cm, and K_0 in cm^2 V^{-1} s^{-1}. Since the zero-field reduced mobility of Ar^+ in He is nearly constant for temperatures below 300 K, a graph of $[{\rm He}]/\tau_{\rm D}$ versus T should yield nearly a straight line, with small deviations when the dependence of K_0 on temperature is included [6]. Measured values of $[{\rm He}]/\tau_{\rm D}$ should be proportional to the temperature thus providing an independent measure of the otherwise difficult to determine electron temperature. Figure 6 shows the theoretical temperature dependence of $[{\rm He}]/\tau_{\rm D}$, where $\tau_{\rm D}$ is calculated using zero-field reduced mobilities of $K_0 = 18.9$ cm^2 V^{-1} s^{-1}

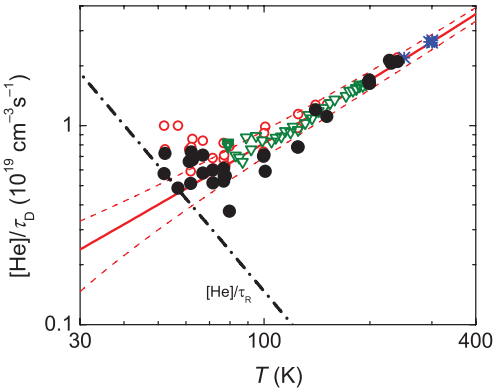

FIG. 6. (Color online) Temperature dependencies of the inverted time constants of diffusion losses $[He]/\tau_D$ and $[He]/\tau_R$. Solid line represents the theoretical temperature dependence of $[He]/\tau_D$ on T, calculated from the zero-field reduced mobility of Ar^+ in He for a thermalized afterglow plasma [47–49]. Dashed lines are calculated for 10 K higher or lower temperatures. The dash-dotted line labeled $[He]/\tau_R$ shows values corresponding to reactive losses due to Ar_2^+ formation at densities $[Ar] = 3 \times 10^{12}$ cm^{-3} and $[He] = 7 \times 10^{17}$ cm^{-3} (see text). In the calculation we used the formula $[He]/\tau_R = k_a[Ar][He]^2 = 9.5 \times 10^{-32}(300/T)^{2.19}[Ar][He]^2$. Data measured with Cryo-FALP I (open triangles) are adapted from [6] as well as data indicated by asterisk symbols measured at 250 and 300 K. Open circles indicate measured $[He]/\tau_L$ and closed circles indicate corresponding experimental $[He]/\tau_D$ calculated for particular [He] and [Ar] using relation $[He]/\tau_D = ([He]/\tau_L - [He]/\tau_R)$.

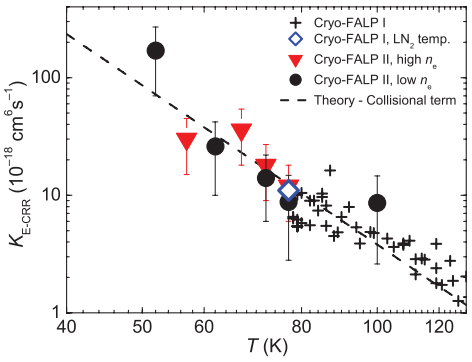

FIG. 7. (Color online) Temperature dependence of the measured ternary recombination rate coefficient $K_{E\text{-}CRR}$ of ternary electron-assisted collisional radiative recombination of Ar^+ ions with electrons. The full circles are the present data measured at lower $n_e(10^8-10^9$ cm$^{-3})$. The data represented by full triangles are measured in our previous studies at higher $n_e(10^9-10^{10}$ cm$^{-3})$ [7]. Data depicted by the open rhomboid at 77 K is compiled from several measurements on Cryo-FALP I. The crosses indicate previous data measured on Cryo-FALP I at temperatures above 77 K (adopted from [6]). The dashed line indicates $K_{E\text{-}CRR}$ calculated by using Stevefelt's formula (4), $K_{E\text{-}CRR} \sim T^{-4.5}$.

at 77 K and 20.5 cm^2 V^{-1} s^{-1} at 300 K [47–49] and a linear interpolation at intermediate temperatures.

To show the sensitivity to small errors in temperature, we also include in Fig. 6 calculated values of $[He]/\tau_D$ for two temperatures that are 10 K higher or lower. As may be seen in Fig. 6, the accuracy of the "diffusion thermometer" deteriorates rapidly below ~70 K because the experimental values $[He]/\tau_L$ include a contribution $[He]/\tau_R$ due to reactive losses in the late afterglow [see Eq. (11)]. We tried to correct the raw "experimental" values $[He]/\tau_L$ (open circles) by subtracting an estimated reactive loss term $[He]/\tau_R$ to obtain the pure diffusion loss rate term $[He]/\tau_D$ (solid circles). The reactive loss term $[He]/\tau_R$ was ascribed to conversion of Ar^+ ions to fast recombining Ar_2^+ ions, using the experimental association ternary rate coefficient k_a of Bohme *et al.* [36] and extrapolating it assuming a temperature dependence of the form $k_a \sim T^{-n}$. From the measured values $k_a(82\text{ K}) = 1.6 \times 10^{-30}$ cm^6 s^{-1} and $k_a(290\text{ K}) = 1 \times 10^{-31}$ cm^6 s^{-1} we calculated $k_a(T) = 9.5 \times 10^{-32}(300/T)^{2.19}$ cm^6 s^{-1}. The size of this correction is included in Fig. 6 (dash-dotted line), the values were calculated for $[Ar] = 3 \times 10^{12}$ cm^{-3} and $[He] = 7 \times 10^{17}$ cm^{-3}. Since the reactive losses increase rapidly at lower temperatures, while the diffusion losses become smaller, the accuracy of the diffusion thermometer becomes poor below 70 K and corrections for reactive losses do not improve it by much. For comparison, in Fig. 6 we also show data from our previous FALP and Cryo-FALP I experiments measured at 250 and 300 K [6]. In that case the whole flow tube was cooled by liquid nitrogen to the same temperature and there was no doubt about temperature equilibration.

The measurements of the diffusion losses corroborate our calculations of the temperature distribution in the flow tube only for temperatures above ~70 K. Nevertheless, this does not necessarily imply a difference between T_W, T_e, and T_{ion} below 70 K. The agreement between experimental data on the rate coefficients for E-CRR and N-CRR and theory (see Secs. III A and III B) also supports the assumption of complete thermalization.

III. RESULTS AND DISCUSSION

A. Temperature dependence of $K_{E\text{-}CRR}$

Figure 7 shows the temperature dependence of $K_{E\text{-}CRR}$ obtained in the present experiment and compares it to previous data measured with the Cryo-FALP I apparatus in the range 77–200 K [6], to previous data measured with the Cryo-FALP II apparatus in the range 57–77 K [7], and to theoretical dependence. The agreement between the experimental data sets is good, even though the electron density n_e in the earlier experiments was much higher $(10^9-10^{10}$ cm$^{-3})$ than in the present experiment $(10^8-10^9$ cm$^{-3})$ and experimental conditions were different. In the present study $K_{E\text{-}CRR}$ was obtained by extrapolation of α_{eff} to zero helium density, as shown in Fig. 4. The present and previous data agree well with the collisional term of the Stevefelt formula [see Eq. (4)], leaving no doubt that the $K_{E\text{-}CRR} \sim T^{-4.5}$ dependence remains valid for Ar^+ ions down to 50 K.

The agreement of the experimental values of $K_{E\text{-}CRR}$ with theory can be taken also as another confirmation that the electron temperature and the measured temperature of the wall of the flow tube are nearly equal. Note also the good agreement

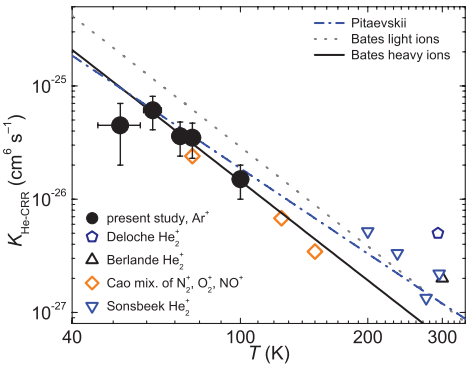

FIG. 8. (Color online) Temperature dependence of the measured ternary recombination rate coefficient $K_{\text{He-CRR}}$ of He-assisted recombination of Ar^+ ions with electrons (full circles). Included are also data from previous experiments [17,18,50,51]. The dotted line follows calculation by Bates [4]; the solid line is scaled for this study using the dependence of the ternary recombination rate coefficient on reduced mass as suggested by Bates [4]. The dash-dotted line indicates theory by Pitaevskii [12].

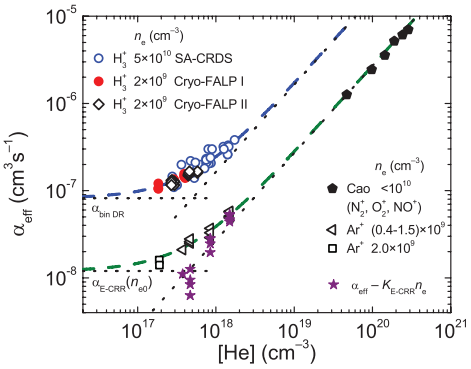

FIG. 9. (Color online) Dependence of the effective recombination rate coefficient α_{eff} on helium number density at 77 K. Present values (open triangles) are plotted together with values obtained by Cao *et al.* [18] (full pentagons) for a mixture of ions, by Varju *et al.* [8], by Dohnal *et al.* [9], and by Glosik *et al.* [19] for H_3^+ and by Kotrik *et al.* [6] for Ar^+ (open squares). The full stars are the present data corrected by subtracting the E-CRR component of α_{eff}. The dashed lines are linear fits to the data (values by Cao were not included in the fit). The dotted lines show the binary and the ternary components of the fitted α_{eff}.

of data obtained at 77 K at very different experimental conditions (it will be again discussed in Sec. IV).

B. Temperature dependence of $K_{\text{He-CRR}}$

The measured temperature dependence of $K_{\text{He-CRR}}$ of ternary recombination of Ar^+ ions with electrons in helium buffer is depicted in Fig. 8, together with examples of data measured in previous experiments with different ions at higher temperatures, predominantly at 300 K [17,18,50,51]. Our data for Ar^+ ions agree well with the calculations of Bates [4] after scaling by the reduced mass factor. The temperature dependence (approximately $T^{-2.9}$) is somewhat stronger than the $T^{-2.5}$ dependence of Pitaevskii [12], presumably because the energy diffusion model of Pitaevskii ignores the discreteness of the electron energy states.

IV. DISCUSSION AND CONCLUSIONS

We have reported on He-assisted ternary recombination of atomic ions below 300 K and rate coefficients of both ternary recombination processes were clearly separated and measured in a well-characterized afterglow plasma at temperatures below 100 K. Careful attention was paid to verifying electron temperatures by measuring the characteristic time constant of ambipolar diffusion τ_D at fixed pressure and flow tube temperature. It was concluded that the plasma particles have nearly the same temperature as the wall of the flow tube, i.e., that $T = T_e = T_{\text{ion}} = T_{\text{He}} = T_W$. However, at the lowest temperatures the verification was complicated by reactive losses.

The measured magnitudes and the temperature dependencies of both ternary recombination rate coefficients $K_{\text{He-CRR}}$ and $K_{\text{E-CRR}}$ of Ar^+ ions agree with theoretical predictions [3,4,12] ($K_{\text{He-CRR}} \sim T^{-2.9}$) in the temperature range from 50 to 100 K and $K_{\text{E-CRR}} \sim T^{-4.5}$ in the range from 50 to 180 K [2] over a broad range of electron and He densities. This observed agreement is not at all obvious. Recent experimental studies of both ternary recombination processes for H_3^+ and D_3^+ ions at temperatures below 300 K gave drastically different results [9,10,22,23], as is demonstrated in Fig. 9 that summarizes the effective binary recombination rate coefficients α_{eff} measured at 77 K in helium afterglow plasmas dominated by different ions. The data obtained by Cao *et al.* [18] for a mixture of molecular ions at very high helium densities are in agreement with the aforementioned results, giving comparable ternary rate coefficients. At their experimental conditions the ternary E-CRR and the binary dissociative recombination can be neglected and He-CRR is by far the dominant recombination process.

The figure also shows data obtained for atomic Ar^+ ions in the present experiments for electron densities $n_e = (0.4-1.5) \times 10^9$ cm^{-3} and He densities $[\text{He}] = (5-20) \times 10^{17}$ cm^{-3}. Some earlier data measured at high n_e and low [He] [6] are also plotted. For atomic Ar^+ ions binary recombination is negligible and both ternary processes He-CRR and E-CRR have comparable rates. The overall rate coefficients can be expressed as $\alpha_{\text{eff}} = \alpha_{\text{He-CRR}} + \alpha_{\text{E-CRR}} = K_{\text{He-CRR}}[\text{He}] + K_{\text{E-CRR}} n_e$. At high [He] and low n_e (triangles) $\alpha_{\text{He-CRR}}$ dominates, while at low [He] and high n_e (open squares) $\alpha_{\text{E-CRR}}$ dominates. The fit of the Ar^+ data gives values $K_{\text{He-CRR}}$ and $K_{\text{E-CRR}}$ in agreement with those obtained by precise analyses (see Figs. 7 and 8). At low [He] the data (triangles) level off due to the contribution from $\alpha_{\text{E-CRR}}$, indicated by a horizontal dashed line (calculated for $n_e = 1 \times 10^9$ cm^{-3}). To show the contribution from $K_{\text{He-CRR}}$ alone we plotted the values $\alpha_{\text{He-CRR}}$ (indicated by full stars) obtained by subtracting $\alpha_{\text{E-CRR}}$ from the measured α_{eff}. We used expression (4) for $\alpha_{\text{E-CRR}}$ and the actual n_e. Note that the corrected data $\alpha_{\text{He-CRR}}$ (stars) and data obtained by Cao *et al.* [18] (pentagons) then follow a straight line $\alpha_{\text{He-CRR}} = K_{\text{He-CRR}}[\text{He}]$ over three orders of magnitude of [He].

The sample of data (upper set of data) obtained in H_3^+-dominated He buffered afterglow plasma are significantly larger. These data were obtained at electron densities from 2×10^9 up to 5×10^{10} cm^{-3} in Cryo-FALP I, Cryo-FALP II, and SA-CRDS experiments [8,9,19]. We did not observe any significant dependence of α_{eff} on n_e that would indicate electron-assisted recombination (see discussion in [9,10,22,23]), so we can expect $\alpha_{\text{eff}} = \alpha_{\text{bin DR}} + \alpha_{\text{He}} = \alpha_{\text{bin DR}} + K_{\text{He}}[\text{He}]$, where $\alpha_{\text{bin DR}}$ is the binary rate coefficient of dissociative recombination of H_3^+ and K_{He} ternary rate coefficients of helium-assisted recombination of H_3^+. The seeming absence of electron-assisted recombination is surprising (see discussion in [9,10]).

Figure 9 strongly suggests that the mechanisms of the ternary helium-assisted processes for Ar^+ and H_3^+ (D_3^+) must be very different. The rate coefficients at low [He] are also different. They reflect dissociative recombination in the case of H_3^+ ($\alpha_{\text{bin DR}}$) and ternary electron-assisted recombination ($\alpha_{\text{E-CRR}}$) in the case of Ar^+.

The present study was, in part, undertaken to learn whether our earlier measurements of the ternary recombination rate coefficients of H_3^+ and D_3^+ [9,10,19,20,23,52] were subject to possible systematic errors. This does not seem to be the case. The good agreement of the helium-assisted ternary channel for Ar^+ with theory [4] strongly corroborates the methods used in the earlier work. We conclude that the very fast helium-assisted ternary recombination of H_3^+ and D_3^+ ions must be due to an entirely different mechanism than that proposed for atomic ions by Bates and Khare [4] and Flannery [3]; for discussion and suggestion of the mechanism see [9,19–21].

The presented experimental results on the ternary electron- and neutral-assisted recombination of atomic Ar^+ ions at temperatures down to 50 K show a remarkable difference in comparison with ternary recombination of H_3^+ and D_3^+ ions. To find differences between ternary recombination of atomic and molecular ions and a possible dependence on type of buffer gas we plan to study ternary recombination of other ions and temperature dependence of recombination processes at temperatures down to 30 K.

ACKNOWLEDGMENTS

This work was partly supported by GACR 205/09/1183, GACR P209/12/0233, SV 267 302, GAUK 353811, GAUK 388811, and GAUK 659112.

[1] M. Larsson and A. Orel, *Dissociative Recombination of Molecular Ions* (Cambridge University Press, Cambridge, 2008).
[2] J. Stevefelt, J. Boulmer, and J. Delpech, Phys. Rev. A **12**, 1246 (1975).
[3] M. R. Flannery, J. Chem. Phys. **95**, 8205 (1991).
[4] D. Bates and S. Khare, Proc. Phys. Soc. London **85**, 231 (1965).
[5] T. Pohl, D. Vrinceanu, and H. R. Sadeghpour, Phys. Rev. Lett. **100**, 223201 (2008).
[6] T. Kotrik, P. Dohnal, S. Roucka, P. Jusko, R. Plasil, J. Glosik, and R. Johnsen, Phys. Rev. A **83**, 032720 (2011).
[7] T. Kotrik, P. Dohnal, P. Rubovic, R. Plasil, S. Roucka, S. Opanasiuk, and J. Glosik, Eur. Phys. J. Appl. Phys. **56**, 24011 (2011).
[8] J. Varju, M. Hejduk, P. Dohnal, M. Jilek, T. Kotrik, R. Plasil, D. Gerlich, and J. Glosik, Phys. Rev. Lett. **106**, 203201 (2011).
[9] P. Dohnal, M. Hejduk, J. Varju, P. Rubovic, S. Roucka, T. Kotrik, R. Plasil, J. Glosik, and R. Johnsen, J. Chem. Phys. **136**, 244304 (2012).
[10] P. Dohnal, M. Hejduk, P. Rubovic, J. Varju, S. Roucka, R. Plasil, and J. Glosik, J. Chem. Phys. **137**, 194320 (2012).
[11] T. C. Killian, S. Kulin, S. D. Bergeson, L. A. Orozco, C. Orzel, and S. L. Rolston, Phys. Rev. Lett. **83**, 4776 (1999).
[12] L. P. Pitaevskii, Sov. Phys. JETP **1**, 919 (1962).
[13] M. Wojcik and M. Tachiya, J. Chem. Phys. **110**, 10016 (1999).
[14] M. Wojcik and M. Tachiya, J. Chem. Phys. **112**, 3845 (2000).
[15] B. L. Whitten, L. W. Downes, and W. E. Wells, J. Appl. Phys. **52**, 1255 (1981).
[16] R. W. Crompton, M. T. Elford, and R. L. Jory, Aust. J. Phys. **20**, 396 (1967).
[17] R. Deloche, P. Monchicourt, M. Cheret, and F. Lambert, Phys. Rev. A **13**, 1140 (1976).
[18] Y. S. Cao and R. Johnsen, J. Chem. Phys. **94**, 5443 (1991).
[19] J. Glosik, R. Plasil, I. Korolov, T. Kotrik, O. Novotny, P. Hlavenka, P. Dohnal, J. Varju, V. Kokoouline, and C. H. Greene, Phys. Rev. A **79**, 052707 (2009).
[20] J. Glosik, I. Korolov, R. Plasil, T. Kotrik, P. Dohnal, O. Novotny, J. Varju, S. Roucka, C. H. Greene, and V. Kokoouline, Phys. Rev. A **80**, 042706 (2009).
[21] J. Glosik, R. Plasil, T. Kotrik, P. Dohnal, J. Varju, M. Hejduk, I. Korlov, S. Roucka, and V. Kokoouline, Mol. Phys. **108**, 2253 (2010).
[22] P. Rubovič, P. Dohnal, M. Hejduk, R. Plašil, and J. Glosík, J. Phys. Chem. A (2013), doi: 10.1021/jp3123192.
[23] R. Johnsen, P. Rubovič, P. Dohnal, M. Hejduk, R. Plasil, and J. Glosík, J. Phys. Chem. A (2013), doi: 10.1021/jp311978n.
[24] M. R. Mahdavi, J. B. Hasted, and M. M. Nakshbandi, J. Phys. B **4**, 1726 (1971).
[25] D. Smith, N. G. Adams, A. G. Dean, and M. J. Church, J. Phys. D: Appl. Phys. **8**, 141 (1975).
[26] J. Glosik, G. Bano, R. Plasil, A. Luca, and P. Zakouril, Int. J. Mass Spectrom. **189**, 103 (1999).
[27] A. J. Yencha, in *Electron Spectroscopy: Theory, Techniques and Applications*, edited by C. R. Bundle and A. D. Baker (Academic Press, London, 1984), Vol. 5.
[28] R. Plasil, I. Korolov, T. Kotrik, P. Dohnal, G. Bano, Z. Donko, and J. Glosik, Eur. Phys. J. D **54**, 391 (2009).
[29] I. Korolov, T. Kotrik, R. Plasil, J. Varju, M. Hejduk, and J. Glosik, Contrib. Plasma Phys. **48**, 521 (2008).
[30] J. D. Swift and M. J. R. Schwar, *Electrical Probes for Plasma Diagnostics* (Elsevier, New York, 1969).
[31] O. Chudacek, P. Kudrna, J. Glosik, M. Sicha, and M. Tichy, Contrib. Plasma Phys. **35**, 503 (1995).
[32] P. Macko, G. Bano, P. Hlavenka, R. Plasil, V. Poterya, A. Pysanenko, O. Votava, R. Johnsen, and J. Glosik, Int. J. Mass Spectrom. **233**, 299 (2004).

[33] O. Novotny, R. Plasil, A. Pysanenko, I. Korolov, and J. Glosik, J. Phys. B **39**, 2561 (2006).
[34] R. Plasil, J. Glosik, V. Poterya, P. Kudrna, J. Rusz, M. Tichy, and A. Pysanenko, Int. J. Mass Spectrom. **218**, 105 (2002).
[35] D. R. Bates, Proc. R. Soc. London, Ser. A **337**, 15 (1974).
[36] D. K. Bohme, D. B. Dunkin, F. C. Fehsendeld, and E. E. Ferguson, J. Chem. Phys. **51**, 863 (1969).
[37] B. M. Smirnov, Sov. Phys. Usp. **20**, 119 (1977).
[38] J. Royal and A. E. Orel, Phys. Rev. A **73**, 042706 (2006).
[39] J. L. McLain, V. Poterya, C. D. Molek, L. M. Babcock, and N. G. Adams, J. Phys. Chem. A **108**, 6704 (2004).
[40] E. Alge, N. G. Adams, and D. Smith, J. Phys. B **16**, 1433 (1983).
[41] F. L. Walls and G. H. Dunn, J. Geophys. Res. **79**, 1911 (1974).
[42] R. Johnsen, Int. J. Mass Spectrom. Ion Processes **81**, 67 (1987).
[43] N. G. Adams, D. Smith, and E. Alge, J. Chem. Phys. **81**, 1778 (1984).
[44] R. Peverall, S. Rosen, J. R. Peterson, M. Larsson, A. Al-Khalili, L. Vikor, J. Semaniak, R. Bobbenkamp, A. N. Maurellis, and W. J. van der Zande, J. Chem. Phys. **114**, 6679 (2001).
[45] P. Spanel, L. Dittrichova, and D. Smith, Int. J. Mass Spectrom. **129**, 183 (1993).
[46] E. Mason and E. McDaniel, *Transport Properties of Ions in Gases* (Wiley, New York, 1988).
[47] L. Viehland, A. Viggiano, and E. Mason, J. Chem. Phys. **95**, 7286 (1991).
[48] W. Lindinger and D. Albritton, J. Chem. Phys. **62**, 3517 (1975).
[49] R. Johnsen and M. A. Biondi, Phys. Rev. A **20**, 221 (1979).
[50] J. Berlande, M. Cheret, R. Deloche, A. Gonfalone, and C. Manus, Phys. Rev. A **1**, 887 (1970).
[51] R. J. van Sonsbeek, R. Cooper, and R. N. Bhave, J. Chem. Phys. **97**, 1800 (1992).
[52] T. Kotrik, P. Dohnal, I. Korolov, R. Plasil, S. Roucka, J. Glosik, C. H. Greene, and V. Kokoouline, J. Chem. Phys. **133**, 034305 (2010).

ARTICLE VII

TITLE: Ternary Recombination of H_3^+ and D_3^+ with Electrons in He–H_2 (D_2) Plasmas at Temperatures from 50 to 300 K

AUTHORS: Rainer Johnsen, Peter Rubovič, Petr Dohnal, Michal Hejduk, Radek Plašil, and Juraj Glosík

JOURNAL: The Journal of Physical Chemistry A 117:9477-9485

DATE: 6 February 2013

DOI: 10.1021/jp311978n

THE JOURNAL OF PHYSICAL CHEMISTRY A

Article

pubs.acs.org/JPCA

Ternary Recombination of H_3^+ and D_3^+ with Electrons in He–H_2 (D_2) Plasmas at Temperatures from 50 to 300 K

R. Johnsen,*[,†] P. Rubovič,[‡] P. Dohnal,[‡] M. Hejduk,[‡] R. Plašil,[‡] and J. Glosík[‡]

[†]Department of Physics and Astronomy, University of Pittsburgh, Pittsburgh, Pennsylvania 15260, United States

[‡]Faculty of Mathematics and Physics, Department of Surface and Plasma Science, Charles University, Prague, Czech Republic

ABSTRACT: We present results of plasma afterglow experiments on ternary electron-ion recombination rate coefficients of H_3^+ and D_3^+ ions at temperatures from 50 to 300 K and compare them to possible three-body reaction mechanisms. Resonant electron capture into H_3* Rydberg states is likely to be the first step in the ternary recombination, rather than third-body-assisted capture. Subsequent interactions of the Rydberg molecules with ambient neutral and charged particles provide the rate-limiting step that completes the recombination. A semiquantitative model is proposed that reconciles several previously discrepant experimental observations. A rigorous treatment of the problem will require additional theoretical work and experimental investigations.

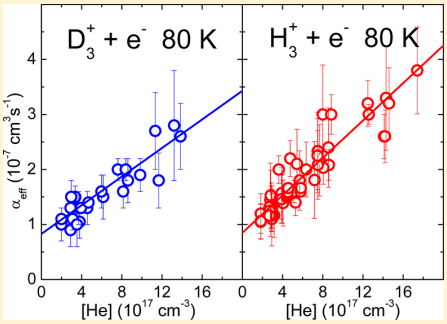

1. INTRODUCTION

The recombination of H_3^+ ions and their deuterated analogs with thermal electrons has been studied for more than four decades, motivated largely by its pivotal role in the chemistry and physics of astrophysical clouds and the atmospheres of the outer planets, applications to man-made discharges, and basic interest. However, a true reconciliation of often discrepant experimental data, and a convergence of theory and experiment have not been achieved, as has been pointed out in recent reviews of the subject (see, e.g., Johnsen and Guberman[1]). This article focuses on three-body recombination of H_3^+ ions, i.e., the enhancement of recombination by collisions with ambient plasma particles, such as electrons, ions, and neutrals. Theoretical[2−5] and experimental[6−8] work on purely binary recombination of H_3^+ has made enormous progress since the advent of storage rings, advanced afterglow techniques, and the modern Jahn–Teller type theories.[2] At this time, the theory reproduces the experimental values of the thermal (Maxwellian) rate coefficients very well, but discrepancies still exist between the calculated resonances and the structures seen in high-resolution storage-ring data, as has been discussed in great detail by Petrignani et al.[9] Some of these resonances may also play a role in the three-body effects discussed here (see section 5).

It is important to realize that third-body assisted recombination does not always lead to experimentally detectable dependences on ambient gas density. We briefly illustrate this point by revisiting the early experiment of Leu et al.[10,11] Their microwave-afterglow measurements yielded an H_3^+ recombination coefficient (2.4×10^{-7} cm^3/s at 300 K) that is far larger (by a factor of nearly 4) than that obtained later (about 0.6×10^{-7} cm^3/s) in low-pressure afterglows[12−14] and storage-ring experiments.[6−8] Leu et al. employed helium as buffer gas, at densities from 4.4×10^{17} to 8.6×10^{17} cm^{-3} at T = 300 K, and from 4.1×10^{17} to 7.8×10^{17} cm^{-3} at 205 K. They found that the recombination rates were independent (within about 5%) of density and that they were independent of the experimental electron densities from 5×10^9 to about 1/20 of that density. Over the limited range of temperatures the measured recombination coefficients varied with temperature as $T^{-1/2}$, exactly what was expected for binary recombination, and hence the authors were confident that they had observed binary recombination of H_3^+, but as we will discuss later, they probably measured a "saturated" three-body reaction that only gives the appearance of binary recombination. A crude estimate of the three-body rate coefficient at 300 K would be given by the ratio $(2.4 \times 10^{-7} - 0.6 \times 10^{-7})/\ 4.4 \times 10^{17} = 4 \times 10^{-25}$ cm^6/s, a rather large value that cannot be ascribed to known three-body mechanism[15] such as collisional radiative recombination in which atoms act as third bodies. We emphasize that the large body of data for ions other than H_3^+ collected by the microwave technique was confirmed later and that three-body effects are not at all common. The gas phase recombination of H_3^+, the simplest triatomic ion, clearly has some unusual features!

Systematic measurements of the neutral-assisted recombination have been carried out in the Prague laboratory over a period of about four years and have recently been extended to unprecedented low temperatures (50 K). Both stationary and

Special Issue: Oka Festschrift: Celebrating 45 Years of Astrochemistry

Received: December 5, 2012
Revised: February 6, 2013
Published: February 6, 2013

   dx.doi.org/10.1021/jp311978n | J. Phys. Chem. A 2013, 117, 9477−9485

flowing afterglow apparatus were employed, always in conjunction with mass spectrometric identification of the recombining ions. In some measurements the traditional Langmuir probe technique was used to determine electron densities. Although accurate recombination coefficients can be obtained by this method, the internal state of the ions remains unspecified. Hence, optical absorption (cavity-ring-down-spectroscopy, CRDS) was added to observe the decay of H_3^+ (D_3^+) ions in known vibrational/rotational states and to measure the dependence of the recombination on the nuclear spin modification (para, ortho, meta). Complete descriptions of the earlier experiments can be found in Glosík et al.,[16−19,22] Varju et al.,[20,23] Kotrík et al.,[21] Plašil et al.,[29] Rubovič et al.,[24] and Dohnal et al.[25−27]

The earliest such measurements,[28] carried out over a small range of helium densities, were consistent with a lack of density dependence. However, as the accuracy of the data improved, and the density range was increased, a dependence of the recombination on neutral (helium) density was invariably observed. The measurements revealed that the three-body coefficients vary with temperature and that they also depend on the nuclear spin states of the H_3^+ (D_3^+) ions (see Varju et al.,[20,23] Plašil et al.,[29] and Dohnal et al.[25,27]).

We limit the discussion to plasmas in which helium is the dominant neutral gas and ignore possible effects of the minority gases that are often present in afterglow experiments, typically argon and hydrogen. Tests showed that small additions of argon have no significant effect. The hydrogen density is kept small ($<10^{13}$ cm^{-3}), sufficient to maintain thermal equilibrium among rotational states (within either the para or ortho manifolds) and to convert precursor ions (mainly Ar^+) rapidly to H_3^+ (D_3^+). We digress briefly to discuss one important measurement that was performed in pure hydrogen to assess the possible effect of H_2.

Amano's[30] pioneering and very influential optical absorption measurements in pure hydrogen afterglows yielded a large recombination coefficient of 1.8×10^{-7} cm^3/s at 300 K, about 3 times larger than the now accepted binary value. Amano did not observe a dependence of the recombination coefficient on hydrogen density in the range from 3.2×10^{15} cm^{-3} to 10 times that value, which seems to indicate an absence of a three-body contribution due to hydrogen. However, as was pointed out earlier, the absence of a density dependence is not conclusive proof that three-body effects are not present. If one were to ascribe the larger observed recombination coefficient entirely to H_2-stabilized recombination (ignoring possible contributions from electrons), the three-body rate would have to be larger than $(1.8 \times 10^{-7} - 0.6 \times 10^{-7})/3.2 \times 10^{15} = 3.75 \times 10^{-23}$ cm^6/s, about 100 times faster than the estimate made earlier for He as third body. This estimate is compatible with that obtained in the experiments of Gougousi et al.[31] In the afterglow experiments described here, the H_2 density was kept below 10^{13} cm^{-3} and hence H_2-assisted recombination should have been negligible. In later work Amano[32] extended his measurements to low temperatures (∼110 K) and found even larger recombination coefficients. Under those conditions, conversion of H_3^+ to H_5^+ is not negligible (see Johnsen[33]) and there is the further complication that the electron densities in Amano's studies were unusually high (∼3×10^{11} cm^{-3}).

Neutral particles are probably not the only third bodies that affect H_3^+ recombination. Two afterglow experiments,[31,34] both performed at low helium densities, indicated that the H_3^+ recombination slowed down in the later afterglow (i.e., at smaller electron densities), but the same was not observed in recombination studies of O_2^+ ions, the "benchmark" ion often used to test experimental procedures. However, this observation has also been ascribed to vibrationally excited H_3^+ ions.[34]

In the following, we will present experimental data on the temperature dependence of neutral assisted recombination, followed by a discussion of possible reaction mechanisms. The proposed mechanisms have in common that they invoke high molecular Rydberg states with principal quantum number n, formed either by third-body assisted capture or by resonant capture into autoionizing states. If such states are sufficiently long-lived, their interactions with third bodies may induce dissociation into stable recombination products, thus making the recombination irreversible. In the case of molecular ions, the ionic core may be rotationally (or vibrationally) excited so that several sets of Rydberg states exist that converge to different ionization limits. One should also be aware that the electron "orbits" can be quite large so that many ambient gas particles will be closer to the ion core than the Rydberg electron. For instance, at gas densities of 3×10^{17} cm^{-3} (∼10 Torr at 300 K), the spherical volume of an $n = 50$ state contains several thousand atoms. The density of charged particles is typically much lower, but above the Inglis−Teller limit[35,36] ($n_{max} \sim 80$ at $n_e = 1 \times 10^9$ cm^{-3}, $n_{max} \sim 60$ at $n_e = 1 \times 10^{10}$ cm^{-3}) the Stark broadening due to neighboring charged particles is on the same order as the energy difference between adjacent Rydberg states.

2. EXPERIMENTAL DATA ON THE TEMPERATURE DEPENDENCE OF THE HELIUM-ASSISTED RECOMBINATION COEFFICIENT

A comprehensive set of rate coefficients of H_3^+ and D_3^+ has been collected in helium-buffered afterglow plasmas in the Prague laboratory. Some of the data were measured earlier, and some were obtained as part of the present investigation. The instruments used and the methods of analysis are the same as those employed in determinations of the binary recombination coefficients and there is no need to repeat detailed descriptions (see, e.g., Kotrík et al.,[37] Dohnal et al.,[38] and Rubovič et al.[24]). In all these measurements the electron and ion temperatures were the same as the gas temperature, the hydrogen and deuterium gases were taken from room-temperature reservoirs, and their nuclear spin states have their "normal" abundances. We will not discuss recent measurements with para-enriched gases (see Varju et al.,[23] Dohnal et al.,[25−27] and Hejduk et al.[39]).

As a precaution, a series of measurements was performed (Dohnal et al.[38]) to rule out the unlikely possibility that the measured dependences on helium density were due to unrecognized systematic errors, for instance in the determinations of electron densities or in the corrections for diffusion losses. In these tests the well-known recombination coefficient of O_2^+ ions was measured at $T = 230$ K for helium densities (in units of cm^{-3}) from 3.8×10^{17} to 5×10^{17}, and at $T = 155$ K from 2.7×10^{17} to 5.6×10^{17}. No detectable variation with density was observed and the absolute values agreed with the known recombination coefficients.

The three-body (ternary) H_3^+ (D_3^+) rate coefficients K_{He} are derived from graphs of the measured "effective" rate coefficient vs the density of helium, assuming that binary recombination (α_{bin}) and ternary recombination simply add, i.e., that

$$\alpha_{eff} = \alpha_{bin} + K_{He}[He] \quad (1)$$

Experimental values of α_{eff} (Figure 1), collected by the SA-CRDS (stationary afterglow −cavity ring-down spectrometer)

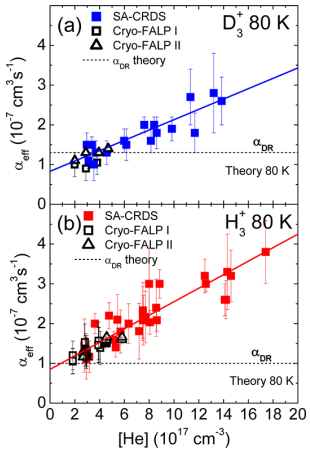

Figure 1. Dependence α_{eff} on helium density at T = 80 ± 3 K, as measured in a stationary afterglow in conjunction with cavity-ring-down spectroscopy (SA-CRDS) and in flowing afterglows (Cryo-FALP I and Cryo-FALP II). (a) D_3^+ data (from Dohnal et al.,[26] Kotrík et al.[21]). (b) H_3^+ data (from Glosík et al.,[18] Varju et al.[23]). The dashed horizontal lines show theoretical values of the binary coefficients (Pagani et al.,[4] Fonseca dos Santos et al.[3]).

and the flowing afterglow (CRYO- FALP I and II), are consistent with a linear dependence over the differing density ranges covered by the experiments. No measurable dependence on electron density was observed, even though the Cryo-FALP I and II data were obtained at low electron densities (typically $n_e = 2 \times 10^9$ cm^{-3}) in the afterglow plasma and the SA-CRDS data were obtained at much higher electron densities (typically 3×10^{10} cm^{-3}).

However, the linear addition of binary and ternary recombination implied by eq 1 is valid only when the two recombination mechanisms occur in parallel, but not when binary and ternary recombination share the same "finite resource", for instance, an intermediate excited state that is formed by electron capture (see section 5). The observations discussed in the Introduction suggest that α_{eff} is more likely to approach a constant value at higher [He]. Hence, the experimental values of K_{He} maybe only approximate first-order values that are valid in the limit of small helium densities.

Figure 2 shows measured K_{He} data for H_3^+ in the temperature range from T = 50 K to T = 350 K, the first such data ever obtained for molecular ions at temperatures below 77 K.

It has been verified in additional studies (Dohnal et al.,[25−27,38] Kotrík et al.[37]) that such plasmas are close to thermal equilibrium ($T_{He} = T_e = T_{ion}$). Although the consistency of the present data with those obtained in earlier experiments is not perfect, the overall temperature dependences are similar. The present experiments covered a wider range of densities and have better accuracy. At temperatures below about 100 K the three-body coefficient falls off with decreasing temperature and then approaches the three-body coefficient for neutral-stabilized recombination. For comparison, we have added experimental data points obtained by Dohnal et al.[38] in plasmas that contained only atomic Ar^+ ions

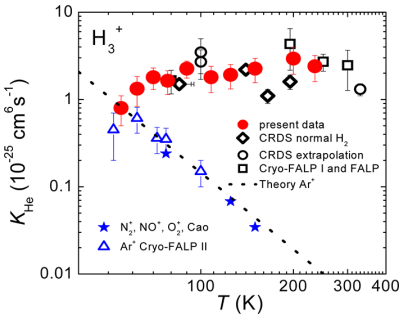

Figure 2. Upper data set: measured variation of K_{He} of H_3^+ ions with gas temperature, obtained when normal hydrogen was used (Varju et al.,[23] Dohnal et al.,[25] Glosík et al.[18]). Lower data set: measured helium-assisted collisional radiative recombination rate coefficient of Ar^+ ions (Dohnal et al.[38]), and earlier results of Cao and Johnsen.[40] Dashed line: theoretical values of the Ar^+ rate coefficient (Bates and Khare[15]).

(in the absence of hydrogen) and those agree very well with earlier data[40] and with theory of neutral assisted collisional radiative recombination (N-CRR, see section 3). At higher temperatures, the latter recombination mechanism makes only a negligible recombination.

Figure 3 shows a similar data set for D_3^+ ions. Here, the rapid decline of the rate coefficient below 100 K is more obvious. In

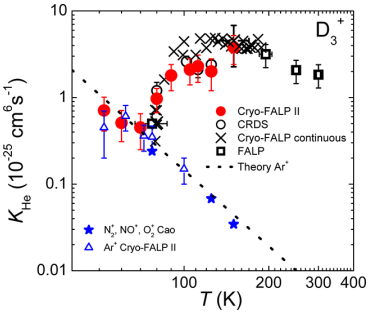

Figure 3. Upper data set: measured variation of K_{He} of D_3^+ ions with gas temperature (Kotrík et al.,[21] Dohnal et al.[26]). Lower data set: measured helium-assisted collisional radiative recombination rate coefficient of Ar^+ ions (Dohnal et al.[38]) and earlier results of Cao and Johnsen.[40] Dashed line: theoretical values of the Ar^+ rate coefficient (Bates and Khare[15]).

these data it is also clear that the D_3^+ ternary rate coefficient rises again below ∼70 K, exactly as is observed for atomic argon ions, removing all doubt that neutral collisional radiative recombination occurs in both cases.

Although H_3^+ and D_3^+ are similar in many respects, there is no reason to believe that they recombine with the same rates or that the three-body rate coefficients should be identical because their rotational and vibrational levels are different. The three-body coefficients exceed those of collisional radiative recombination in both cases at all but the lowest temperatures. Also, the temperature dependence clearly does not obey a simple inverse power-law dependence on temperature, such as is often seen in three-body reactions such as ion−molecule association reactions. A casual inspection of the data, especially those for D_3^+, suggests that the three-body recombination

dx.doi.org/10.1021/jp311978n | J. Phys. Chem. A 2013, 117, 9477−9485

involves an activation energy or a resonance that requires a minimum energy.

3. MODELS OF THREE-BODY ELECTRON-ION RECOMBINATION OF H_3^+ AND D_3^+

Many, if not most, molecular ions recombine by the direct mechanism. Here, the captured electron induces rapid dissociation and there is insufficient time for stabilizing collisions with third bodies. When, as is the case in indirect recombination, the electron is first captured into autoinizing Rydberg states, collisions with third bodies can affect their subsequent evolution, if the lifetime of such states is long enough. The density of third bodies here enters in the "stabilizing" step. It is also possible, though, that the third bodies play a role in the formation of Rydberg states, as in collisional radiative recombination. It is not obvious which of the two mechanisms is more important and whether the capture step or the stabilization step are rate-limiting.

The earliest attempts[31] to explain the peculiar recombination in H_3^+ containing afterglow plasmas (at low helium densities of 3×10^{16} cm^{-3} at $T = 300$ K) were made at a time when theoretical calculations predicted a very small binary recombination coefficient. Gougousi et al.[31] observed that the recombination rate coefficient declined in the late afterglow, a finding that was quite similar to that found in earlier afterglow experiments by Smith and Španěl.[34] Gougousi et al. proposed a model in which an electron was captured into a long-lived Rydberg state with a vibrationally excite core, followed by electron induced l-mixing (l being the Rydberg electron's angular momentum) and eventual stabilization by a reaction with ambient hydrogen. In hindsight, the lifetimes used in their model were probably too long, and improved theories[2] showed that binary recombination was not as slow as earlier theories had suggested. The experimental observations of Gougousi et al. and Smith and Španěl, however, should not be dismissed as "early data".

When later afterglow experiments (Glosík et al.,[16−19,22] Kotrík et al.,[21] Dohnal et al.[25]) showed that the recombination rate increased with the density of the buffer gas (helium), the authors developed an approximate model in which electrons of low angular momentum ($l = 1$) are captured into rotationally excited Rydberg states, subsequently suffer l-mixing in collisions with helium, and are eventually stabilized. As will be discussed later, rather large l-mixing rates for high Rydberg states have to be invoked to obtain agreement with experiment. An alternate mechanism (Johnsen and Guberman[1]) invokes three-body capture into lower Rydberg states that have higher l-mixing rates. This estimate, however, relies on the approximation that states with binding energies less than $-4kT$ (the so-called "bottleneck") are in thermal Saha equilibrium, which is not necessarily true if those states are subject to stabilization other than by collisional energy loss.

In the following, we will use the following abbreviations: E-CRR and N-CRR denote electron or neutral assisted collisional radiative recombination of atomic ions. We use E-CDR and N-CDR (electron or neutral collisional dissociative recombination) for molecular ions that can be stabilized by dissociation. In reality, all these processes can occur together, do not add in a simple manner, and are difficult to separate.

We begin with a brief introduction to the essential properties of collisional radiative recombination for ions with an atomic core. Though neither of these processes provides an adequate explanation for the three-body effect observed in the case of recombining H_3^+ plasmas, some aspects of the problem are best understood by first considering atomic ions before examining modifications that should be made in the case of molecular ions. Electron assisted collisional radiative recombination (E-CRR) involves three-body capture of an electron by the ion in the presence of other electrons. One of the electrons is captured into a high Rydberg state whereas the second electron carries away the excess energy. Subsequent collisions with ambient electrons then cause a net downward cascade that eventually makes reionization impossible.

The rate coefficient for E-CRR is given by (see, e.g., Stevefelt et al.[41])

$$\alpha_{\text{E-CRR}} = 2.7 \times 10^{-20}(T_e/300)^{-4.5} n_e \ [\text{cm}^3/\text{s}] \tag{2}$$

Here and in the following we will ignore the additional terms that represent radiative effects. The validity of eq 2 at very low temperatures T_e (down to 52 K) was recently verified for Ar^+ ions in a helium-buffered afterglow plasma in a Cryo-FALP II experiment (Kotrík et al.,[27,42] Dohnal et al.[38]). Excellent agreement of experimental and theoretical values was obtained.

The capture into high Rydberg states (a few kT below the ionization limit) is much faster than that given by the formula above, but most of the Rydberg atoms will be reionized, rather than recombined. The capture rate coefficient can be calculated from the detailed balance between capture of free electrons and ionization of Rydberg atoms in thermal Saha equilibrium as

$$\alpha_{\text{cap}}(n) = n^2 {\lambda_{\text{th}}}^3 e^{\varepsilon_n} k_{\text{ion}} n_e \ [\text{cm}^3/\text{s}] \tag{3}$$

Here λ_{th} is the thermal de Broglie wavelength

$${\lambda_{\text{th}}}^3 = (h^2/(2\pi m_e kT))^{3/2} \tag{4}$$

and ε_n is the ionization energy of a Rydberg atom (13.6 [eV]/n^2) with principal quantum number n, divided by kT_e [eV], i.e.

$$\varepsilon_n = \frac{13.6}{n^2 kT_e} \tag{5}$$

The electron ionization coefficient k_{ion} in eq 3 is quite accurately known. Vriens and Smeets[43] derived the semi-empirical analytical formula

$$k_{\text{ion}} = \frac{9.56 \times 10^{-6}(kT_e)^{-1.5} \exp(-\varepsilon_n)}{{\varepsilon_n}^{2.33} + 4.38{\varepsilon_n}^{1.72} + 1.32\varepsilon_n} \ [\text{cm}^3/\text{s}] \tag{6}$$

Here, kT_e has to be inserted in units of electronvolts. More elaborate calculations by Pohl et al.[44] have confirmed the validity of this formula, and Vrinceanu[45] has shown that the ionization coefficient is only weakly dependent on the electronic angular momentum. If one now makes the simple assumption that low Rydberg states with binding energies above kT cannot be reionized, the capture rate coefficient of eq 3 in conjunction with eq 6 provides a rather good estimate of the E-CRR rate of eq 2 that, however, is somewhat fictitious because it ignores the contribution of downward n-changing collisions. Capture into higher Rydbergs is much faster than α_{CRR} of eq 2. For instance, capture into a range of Rydberg states from $n = 40$ to $n = 80$ at $n_e = 1 \times 10^{10}$ cm^{-3} proceeds with an effective binary capture rate coefficients of $\alpha_{\text{cap}} \sim 1 \times 10^{-6}$ cm^3/s at $T_e = 300$ K, $\alpha_{\text{cap}} \sim 5 \times 10^{-6}$ cm^3/s at $T_e = 100$ K. Note that the equilibrium between capture and collisional ionization will be maintained on a time scale of $1/k_{\text{ion}}\, n_e$, about 10^{-8} s for $n = 80$ (at 300 K and $n_e = 1 \times 10^{10}$ cm^{-3}), which is

dx.doi.org/10.1021/jp311978n | J. Phys. Chem. A 2013, 117, 9477−9485

much shorter than the recombination time scale of afterglow experiments.

In the case of atomic ion cores the capture into high Rydberg states is almost entirely compensated by reionization, but the same need not be true for molecular cores that, at least in principle, can be stabilized by predissociation into fragments that can no longer be ionized. This is the basic idea of the collisional dissociative recombination (E-CDR), first prosed by Collins.[46] If one assumes that all Rydberg atoms with p from 40 to 80 predissociate rapidly, the effective recombination coefficient approaches the capture coefficient that rises linearly with n_e and is very large, $\sim 1 \times 10^{-6}$ cm^3/s at T_e = 300 K and n_e = 1×10^{10} cm^{-3}, $\sim 5 \times 10^{-6}$ cm^3/s at 100 K. The effective recombination coefficient will rise with n_e until the reionization rate exceeds the predissociation rate and then levels off. However, the assumption that a large fraction of the Rydberg predissociate rapidly is probably not realistic. The capture populates all allowed angular momentum states evenly (because the inverse, ionization, is only weakly l-dependent) but only very few of those, namely those with small l are likely to predissociate (see Chupka[47]). If only ions with low l, e.g., in l = 1, are capable of predissociating, the estimates of the E-CDR rate coefficient will be reduced by the factor $(2l + 1)/n^2$, approximately 10^{-3} at n = 50. One might presume that l-mixing by electrons would be effective in converting high-l ions to predissociating l-states. The l-mixing rate by electrons from a given l' to a different l is indeed very large (Dutta et al.[48]), but the rate for converting a random l to a given l' is smaller by the factor $(2l' + 1)/[n^2 - (2l' + 1)]$, again a number on the order of 10^{-3}. Thus, it appears unlikely that E-CDR is an important process under the conditions of the afterglow experiments, unless Rydberg molecules in high l-states dissociate rapidly or are destroyed by some other reaction. If E-CDR were important, its rate should increase quite fast with decreasing temperature and lead to a strong dependence on electron density. This, however, is not what is experimentally observed.

Collisional radiative recombination, however, should become noticeable at very low temperatures and high electron densities. For instance, at 100 K and $n_e = 1 \times 10^{10}$ cm^{-3} eq 2 gives $\alpha_{CRR} \sim 4 \times 10^{-8}$ cm^3/s.

Similar considerations apply to neutral-assisted recombination processes. The approximation made in the above estimates of the electron-assisted three-body capture is not applicable in the case of neutral-assisted capture. Ionization of Rydberg states by helium atoms as opposed to electrons is slower by about 10 orders of magnitude (see Lebedev[49]). Hence, one would obtain extremely small rates of capture into high Rydberg states. This estimate is inappropriate because those states are populated predominantly by multiple electron-atom collisions that gradually reduce the total energy. A more reasonable estimate can be based on the treatment by Flannery,[50] who obtained the following rate coefficient for the neutral assisted recombination of atomic ions:

$$\alpha = 8\pi \frac{m_e}{M_{atom}} R_0 R_e^2 \left(\frac{8kT}{\pi m_e}\right)^{1/2} \sigma_{e,atom} n_{atom} \tag{7}$$

Here, m_e and M_{atom} denote the masses of the electron and gas atoms (e.g., helium), $\sigma_{e,atom}$ is the electron-atom momentum transfer cross section, and $R_e = e^2/kT$ (=5×10^{-6} cm at 300 K). R_0 is the trapping radius. The assumption is made that an electron that collides with an atom inside this radius recombines with unit probability, whereas those colliding outside that radius will escape recombination. If R_0 is taken as $2R_e/3$, the recombination coefficient decreases with temperature as $T^{-2.5}$ and agrees with the energy-diffusion model of Pitaevskii.[51] In the case of recombination in ambient helium (using $\sigma_{e,atom} = 5 \times 10^{-16}$ cm^2), one obtains

$$\alpha(T) = 2.1 \times 10^{-27} (T/300)^{-2.5} n(\mathrm{He})\ [\mathrm{cm}^3/\mathrm{s}] \tag{8}$$

A smaller (by about 40%) rate coefficient was obtained by Bates and Khare[15] in their classical treatment of the problem. At temperatures above 100 K, this recombination coefficient is far smaller than what is needed to explain the neutral assisted coefficient in the H_3^+ recombination studies. However, at temperatures below 50 K and n(He) = 6×10^{17} cm^{-3} $\alpha(T)$ of eq 8 exceeds 1×10^{-7} cm^3/s, which is clearly not negligible.

It is difficult to construct a general theory of third-body assisted recombination of molecular ions because the decay of molecular ions in high Rydberg states depends critically on the specific molecule. However, one can estimate the relative efficiencies of helium and electrons in leading to recombination from the ratio of the rates in eqs 2 and 8. At T_e = 300 K, one ambient electron has about the same stabilizing effect as 10^7 helium atoms. If one now, as before, assumes that high Rydberg atoms can also be stabilized by predissociation, it seems reasonable to expect that the flux into such states is controlled by helium atoms with an efficiency that is smaller by 10^7 compared to that of electrons. For example, a density of ambient electrons of $n_e = 1 \times 10^{10}$ cm^{-3} would have an effect similar to that of helium with density n(He) = 1×10^{17} cm^{-3}. Such conditions are fairly typical in experiments. Again, however, the magnitude of N-DRR is expected to be significant only if a very large number of Rydbergs states can predissociate, which seems unlikely. Also, the N-DRR rate coefficient would increase as the temperature is reduced, rather than exhibiting a drastic decline, such as that seen in the D_3^+ data below 100 K (Figure 3).

We conclude that that neither E-CDR nor N-CDR provides a compelling or even plausible explanation for the experimental findings. However, at very low temperatures collisional radiative recombination, given by eqs 2 and 8, becomes competitive with binary recombination. It may seem surprising that collisional dissociative recombination is less important than collisional radiative recombination. The reason is that dissociation is effective only for states of low l, whereas collisional stabilization also occurs for states with high l and much higher statistical weights.

4. RESONANT CAPTURE AND L-MIXING MODEL

A more promising mechanism of the helium-assisted recombination may be electron capture of a p-electron into an autoionizing resonance with a rotationally excited core, followed by a helium-induced change of the Rydberg electron's angular momentum (l-mixing), and final stabilization by predissociation or perhaps some other stabilizing mechanism. This is the model that has been invoked in several earlier publications.[16,21] Calculations of the lifetimes (or "time delays") of such resonances show that they can be indeed quite large (100−1000 ps) but the subsequent collisions that lead to irreversible recombination are more difficult to quantify. Essentially, the effective rate coefficient is estimated as

$$\alpha_{eff} = f \alpha_{cap} k_l n(\mathrm{He})/\nu_a\ [\mathrm{cm}^3/\mathrm{s}] \tag{9}$$

dx.doi.org/10.1021/jp311978n | J. Phys. Chem. A 2013, 117, 9477−9485

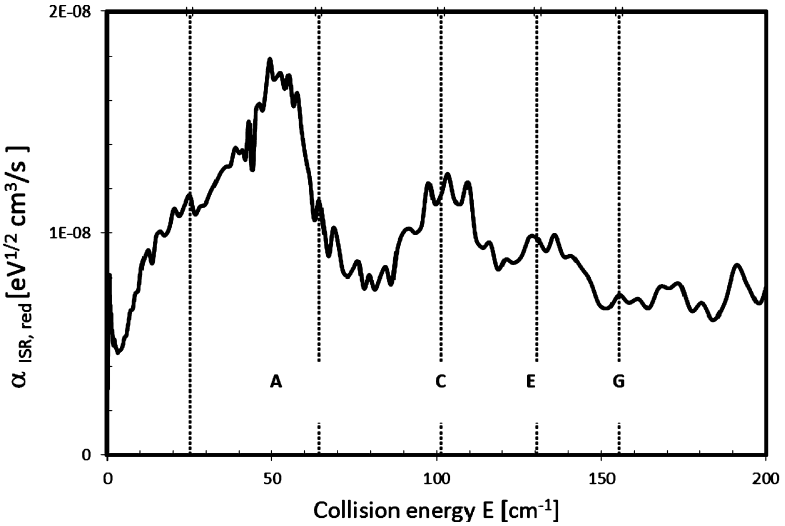

Figure 4. Reduced H_3^+ rate coefficient observed in storage-ring experiments as a function of collision energy, drawn from data supplied by Petrignani.[53] Vertical dashed lines indicate the energies at which the calculated lifetimes[16] of (1, 1) to (2, 1) resonances have maxima. The energies C, E, and G correspond to resonant capture into n = 39, 50, and 78, respectively.

where $\nu_a = 1/\tau_a$ is the reciprocal of the autoionizing lifetime, α_{cap} denotes the capture coefficient, and k_l is the l-mixing rate from the initial p-state to higher angular momenta. The factor f denotes the fraction of the H_3^+ ions that are capable of capturing electrons, e.g., are in an appropriate rotational state. That number is estimated to be about 0.25. If one uses $\tau_a = 10^{-10}$ s, $\alpha_{cap} = 3 \times 10^{-7}$ cm^3/s, and $k_l = 3 \times 10^{-8}$ cm^3/s, one obtains a three-body rate coefficient of 2.25×10^{-25} cm^6/s, in good agreement with the experimental value assuming that Rydberg states from p = 40−80 contribute. Equation 9 is valid only in the limit of vanishing helium density. At finite helium densities, l-mixing also depletes the resonant state. Hence, eq 9 should be replaced by

$$\alpha_{eff} = f\alpha_{cap}\frac{k_l n(\mathrm{He})}{k_l n(\mathrm{He}) + \nu_a} \quad (10)$$

which agrees with formula 9 in the limit n(He) = 0. At a helium density of 3×10^{17} cm^{-3}, α(He) is now only about 50% of that given by eq 9. At higher helium densities it "saturates" at $f\alpha_{cap}$ and the differential three-body rate $(d\alpha_{eff}/dn(\mathrm{He})$ approaches zero. The saturation should be taking into account in comparisons of experimental data to model calculations. We note also that eq 10 only considers l-mixing by helium atoms. If one includes the much faster l-mixing by electrons, the "saturation" would set in at lower helium densities under many experimental conditions.

The assumption that the l-mixing rate coefficient due to helium is given by $k_l = 3 \times 10^{-8}$ cm^3/s, independent of the principal quantum number, is in conflict with the theoretical conclusion of Hickman[52] that for higher n it should decline as $n^{-2.7}$. Also, the theories of l-mixing consider only mixing from $l \geq 2$. The rates for mixing from l = 0, 1 to higher l are actually smaller because the quantum defects are larger. Unfortunately, there are no direct measurements of l-mixing coefficients for high p for molecular ions to reach a clear decision.

The assumption that the autoionizing high-l Rydberg states formed by l-mixing predissociate much faster than they autoionize is also not obvious, and there is no good argument that rules out the opposite assumption. In the following section we will explore a modification of the resonant-capture model that is, in part, based on experimental observations. In a more rigorous treatment, multiple capture resonances should be considered and their contributions should be added.

5. COMPLEX MODEL

At low electron densities binary rotational capture will always be a faster route to Rydberg states than three-body assisted capture. Hence, we will neglect contributions due to three-body capture. The resonant lifetimes that were used in earlier treatments were calculated from the matrix that describes the rotational capture of p-electrons and their release assuming that the ionic core, except for changing its rotational state, remains unaffected. Other channels, such as predissociation or vibrational excitation were deemed to play no significant role. It seems possible, however, that the rotational resonances lead to more complicated complexes, in which the ionic core becomes highly vibrationally excited and eventually decays into dissociating channels. This conjecture motivated us to examine the energy dependence of the H_3^+ recombination that has been observed in storage-ring experiments

The high-resolution storage-ring data on H_3^+ recombination Petrignani et al.[9,53] show several recombination peaks at energies from 40 to 160 cm^{-1} (0.005−0.02 eV) that are not predicted by theory. As shown in Figure 4, their positions correlate with the calculated[16] positions of the lifetime maxima for the rotational resonances from the (1, 1) to the (2, 1) (excitation energy of 173 cm^{-1}) rotational states of para-H_3^+. In Figure 5 of Petrignani et al. the peaks are labeled C and E (we labeled the next higher peak "G"). In this graph, the "raw" (referring to narrow, non-Maxwellian energy distributions) rate coefficients have been reduced by multiplying with the square root of the collision energy to remove the overall energy dependence. It is still not entirely clear whether or not H_3^+ recombination measurements in storage rings are free from possible effects due to electric stray fields.

One could dismiss the correlation as coincidence, but resonant capture by H_3^+ in the (1, 1) state, the rotational ground state of para-H_3^+, is a natural first step in complex formation. Helium, of course is absent in the storage ring, and the electron density is much lower than in afterglow experiments. Hence, it appears that some of the long-lived rotational resonances actually lead to binary recombination. The largest (very broad) peak in the storage ring data at 50 cm^{-1} (labeled A) has no counterpart in the lifetime graph of (1, 1) to (2, 1) resonances and probably has a different origin. Storage ring data by Kreckel et al.[54] (see their Figure 8) indicate that the central part of peak "A" remained the same when para-enriched rather than normal hydrogen was fed to the ISR ion source. Peak "A" may reflect a rotational resonance from the para (2, 1) to the (3, 1) rotational state. If this assignment is correct, this resonance could contribute to afterglow recombination at T = 300 K, but it should not play a role at very low temperatures, because the abundance of the (2, 1) rotational state would be small.

Returning to three-body effects, we now assume that the Rydberg states formed by rotational capture of a p-electron actually interact with the ion core and form an ensemble of complexes with lifetimes that exceed those given by the lifetime matrix. We further assume that the complexes can autoionize, dissociate in the absence of third-body interactions, and that the dissociation rate can be enhanced by third bodies. The resulting recombination rate coefficient in terms of several, however not well-known, rate coefficients has the form

$$\alpha_{\mathrm{eff}}(He) = \alpha_{\mathrm{cap}} \frac{k_{\mathrm{He}} n(\mathrm{He}) + k_e n_e + \nu_{\mathrm{diss},0}}{k_{\mathrm{He}} n(\mathrm{He}) + k_e n_e + \nu_{\mathrm{diss},0} + \nu_a} \qquad (11)$$

The effective recombination coefficient is the product of a capture rate coefficient and the ratio of recombination channels to all decay channels. It is similar to eq 10, but the rate coefficients have different meanings. Here, k_{He} and k_e denote the net rate coefficients for complex stabilization (i.e., leading to predissociation rather than collisional ionization) by helium atoms or electrons, respectively. $\nu_{\mathrm{diss},0}$ is the predissociation rate in the absence of third bodies, and ν_a is the autoionization frequency. We prefer to use decay frequencies rather than lifetimes, because an ensemble of complexes does not necessarily decay with a single exponential time constant.

The coefficients in eq 11 are not known and it is not likely that they can be deduced from simple theoretical arguments. However, it is easy to find values that approximately reproduce the experimental data. Figure 5 shows a fit of eq 11 to data obtained at T = 300 K for three different electron densities. The autoionization rate has been chosen as $\nu_a = 8 \times 10^8$ 1/s such that the model agrees with those of the Prague experiments rather than with those of Leu et al.[10]

The data by Smith and Španěl[34] and by Gougousi et al.[31] are shown with upward arrows, from the values that they observed at low n_e (late afterglow) to those at high n_e (early afterglow). If one chooses $k_e = 10^7 k_{\mathrm{He}}$, the same "efficiency factor" used in section 3, the model roughly reproduces the range of rate coefficients observed in those experiments at different n_e. A precise fitting of those data is not possible and would be pointless because the accuracy of those data at low n_e is considerably worse than at high electron densities. At high n(He) the model gives a weaker dependence on n_e, in agreement with the findings by both Leu et al.[10] and the Prague experiments. Although a linear extrapolation of the Prague data to n(He) = 0 is not strictly compatible with the model, it results in a binary value that is only slightly too high.

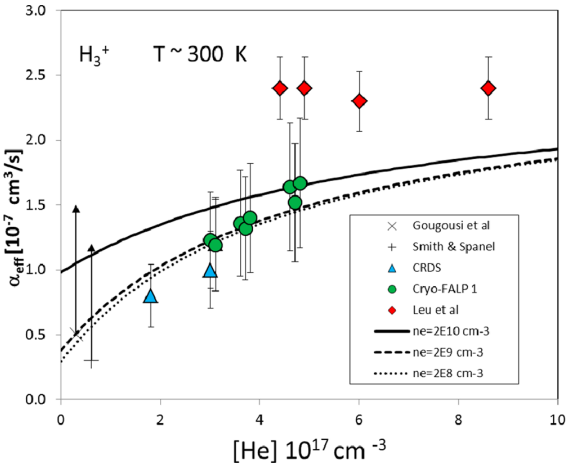

Figure 5. Comparison of eq 11 to experimental data at T = 300 K. The following values were used for the rate coefficients and decay rates: $\alpha_{\mathrm{cap}} = 2.55 \times 10^{-7}$ cm^3/s, $k_{\mathrm{He}} = 2 \times 10^{-9}$ cm^3/s, $k_e = 5 \times 10^{-2}$ cm^3/s, $\nu_{\mathrm{diss},0} = 1 \times 10^8$ 1/s, $\nu_a = 8 \times 10^8$ 1/s. See text for additional explanations. Data points from Gougousi et al.,[31] Smith and Spanel,[34] CRDS and Cryo-FALP I from Glosík et al.[18] and Leu et al.[11]

Our exploratory model provides a common framework that makes the apparent discrepancies between experimental data easier to accept. Obviously, the model is crude because it uses the same rate coefficients for all members of the ensemble of complexes. This is unavoidable, given the severe lack of knowledge of the relevant parameters. It is also difficult to estimate how the effective recombination coefficients would vary with temperature. At low electron temperatures resonant capture can only occur into Rydberg states with smaller principal quantum numbers and the spacing between states will increase. Thus, one might expect that three-body effect would become smaller at low temperatures. The changing rotational distribution of H_3^+ is likely to have an effect also.

In the complex model, collisions with third bodies enhance the recombination rate at the expense of the autoionization rate ν_a. If ν_a is vanishingly small, however, then (see eq 11) the recombination rate is limited by electron capture and third-body effects disappear. In the simplified theory of Jungen and Pratt[5] electrons are captured by vibrational excitation mediated by the linear Jahn−Teller effect and autoionization is assumed to be negligible. Because their theory reproduces the rate coefficients measured in storage rings quite well, the agreement can be seen as a possible argument against the complex model. However, in a later and more detailed paper Jungen and Pratt[55] conclude that purely rotational capture into autoionizing states should also be considered and that recombination in that case would not be capture limited. It is difficult to go further without knowing the relative efficiencies of the capture mechanisms.

6. CONCLUSIONS

The multiyear efforts to elucidate the ternary recombination of H_3^+ and D_3^+ ions, in particular the novel extension to very low temperatures, have resulted in a rather unique set of data. It is particularly pleasing to see that the traditional three-body reaction (i.e., the Bates and Khare mechanism[15]) becomes

detectable at temperatures below 70 K. This observation strongly supports the validity of the afterglow methods used here.

It appears that many of the seeming discrepancies between afterglow recombination data on H_3^+ (D_3^+) can be traced to third-body effects involving both neutral and charged particles. Although these measurements of third-body assisted recombination have narrowed the range of plausible mechanisms, developing a quantitative theoretical model is seriously hampered by the lack of needed data, especially on rates of predissociation, their dependence on angular momentum, and coupling between electronic and core degrees of freedom. The tentative model proposed here presents an attempt to develop a common framework that seeks to reconcile experimental observations.

The data obtained in helium-buffered plasmas are nearly complete, but there is a lack of data in other rare gases. Neon might be a good choice for further work because the momentum transfer between electrons and neon is far smaller than with helium. The only experiment in neon buffer[56] was done at a single pressure and does not permit any inferences regarding pressure dependences. Hence, we did not discuss this work but note that it resulted in smaller recombination coefficients than those obtained with helium buffer gas.

There remains some doubt about the role that electrons play as stabilizing body because the only two experiments[34,31] that point to electron-stabilized recombination may have alternate explanations. Additional experiments, especially measurements at very low temperatures, may be worth the effort.

Finally, it would certainly be highly desirable to have more theoretical information on the configuration interaction between electronic and core excitations in H_3^+ Rydberg states, and to identify clearly the origin of the resonance peaks that are seen in storage-ring experiments.

AUTHOR INFORMATION

Corresponding Author

*Phone: 412-624-9285. E-mail: rj@pitt.edu.

Notes

The authors declare no competing financial interest.

ACKNOWLEDGMENTS

This work was partly financed by the research grant OC10046 from the Ministry of Education of the Czech Republic and was partly supported by GACR (205/09/1183, P209/12/0233), by SV 267 302, by GAUK 353811, GAUK 406011, GAUK 659112, and by COST Action CM0805 (The Chemical Cosmos). We thank A. Petrignani for supplying numerical data on the storage ring results

REFERENCES

(1) Johnsen, R.; Guberman, S. L. Dissociative Recombination of H_3^+ Ions with Electrons: Theory and Experiment. *Adv. At., Mol., Opt. Phys.* **2010**, *59*, 75−127.

(2) Kokoouline, V.; Greene, C. H. Unified Theoretical Treatment of Dissociative Recombination of D3h Triatomic Ions: Application to H_3^+ and D_3^+. *Phys. Rev. A: At., Mol., Opt. Phys.* **2003**, *68*, 012703-1−23.

(3) Fonseca dos Santos, S.; Kokoouline, V.; Greene, C. H. Dissociative Recombination of H_3^+ in the Ground and Excited Vibrational States. *J. Chem. Phys.* **2007**, *127*, 124309-1−8.

(4) Pagani, L.; Vastel, C.; Hugo, E.; Kokoouline, V.; Greene, C. H.; Bacmann, A.; Bayet, E.; Ceccarelli, C.; Peng, R.; Schlemmer, S. Chemical Modeling of L183 (L134N): An Estimate of the Ortho/Para H_2 ratio. *Astron. Astrophys.* **2009**, *494*, 623−636.

(5) Jungen, Ch.; Pratt, S. T. Jahn-Teller Interactions in the Dissociative Recombination of H_3. *Phys. Rev. Lett.* **2009**, *102*, 023201-1−4.

(6) McCall, B. J.; Huneycutt, A. J.; Saykally, R. J.; Djuric, N.; Dunn, G. H.; Semaniak, J.; Novotny, O.; Al-Khalili, A.; Ehlerding, A.; Hellberg, F.; et al. Dissociative Recombination of Rotationally Cold H_3^+. *Phys. Rev. A: At., Mol., Opt. Phys.* **2004**, *70*, 052716-1−12.

(7) Wolf, A.; Kreckel, H.; Lammich, L.; Strasser, D.; Mikosch, J.; Glosík, J.; Plašil, R.; Altevogt, S.; Andrianarijaona, V.; Buhr, H.; et al. Effects of Molecular Rotation in Low-Energy Electron Collisions of H_3^+. *Philos. Trans. R. Soc. A.* **2006**, *364*, 2981−2997.

(8) Kreckel, H.; Motsch, M.; Mikosch, J.; Glosík, J.; Plašil, R.; Altevogt, S.; Andrianarijaona, V.; Buhr, H.; Hoffmann, J.; Lammich, L.; et al. High-Resolution Dissociative Recombination of Cold H_3^+ and First Evidence for Nuclear Spin Effects. *Phys. Rev. Lett.* **2005**, *95*, 263201-1−4.

(9) Petrignani, A.; Altevogt, S.; Berg, M. H.; Bing, D.; Grieser, M.; Hoffmann, J.; Jordon-Thaden, B.; Krantz, C.; Mendes, M.; Novotny, O.; et al. Resonant Structure of Low-Energy H_3^+ Dissociative Recombination. *Phys. Rev. A: At., Mol., Opt. Phys.* **2011**, *83*, 032711-1−10.

(10) Leu, M. T.; Biondi, M. A.; Johnsen, R. Measurements of Recombination of Electrons with H_3^+ and H_5^+ Ions. *Phys. Rev. A: At., Mol., Opt. Phys.* **1973**, *8*, 413−419.

(11) Leu, M. T. *Ph.D. thesis*, University of Pittsburgh, Pittsburgh, PA, USA, 1972.

(12) Macko, P.; Bánó, G.; Hlavenka, P.; Plašil, R.; Poterya, V.; Pysanenko, A.; Votava, O.; Johnsen, R.; Glosík, J. Afterglow Studies of H_3^+(v = 0) Recombination Using Time Resolved CW-Diode Laser Cavity Ring-Down Spectroscopy. *Int. J. Mass Spectrom.* **2004**, *233*, 299−304.

(13) Plašil, R.; Glosík, J.; Poterya, V.; Kudrna, P.; Rusz, J.; Tichý, M.; Pysanenko, A. Advanced Integrated Stationary Afterglow Method for Experimental Study of Recombination processes of H_3^+ and D_3^+ Ions With electrons. *Int. J. Mass Spectrom.* **2002**, *218*, 105−130.

(14) Laubé, S.; Le Padellec, A.; Sidko, O.; Rebrion-Rowe, C.; Mitchell, J. B. A.; Rowe, B. R. New FALP-MS Measurements of H_3+, D_3^+ and HCO^+ Dissociative Recombination. *J. Phys. B: At., Mol. Opt. Phys.* **1998**, *31*, 2111−2128.

(15) Bates, D. R.; Khare, S. P. Recombination of Positive Ions with Electrons in a Dense Gas. *Proc. Phys. Soc.* **1965**, *85*, 231−243.

(16) Glosík, J.; Korolov, I.; Plašil, R.; Novotny, O.; Kotrík, T.; Hlavenka, P.; Varju, J.; Mikhailov, I. A.; Kokoouline, V.; Greene, C. H. Recombination of H_3^+ ions in the Afterglow of a He−Ar−H_2 Plasma. *J. Phys. B: At., Mol. Opt. Phys.* **2008**, *41*, 191001−191009.

(17) Glosík, J.; Plašil, R.; Korolov, I.; Novotny, O.; Kotrík, T. Multicollision Character of Recombination of H_3^+ Ions in Afterglow Plasma. *J. Phys.: Conf. Ser.* **2009**, *192*, 012005 (8 pages).

(18) Glosík, J.; Plašil, R.; Korolov, I.; Kotrík, T.; Novotny, O.; Hlavenka, P.; Dohnal, P.; Varju, J.; Kokoouline, V.; Greene, C. H. Temperature Dependence of Binary and Ternary Recombination of H_3^+ ions with Electrons. *Phys. Rev. A: At., Mol., Opt. Phys.* **2009**, *79*, 052707-1−10.

(19) Glosík, J.; Korolov, I.; Plašil, R.; Kotrík, T.; Dohnal, P.; Novotny, O.; Varju, J.; Roučka, Š.; Greene, C. H.; Kokoouline, V. Binary and Ternary Recombination of D_3^+ Ions with Electrons in He-D_2 plasma. *Phys. Rev. A: At., Mol., Opt. Phys.* **2009**, *80*, 042706-1−9.

(20) Varju, J.; Roučka, Š.; Kotrík, T.; Plašil, R.; Glosík, J. Application of NIR − CRDS for State Selective Study of Recombination of Para and Ortho H_3^+ Ions with Electrons in Low Temperature Plasma. *J. Phys.: Conf. Ser.* **2010**, *227*, 012026 (4 pages).

(21) Kotrík, T.; Dohnal, P.; Korolov, I.; Plašil, R.; Roučka, S.; Glosík, J.; Greene, C. H.; Kokoouline, V. Temperature Dependence of Binary and Ternary Recombination of D_3^+ Ions with Electrons. *J. Chem. Phys.* **2010**, *133*, 034305−034313.

(22) Glosík, J.; Plašil, R.; Kotrík, T.; Dohnal, P.; Varju, J.; Hejduk, M.; Korolov, I.; Roučka, Š.; Kokoouline, V. Temperature Dependence of

Binary and Ternary Recombination of D_3^+ ions with Electrons. *Mol. Phys.* **2010**, *108*, 2253−2264.
(23) Varju, J.; Hejduk, M.; Dohnal, P.; Jílek, M.; Kotrík, T.; Plašil, R.; Gerlich, D.; Glosík, J. Nuclear Spin Effect on Recombination of H_3^+ Ions with Electrons at 77 K. *Phys. Rev. Lett.* **2011**, *106*, 203201−203205.
(24) Rubovič, P.; Dohnal, P.; Hejduk, M.; Plašil, R.; Glosík, J. Binary Recombination of H_3^+ and D_3^+ Ions with Electrons in Plasmas at 50 − 230 K. *J. Phys. Chem. A* **2013**, DOI: 10.1021/jp3123192.
(25) Dohnal, P.; Hejduk, M.; Varju, J.; Rubovič, P.; Roučka, Š; Kotrík, T.; Plašil, R.; Glosík, J.; Johnsen, R. Binary and Ternary Recombination of Para-H_3^+ and Ortho-H_3^+ with Electrons: State Selective Study at 77−200 K. *J. Chem. Phys.* **2012**, *136*, 244304-1−14.
(26) Dohnal, P.; Hejduk, M.; Rubovič, P.; Varju, J.; Roučka, Š.; Plašil, R.; Glosík, J. Binary and Ternary Recombination of D_3^+ Ions at 80−130 K: Application of Laser Absorption Spectroscopy. *J. Chem. Phys.* **2012**, *137*, 194320-1−8.
(27) Dohnal, P.; Hejduk, M.; Varju, J.; Rubovič, P.; Roučka, S.; Kotrík, T.; Plašil, R.; Johnsen, R.; Glosík, J. Binary Recombination of Para- and Ortho-H3+ with Electrons at Low Temperatures. *Philos. Trans. R. Soc. A* **2012**, *370*, 5101−5108.
(28) Glosík, J.; Plašil, R.; Poterya, V.; Tichy, M.; Pysanenko, A. Experimental Study of Recombination of H_3^+ Ions with Electrons Relevant for Interstellar and Planetary Plasmas. *J. Phys. B: At. Mol. Opt. Phys.* **2001**, *34*, L458−L494.
(29) Plašil, R.; Varju, J.; Hejduk, M.; Dohnal, P.; Kotrík, T.; Glosík, J. Experimental Study of Para- and Ortho-H_3^+ Recombination. *J. Phys Conf. Ser* **2011**, *300*, 012023 (8 pages).
(30) Amano, T. Is the Dissociative Recombination of H_3^+ Really Slow? A New Spectroscopic Measurement of the Rate Constant. *Astrophys. J., Lett.* **1988**, *329*, L121−L124.
(31) Gougousi, T.; Johnsen, R.; Golde, M. F. Recombination of H_3^+ and D_3^+ Ions in a Flowing Afterglow Plasma. *Int. J. Mass Spectrom.* **1995**, *149*−*150*, 131−151.
(32) Amano, T. The Dissociative Recombination Rate Coefficients of H_3^+, HN_2^+, and HCO. *J. Chem. Phys.* **1990**, *92*, 6492−6501.
(33) Johnsen, R. Kinetic Processes in Recombining H_3^+ Plasmas. *Philos. Trans. R. Soc. A* **2012**, *370*, 5109−5117.
(34) Smith, D.; Španěl, P. Dissociative Recombination of H_3^+. Experiment and Theory reconciled. *Chem. Phys. Lett.* **1993**, *211*, 454−460.
(35) Inglis, D. R.; Teller, E. Ionic Depression of Series Limits in One-Electron Spectra. *Astrophys. J.* **1939**, *90*, 439−448.
(36) Mitrafanov, A. V. On a Revised Version of the Inglis-Teller Formula. *Soviet Astronomy-AJ* **1973**, *16*, 867−869.
(37) Kotrík, T.; Dohnal, P.; Rubovič, P.; Plašil, R.; Roučka, S.; Opanasiuk, S. Glosík. Cryo-FALP Study of Collisional-Radiative Recombination of Ar+ Ions at 40−200 K. *Eur. Phys. J.: Appl. Phys.* **2011**, *56*, 24011−24016.
(38) Dohnal, P.; Rubovič, P.; Kotrík, T.; Hejduk, M.; Plašil, R.; Johnsen, R.; Glosík, J. Ternary Recombination of Ar^+ with Electrons in He at Temperatures 50−100 K. To be published.
(39) Hejduk, M.; Dohnal, P.; Varju, J.; Rubovič, P.; Plašil, R.; Glosík, J. Nuclear Spin State-Resolved Cavity Ring-Down Spectroscopy Diagnostics of a Low-Temperature H_3+−Dominated Plasma. *Plasma Sources Sci. Technol.* **2012**, *21*, 024002−024011.
(40) Cao, Y. S.; Johnsen, R. Neutral Stabilized Electron-ion Recombination in Ambient Helium Gas. *J. Chem. Phys.* **1991**, *94*, 5443−5446.
(41) Stevefelt, J.; Boulmer, J.; Delpech, J. Collisional-Radiative Recombination in Cold Plasmas. *Phys. Rev. A: At., Mol., Opt. Phys.* **1975**, *12*, 1246−1251.
(42) Kotrík, T.; Dohnal, P.; Roučka, S.; Jusko, P.; Plašil, R.; Glosík, J.; Johnsen, R. Collisional Radiative Recombination $Ar^+ + e + e$; Experimental Study at 77−180 K. *Phys. Rev. A: At., Mol., Opt. Phys.* **2011**, *83*, 032720-1−032720-8.
(43) Vriens, L.; Smeets, H. M. Cross-section and Rate Formulas for Electron Impact Ionization, Excitation, and Total Population of Excited Atoms. *Phys. Rev. A: At., Mol., Opt. Phys.* **1980**, *22*, 940−951.
(44) Pohl, T.; Vrinceanu, D.; Sadeghepour, H. R. Rydberg Atom Formation in Ultracold Plasmas: Small Energy Transfer with Large Consequences. *Phys. Rev. Lett.* **2008**, *100*, 223201-1−3.
(45) Vrinceanu, D. Electron Impact Ionization of Rydberg Atoms. . *Phys. Rev. A: At., Mol., Opt. Phys* **2005**, *72*, 022722-1− 8.
(46) Collins, C. B. Collisional-Dissociative Recombination of Electrons with Molecules. *Phys. Rev. A: At., Mol., Opt. Phys.* **1965**, *140*, 1850−1857.
(47) Chupka, W. A. Factors Affecting Lifetimes and Resolution of Rydberg States Observed in Zero-Electron-Kinetic-Energy Spectroscopy. *J. Chem. Phys.* **1993**, *98*, 4520−4530.
(48) Dutta, S. K.; Feldbaum, D.; Walz-Flannigan, A.; Guest, J. R.; Raithel, G. High-Angular-Momentum States in Cold Rydberg Gases. *Phys. Rev. Lett.* **2001**, *86*, 3993−3996.
(49) Lebedev, V. S. Ionization of Rydberg atoms by neutral particles. I. Mechanism of the Perturber-Quasifree-Electron Scattering. *J. Phys. B: At. Mol. Opt. Phys.* **1991**, *24*, 1977−1991.
(50) Flannery, M. R. Transportcollisional Master Equations for Termolecular Recombination as a Function of Gas Density. *J. Chem. Phys.* **1991**, *95*, 8205−8226.
(51) Pitaevskii, L. P. Electron Recombination in an Atomic Gas. *Sov. Phys. JETP* **1962**, *15*, 919−921.
(52) Hickman, A. P. Theory of Angular Momentum Mixing in Rydberg-Atom-Rare-Gas Collisions. *Phys. Rev. A: At., Mol., Opt. Phys.* **1978**, *18*, 1339−1342.
(53) Petrignani, A. Private communication. 2012.
(54) Kreckel, H.; Novotny, O.; Crabtree, K. N.; Buhr, H.; Petrignani, A.; Tom, B. A.; Thomas, R. D.; Berg, M. H.; Bing, D.; Grieser, M.; et al. High-Resolution Storage-Ring Measurements of the Dissociative Recombination of H_3^+ Using a Supersonic Expansion Ion Source. *Phys. Rev. A: At., Mol., Opt. Phys.* **2010**, *82*, 042715-1−11.
(55) Jungen, Ch.; Pratt, S. T. Low-Energy Dissociative Recombination in Small Polyatomic Molecules. *J. Chem. Phys.* **2010**, *133*, 214303-1−9.
(56) Macdonald, J. A.; Biondi, M. A.; Johnsen, R. Recombination of Electrons with H_3^+ and H_5^+ Ions. *Planet. Space Sci.* **1984**, *32*, 651−654.

ARTICLE VIII

TITLE: Binary Recombination of H_3^+ and D_3^+ Ions with Electrons in Plasma at 50–230 K

AUTHORS: Peter Rubovič, Petr Dohnal, Michal Hejduk, Radek Plašil, and Juraj Glosík

JOURNAL: The Journal of Physical Chemistry A 117:9626-9632

DATE: 27 March 2013

DOI: 10.1021/jp3123192

THE JOURNAL OF PHYSICAL CHEMISTRY A

Article

pubs.acs.org/JPCA

Binary Recombination of H_3^+ and D_3^+ Ions with Electrons in Plasma at 50−230 K

Peter Rubovič, Petr Dohnal, Michal Hejduk, Radek Plašil,* and Juraj Glosík

Department of Surface and Plasma Science, Faculty of Mathematics and Physics, Charles University, Prague 18000, Czech Republic

ABSTRACT: The results of an experimental study of the H_3^+ and D_3^+ ions recombination with electrons in afterglow plasmas in the temperature range 50−230 K are presented. A flowing afterglow apparatus equipped with a Langmuir probe was used to measure the evolution of the electron number density in the decaying plasma. The obtained values of the binary recombination rate coefficient are $\alpha_{\mathrm{bin}H_3^+} = (6.0 \pm 1.8) \times 10^{-8}(300/T)^{0.36\pm0.09}$ cm^3 s^{-1} for H_3^+ ions in the temperature range 80−300 K and $\alpha_{\mathrm{bin}D_3^+} = (3.5 \pm 1.1) \times 10^{-8}(300/T)^{0.73\pm0.09}$ cm^3 s^{-1} for D_3^+ ions in the temperature range 50−300 K. This is the first measurement of the binary recombination rate coefficient of H_3^+ and D_3^+ ions in a plasma experiment down to 50 K.

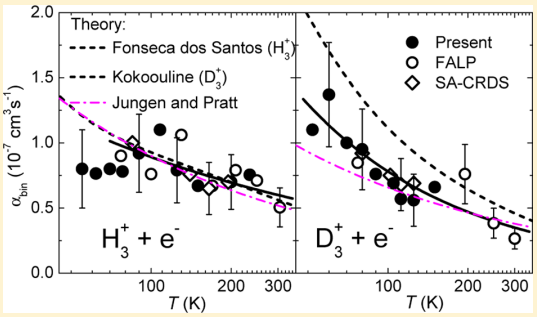

I. INTRODUCTION

The recombination of the simplest polyatomic ion H_3^+ (and to some extent of its deuterated isotopologues) with electrons has been the subject of extensive study by both experimental and theoretical physicists during the previous fifty years.[1] This process is fundamental for modeling of astrophysical diffuse clouds[2] and other hydrogen containing plasmas. The long history of H_3^+ recombination studies has been summarized in a number of reviews[3−8] and in the thorough book by Larsson and Orel.[9] The once puzzling disagreements in magnitude of recombination rate coefficients obtained in different types of experiments have been largely resolved by taking into account third-body stabilized recombination processes that can substantially enhance the overall recombination in plasmas over the pure binary recombination rate coefficients measured in beam type experiments.[10,11] Moreover, the large discrepancy between experimentally obtained recombination rate coefficients and some early quantum mechanical calculations[12] has been successfully resolved by including the role of the Jahn−Teller effect.[13−16] Theoretical predictions now agree very well with values obtained in ion-storage-rings experiments[17−20] and in afterglow experiments.[4,10,11,21,22]

In comparison, the neutral assisted ternary recombination of H_3^+ and D_3^+ ions with electrons as found in helium buffered afterglow experiments is still not fully understood. The recombining H_3^+ and D_3^+ ions form long living metastable Rydberg states[11,21] with lifetimes in the order of hundreds of picoseconds. At pressures above 100 Pa, this is long enough for several collisions with particles of the buffer gas prior to recombination. Although some mechanisms for these interactions have been proposed,[8,11] none of them fully explains the experimental data. This topic is thoroughly discussed in another article in this volume[23] together with new experimental data on the ternary helium assisted recombination of H_3^+ or D_3^+ ions with electrons.

The theory of the dissociative recombination of H_3^+ ions with electrons also predicts a large difference between the recombination of *ortho*- and *para*-H_3^+ (more than 10 times at 10 K, 2.5 times at 80 K and no difference above 300 K).[15] This was partially confirmed by storage ring measurements conducted using normal and para-enriched hydrogen (normal hydrogen contains 25% of *para*-H_2 and 75% of *ortho*-H_2—i.e., the population of the rotational states of H_2 in thermodynamic equilibrium at 300 K).[18,24−26] Tom et al.[25] found that *para*-H_3^+ recombines about twice as fast as *ortho*-H_3^+ at low collisional energies (10 K). The rotational temperature of H_3^+ ions in this experiment was probably higher than 300 K (see discussion in refs 20 and 26). In recent stationary afterglow experiments[27−29] a cavity ring down spectrometer (CRDS) was used to probe the decay of ions in specific rotational states and to determine the state specific recombination coefficients. According to these experiments at 77 K *para*-H_3^+ ions recombine three to 10 times faster (if the error bars are taken into account) than *ortho*-H_3^+ ions. In these experiments, the H_3^+ ions were in thermodynamic equilibrium (TDE) with the helium buffer gas; i.e., the measured kinetic and rotational temperatures of the H_3^+ ions were close to the wall temperature, $T_{\mathrm{kin}} = T_{\mathrm{rot}} = T_{\mathrm{He}} = T_{\mathrm{wall}}$.

Another afterglow experiment with spectroscopically resolved number densities of the recombining H_3^+ ions was conducted by Amano in pure hydrogen in the early nineties.[30]

Special Issue: Oka Festschrift: Celebrating 45 Years of Astrochemistry

Received: December 14, 2012
Revised: March 6, 2013
Published: March 27, 2013

   dx.doi.org/10.1021/jp3123192 | J. Phys. Chem. A 2013, 117, 9626−9632

His value of recombination rate coefficient $\alpha = 1.8 \times 10^{-7}$ cm^3 s^{-1} at 273 K and measured at pressure below 100 Pa is rather high and it probably indicates a very effective H_2 assisted ternary recombination.

The recombination of D_3^+ ions with electrons was also studied in storage ring experiments[31] and in plasmatic experiments.[4,21,32] Up to now there is only one study in a D_3^+ dominated plasma with spectroscopically resolved recombining ions.[33] In that experiment the measured kinetic and rotational temperatures of the recombining ions was also close to the buffer gas temperature (for details see ref 33).

In addition to the ternary neutral assisted recombination, an entirely different ternary process that can enhance the overall recombination rate in low temperature afterglow plasma is electron assisted ternary recombination (collisional radiative recombination, E-CRR).[34] At 80 K and an electron number density of $n_e = 5 \times 10^{10}$ cm^{-3} the predicted effective binary recombination rate coefficient due to E-CRR is 5×10^{-7} cm^3 s^{-1}—much larger than the actual values measured in H_3^+ or D_3^+ dominated afterglow plasmas under the same conditions.[28,33] The thorough analysis of experimental data made by Dohnal et al.[28] has shown that the E-CRR contribution to the overall recombination rate in their experiments is more than order of magnitude lower than that predicted by the theory of E-CRR.[34] We have recently studied the E-CRR of Ar^+ ions in the temperature range 50−200 K,[35,36] and we have obtained reasonable agreement with the theory. It is rather puzzling that we can measure value for the recombination rate coefficient close to the calculated one for the atomic ion Ar^+ and not for the molecular ion H_3^+. Recently, Shuman et al.[37] observed the dependence of the mutual neutralization of Ar^+ ions with various molecular anions on electron number density. Although the process they proposed is different than E-CRR (and 10−100 times faster), it is clear that the magnitude of the electron induced enhancement of the recombination rate of more complicated species (e.g., molecular ions) is still an open question (especially given the lack of experimental data on the subject). One of the motivations for the present experiments was to study the role of E-CRR on the overall recombination of H_3^+/D_3^+ ions in an afterglow plasma.

In this article we will present the results of our study of the recombination of H_3^+ and D_3^+ ions with electrons in the temperature range 50−230 K, extending our previous measurement down to 50 K. The present measurements were performed with better temperature stability and over a broader range of pressures than in our previous flowing afterglow experiments[10,11,21] to gain better accuracy of obtained binary and ternary recombination rate coefficients. To the best of our knowledge this is the first study of recombination of these molecular ions in an afterglow plasma below 80 K.

II. EXPERIMENT

In this study we used a Cryo-FALP II apparatus—a modification of the standard FALP (Flowing Afterglow with Langmuir Probe) device. The details of the FALP technique may be found in refs 9 and 38. The current experimental setup is described in ref 36 so only a short description will be given here.

The helium buffer gas is ionized in a microwave discharge in the upstream glass section of the flow tube, enters the stainless steel flow tube, and is pumped out by a Roots pump located at the other end of the flow tube. Argon is added a few centimeters downstream from the discharge to remove metastable helium atoms and to form an Ar^+ dominated plasma. Further downstream, H_2 or D_2 is added to form H_3^+ or D_3^+ dominated plasmas. The sequence of ion−molecule reactions leading to the formation of H_3^+ (D_3^+) dominated plasma is discussed, e.g., in refs 5 and 39. The decrease of the electron number density along the flow tube is measured by means of axially movable Langmuir probe.

In our previous SA-CRDS (stationary afterglow with cavity ring down spectrometer) experiments[27−29,33,40] conducted under conditions (pressure, temperature, and gas composition) similar to those in the present experiment, the measured kinetic and rotational temperatures of the H_3^+ or D_3^+ ions in the afterglow were close to the buffer gas temperature. Therefore, we have good reason to suppose that the internal temperature of the recombining ions is close to the buffer gas temperature also in the presented study which essentially extends previous measurements down to 50 K. Nevertheless, as discussed below, the actual *para*-H_3^+ to *ortho*-H_3^+ ratio could have been slightly shifted in favor of *ortho*-H_3^+ at temperatures below 80 K.

The electron temperature T_e was not directly measured in these (SA-CRDS and Cryo-FALP II) experiments. Recently, we have studied the collisional radiative recombination of Ar^+ ions with electrons, a process with a steep dependence on electron temperature.[35,36] The results were in overall agreement with the theory of E-CRR[34] indicating that T_e was not significantly higher than the buffer gas temperature. Another indirect measure of the value of T_e is the rate of ambipolar diffusion. Ambipolar diffusion time constants measurements for the Ar^+ ions in helium gas, performed using the same experimental setup as in present study,[35] confirmed that in the studied range 80−200 K the measured ambipolar diffusion is close to the expected value, i. e. again that the electron temperature is not higher than the buffer gas temperature (within experimental error of 10%).

III. DETERMINATION OF THE BINARY RECOMBINATION RATE COEFFICIENTS

Here and in the following text we will refer to the recombining ions as H_3^+, but the same considerations apply to D_3^+ ions unless stated otherwise.

It has been shown in previous afterglow experiments[4,10,11,21] that the recombination losses due to the ternary helium assisted recombination of H_3^+ or D_3^+ ions can be comparable to that due to the dissociative recombination at buffer gas pressures of a few hundred pascals. Furthermore, at low temperatures and high densities of H_2 and He, H_5^+ cluster ions, which quickly recombine with electrons with a recombination rate coefficient $\alpha_5 \sim 10^{-6}$ cm^3 s^{-1}, are formed in three body association reactions.[41,42]

The overall losses of charged particles in a H_3^+ dominated plasma with a small fraction of H_5^+ ions, following the derivation in refs 35 and 42 can be described by the equation

$$\frac{dn_e}{dt} = \frac{d[H_3^+]}{dt} = -\alpha_{bin}[H_3^+]n_e - \alpha_5 R[H_3^+]n_e - K_{He}[He][H_3^+]n_e - K_{E\text{-}CRR}[H_3^+]n_e^2 - \frac{n_e}{\tau_D} - \frac{n_e}{\tau_R} \quad (3)$$

where n_e is the electron number density, $[H_3^+]$ is the number density of H_3^+ ions, [He] is the number density of neutral buffer gas atoms (helium in this experiment), α_{bin} is the binary

dx.doi.org/10.1021/jp3123192 | J. Phys. Chem. A 2013, 117, 9626−9632

recombination rate coefficient of H_3^+ ions, α_5 is the H_5^+ binary recombination rate coefficient, $R = [H_5^+]/[H_3^+] \approx K_C[H_2]$ (K_C is the equilibrium constant, the ratio R is equal to $K_C[H_2]$ if R does not change in time), K_{He} is the ternary recombination rate coefficient of neutral assisted ternary recombination (N-CRR), $K_{E\text{-}CRR}$ is the ternary recombination rate coefficient of electron assisted collisional radiative recombination (E-CRR), τ_D is the time constant of ambipolar diffusion, and τ_R is the time constant of losses due to reactions with impurities and consequent fast recombination of formed ions. Assuming that H_3^+ is the dominant ion in the decaying plasma, and that the plasma is quasineutral, eq 3 can be then simplified:

$$\frac{dn_e}{dt} = -\alpha_{eff} n_e^2 - \frac{n_e}{\tau_L} \quad (4)$$

where

$$\alpha_{eff} = \alpha_{extrap} + \alpha_5 K_C[H_2] = \alpha_{eff0} + K_{He}[He] + \alpha_5 K_C[H_2] \quad (5)$$

is the effective binary recombination rate coefficient, and $1/\tau_L = 1/\tau_D + 1/\tau_R$. The α_{extrap} is part of the effective recombination rate coefficient independent of hydrogen number density. In the limit of vanishing helium and hydrogen densities, α_{eff} ($[H_2] \rightarrow 0$, $[He] \rightarrow 0$) = $\alpha_{eff0} = (\alpha_{bin} + K_{E\text{-}CRR} n_e)$.

In the previous paragraph we have assumed that losses by N-CRR and E-CRR can be linearly added. This assumption might not be necessarily correct because of competition between both ternary processes.[43] At temperatures above 100 K and electron number densities $n_e \sim 10^9$ cm^{-3}, the predicted losses due to E-CRR[34] are negligible in comparison with the losses due to dissociative recombination of H_3^+ (or D_3^+). At lower temperatures the losses due to E-CRR could be comparable with those from the dissociative recombination reaction. Nevertheless, we decided not to evaluate the $K_{E\text{-}CRR}$ from the measured decay of the electron number density. If the E-CRR is present, it would be included in the α_{eff0} term of eq 5, because the H_2 and He dependent terms are evaluated separately (see below).

The "integral data analysis" described in ref 44 enables us to evaluate the effective recombination rate coefficient, α_{eff}, and the time constant, τ_L, from the measured evolution of the electron number density.

To correct for the presence of H_5^+ ions, we measured the dependence of the effective recombination rate coefficient, α_{eff}, on the H_2 number density at each temperature and pressure. Examples of such dependences are plotted in Figure 1.

The recombination rate coefficients of H_3^+ ions with electrons at a given temperature and pressure $\alpha_{extrap}(T, [He])$ = $\alpha_{eff}(T,[He],[H_2]\rightarrow 0)$, are then obtained by linear extrapolation of the measured α_{eff} to $[H_2] = 0$, as shown in Figure 1. The steepness of the slope fitted to these data increased with helium density and decreasing temperature. The number density of H_2 was always kept above 5×10^{11} cm^{-3} because it has to be high enough to form H_3^+ rapidly from the Ar^+ precursor ions and to maintain a constant *para*- to *ortho*-H_3^+ ratio. Otherwise, the faster recombining species would be depleted preferentially. We perform calculations of the chemical kinetics to determine the best conditions for the experiment. The discussions in refs 4 and 11 suggest that at conditions similar to the present experiment, the number density of H_2 should be greater than 10^{12} cm^{-3}. In this study $[H_2]$ was in the range 5×10^{11} to 2×10^{13} cm^{-3}, sufficient to maintain the *para*-H_3^+ to *ortho*-H_3^+ ratio at the value appropriate for the *para*/*ortho* composition of the H_2 gas used.[40,45]

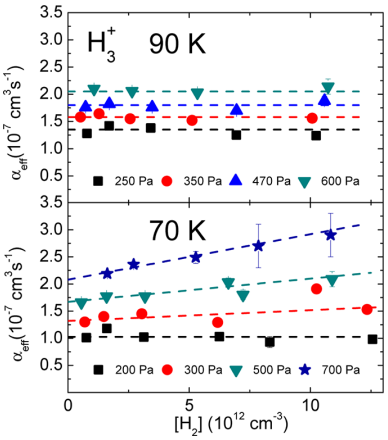

Figure 1. Dependence of the measured effective recombination rate coefficient of recombination of H_3^+ ions with electrons on H_2 number density at 90 K (upper panel) and 70 K (lower panel). Dashed lines are linear fits to the data. The extrapolation of these fits to $[H_2] = 0$ gives the value of $\alpha_{extrap}(T,[He])$ at the given temperature and pressure.

Examples of measured dependences of α_{eff} on the helium number density for H_3^+ and for D_3^+ are plotted in Figure 2.

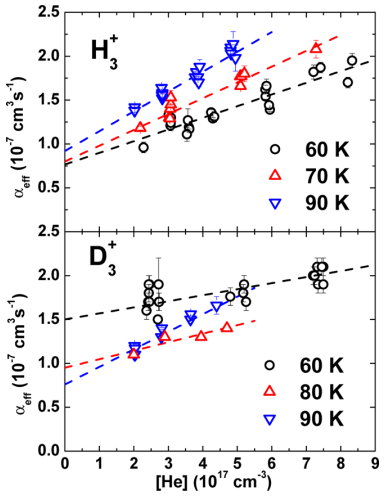

Figure 2. Upper panel: dependence of the effective recombination rate coefficient of recombination of H_3^+ ions with electrons on the helium buffer gas density measured at each of the following temperatures: 60, 70, and 90 K. Lower panel: as in the upper panel but for D_3^+ ions at the temperatures 60, 80, and 90 K. The dashed lines are linear fits to the data. The displayed errors are statistical errors.

These data were obtained at number densities of H_2 in the range 1×10^{12} to 7×10^{12} cm^{-3}. In general, the binary and the ternary recombination rate coefficients can be obtained from the dependences plotted in Figure 2, as is discussed, e.g., in ref 28. At low temperatures (especially at 50 K) and at higher helium densities the formation of H_5^+ (D_5^+) would cause an additional increase in the effective recombination rate

dx.doi.org/10.1021/jp3123192 | J. Phys. Chem. A 2013, 117, 9626−9632

coefficient. The binary α_{eff0} and the ternary K_{He} recombination rate coefficients at a given temperature were thus obtained using eq 5 from the dependence of $\alpha_{extrap}(T,[He])$ on the helium number density. The errors displayed in Figures 1 and 2 are statistical errors of the fit to the time decay of electron number density.

IV. RESULTS AND DISCUSSION

The measured dependence of the binary recombination rate coefficient α_{bin} (α_{eff0}, see below) of the recombination of H_3^+ ions with electrons on temperature is plotted in Figure 3. The

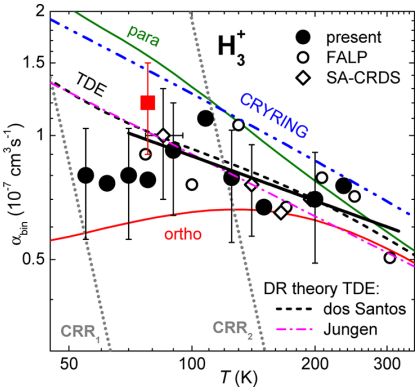

Figure 3. Temperature dependence of the binary recombination rate coefficient for the recombination of H_3^+ ions with electrons. Present Cryo-FALP II data are indicated by full circles. Open rhomboids indicate values measured by Varju et al.[27] and Dohnal et al.[28] using the SA-CRDS apparatus with spectroscopic identification of the recombining ions. Open circles are binary recombination rate coefficients measured in this laboratory using the FALP technique (see discussion in refs 11 and 28). The dashed double dotted line shows data measured at the storage ring CRYRING.[19] The dashed, and the dot dashed, lines marked TDE are theoretical calculations by Fonseca dos Santos[15] and Pratt and Jungen,[46] respectively. The dotted lines marked CRR$_1$ and CRR$_2$ indicate calculated[34] recombination rate coefficient for E-CRR at electron number densities of 10^9 and 5×10^{10} cm^{-3}, respectively. The thick full straight line is a fit to the FALP, Cryo-FALP II, and SA-CRDS data in the range 80−300 K: $\alpha_{binH_3^+} = (6.0 \pm 1.8) \times 10^{-8}(300/T)^{0.36\pm0.09}$ cm^3 s^{-1}. The full lines labeled para and ortho are recombination rate coefficients calculated by Fonseca dos Santos[15] for *para*-H_3^+ and *ortho*-H_3^+ ions. The full square is the value of α_{bin} measured using the Cryo-FALP II apparatus with para-enriched H_2 instead of normal H_2.

present data are plotted as full circles. Values from previous FALP,[11] SA-CRDS,[27,28] and CRYRING[19] experiments are also plotted in Figure 3 together with the thermal dissociative recombination rate coefficients calculated by Fonseca dos Santos et al.[15] and by Pratt and Jungen.[16,46] We computed the thermal values from the energy dependent recombination rate coefficients published by Pratt and Jungen.[46] The estimated errors of the measured recombination rate coefficients α_{bin} are ±30%.[47] The main contributions of the systematic errors arise from the electron number density measurement by Langmuir probe and from uncertainties in the determination of pressure and gas flows. The statistical error from the aforementioned fitting steps (less than 10%) is negligible in comparison with the systematic one.

The dotted lines in Figure 3 labeled CRR$_1$ and CRR$_2$ are effective binary recombination rate coefficients of E-CRR ($\alpha_{E\text{-}CRR}$) at electron number density of 10^9 cm^{-3} (a typical value for the present Cryo-FALP II experiment) and 5×10^{10} cm^{-3} (a typical value for the SA-CRDS experiment), calculated from the dependence $\alpha_{E\text{-}CRR} = 3.8 \times 10^{-9}\ T^{-4.5}\ n_e$ cm^3 s^{-1} (see ref 34), respectively. Note that at $T \sim 80$ K, the difference between the values of α_{bin} obtained in the present study and in the previous SA-CRDS experiment[27] is less than 2×10^{-8} cm^3 s^{-1}. This suggests that the effect of E-CRR on the recombination of H_3^+ ions with electrons is at least 20 times lower than predicted by theory of E-CRR.[34] A substantial increase of the recombination rate coefficient below 80 K (in accordance with the $T^{-4.5}$ temperature dependence of $\alpha_{E\text{-}CRR}$) was not observed. This leads to the conclusion that under our experimental conditions $\alpha_{eff0} = \alpha_{bin}$.

We have previously measured the rate coefficients of E-CRR of Ar^+ ions using the same setup as in current experiment[35,36] and we have found good agreement with theory of E-CRR.[34] We do not have an explanation for the seeming absence of E-CRR in the H_3^+ dominated plasma investigated here.

The thick full straight line plotted in Figure 3 is the fit of the FALP, Cryo-FALP II, and SA-CRDS data in the temperature range 80−300 K giving the value $\alpha_{binH_3^+} = (6.0 \pm 1.8) \times 10^{-8}(300/T)^{0.36\pm0.09}$ cm^3 s^{-1}. We included in the fit only the data for which we have information about the internal state of the recombining ions. The agreement of the present data with our previous afterglow experiments, storage ring values and with the theoretical calculations is very good. Below 80 K the experimental values begin to deviate from the theoretical ones. To form H_3^+ ions, we used normal H_2 from a 300 K reservoir, with a *para*- to *ortho*-H_2 ratio of 1:3. The *para*- to *ortho*-H_2 equilibrium ratio at 50 K is approximately 3:1. We suspect that this huge difference could shift the population of H_3^+ ions toward *ortho*-H_3^+. At 77 K where the *para*- to *ortho*-H_2 equilibrium ratio is 1:1, the resulting percentage of *para*-H_3^+ states was 45 ± 2% depending on conditions (see Figure 10 in Hejduk et al.[40]). There is a difference in magnitude of the recombination rate coefficients of *para*- and *ortho*-H_3^+ below 300 K. *para*-H_3^+ recombines 2 times faster than *ortho*-H_3^+ at 10 K as measured in storage ring experiment CRYRING[25] or 3−10 times faster at 80 K as measured in our stationary afterglow experiment.[27] The theory[15] suggests that *para*-H_3^+ recombines 2.5 times faster than *ortho*-H_3^+ at 80 K (Figure 3). This would lead to substantial decrease of measured α_{bin} if the fraction of *ortho*-H_3^+ ions was enhanced with respect to the equilibrium population of states of the H_3^+ ions.

To see the influence of the different *para*- to *ortho*-H_3^+ ratios on the overall recombination in plasma, we used hydrogen with an enriched fraction of *para*-H_2 at otherwise identical conditions as in presented experiments with normal H_2. The para-enriched hydrogen was produced using apparatus described in ref 40. According to the measurements of the reaction rate coefficient of the reaction of N^+ with H_2,[48] the produced H_2 gas contained 99.5 ± 0.5% molecules in *para*-H_2 states. Using this *para*-H_2-enriched gas to form the H_3^+ dominated plasma, the obtained value of the binary recombination rate coefficient was $(1.2 \pm 0.3) \times 10^{-7}$ cm^3 s^{-1} at 80 K in comparison with the value of $(0.8 \pm 0.3) \times 10^{-7}$ cm^3 s^{-1} obtained using normal H_2. The result is plotted in Figure 3 as a full square. Unfortunately, we are not able to measure in situ the *para*- to *ortho*-H_3^+ ratio in the present Cryo-

dx.doi.org/10.1021/jp3123192 | J. Phys. Chem. A 2013, 117, 9626−9632

FALP II setup. The fraction of *para*-H_3^+ ions obtained in SA-CRDS experiment at 80 K when para-enriched H_2 was used was 70−75%.[40] We suppose that the *para*-H_3^+ fraction in our Cryo-FALP II experiment is similar.

The experiments with D_3^+ dominated plasmas were similar to those with H_3^+ dominated plasmas. We measured the dependence of the effective recombination rate coefficient on the D_2 number density at particular temperatures and pressures and obtained the binary α_{bin} and the ternary K_{He} recombination rate coefficients for the recombination of D_3^+ ions with electrons. The measured binary recombination rate coefficients of recombination of D_3^+ ions with electrons are plotted in Figure 4 together with values from previous SA-CRDS,[33]

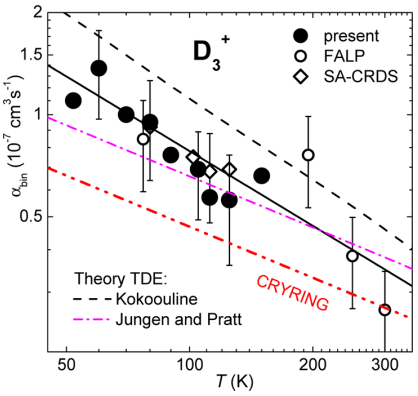

Figure 4. Temperature dependence of the measured binary recombination rate coefficient for the recombination of D_3^+ ions with electrons. Full circles indicate the present data obtained in the Cryo-FALP II experiment. Open rhomboids are the values obtained in SA-CRDS experiment.[33] Open circles are data from previous FALP[21] experiments. The dashed double dot line indicates results from the storage ring CRYRING.[31] The theoretical calculations of Kokoouline[49] and Pratt and Jungen[46] are plotted as dashed lines and dot dashed lines, respectively. The full straight line is a fit to the FALP, Cryo-FALP II, and SA-CRDS data in the range 50−300 K: $\alpha_{binD_3^+} = (3.5 \pm 1.1) \times 10^{-8}(300/T)^{0.73\pm0.09}$ cm^3 s^{-1}.

FALP,[21] and CRYRING[31] experiments. The theoretical dependences calculated by Kokoouline[49] and by Pratt and Jungen[46] are also plotted in Figure 4. We calculated the recombination rate coefficients labeled Jungen and Pratt in Figure 4 by thermally averaging their energy dependent recombination rates published in ref 46. The full straight line plotted in Figure 4 is the fit to the FALP, Cryo-FALP II, and SA-CRDS data in the range 50−300 K, giving a value for recombination rate coefficient $\alpha_{binD_3^+} = (3.5 \pm 1.1) \times 10^{-8}(300/T)^{0.73\pm0.09}$ cm^3 s^{-1}. The theory[49] predicts that the difference between the recombination rate coefficients of each nuclear spin state modification of D_3^+ (ortho, para, and meta) is only small and not so pronounced as in the case of H_3^+. For example at 50 K *ortho*-D_3^+ should recombine 1.5 times faster than *meta*-D_3^+. Moreover, the relative population of nuclear spin modifications in the D_2 gas used in the experiment is close to the equilibrium value even at 60 K due to the closer spacing of the rotational energy levels of D_2 in comparison with H_2. At 300 K the *para*-D_2 to *ortho*-D_2 equilibrium ratio is 2, at 60 K the *para*-D_2 to *ortho*-D_2 equilibrium ratio is 1.8. Therefore, we suppose that the *ortho*/*para*/*meta*-D_3^+ ratio is maintained in the whole temperature range used in this study. This is probably why the values for the D_3^+ recombination rate coefficient obtained below 80 K continue to follow the $T^{-0.73}$ dependence (the full line plotted in Figure 4). As in the case of H_3^+, the results obtained for D_3^+ are in good agreement with theoretical calculations and with other experiments. No substantial difference between present values and values obtained in SA-CRDS experiment[33] conducted at order of magnitude higher n_e was observed. As in the case of H_3^+ dominated plasma we have seen no substantial influence of E-CRR on the overall recombination of D_3^+ ions with electrons over the range of experimental conditions.

Together with binary recombination rate coefficients α_{bin} we also evaluated the ternary recombination rate coefficients K_{He} for the recombination of H_3^+ and D_3^+ ions with electrons in the temperature range 50−230 K. These results are published elsewhere[23] together with a thorough discussion of possible ternary recombination processes occurring in low temperature plasmas. The temperature range 80−300 K was already covered in our previous experiments;[11,21,28,33] the present data were measured over wider temperature and pressure ranges than in the FALP[11,21] experiments and with better accuracy and temperature stability. The agreement with these previous studies is good.

V. CONCLUSION

We have measured the binary and the ternary recombination rate coefficient for the recombination of H_3^+ and D_3^+ ions with electrons in the temperature range 50−230 K. The results are in good agreement with previous afterglow experiments (FALP and SA-CRDS), storage ring data, and theoretical calculations. The obtained binary recombination rate coefficients follow the dependence $\alpha_{binH_3^+} = (6.0 \pm 1.8) \times 10^{-8}(300/T)^{0.36\pm0.09}$ cm^3 s^{-1} for H_3^+ in the temperature range 80−300 K and $\alpha_{binD_3^+} = (3.5 \pm 1.1) \times 10^{-8}(300/T)^{0.73\pm0.09}$ cm^3 s^{-1} for D_3^+ in the temperature range 50−300 K. We have seen no enhancement of the measured recombination rate coefficient of H_3^+ and D_3^+ ions due to E-CRR even at the lowest temperature. This is in agreement with our previous SA-CRDS experiments[27,33] conducted at higher electron number densities than in present study. The addition of para-enriched H_2 instead of normal H_2 led to the increase of the binary recombination rate coefficient at 80 K from $(0.8 \pm 0.3) \times 10^{-7}$ cm^3 s^{-1} with normal H_2 to $(1.2 \pm 0.3) \times 10^{-7}$ cm^3 s^{-1} with para-enriched H_2. This is the first measurement of the recombination rate coefficient of H_3^+ and D_3^+ ions in a plasma experiment down to 50 K.

AUTHOR INFORMATION

Corresponding Author

*Phone: +420221912224. E-mail: radek.plasil@mff.cuni.cz.

Author Contributions

The manuscript was written through contributions of all authors. All authors have given approval to the final version of the manuscript.

Notes

The authors declare no competing financial interest.

ACKNOWLEDGMENTS

We thank Rainer Johnsen for helpful discussion and comments. This work was partly supported by GACR (205/09/1183, P209/12/0233), SV 267 302, GAUK 353811, GAUK 406011,

GAUK 659112, and COST Action CM0805 (The Chemical Cosmos).

REFERENCES

(1) Oka, T. in *Dissociative Recombination of Molecular Ions with Electrons*; Guberman, S. L., Ed.; Kluwer Academic/Plenum Publishers: New York, USA, 2003; pp 209−220

(2) Herbst, E.; Klemperer, W. The Formation and Depletion of Molecules in Dense Interstellar Clouds. *Astrophys. J.* **1973**, *185*, 505−533.

(3) Larsson, M. Experimental Studies of the Dissociative Recombination of H_3^+. *Philos. Trans. R. Soc. A* **2000**, *358*, 2433−2444.

(4) Glosik, J.; Plasil, R.; Kotrik, T.; Dohnal, P.; Varju, J.; Hejduk, M.; Korolov, I.; Roucka, S.; Kokoouline, V. Binary and Ternary Recombination of H_3^+ and D_3^+ Ions with Electrons in Low Temperature Plasma. *Mol. Phys.* **2010**, *108*, 2253−2264.

(5) Plasil, R.; Glosik, J.; Poterya, V.; Kudrna, P.; Rusz, J.; Tichy, M.; Pysanenko, A. Advanced Integrated Stationary Afterglow Method for Experimental Study of Recombination of Processes of H_3^+ and D_3^+ Ions with Electrons. *Int. J. Mass Spectrom.* **2002**, *218*, 105−130.

(6) Smith, D.; Spanel, P. Dissociative Recombination of H_3^+ and Some Other Interstellar Ions: a Controversy Resolved. *Int. J. Mass Spectrom.* **1993**, *129*, 163−182.

(7) Johnsen, R. A Critical Review of H_3^+ Recombination Studies. *J. Phys.: Conf. Ser.* **2005**, *4*, 83−91.

(8) Johnsen, R.; Guberman, S. L. Dissociative Recombination of H_3^+ Ions with Electrons: Theory and Experiment. *Adv. At., Mol., Opt. Phys.* **2010**, *59*, 75−128.

(9) Larsson, M.; Orel, A. *Dissociative Recombination of Molecular Ions*; Cambridge University Press: Cambridge, U.K., 1995.

(10) Glosik, J.; Korolov, I.; Plasil, R.; Novotny, O.; Kotrik, T.; Hlavenka, P.; Varju, J.; Mikhailov, I. A.; Kokoouline, V.; Greene, C. H. Recombination of H_3^+ Ions in the Afterglow of a He-Ar-H_2 Plasma. *J. Phys. B-At. Mol. Opt.* **2008**, *41*, 191001.

(11) Glosik, J.; Plasil, R.; Korolov, I.; Kotrik, T.; Novotny, O.; Hlavenka, P.; Dohnal, P.; Varju, J.; Kokoouline, V.; Greene, C. H. Temperature Dependence of Binary and Ternary Recombination of H_3^+ Ions with Electrons. *Phys. Rev. A* **2009**, *79*, 052707.

(12) Michels, H. H.; Hobbs, R. H. Low-Temperature Dissociative Recombination of e + H_3^+. *Astrophys. J.* **1984**, *286*, L27−L29.

(13) Kokoouline, V.; Greene, C. H.; Esry, B. D. Mechanism for the Destruction of H_3^+ Ions by Electron Impact. *Nature* **2001**, *412*, 891−894.

(14) Kokoouline, V.; Greene, C. H. Unified Theoretical Treatment of Dissociative Recombination of D_{3h} Triatomic Ions: Application to H_3^+ and D_3^+. *Phys. Rev. A* **2003**, *68*, 012703.

(15) Fonseca dos Santos, S.; Kokoouline, V.; Greene, C. H. Dissociative Recombination of H_3^+ in the Ground and Excited Vibrational States. *J. Chem. Phys.* **2007**, *127*, 124309.

(16) Jungen, Ch.; Pratt, S. T. Jahn-Teller Interactions in the Dissociative Recombination of H_3^+. *Phys. Rev. Lett.* **2009**, *102*, 023201.

(17) McCall, B. J.; Honeycutt, A. J.; Saykally, R. J.; Geballe, T. R.; Djuric, N.; Dunn, G. H.; Semaniak, J.; Novotny, O.; Al-Khalili, A.; Ehlerding, A.; et al. An Enhanced Cosmic-Ray Flux Towards ζ Persei Inferred from a Laboratory Study of the H_3^+-e^- Recombination Rate. *Nature* **2003**, *422*, 500−502.

(18) Kreckel, H.; Motsch, M.; Mikosch, J.; Glosik, J.; Plasil, R.; Altevogt, S.; Andrianarijaona, V.; Buhr, H.; Hoffman, J.; Lammich, L.; et al. High-Resolution Dissociative Recombination of Cold H_3^+ and First Evidence for Nuclear Spin Effects. *Phys. Rev. Lett.* **2005**, *95*, 263201.

(19) McCall, B. J.; Honeycutt, A. J.; Saykally, R. J.; Djuric, N.; Dunn, G. H.; Semaniak, J.; Novotny, O.; Al-Khalili, A.; Ehlerding, A.; Hellberg, F.; et al. Dissociative Recombination of Rotationally Cold H_3^+. *Phys. Rev. A* **2004**, *70*, 052716.

(20) Petrignani, A.; Altevogt, S.; Berg, M. H.; Bing, D.; Grieser, M.; Hoffman, J.; Jordon-Thaden, B.; Krantz, C.; Mendes, M. B.; Novotny, O.; et al. Resonant Structure of Low-Energy H_3^+ Dissociative Recombination. *Phys. Rev. A* **2011**, *83*, 032711.

(21) Kotrik, T.; Dohnal, P.; Korolov, I.; Plasil, R.; Roucka, S.; Glosik, J.; Greene, C. H.; Kokoouline, V. Temperature Dependence of Binary and Ternary Recombination of D_3^+ Ions with Electrons. *J. Chem. Phys.* **2010**, *133*, 034305.

(22) Glosik, J.; Plasil, R.; Korolov, I.; Novotny, O.; Kotrik, T. Multicollision Character of Recombination of H_3^+ Ions in Afterglow Plasma. *J. Phys.: Conf. Ser.* **2009**, *192*, 012005.

(23) Johnsen, R.; Rubovic, P.; Dohnal, P.; Hejduk, M.; Plasil, R.; Glosik, J. Ternary Recombination of H_3^+ and D_3^+ with Electrons in He-H_2 (D_2) Plasmas at Temperatures from 50 to 300 K. Elsewhere in this volume. *J. Phys. Chem. A* **2013**, DOI: 1021/jp311978n.

(24) Wolf, A.; Kreckel, H.; Lammich, L.; Strasser, D.; Mikosch, J.; Glosik, J.; Plasil, R.; Altevogt, S.; Andrianarijaona, V.; Buhr, H.; et al. Effects of Molecular Rotation in Low-Energy Electron Collisions of H_3^+. *Philos. Trans. R. Soc. A* **2006**, *364*, 2981−2997.

(25) Tom, B. A.; Zhaunerchyk, V.; Wiczer, M. B.; Mills, A. A.; Crabtree, K. N.; Kaminska, M.; Geppert, W. D.; Hamberg, M.; af Ugglas, M.; Vigren, E.; et al. Dissociative Recombination of Highly Enriched Para-H_3^+. *J. Chem. Phys.* **2009**, *130*, 031101.

(26) Kreckel, H.; Novotny, O.; Crabtree, K. N.; Buhr, H.; Petrignani, A.; Tom, B. A.; Thomas, R. D.; Berg, M. H.; Bing, D.; Grieser, M.; et al. High-Resolution Storage-Ring Measurements of the Dissociative Recombination of H_3^+ Using a Supersonic Expansion Ion Source. *Phys. Rev. A* **2010**, *82*, 042715.

(27) Varju, J.; Hejduk, M.; Dohnal, P.; Jilek, M.; Kotrik, T.; Plasil, R.; Gerlich, D.; Glosik, J. Nuclear Spin Effect on Recombination of H_3^+ Ions with Electrons at 77 K. *Phys. Rev. Lett.* **2011**, *106*, 203201.

(28) Dohnal, P.; Hejduk, M.; Varju, J.; Rubovic, P.; Roucka, S.; Kotrik, T.; Plasil, R.; Glosik, J.; Johnsen, R. Binary and Ternary Recombination of Para-H_3^+ and Ortho-H_3^+ with Electrons: State Selective Study at 77−200 K. *J. Chem. Phys.* **2012**, *136*, 244304.

(29) Dohnal, P.; Hejduk, M.; Varju, J.; Rubovic, P.; Roucka, S.; Kotrik, T.; Plasil, R.; Johnsen, R.; Glosik, J. Binary Recombination of Para- and Ortho-H_3^+ with Electrons at Low Temperatures. *Philos. Trans. R. Soc. A* **2012**, *370*, 5101−5108.

(30) Amano, T. The Dissociative Recombination Rate Coefficients of H_3^+, HN_2^+ and HCO^+. *J. Chem. Phys.* **1990**, *92*, 6492−6501.

(31) Le Padellec, A.; Larsson, M.; Danared, H.; Larson, A.; Peterson, J. R.; Rosen, S.; Semaniak, J.; Stromholm, C. A Storage Ring Study of Dissociative Excitation and Recombination of D_3^+. *Phys. Scr.* **1998**, *57*, 215−221.

(32) Poterya, V.; Glosik, J.; Plasil, R.; Tichy, M.; Kudrna, P.; Pysanenko, A. Recombination of D_3^+ ions in the Afterglow of a He-Ar-D_2 Plasma. *Phys. Rev. Lett.* **2002**, *88*, 044802.

(33) Dohnal, P.; Hejduk, M.; Rubovic, P.; Varju, J.; Roucka, S.; Plasil, R.; Glosik, J. Binary and Ternary Recombination of D_3^+ Ions at 80−130 K: Application of Laser Absorption Spectroscopy. *J. Chem. Phys.* **2012**, *137*, 194320.

(34) Stevefelt, J.; Boulmer, J.; Delpech, J. F. Collisional-Radiative Recombination in Cold Plasmas. *Phys. Rev. A* **1975**, *12*, 1246−1251.

(35) Kotrik, T.; Dohnal, P.; Roucka, S.; Jusko, P.; Plasil, R.; Glosik, J.; Johnsen, R. Collisional-Radiative Recombination Ar^+ + e + e: Experimental Study at 77−180 K. *Phys. Rev. A* **2011**, *83* (3), 032720.

(36) Kotrik, T.; Dohnal, P.; Rubovic, P.; Plasil, R.; Roucka, S.; Opanasiuk, S.; Glosik, J. Cryo-FALP Study of Collisional-Radiative Recombination of Ar^+ Ions at 40−200 K. *Eur. Phys. J. Appl. Phys.* **2011**, *56*, 24011.

(37) Shuman, S.; Miller, T. M.; Bemish, R. J.; Viggiano, A. A. Electron-Catalyzed Mutual Neutralization of Various Anions with Ar^+: Evidence of a New Plasma Process. *Phys. Rev. Lett.* **2011**, *106*, 018302.

(38) Smith, D.; Adams, N. G.; Dean, A. G.; Church, M. J. The Application of the Langmuir Probes to the Study of the Flowing Afterglow Plasmas. *J. Phys. D: Appl. Phys.* **1975**, *8*, 141−152.

(39) Novotny, O.; Plasil, R.; Pysanenko, A.; Korolov, I.; Glosik, J. The Recombination of D_3^+ and D_5^+ Ions with Electrons in Deuterium Containing Plasma. *J. Phys. B-At. Mol. Opt. Phys.* **2006**, *39*, 2561−2569.

(40) Hejduk, M.; Dohnal, P.; Varju, J.; Rubovic, P.; Plasil, R.; Glosik, J. Nuclear Spin State-Resolved Cavity Ring-Down Spectroscopy

Diagnostics of a Low-Temperature H_3^+ Dominated Plasma. *Plasma Sources Sci. Technol.* **2012**, *21*, 024002.
(41) Hiraoka, K. A determination of the Stabilities of $H_3^+(H_2)_n$ with n = 1−9 from Measurements of the Gas Phase Ion Equilibria $H_3^+(H_2)_{n-1} + H_2 = H_3^+(H_2)_n$. *J. Chem. Phys.* **1987**, *87*, 4048−4055.
(42) Glosik, J.; Novotny, O.; Pysanenko, A.; Zakouril, P.; Plasil, R.; Kudrna, P.; Poterya, V. The Recombination of H_3^+ and H_5^+ Ions with Electrons in Hydrogen Plasma: Dependence on Temperature and on Pressure of H_2. *Plasma Sources Sci. Technol.* **2003**, *12*, S117−S122.
(43) Bates, D. R. Recombination and Electrical Networks. *Proc. R. Soc. London A* **1974**, *337*, 15−20.
(44) Korolov, I.; Kotrik, T.; Plasil, R.; Varju, J.; Hejduk, M.; Glosik, J. Application of Langmuir Probe in Recombination Dominated Afterglow Plasma. *Contrib. Plasma Phys.* **2008**, *48*, 521−526.
(45) Grussie, F.; Berg, M. H.; Crabtree, K. N.; Gartner, S.; McCall, B. J.; Schlemmer, S.; Wolf, A.; Kreckel, H. The Low-Temperature Nuclear Spin Equilibrium of H_3^+ in Collisions with H_2. *Astrophys. J.* **2012**, *759*, 21.
(46) Pratt, T.; Jungen, Ch. Dissociative Recombination of Small Polyatomic Molecules. *J. Phys.: Conf. Ser.* **2011**, *300*, 012019.
(47) Glosik, J.; Bano, G.; Plasil, R.; Luca, A.; Zakouril, P. Study of the Electron Ion Recombination in High Pressure Flowing Afterglow: Recombination of $NH_4^+(NH_3)_2$. *Int. J. Mass Spectrom.* **1999**, *189*, 103−113.
(48) Zymak, I.; Hejduk, M.; Mulin, D.; Plasil, R.; Glosik, J.; Gerlich, D. Low Temperature Ion Trap Studies of $N^+(^3P_{ja}) + H_2(j) \rightarrow NH^+ + H$. *Astrophys. J.* **2013**, in press.
(49) Pagani, L.; Vastel, C.; Hugo, E.; Kokoouline, V.; Greene, C. H.; Backmann, A.; Bayet, E.; Ceccarelli, C.; Peng, R.; Schlemmer, S. Chemical Modeling of L183 (L134N): an Estimate of the Ortho/Para H_2 Ratio. *Astron. Astrophys.* **2009**, *494*, 623−636.

COLOPHON

This document was typeset using LaTeX with the typographical look-and-feel `classicthesis`. Figures were created using `OriginLab`. The text was written in `Kile`.

Printed June 2, 2014.